NATIONAL AND KAPODISTRIAN UNIVERSITY OF ATHENS

SCHOOL OF SCIENCE – FACULTY OF PHYSICS DIVISION
OF ENVIRONMENTAL PHYSICS

PhD Thesis

Extreme value analysis of environmental parameters and quantification of the associated uncertainty

Platon
Patlakas

Athens 2020

Σχολή Θετικών Επιστημών, Τμήμα Φυσικής, Τομέας Φυσικής Περιβάλλοντος - Μετεωρολογίας

Διδακτορικό Δίπλωμα Φυσικών Επιστημών

Τίτλος: «Εκτίμηση ακραίων τιμών περιβαλλοντικών παραμέτρων και ποσοτικοποίηση της αντίστοιχης αβεβαιότητας»

Title: “Extreme value analysis of environmental parameters and quantification of the associated uncertainty”

Συγγραφέας: Πλάτων Πατλάκας

Αριθμός Μητρώου: 2014518

Τριμελής επιτροπή:

Γεώργιος Κάλλος (επιβλέπων)

Γεώργιος Γαλάνης

Σαράντης Σοφιανός

Αθήνα 2020

Λέξεις κλειδιά: Περίοδοι επαναφοράς, Θεωρία ακραίων τιμών, Επιπτώσεις ακραίων καιρικών φαινομένων, Ατμοσφαιρικά μοντέλα πρόγνωσης καιρού

Key words: Return periods, Extreme value theory, Impact of extreme weather events, Atmospheric modeling systems

0000468115

ΕΚΠΑ 07/12/2020
Α. Π.: Εισερχ. 58744

ΕΛΛΗΝΙΚΗ ΔΗΜΟΚΡΑΤΙΑ
Εθνικόν και Καποδιστριακόν Πανεπιστήμιον Αθηνών
ΙΔΡΥΘΕΝ ΤΟ 1837

Τμήμα Φυσικής
Τομέας Φυσικής Περιβάλλοντος – Μετεωρολογίας
Πανεπιστημιούπολη, Ζωγράφου 15784
Τηλ.: 210 727 6830, Fax: 210 727 6791

Αθήνα, 3 Δεκεμβρίου 2020

ΠΡΑΚΤΙΚΟ ΕΞΕΤΑΣΗΣ ΤΗΣ ΔΙΔΑΚΤΟΡΙΚΗΣ ΔΙΑΤΡΙΒΗΣ
του κ. ΠΛΑΤΩΝΑ ΠΑΤΛΑΚΑ

Οι υπογράφοντες το παρόν πρακτικό εξέτασης αποτελούμε τα μέλη της επταμελούς Εξεταστικής Επιτροπής που ορίστηκε από τη Συνέλευση του Τμήματος Φυσικής την 18/5/2020, για την κρίση της Διδακτορικής Διατριβής του κυρίου **Πλάτωνα Πατλάκα** με θέμα:

«Εκτίμηση ακραίων τιμών περιβαλλοντικών παραμέτρων και ποσοτικοποίηση της αντίστοιχης αβεβαιότητας»

Η επταμελής Εξεταστική Επιτροπή απαρτίστηκε από τους κ.κ. : **Γεώργιο Κάλλο**, Ομότιμο Καθηγητή Τμήματος Φυσικής-ΕΚΠΑ (επιβλέπων), **Σαράντη Σοφιανό**, Αναπληρωτή Καθηγητή Τμήματος Φυσικής-ΕΚΠΑ, **Γεώργιο Γαλάνη**, Καθηγητή, Σχολή Ναυτικών Δοκίμων, **Έλενα Φλόκα**, Καθηγήτρια Τμήματος Φυσικής-ΕΚΠΑ, **Εμμανουήλ Αναγνώστου**, Καθηγητή, University of Connecticut, USA, **Παναγιώτη Νάστο**, Καθηγητή Τμήματος Γεωλογίας & Γεωπεριβάλλοντος, ΕΚΠΑ, και **Ιωάννη Πυθαρούλη**, Αναπληρωτή Καθηγητή Τμήματος Γεωλογίας, ΑΠΘ.

Τα παραπάνω μέλη της Εξεταστικής Επιτροπής, υποβάλαμε τον υποψήφιο διδάκτορα σε προφορική εξέταση μέσω τηλεδιάσκεψης (e-presence) την **Πέμπτη 3 Δεκεμβρίου 2020** και ώρα 16:00. Η διδακτορική διατριβή είχε έγκαιρα υποβληθεί στα μέλη της Εξεταστικής Επιτροπής.

Συμπεράναμε ομόφωνα από αυτήν την εξέταση ότι:

α) Το περιεχόμενο της διατριβής του κ. Πλάτωνα Πατλάκα είναι πρωτότυπο και προάγει την επιστήμη στο χώρο της Φυσικής της Ατμόσφαιρας.
β) Καλύπτει τις απαιτήσεις από την άποψη περιεχομένου, δομής, βιβλιογραφικής τεκμηρίωσης και πρωτοτυπίας.
γ) Έχει καταλήξει σε συμπεράσματα που έχουν δημοσιευθεί σε έγκυρα διεθνή επιστημονικά περιοδικά και σε διεθνή επιστημονικά συνέδρια με κρίση.
δ) Ο υποψήφιος παρουσίασε την υπό κρίση διατριβή του, ανέδειξε με σαφήνεια και επιστημονική πληρότητα τους στόχους, περιέγραψε τη μεθοδολογία και τεκμηρίωσε τη συνεισφορά και τα αποτελέσματα της διατριβής, απάντησε δε απόλυτα ικανοποιητικά και με πληρότητα στις ερωτήσεις που του υποβλήθηκαν από τα μέλη της Εξεταστικής Επιτροπής. Από την προφορική αυτή εξέταση απέδειξε ότι κατέχει σε βάθος την επιστημονική περιοχή του θέματος της διδακτορικής διατριβής.

Στη συνέχεια τα μέλη της Εξεταστικής Επιτροπής αποσύρθηκαν σε σύσκεψη.

Μετά από σχετική συζήτηση μεταξύ των μελών της, η Εξεταστική Επιτροπή έκρινε τη διατριβή του κ. Πλάτωνα Πατλάκα σημαντική και πρωτότυπη, με αξιόλογη συμβολή στην Επιστήμη, αποφάσισε να αποδεχθεί τη διδακτορική αυτή διατριβή και με ιδιαίτερη ικανοποίηση εισηγείται την **απονομή στον κύριο Πλάτωνα Πατλάκα του τίτλου του Διδάκτορα των Φυσικών Επιστημών του Εθνικού και Καποδιστριακού Πανεπιστημίου Αθηνών με βαθμό «Άριστα».**

Η επταμελής Εξεταστική Επιτροπή

GEORGIOS KALLOS
Digitally signed by GEORGIOS KALLOS
Date: 2020.12.04 13:30:09 +02'00'

Γεώργιος Κάλλος
Ομότιμος Καθηγητής

SARANTIS SOFIANOS
Digitally signed by SARANTIS SOFIANOS
Date: 2020.12.04 20:13:49 +02'00'

Σαράντης Σοφιανός
Αναπληρωτής Καθηγητής

Γεώργιος Γαλάνης
Καθηγητής

ELENA FLOKA
Digitally signed by ELENA FLOKA
Date: 2020.12.08 18:08:26 +02'00'

Έλενα Φλόκα
Καθηγήτρια

Εμμανουήλ Αναγνώστου
Καθηγητής

PANAGIOTIS NASTOS
Digitally signed by PANAGIOTIS NASTOS
DN: c=GR, l=Athens, o=National and Kapodistrian University of Athens, ou=Department of Geology and Geoenvironment, ou=Class A - Private Key created and stored in hardware CSP, sn=NASTOS, givenName=PANAGIOTIS, serialNumber=96285568454, cn=PANAGIOTIS NASTOS, email=nastos@geol.uoa.gr
Date: 2020.12.04 19:51:29 +02'00'

Παναγιώτης Νάστος
Καθηγητής

Ioannis Pytharoulis
Digitally signed by Ioannis Pytharoulis
Date: 2020.12.04 15:55:05 +02'00'

Ιωάννης Πυθαρούλης
Αναπληρωτής Καθηγητής

Acknowledgments

The writing of this PhD Thesis has been challenging in many aspects. Toward the successful completion several people throughout the years have played their own important role and thus I feel the need to acknowledge their contribution.

First and foremost, I would like to express my sincere appreciation to my advisor Professor George Kallos for giving me the opportunity to work on this particular field of research and for the continuous support during my PhD study and related research.

I would also like to thank the rest of my advising committee: Professors George Galanis and Sarantis Sofianos for their insightful comments. Furthermore, I would like to thank the examination committee for their suggestions, which improved the content of this Thesis and especially Professor Helena Flocas for her support.

I would like to thank all the past and present members of the Atmospheric Modeling and Weather Forecasting group of University of Athens for their collaboration. Especially I want to thank my friend Dimitris Diamantis who helped me in technical and data retrieval issues as without him the preparation of this Thesis would last more. Special thanks to my friend Christos Stahopoulos with whom I have been sharing ideas, problems and support and a successful collaboration regarding our common Scholarship. I would also like to thank my friends Dr Bartsotas and Dr Kalogeri for their comments and advice through my dissertation writing and Professor George Galanis for his support from the very beginning.

This work has been supported by the following projects: “MARINA Platform”, “MedSea”, “IRPWind” and the scholarship entitled “Study of Extreme Environmental Events with Numerical Weather Prediction Models and Stochastic Processes”.

For the evaluation of the dataset used in this Thesis I would like acknowledge the BMWi (Bundesministerium fuer Wirtschaft und Energie), the PTJ (Projekttraeger Juelich, project executing organization), the Crown Estate (Marine data exchange) and the European Marine Observation and Data Network (EMODnet) for the observations provided.

Finally, I would like to express my gratitude to my parents, my brothers and my wife, for their support and encouragement through all these years.

Athens, Platon Patlakas

October 2020

Στην Έλενα

Abstract

Extreme weather is a term generally used for describing weather patterns with a low frequency of occurrence, from the strong cyclonic presence to extreme sea state or extensive heat waves. Such events can be associated with severe social and economic consequences. Therefore, their analysis and in-depth understanding is more than critical not only for the pure scientific interest but also for its impact in the society and economy. In this context, the potential risk from extreme weather can be expressed through the concept of return periods. These are based on Extreme Value Theory and they are practically a statistical estimate for the recurrence of extreme phenomena based on limited data. The scope of this dissertation, therefore, is to quantify risk associated to atmospheric and wave parameters in terms of return periods employing different approaches, extreme value methodologies and tools.

The overall analysis is performed through three proposed approaches, focusing on grid-points (single locations), employing a characteristic value of an entire region and studying the phenomena themselves. Beginning with the first approach, wind speed probability distribution is examined focusing on both its higher and lower values alongside the duration of the event. The main purpose is to determine the probability of occurrence of extreme events by combining their intensity and duration, adopting the concept of return periods, and to quantify the associated uncertainty. Among the highlights in the study of low wind events was that the Maximum Likelihood method for the parameter-fitting was found to be suitable in the Intensity Given Duration approach. In the Duration Given Intensity approach the Rayleigh distribution outperformed other theoretical distributions in the application of AM methodology. Regarding the wind speed probability distribution upper tail, the intensity, duration and frequency of the events were found to be highly affected by the topography.

There are several sectors that apart from the traditional approaches that are applied in single locations they also require additional information on a regional basis. Therefore, in the present work, an effort towards the characterization of wide areas according to their extremes is made. To achieve this, several regional-scale summary measures are proposed. These summarize the performance of the region into a singular value and can help identify selected cases and support an overall risk assessment from particular scenarios. It was found that the spatially maximum values or high spatial quantiles should not be selected as extreme indices for large

areas as their performance deviates. Also, in general, the events are characterized by lower return periods in terms of significant wave height. Through this process a transition is made from the grid-oriented approach to one characterizing a region. However, an additional finding was that the extremity of a variable under study may have different impact depending on the weather pattern associated to.

This issue was addressed emphasizing also in weather phenomena with distinct characteristics through an object-oriented approach. Thus, the probability of occurrence of an event is estimated based on different environmental parameters, an element necessary in the modeling of damages. For the application of the proposed methodology, the Mediterranean cyclones with tropical characteristics were selected as a phenomenon to be investigated. The aim was to identify the areas at risk and estimate the extremity of such cyclones. The most affected regions were found to be mainly in the central and the western Mediterranean both regarding extreme winds and waves. In the estimation of their return periods, a similar behavior among the methods applied was met.

The employment of different meteorological parameters and methodologies to estimate the above can be valuable from a climatic point of view and help towards the implementation of more targeted measures to deal with potential damages. This can be of great assistance to many sectors and in particular to decision makers and stakeholders.

Περίληψη

Σε ένα περιβάλλον με συνεχώς μεταβαλλόμενες κλιματολογικές συνθήκες, είναι περισσότερο από απαραίτητο να κατανοηθούν και να αναλυθούν ακραία καιρικά φαινόμενα με κοινωνικές και οικονομικές επιπτώσεις. Η συχνότητα και η ένταση τέτοιων φαινομένων διαδραματίζουν κρίσιμο ρόλο που επηρεάζουν μεγάλο αριθμό κοινωνικοοικονομικών δραστηριοτήτων και διαφόρων τομέων όπως η πολιτική προστασία, οι κατασκευές, ο τουρισμός, οι υπεράκτιες και παράκτιες εφαρμογές, η ασφάλιση και αντασφάλιση, η ναυτιλία και οι μεταφορές. Είναι προφανές επομένως, το έντονο ενδιαφέρον από τους επιστήμονες λόγω της δυνατότητάς τους να προκαλέσουν εκτεταμένες ζημιές και επιπτώσεις στους ανθρώπους, στις υποδομές και στη φύση. Ακραία φαινόμενα θεωρούνται εκείνα που παρουσιάζουν μικρή συχνότητα εμφάνισης γενικότερα, από την έντονη κυκλωνική παρουσία μέχρι εκτεταμένους καύσωνες. Στόχος της παρούσας διατριβής, επομένως, είναι εκτίμηση της συχνότητας εμφάνισης ατμοσφαιρικών και κυματικών παραμέτρων και η πρόταση τριών διαφορετικών προσεγγίσεων, μέσα από σημεία του πλέγματος, μέσα από ένα συγκεντρωτικό μέτρο, χαρακτηριστικό μίας ολόκληρης περιοχής και μέσα από τα ίδια τα φαινόμενα προς μελέτη.

Σε αυτήν την κατεύθυνση, ο πιθανός κίνδυνος μπορεί να εκφραστεί μέσω της έννοιας των περιόδων επαναφοράς. Αυτές βασίζονται στην Θεωρία Ακραίων Τιμών και είναι ουσιαστικά μία στατιστική εκτίμηση για την επανεμφάνιση ακραίων φαινόμενων βασιζόμενη σε δεδομένα μικρότερου εύρους. Παρόλο που, υπάρχουν διαφορετικές προσεγγίσεις που προτείνονται για την εκτίμηση του μεγέθους και του διαστήματος επανεμφάνισης των γεγονότων, οι μέθοδοι Annual Maxima, Peaks Over Threshold και Method of Independent Storms ανταποκρίνονται σε μεγάλο βαθμό στις προκλήσεις όντας αρκετά αποδοτικές. Αυτές οι μέθοδοι χρησιμοποιούνται εκτενώς στην παρούσα διατριβή συμπληρώνοντας η μία την άλλη και συζητώντας τις πιθανές αδυναμίες που παρουσιάζει κάθε μία ξεχωριστά.

Τα αναγκαία δεδομένα στα οποία βασίστηκε η μελέτη προέρχονται από ατμοσφαιρικά και κυματικά μοντέλα μέσης κλίμακας. Πιο συγκεκριμένα αξιοποιήθηκε η βάση ατμοσφαιρικών και κυματικών δεδομένων που δημιουργήθηκε από την Ομάδα Ατμοσφαιρικών Μοντέλων και Πρόγνωσης του Καιρού (ΕΚΠΑ) στα πλαίσια του Ευρωπαϊκού Προγράμματος Marina (Marina Database). Η βάση δεδομένων βασίστηκε στις προσομοιώσεις του ατμοσφαιρικού μοντέλου Σκίρων και του κυματικού μοντέλου WAM. Επίσης το δεύτερο κομμάτι της διατριβής βασίστηκε

στο ατμοσφαιρικό μοντέλο RAMS/ICLAMS συζευγμένο με το κυματικό μοντέλο WAM. Για τις ανάγκες της έρευνας, αναπτύχθηκε αντίστοιχος αλγόριθμος για τον υπολογισμό των ριπών του ανέμου κοντά στην επιφάνεια του εδάφους. Η ικανότητα του αλγορίθμου για την εκτίμηση της συγκεκριμένης παραμέτρου αξιολογήθηκε με τη χρήση ειδικευμένων παρατηρήσεων.

Έχοντας σαν βάση τα παραπάνω, σε πρώτη φάση εξετάζεται η κατανομή της ταχύτητας ανέμου δίνοντας βάση τόσο στις υψηλές όσο και στις χαμηλές τιμές της σε συνδυασμό με την διάρκεια του φαινομένου. Η εφαρμογή γίνεται τόσο σε χαρακτηριστικά σημεία του πλέγματος των μοντέλων όσο και σε ολόκληρες περιοχές. Ο κύριος στόχος είναι να καθοριστεί η πιθανότητα εμφάνισης ακραίων γεγονότων συνδυάζοντας ένταση και διάρκεια μέσα από την χρήση περιόδων επαναφοράς και να ποσοτικοποιηθεί η σχετική αβεβαιότητα. Ξεκινώντας με τη διερεύνηση της διάρκειας και της συχνότητας των γεγονότων χαμηλής ταχύτητας ανέμου, ακολουθούνται δύο προσεγγίσεις, η μέθοδος "Intensity given duration" (IGD) και η "Duration given intensity" (DGI). Η πρώτη παρέχει περισσότερες πληροφορίες ταυτόχρονα καθώς τα αποτελέσματα εκφράζονται μέσω καμπυλών έντασης - διάρκειας - συχνότητας (intensity-duration-frequency - IDF). Ταυτόχρονα, οι ακραίες τιμές ταχύτητας ανέμου μελετώνται μέσω της πρώτης προσέγγισης. Δοκιμάζονται διαφορετικά εργαλεία και κατανομές πιθανότητας προκειμένου να ποσοτικοποιηθεί η αβεβαιότητα που χρησιμοποιείται από τη χρήση αυτών των μεθοδολογιών. Η σύγκλιση των τελικών αποτελεσμάτων συζητείται και δοκιμάζεται η εφαρμογή σε ευρύτερες περιοχές.

Για την εφαρμογή των DGI και IGD, χρησιμοποιείται η μέθοδος των ετήσιων μέγιστων / ελάχιστων (AM). Εξετάζεται η καταλληλόλητα δύο τεχνικών για την εκτίμηση των παραμέτρων της κατανομής, της μεθόδου method of moments (MoM) και της Maximum Likelihood (ML). Αυτές δοκιμάστηκαν παράλληλα με τη μέθοδο IGD με τα αποτελέσματα να στηρίζουν την εφαρμογή της ML. Στη συνέχεια, εξετάζεται η απόδοση της μεθοδολογίας DGI χρησιμοποιώντας τέσσερις διαφορετικές θεωρητικές κατανομές πιθανότητας στην εφαρμογή της μεθόδου AM αποκαλύπτοντας ότι:

• Κατά τη χρήση της κατανομής Gumbel και Weibull παρατηρείται συνεχής υποτίμηση.

• Η εφαρμογή της G.E.V. οδήγησε σε αποτέλεσμα χωρίς ιδιαίτερο μοτίβο και μεγάλες αποκλίσεις.

• Τα καλύτερα αποτελέσματα επιτεύχθηκαν χρησιμοποιώντας τη κατανομή Rayleigh.

Όσον αφορά τη μελέτη της ουράς της κατανομής του ανέμου, οι καμπύλες IDF βρέθηκαν να επηρεάζονται ιδιαίτερα από την τοπογραφία. Ειδικά στην ξηρά υπάρχει αυξημένη χωρική μεταβλητότητα των παραμέτρων της λογαριθμικής συνάρτησης που χρησιμοποιείται για την εφαρμογή. Ο ορισμός της διάρκειας σε μία ώρα οδηγεί στην κλασική προσέγγιση της AM με τα αποτελέσματα να δοκιμάζονται έναντι της POT. Τα παρεχόμενα αποτελέσματα αποτελούν εναλλακτικές πληροφορίες σχετικά με την κλιματολογία της περιοχής μελέτης. Τέτοιες πληροφορίες μπορούν να περιληφθούν σε τεχνικές εκτίμησης κινδύνου και μπορούν να εφαρμοστούν, μεταξύ άλλων, για ενεργειακές δραστηριότητες.

Η συντριπτική πλειονότητα αυτών των μελετών βασίζεται σε χρονοσειρές σε συγκεκριμένα σημεία. Προς μια καλύτερη κατανόηση και πιο στοχοθετημένο αποτέλεσμα, προτείνεται ένα περιφερειακό συνοπτικό μέτρο εκτίμησης περιόδων επαναφοράς ακραίων καιρικών φαινομένων. Αυτό επιτυγχάνεται αξιοποιώντας διαφορετικές ατμοσφαιρικές και ωκεάνιες παραμέτρους όπως η ταχύτητα του ανέμου και το σημαντικό ύψος κύματος. Επιπρόσθετα, μέσω του του προτεινόμενου συγκεντρωτικού (συνοπτικού) μέτρου στο οποίο βασίζεται η μελέτη, λαμβάνονται υπόψη αρκετά χαρακτηριστικά των φαινομένων, όπως η τοποθεσία, η διαδρομή, η χωρική έκταση και η διάρκεια. Οι περίοδοι επαναφοράς μπορούν να αποτελέσουν ένα πολύτιμο μέτρο για τη σύγκριση πραγματικών και παρελθόντων γεγονότων και για τον προσδιορισμό των επιπτώσεών τους. Μια τέτοια προσέγγιση είναι πολύτιμη σε ορισμένους από τους πιο επηρεαζόμενους και με μεγάλες πιθανές απώλειες κλάδους όπως οι κατασκευές και η αντασφάλιση. Τα συνοπτικά μέτρα μπορούν να βοηθήσουν στον προσδιορισμό επιλεγμένων περιπτώσεων και να υποστηρίξουν μια συνολική εκτίμηση κινδύνου από επιλεγμένα σενάρια. Θα πρέπει να σημειωθεί ότι η αβεβαιότητα που συνδέεται με τη δημιουργία του προτεινόμενου μέτρου και την αναπαράσταση των τοπικών χαρακτηριστικών πρέπει να διερευνηθεί περαιτέρω σε εφαρμογές.

Ακολουθώντας αυτήν την προσέγγιση, πραγματοποιείται ανάλυση των χαρακτηριστικών των ακραίων ανέμων και των κυμάτων των καταιγίδων στη Μεσόγειο Θάλασσα αξιοποιώντας τη βάση δεδομένων Marina. Η λεκάνη χωρίζεται σε πέντε περιοχές ανάλογα με τη συμπεριφορά των ακραίων τιμών για την ταχύτητα του ανέμου και το σημαντικό ύψος κύματος ξεχωριστά. Σε κάθε έναν από αυτούς τους τομείς εφαρμόζονται διάφοροι δείκτες. Η επαναληψιμότητα των

ακραίων τιμών τους συζητείται μέσω της εφαρμογής των μεθόδων AM και POT. Μέσα από αυτή τη διαδικασία γίνεται η μετάβαση από την προσέγγιση με πλέγμα σε μια με βάση ένα συνοπτικό μέτρο. Με αυτόν τον τρόπο γίνεται η εκτίμηση της πιθανότητας εμφάνισης ακραίων φαινομένων μέσα από τον άνεμο και το κύμα αναλόγως με την επίπτωση αυτών στις προκαθορισμένες ζώνες ενδιαφέροντος.

Σε κάθε περίπτωση, η εφαρμογή της θεωρίας ακραίων τιμών απαιτεί την ανεξαρτησία των δεδομένων προς επεξεργασία. Η ανεξαρτησία διασφαλίζεται μέσω διαφορετικών στατιστικών μεθοδολογιών. Ένας επιπλέον στόχος της συγκεκριμένης διατριβής είναι η προσπάθεια αυτό να επιτευχθεί μέσω μιας φυσικής διαδικασίας. Προς αυτήν την κατεύθυνση έμφαση δίνεται σε καιρικά φαινόμενα με ξεχωριστά χαρακτηριστικά και όχι σε χρονοσειρές. Σαν αποτέλεσμα, το πρόβλημα της ανεξαρτησίας διασφαλίζεται με φυσικό τρόπο, καθώς η έναρξη και η λήξη ενός καιρικού γεγονότος είναι ανιχνεύσιμες. Το πιο σημαντικό όμως είναι ότι το αποτέλεσμα προκύπτει μέσω μιας αντικειμενοστρεφούς προσέγγισης. Έτσι η πιθανότητα εμφάνισης ενός φαινομένου εκτιμάται με βάση διαφορετικές περιβαλλοντικές παραμέτρους, στοιχείο απαραίτητο στη μοντελοποίηση ζημιών. Για την εφαρμογή της προτεινόμενης μεθοδολογίας επιλέχθηκαν οι Μεσογειακοί κυκλώνες με τροπικά χαρακτηριστικά σαν φαινόμενο προς έρευνα.

Το τελευταίο κομμάτι της διατριβής στοχεύει, επομένως, στον καθορισμό των περιοχών που εκτίθενται σε κίνδυνο και στην ανάπτυξη ενός συνοπτικού μέτρου για την πιθανότητα εμφάνισης τέτοιων κυκλώνων στη Μεσόγειο. Το πρώτο εκφράζεται μέσω της χωρικής κατανομής των προσβεβλημένων περιοχών σε όλα τα στάδια της ζωής των φαινομένων, ενώ το δεύτερο χρησιμοποιεί ακραίους δείκτες που συνοψίζουν την ένταση της καταιγίδας και τη χωρική της έκταση.

Η σφοδρότητα ενός τέτοιου φαινομένου περιγράφεται χρησιμοποιώντας μόνο μία τιμή και τα αποτελέσματα αυτών των δεικτών μέσα από την έννοια των περιόδων επαναφοράς. Για την ανάλυση χρησιμοποιήθηκαν δεδομένα στο ισοβαρικό επίπεδο των 925 hPa και στην επιφάνεια του εδάφους (ταχύτητα ανέμου, ριπές ανέμου και σημαντικό ύψος κύματος). Για τις ανάγκες της μελέτης αξιοποιήθηκε το συζευγμένο σύστημα RAMS/ICLAMS – WAM σε υψηλή χωρική ανάλυση για τη προσομοίωση 52 περιπτωσιολογικών μελετών σε μια περίοδο 25 ετών.

Η χωρική έκταση των περιοχών που επηρεάζονται από τους κυκλώνες ποσοτικοποιείται χρησιμοποιώντας δύο διαφορετικές τιμές αναφοράς, μία για τον άνεμο στα 925 hPa και μία για

το σημαντικό ύψος κύματος. Όσον αφορά τον άνεμο, οι περιοχές που εκτίθενται σε κίνδυνο βρίσκονται κυρίως στην κεντρική και τη δυτική Μεσόγειο με ένα μέγιστο να παρατηρείται στον Κόλπο του Λέοντα. Οι περιοχές που επηρεάζονται από το κύμα είναι παρόμοιες με αυτές της ταχύτητας του ανέμου με υψηλότερες τιμές στην ανοιχτή θάλασσα.

Εκτός από την εύρεση των περιοχών που εκτίθενται σε κίνδυνο, οι περίοδοι επαναφοράς των κυκλώνων μελετώνται με όρους ανέμου και κυμάτων. Για το λόγο αυτό χρησιμοποιούνται τρεις ακραίοι δείκτες (μέση τιμή, 95ο ποσοστημόριο και μέγιστη τιμή) μαζί με δύο διαφορετικές προσεγγίσεις της Θεωρίας Ακραίων Τιμών (AM και MIS). Στον άνεμο οι διαφορές μεταξύ των δύο προσεγγίσεων είναι ασήμαντες και εντός των διαστημάτων εμπιστοσύνης. Η MIS παράγει μικρότερα διαστήματα εμπιστοσύνης σε σύγκριση με την AM λόγω του γεγονότος ότι λαμβάνει υπόψη περισσότερες τιμές. Επιπλέον, η AM χαρακτηρίζεται από ταχύτερη σύγκλιση, κάτι που βρέθηκε επίσης καθώς προχωράμε από τις μέσες τιμές προς τα μέγιστα. Η εκθετικότητα αυξάνεται και αυτό οφείλεται στο ότι η χρήση του μέσου όρου οδηγεί σε πιο ομαλά αποτελέσματα. Όσον αφορά το σημαντικό ύψος κύματος, η σύγκλιση είναι παρόμοια τόσο για την AM όσο και για τη MIS.

Η προτεινόμενη μεθοδολογία είναι πολύτιμη από κλιματολογικής απόψεως, καθώς μπορούν να αντληθούν πληροφορίες σχετικά με τις περιοχές που εκτίθενται σε Μεσογειακούς κυκλώνες με τροπικά χαρακτηριστικά καθώς και τις περιόδους επαναφοράς τους. Η χρήση διαφορετικών παραμέτρων για την εκτίμηση των παραπάνω μπορεί να βοηθήσει στην εφαρμογή στοχευμένων μέτρων.

Table of Contents

Glossary of terms

Abbreviation	Definition	Abbreviation	Definition
RP	Return Period	**IDF**	Intensity, Duration, Frequency
EVA	Extreme Value Analysis	**IGD**	Intensity Given Duration
EV	Extreme Value	**DGI**	Duration Given Intensity
AM	Annual Maxima	**CDF**	Cumulative Distribution Function
POT	Peaks Over Threshold	**PDF**	Probability Density Function
MIS	Method of Independent Storms	**NC diagnostics**	Threshold selection model
GEV	Generalized Extreme Value Distribution	**SST**	Sea Surface Temperature
GPD	Generalized Pareto Distribution	**Wg**	Wind gust
IID	Independent and Identically Distributed criterion.	**EI**	Era Interim dataset
ML	Maximum Likelihood	**Medicane**	Mediterranean Cyclone with tropical transition
MoM	Method of Moments	**R2**	Coefficient of Determination
Sw3q90	The cube root of the sum of variable, cubed above the domain climatological 90% quantile	**r**	Pearson correlation coefficient
Sfq95	The sum of the fraction of the variable divided by the grid-point climatological 95% quantile	**RMSE**	Root Mean Square Error
Sfq95q99	The sum of the fraction of the extreme value divided by the length of the distribution tail	**NSE**	Nash-Sutcliffe model efficiency coefficient
		$\tilde{x}$	Sample mean

1 Introduction

1.1 Motivation

In a global environment with constantly changing climatic conditions, it is more than necessary to understand and analyze extreme weather events with both social and economic implications. Such events have affected humanity since the beginning of its existence in several ways and vice versa. The frequency and intensity of such phenomena play a crucial role affecting a great number of socioeconomic activities and various sectors such as civil protection, constructions, tourism, offshore energy applications (both renewable and not), insurance and reinsurance, food security, shipping and transportation, natural inhabitant and cultural heritage security. At the same time, the investigation of the effects of climate change on extreme events (Intergovernmental Panel on Climate Change - IPCC, etc.) is an open subject of study.

An increase regarding disasters is observed during the last years (United Nations Office for Disaster Risk Reduction - UNISDR, 2013). Such disasters are associated to hazards that generate impacts on social, ecological, and/or technical systems. This increase can be partially attributed to the population growth. This has led to an expansion of the habitable areas into hazard-prone zones facing increased risk (McPhillips et al., 2018; Bouwer, 2010; Chang & Franczyk, 2008; IPCC, 2012). In global scales, more than 50% of the world's population now lives in cities, something associated with the rapid growth of megacities (United Nations Department of Economic and Social Affairs, 2014). At the same time according to Eurostat (https://ec.europa.eu/eurostat/statistics-explained/index.php/ Archive: Coastal_regions_-_population_statistics), in 2011, 40.8 % of the EU-27 population lived in coastal regions, which covered 40.0 % of EU-27 territory. These regions are exposed to direct impacts from coastal storms and sea-level rise (Neumann et al., 2015).

Moreover, offshore, near shore and coastal activities are flourishing. Beginning with energy, Europe has a leading role in the offshore wind energy production worldwide with more than 11GW of installed grid-connected capacity mostly located in the Northern Europe (North Sea, the Irish Sea and the Baltic Sea). The European commission has set targets to cover the 7.7% of the electrical demand of Europe from offshore wind energy until 2030. This corresponds to approximately 66GW of installed offshore wind power capacity (EWEA). Additionally there is a

high interest in natural gas exploration in blocks located mainly in central and western Mediterranean. Seismic studies and scans are continuously performed during the last years, drawing the attention of global markets. The EU is also home to the world's largest shipping fleet including approximately 23000 vessels (450 million gross tons) at the start of 2014. The EU shipping industry contributed €145 billion to EU GDP in 2012. Almost 90% of everything used within EU such as clothes, food, oil, gas, cars and electrical appliances arrives by ship, often travelling thousands of kilometres before reaching its destination. Additionally, the Suez Canal, an artificial sea-level waterway in Egypt, connects the Mediterranean Sea to the Red Sea through the Isthmus of Suez. The canal practically is part of a more direct, safe and economic route between the North Atlantic and northern Indian oceans via the Mediterranean and Red seas further increasing the marine traffic in the Mediterranean basin. Finally, local economies are highly affected by the interaction with the sea. Tourism has a key role in the economy of the Mediterranean region. The industry is highly affected by a variety of extreme events. Cyclonic activity may pose a threat to the infrastructure but tourism flourishes during the summer period where cyclones are rather rare. Heat waves, droughts and sea level rise on the other hand could cause significant problems. Apart from tourism, a considerable part of the coastal activities has to do with fisheries that are highly affected from extreme wind and waves and intense cyclonic activity.

It is obvious that extreme events are of interest to scientists and managers because of their potential to cause extensive damage and impacts on people, infrastructure, and nature. It is also clear that the term extreme events should be generally and widely used in non-frequent events that may have different characteristics, effects and implications. In the structural design of wind turbines, for example, probabilistic approaches of risk assessment are adopted in order to optimize the constructions in terms of profit and durability and avoid time and cost overruns that can compromise the economic viability of the project. To this end different approaches are used for estimating conditions that contribute to or form potential threats for wind turbines such as extreme wind speed. These approaches are focused in the study of the wind speed probability distribution main body and upper tail which is used both for the estimation of the energy potential and the extreme wind events that characterize the area under consideration. However, a better understanding of the environmental resources behavior requires additional information that can be used towards a more integrated research in the field of wind farm

siting. For this reason, apart from the mainstream approaches described shortly above, the concept of low wind speed event is introduced. The existence and the frequency of such events are positively correlated with the existence of high-pressure systems. These systems are characterized by light winds at the surface, cover large areas and can last up to several days depending on the local climate. This form of extreme conditions can cause several problems in electricity networks since several turbines are affected simultaneously. There are more than one definition of calm conditions related to light winds since different authors use various ways to define it and refer to a range of conditions. A characteristic example is the definition implied by Smith (1989). According to this, calm conditions are specified when the mean wind speed is comparable to or less than the root-mean-square turbulent horizontal velocity. It becomes obvious that for a more comprehensive analysis, the study of the intensity, duration and frequency of non-frequent (extreme) events focusing both in the upper and lower tail of wind speed probability distribution is necessary. The quantification of this risk and the associated uncertainty is one of the main questions and objectives addressed in the current thesis.

In this direction, risk can be expressed through the concept of return periods that is a statistical estimator for extreme phenomena reoccurrence based on data of shorter range. Although, there are different approaches proposed for the estimation of the magnitude and reoccurrence interval of events, Annual Maxima and Peaks Over Threshold methods (Coles, 2001) meet great acceptance for their effectiveness. Cook (1985) suggested that for Annual Maxima method, extreme wind speed is often well represented by Gumbel distribution. The same author (1982) used the dynamic pressure to achieve a faster convergence and better distribution fitting. A more recent study was held by Larsén et al. (2011) where an extreme wind speed atlas is created based on the principles of Generalized Extreme Value (GEV) theory and the Annual Maxima (AM) method. Peaks Over Threshold (POT) methodology is employed for studies based on smaller time series and the use of exponential is supported (Abild et al., 1992). As in the first case, the wind speed square is found to fit better, especially in areas with low wind speeds and in cases where the wind speed distribution is not skewed enough for an exponential quick convergence to the distribution tail (Caires και Sterl, 2004; Galambos, 1987; Cook, 1982). These extreme value analysis methods are also used to more targeted studies of extremes based on similar characteristics such as the year season or the direction (Cook, 1982). The necessity for bigger datasets that do not violate the principles of Extreme Value (EV) theory

led to the introduction of other methodologies such as the Method of Independent Storms (MIS) (Harris, 1998) and the EV theory based on the r largest annual events (Smith, 1986). At the same time different approaches are proposed by Lopatoukhin et al. (2000) for the estimation of extreme wind wave heights such us the Initial Distribution Method (IDM). Breivik et al. (2014) studied wind and wave extremes using large ensembles and computed a non-parametric Direct Return Estimate (DRE) from the tail of the fitted distribution function. This was used for the estimation of the 100-year marine wind speed over the Globe.

Most of such studies focus on gridded time series. Towards a better understanding and more targeted outcome a regional summary measure of the storminess of severe windstorms expressed in terms of return periods (RP) is proposed. The RP of a storm can be addressed in this way through different atmospheric and ocean parameters such as wind speed and significant wave height. Additionally, through the scalar measure several characteristics of the meteorological storminess are also taken into account such as the location, path, spatial extent and the duration. The RP of storms can be a valuable measure in comparing actual and past events and in determining their impact. Such an approach would be valuable in some of the most affected and with a great loss potential industries like constructions and reinsurance (MunichRe, 2000; SwissRe, 2000). The summary measures can help to identify the case studies selected and support an overall risk assessment from selected scenarios. So, the demand for regional-scale RP estimation derives primarily from the straightforward use in practical applications. It should be noted that the uncertainties associated to the measures creation and the misrepresentativity of local features need to be further investigated in applications.

Studies documenting the extreme wind climate of Europe are based on different methodologies and input data. Many of them are focused on the characterization of the wind climate in local and regional scales and use observations (Dukes and Palutikof, 1995; Kristensen et al., 1999; Sacre, 2002; Barring and von Storch, 2004; Alexander et al., 2005; Smits et al., 2005; Walter et al., 2006). Other studies, in larger scales are using a variety of datasets from in situ and satellite observations to reanalysis datasets (Lamb, 1991; Schinke, 1993; Kaas et al., 1996; Alexandersson et al., 1998; Schmith et al., 1998; Miller, 2003; Yan et al., 2002; 2006; Monahan, 2006). Della-Marta et al. (2009) has used reanalysis products for the estimation of a summary measure describing the storminess of winter storms attempting to assign RPs to known historical storm events on a European scale. His approach did not pay special attention to long-

term non-stationarities while the measure used covered the whole European continent. His results include extreme wind climatologies and the RPs of prominent high-impact events and have been an inspiration for a more comprehensive analysis.

Towards this way an analysis of both the extreme wind and wave characteristics of the European continent separated in sub-regions with similar extreme characteristics is interesting. A first categorization could be in three major subsectors with distinct characteristics, the continental Europe, the offshore areas in northern Europe (North Atlantic, North Sea etc) and the Mediterranean basin. A second categorization for each of these sub-regions based on statistical tools can define even smaller areas with similar extreme behavior. A sub-regional summary measure can be applied and the return periods of windstorms in terms of wind and wave parameters can be defined. Moving from the classical gridded approach to one based on summary measures and extreme indices is also under investigation within this thesis.

In any case, the application of the extreme value theory requires the independency of the data to be processed. The independency is ensured via different statistical methodologies. The question is, therefore, if this could also be achieved through a physical process. To do so, a quite different approach and point of view are required. Towards this way, the focus should be given in weather events with distinct characteristics and not in timeseries, solving several issues at once. Beginning with the independency problem, it will be ensured from a physical perspective since there are ways to define the beginning and the end of a weather event such as the generation and dissipation of a cyclone or the start and the end of a local wind (e.g. Etesians - Dafka et al., 2018). Most important, the outcome will be derived through an object-oriented approach, meaning that the extremity of an event can be approached in terms of multiple environmental parameters simultaneously, essential in damage modeling. A characteristic example is that strong winds in dry weather do not have the same impact with strong winds accompanied by heavy precipitation. In the second case the precipitation affects the soil making it easier for strong winds to cause tree falls and electricity outages. Last but not least, an event-oriented approach would require less computer power needs. Thus, more focus could be given on resolution and expensive microphysical schemes in the model simulations of the cases under study. These questions pose an additional motivation for the present thesis focusing on the intensity, duration and frequency of the events and moving gradually from a gridded to a summary measure and finally an event-oriented approach.

1.2 Objectives

The main objective of this study is the quantification of the extremity and the associated uncertainty of different atmospheric parameters.

The particular objectives of this Thesis can be outlined as follows:

- Study the intensity, duration and frequency of non-frequent weather events through different atmospheric and wave parameters.
- Explore the cons and pros of numerous approaches and suggest new ones.
- Quantify the impact of the proposed techniques and identify the potential problems in applications.

This study is aiming at the investigation of both the upper and lower tail of the wind speed probability distribution in a spatial (gridded) approach. The selected study areas are the Mediterranean Basin and the North Sea. An alternative process based on a summary measure through the categorization of the Mediterranean Basin in sub-regions is proposed. Moreover, a novel object (event) oriented approach is suggested and tested through its application in Mediterranean cyclones taking at the same time more atmospheric and ocean parameters into consideration.

1.3 Thesis outline

This Thesis is organized in seven chapters.

Chapter 1 contains a summary regarding the description and the effects of extreme weather events and an insight on the literature and issues related to them. It is a synopsis of the questions led to the findings presented in this Thesis.

Chapter 2 provides the theoretical background related to the basic characteristics of the wind and wave parameters and their extreme nature.

Chapter 3 includes the general methodology adopted in the chapters to follow. More specifically, it provides the basic principles of the Extreme Value Theory alongside the statistical tools suggested.

Chapter 4 discusses the main findings from the wind speed, intensity duration and frequency analysis through a point-to-point (gridded) approach.

Chapter 5 describes the findings of a sub-regional (summary -measure) approach in the study of extremes in the Mediterranean Sea.

Chapter 6 is about the estimation of the extremity of weather events in the Mediterranean Basin from an object-oriented approach. The methodology is focusing in Tropical Like Cyclones (Medicanes).

Chapter 7 is a summary of the main findings and suggestions for future work.

2 General background

2.1 Scales of Atmospheric Motions

As described in the previous chapter atmospheric motions are generally generated by geographic variations in heating of the earth surface by meridional gradients of insolation and other factors such as the earth's rotation, land-sea coverage, albedo variations and others. The heating variations on the atmosphere create the atmospheric motions which act in a way to offset the variations themselves. The total energy balance of the atmospheric system is preserved. It can be expressed through the variance of the atmospheric variables, distributed among different timescales (Holton, 2004). Within the system, energy is transferred from large scale eddies to smaller scales, dissipating into heat through viscosity (molecular scale process). This procedure called the energy cascade (Figure 2-1).

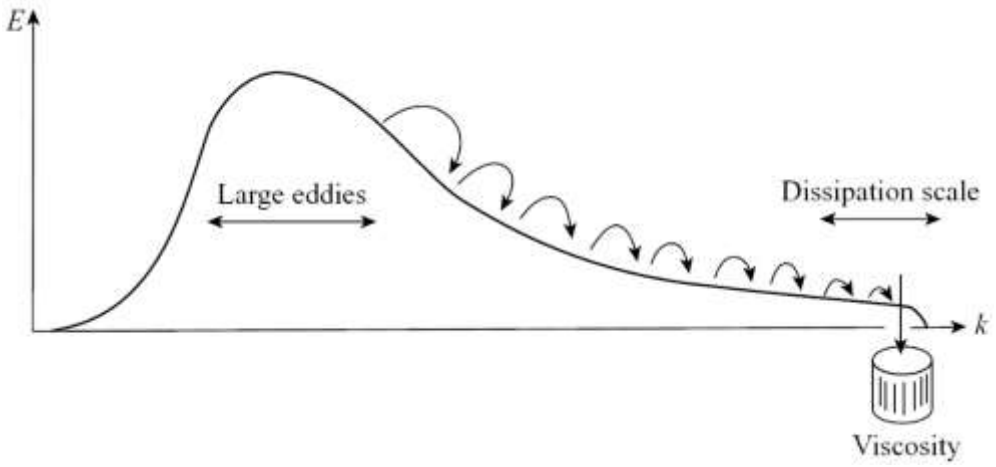

Figure 2-1: The energy cascade (Davidson, 2013).

In such a variance spectrum the area under the curve between two frequencies or wavelengths represents the energy contributed by this range of frequencies or wavelengths to the total energy of the system. There are two types of energy spectra. The first is spatial oriented giving the energy distribution over different wavelengths. The second is temporal, providing the distribution of energy over periods or frequencies. These two points of view are

correlated and the spectrum can be expressed both in frequencies and wavelengths (Fiedler and Panofsky, 1970).

Considering wind, the relative spectral intensity over frequencies describes the kinetic energy on a certain frequency. The Power Spectral Density (PSD) is one of a variety of tools used to analyze wind speed variability. In figure 2-2 there is a characteristic example of such spectra. The left peak corresponds to four days and is associated to migratory pressure systems of a synoptic weather map scale. The second peak as we move to higher frequencies refers to the diurnal cycle. The last one occurs at a period of one minute and is associated to mechanical and/or thermodynamical type of turbulence. The frequencies between the last two peaks that correspond to time periods between ten minutes and two hours is characterized by low variation. This area is called the spectral gap. Van der Hoven (1957) showed some relation between the spectral gap shape and surface roughness under some circumstances.

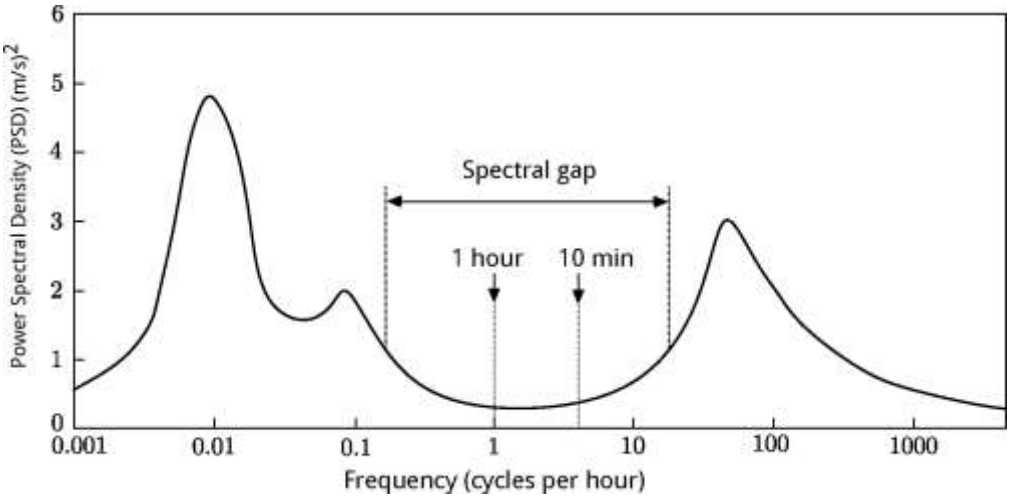

Figure 2-2: Horizontal wind Power Spectral Density (*Van der Hoven, 1957*)

From an atmospheric sciences perspective based on the duration and the spatial coverage, these motions can be divided in six categories: Molecular, Turbulent, Convective, Meso-scale, Synoptic-scale, Large or Planetary (Table 2-1).

Table 2-1: Scales of Atmospheric Motion

	Scale	Length Scale (m)	Time Scale (sec)	Systems/Importance
Coriolis not important	Molecular	10^{-7} - 10^{-2}	10^{-1}	(Neglected)
	Turbulent	10^{-2} – 10^{3}	10^{1}	Sea surface interaction, wind stress & wave formation
	Convective	10^{3} – 10^{4}	10^{3}	Thunderstorm cells
Coriolis important	Meso-scale	10^{4} - 10^{5}	10^{4}	Sea-breeze circulations, coastal fronts
	Synoptic-scale	10^{5} - 10^{6}	10^{5}	Major storms
	Large	> 10^{6}	10^{6}	Thermodynamic factors important, seasonal circulations

The **molecular scale** circulations are of the magnitude of a few seconds. The energy dissipation is performed in these scales and the importance in the atmosphere is considered negligible.

Turbulent circulations last under a few minutes and have a size smaller than 1 km. Processes like heat transfer and air-land-ocean interaction or wind gusts fall within this category.

Convective scales have a magnitude of around one km and are associated with processes like thunderstorm cells ant local convective activity.

Meso-scale systems range from a few to about a hundred kilometers in horizontal distance. As a rule of thumb, the vertical velocity often equals or exceeds horizontal velocities. Typical circulations are major storms, tornadoes, and small tropical storms.

Synoptic scale circulations range from several days to weeks. Their sizes reach up to 5000 km. Synoptic scale features are the high pressure systems like the Siberian anticyclone, low pressure systems like extra-tropical and mid-latitude cyclones or hurricanes and frontal activity.

Regarding the **Large (Planetary)** scale circulation the size extends to tens of thousands km and can last up to several months or years such in the monsoonal activity or the El Nino.

2.2 Atmospheric Boundary Layer

The part of the atmosphere influenced directly by the roughness and energy balance of the Earth's surface is known as the Atmospheric Boundary Layer (ABL). It has an important impact on the atmospheric behavior and its proper representation is crucial in the success of climate modeling and numerical weather prediction (Hu, 2015). It extends from about 100m above ground to up to more than 1-2km (and even higher in desert areas) and responds to surface forcing within a timescale of about an hour or less. Its characteristics are highly affected by the nature of the underlying surface (Mason & Thomson, 2015) and more specifically by different mechanical and thermal effects (Stull 2012).

The mechanical part is associated to the friction between the wind and the ground. The winds near the surface are affected most from the friction forces leading to a deceleration. This influence gradually decreases with height resulting in a vertical wind shear and thus, mechanical turbulence. This turbulence and the drag between the atmosphere and the surface is the main mechanism by which the energy in the large-scale motion is dissipated. The energy source for the thermal effects to take place is the sun. The solar radiation and the interaction with the ground result in spatiotemporal variability in the surface temperature. This variability determines the presence and strength of convective turbulence affecting the wind speed profile within the layer resulting in three stability states inside the ABL, the unstable, the stable and the neutral conditions (Figure 2-3).

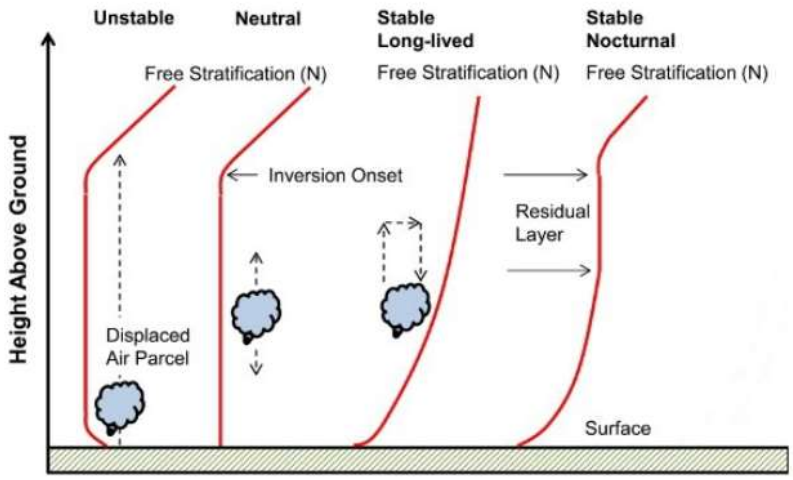

Figure 2-3: Atmospheric planetary boundary layer schematic showing stable, neutral, and unstable conditions (Aliabadi et al., 2016).

Unstable conditions prevail when turbulence is driven mainly through convection. The general pattern for this is the existence of dense air masses above warmer and/or more humid air masses. This arises from the circumstance where the land/sea surface is hotter than the air overhead. The warm air is rising and strong vertical mixing is observed. Over land the ABL becomes unstable approximately when the sun rises and the land surface is radiatively heated. The exact opposite is happening offshore due to the great heat capacity of the water and the smaller variability in Sea Surface Temperature (SST). In such cases, during the night the overlaying air masses lose heat due to radiative transfer and due to the higher SST the temperature of the near-surface air masses is higher as compared to the layers above leading to instability and mixing. This instability and the humid advecting air can result in convection systems.

The stable ABL is generally generated by surface radiative cooling or advection of warm air over a cooler surface. A characteristic example is through the air land interaction during the night. The bottom portion of the layer is cooled by its contact with the ground resulting in increased thermal stability. Similar conditions can be found also when warm air masses move over the cold ocean. This can lead to the formation of fog or low stratus. Stable boundary layer is also associated with the appearance of internal gravity waves, drainage flows, inertial oscillations, and nocturnal jets. The last is met when winds in higher layers may accelerate to

super-geostrophic speeds accompanied with sporadic turbulence near surface. The stable boundary layer top is poorly defined as it smoothly blends into the atmosphere above it, considered however rather shallow (20-500m).

Turbulence in neutral conditions is of mechanical origin depending mainly in the wind shear vertical distribution and ground friction. Such conditions are rarely encountered in the atmosphere. However, during overcast skies and strong surface geostrophic winds, the atmospheric boundary layer may be considered near-neutral.

2.2.1 Air-sea interaction

The two most important systems in terms of dynamics of weather and climate are the atmosphere and the ocean. Thus the interface between them is the means for energy exchange. This role is granted to ocean waves. Taking all the above into consideration a realistic description of the physical processes at this interface is essential for a reliable determination of the air-sea fluxes of momentum and the atmospheric structure in general. The energy transfers from the atmosphere to the ocean through the horizontal forces from the surface winds to the wave field (Stull 2012, Bouws et al. 1998, Komen et al., 1996). This is called wind stress and given by:

$$\tau = \rho_\alpha C_D U_{10}^2 \qquad (2\text{-}1)$$

Where ρ_α is the air density, C_D is the drag coefficient and U_{10} is the wind speed at 10m.

The friction velocity is defined by the effective interface shear stress as $u^* = \sqrt{\tau/\rho_\alpha}$ and serves as the velocity scale of the turbulent flow in the entire surface layer. Through the two equations above it is concluded that $C_D = \frac{u_*^2}{u_{10}^2}$. The drag is a function of wind speed and surface stability. In unstable conditions the drag has been found to increase leading to a simultaneous increase in stress. Based on the similarity theory of Monin and Obukhov, the wind speed profile within the surface layer takes the following form (Liu et al., 1979; Stull, 1988):

$$|U(z)| = \frac{u^*}{\kappa}\left(ln\frac{z}{z_0} - \psi(\zeta)\right) \qquad (2\text{-}2)$$

Where κ is the Von Karman constant, z_0 is the roughness length, z the height and and ψ(ζ) is a stability function based on the Businger–Dyer model (Liu et al., 1979).

Under neutral conditions, ψ(ζ)= 0 and wind speed takes the shape of the well-known logarithmic profile. Under stable conditions ψ(ζ) is positive while the profile contains more shear near the surface compare to the neutral case. A negative stability function is associated with unstable conditions and less shear. It should be noted that similar formulations exist for air temperature and humidity as well. Considering all these, the drag coefficient and friction velocity under neutral and unstable conditions can be expressed as follows:

Neutral conditions:

$$C_D = \frac{\kappa^2}{ln\left(\frac{z}{z_0}\right)^2} \qquad (2\text{-}3)$$

$$u_* = \frac{\kappa\, u_{10}}{ln\left(\frac{z}{z_0}\right)} \qquad (2\text{-}4)$$

Unstable conditions:

Here the thermal effects dominate. Thus for the estimation of the drag coefficient they are also taken into consideration through ψ(ζ).

$$C_D = \frac{\kappa^2}{\left(ln\left(\frac{z}{z_0}\right) - \psi(\zeta)\right)^2} \qquad (2\text{-}5)$$

$$u_* = \frac{\kappa\, u_{10}}{ln\left(\frac{z}{z_0}\right) - \psi(\zeta)} \qquad (2\text{-}6)$$

2.2.2 Winds at the lower part of the atmosphere

The surface layer is the layer of the atmosphere most affected by the interaction with the surface. It is characterized by turbulence, large gradients of tangential velocity and large concentration gradients of any substances (temperature, moisture, etc) transported to or from the interface. It is the lowest part of the atmospheric boundary layer (typically the bottom 10% where the log wind profile is valid) and varies in heights between 2 and 200 m. The so-called

constant flux layer is quite important since it is the layer where extreme phenomena directly affect the bio system.

The winds near the surface are highly affected by the atmospheric stability. Taking the equations of Chapter 2.2.1 into consideration, wind speed at a height z can be calculated through the logarithmic law (Stull 2012). Considering that ψ(ζ) is depending on the height (z) and the Monin Obukhov length (L), wind speed (U) is given by:

$$U(z) = \frac{u_*}{\kappa}\left[ln\frac{z}{z_0}\psi\left(\frac{z}{L}\right)\right] \qquad (2\text{-}7)$$

The profile and the intensity of wind speed inside the surface layer is affected by the thermal and mechanical surface effects. These are correlated to the climatic and microclimatic conditions of the area of interest. In this thesis, all stability layers are quite important. In stable conditions, for example, light winds are favorable, something investigated in the present study. At the same time however, rapid changes can take place with sporadic turbulence and gusts near the surface. On the other hand, neutral or near-neutral conditions are associated to strong winds blow over the area. In unstable conditions despite that the thermal effects prevail; the presence of surface gusts is favorable causing damages.

Over the ocean everything is somehow different. In contrast with land where winds exactly above the surface are zero, in a moving water surface this cannot be always assumed. The sea is a fluid and as all fluids it can move in three dimensions. As a result the wind forcing can affect the water movement in all of them. The most obvious, however, is the generation of waves which subsequently affect the wind profile structure. So, the description of the momentum exchange between the atmosphere and the ocean is multiparametric and up to today investigated. Generally, the roughness over the sea is smaller compared to over the land meaning that offshore winds tend to be closer to the geostrophic flow and generally characterized by higher values. Apparently, the wind shear over the sea is also smaller than that over land. Exceptions where the effects of roughness on the near surface turbulence tend to be comparable to that over land are quite few (Petersen et al., 1998). Marine winds are affected by the air-sea processes such as mechanical and convective turbulence as energy is transferred and converted into waves.

2.3 Wind and wave characteristics

Wind speed affects aviation and maritime operations, construction projects, and energy systems while its extremes may affect in various ways the socioeconomic activities and everyday life. Low wind speeds can be associated to the slow dispersion of pollutants or low productivity of wind energy applications. On the other hand, extreme wind speed can cause several problems in structures and the infrastructure in general. It is often used for the categorization of extreme weather events. One of the most characteristic categorizations is performed through the Saffir–Simpson hurricane wind scale (SSHWS – Table 2-2). This is used for the classification of hurricanes that exceed the intensities of tropical depressions and tropical storms. These are separated into five categories distinguished by the intensities of their sustained winds.

Table 2-2: The Saffir–Simpson hurricane wind scale (https://www.nhc.noaa.gov/aboutsshws.php).

Category	Sustained Winds	Types of Damage Due to Hurricane Winds
1	33–42 m/s 74-95 mph 64-82 kt 119-153 km/h	**Very dangerous winds will produce some damage:** Well-constructed frame homes could have damage to roof, shingles, vinyl siding and gutters. Large branches of trees will snap and shallowly rooted trees may be toppled. Extensive damage to power lines and poles likely will result in power outages that could last a few to several days.
2	43–49 m/s 96-110 mph 83-95 kt 154-177 km/h	**Extremely dangerous winds will cause extensive damage:** Well-constructed frame homes could sustain major roof and siding damage. Many shallowly rooted trees will be snapped or uprooted and block numerous roads. Near-total power loss is expected with outages that could last from several days to weeks.
3 (major)	50–58 m/s 111-129 mph 96-112 kt 178-208 km/h	**Devastating damage will occur:** Well-built framed homes may incur major damage or removal of roof decking and gable ends. Many trees will be snapped or uprooted, blocking numerous roads. Electricity and water will be unavailable for several days to weeks after the storm passes.
4 (major)	58–70 m/s 130-156 mph 113-136 kt 209-251 km/h	**Catastrophic damage will occur:** Well-built framed homes can sustain severe damage with loss of most of the roof structure and/or some exterior walls. Most trees will be snapped or uprooted and power poles downed. Fallen trees and power poles will isolate residential areas. Power outages will last weeks to possibly months. Most of the area will be uninhabitable for weeks or months.
5 (major)	≥ 70 m/s ≥ 157 mph ≥ 137 kt ≥ 252 km/h	**Catastrophic damage will occur:** A high percentage of framed homes will be destroyed, with total roof failure and wall collapse. Fallen trees and power poles will isolate residential areas. Power outages will last for weeks to possibly months. Most of the area will be uninhabitable for weeks or months.

The Saffir-Simpson Hurricane Wind Scale is based on a hurricane's sustained wind speed estimating empirically potential property damage. The same classification is also used to define tropical depressions (≤17 m/s) and tropical storms (18-32 m/s). It should be noted that hurricanes reaching Category 3 and higher are considered capable for significant loss of life and damage. Similar categorizations can be found in different parts of the world such North Pacific.

Regarding ocean waves, they are as well characterized by various spatiotemporal timescales ranging from long waves such as the tides caused by the gravitational force of the Sun and Moon to small scale ones generated by the forcing of the wind on the sea surface. The last, also known as wind waves have the highest contribution to the energy spectrum of the wave energy distribution with periods between 0.5 and 30 sec.

Wind generated waves form as a result of wind stress. Additional forces are the gravitational and the water buoyancy. They are directly affected by the wind intensity and duration but also by the fetch extent due to the nature of the ocean surface. The waves directly affected by wind in a local scale have different characteristics from those generated locally and traveled away from the perturbation (eg. storm). The first are considered irregular and short crested while the second, also known as swells, presume a regular and long-crested form and a higher phase speed. These two wave forms may coexist in local scales forming a wave field with waves of different amplitudes, periods and directions.

The sea state is considered to be the general conditions of the ocean's free surface with respect to wind waves and swell at a certain location and moment. The sea state can be characterized by statistics including the wave height, period, and power spectrum. A proposed definition regarding the sea stated is proposed by H.P. Douglas (Table 2-3). The Douglas sea scale, also called the "international sea and swell scale" is used for the estimation the roughness of the sea for navigation.

Table 2-3: Douglas state of the sea (wind sea) scale (http://www.eurometeo.com/english/read/doc_douglas).

Degree	Height (m)	Description
0	No wave	Calm (Glassy)
1	0–0.10	Calm (rippled)
2	0.10–0.50	Smooth
3	0.50–1.25	Slight
4	1.25–2.50	Moderate
5	2.50–4.00	Rough
6	4.00–6.00	Very rough
7	6.00–9.00	High
8	9.00–14.00	Very high
9	14.00+	Phenomenal

The scale has also a second categorization for the description of the presence of swell in the area of interest (Table 2-4).

Table 2-4: Swell classification (http://www.eurometeo.com/english/read/doc_douglas).

Degrees	Description
0	No swell
1	Very Low (short or average and low wave)
2	Low (long and low wave)
3	Light (short and moderate wave)
4	Moderate (average and moderate wave)
5	Moderate rough (long and moderate wave)
6	Rough (short and high wave)
7	High (average and high wave)
8	Very high (long and high wave)
9	Confused (wavelength and height indefinable)

There is also a categorization of the weather state in general that depends on sea state conditions but is also associated with wind speed. The so-called Beaufort scale (Table 2-5) is neither an exact nor an objective scale. It was based on visual and subjective observations from ships. The corresponding wind speed values were determined at later time.

Table 2-5: The Beaufort scale (https://www.spc.noaa.gov/faq/tornado/beaufort.html)

Force	Wind speed (m/s)	Wave height (m)	WMO Classification	Wind effects on the water	Wind effects on land
0	< 0.5	0	Calm	Sea surface smooth and mirror-like	Calm, smoke rises vertically
1	0.5–1.5	0 – 0.3	Light Air	Scaly ripples, no foam crests	Smoke drift indicates wind direction, still wind vanes
2	1.6–3.3	0.3–0.6	Light Breeze	Small wavelets, crests glassy, no breaking	Wind felt on face, leaves rustle, vanes begin to move
3	3.4–5.5	0.6–1.2	Gentle Breeze	Large wavelets, crests begin to break, scattered whitecaps	Leaves and small twigs constantly moving, light flags extended
4	5.5–7.9	1–2	Moderate Breeze	Small waves, becoming longer, numerous whitecaps	Dust, leaves, and loose paper lifted, small tree branches move
5	8–10.7	2–3	Fresh Breeze	Moderate waves taking longer form, many whitecaps, some spray	Small trees in leaf begin to sway
6	10.8–13.8	3–4	Strong Breeze	Larger waves, whitecaps common, more spray	Larger tree branches moving, whistling in wires
7	13.9–17.1	4–5.5	Near Gale	Sea heaps up, white foam streaks off breakers	Whole trees moving, resistance felt walking against wind
8	17.2–20.7	5.5–7.5	Gale	Moderately high waves of greater length, edges of crests begin to break into spindrift, foam blown in streaks	Twigs breaking off trees, generally impedes progress
9	20.8–24.4	7–10	Strong Gale	High waves, sea begins to roll, dense streaks of foam, spray may reduce visibility	Slight structural damage occurs, slate blows off roofs
10	24.5–28.4	9–12.5	Storm	Very high waves with overhanging crests, sea white with densely blown foam, heavy rolling, lowered visibility	Seldom experienced on land, trees broken or uprooted, "considerable structural damage"
11	28.5–32.6	11.5–16	Violent Storm	Exceptionally high waves, foam patches cover sea, visibility more reduced	
12	≥ 32.7	≥ 14	Hurricane	Air filled with foam, sea completely white with driving spray, visibility greatly reduced	

Despite its subjectivity, the scale is widely used in many countries such as the Netherlands, Germany, Greece and Malta.

Beginning with wind, several characteristics are addressed in the lines to follow from the theoretical distribution function better describing it to its extremes. The same layout is used also for the wave characteristics.

2.3.1 Frequency distribution of wind speed

Wind speed frequency distribution can provide information regarding the behavior of wind speed. Its description can be essential among others for the design of buildings and structures. Current methods are based on statistical analysis in particular locations showing different populations depending on the regional and local characteristics. A way to study the wind speed frequency at a particular location is through the fit of a probability distribution function to the observed data. Although different probability distributions have been proposed and tested, it is accepted that the Weibull distribution gives a good representation of hourly mean wind speeds over a year.

The frequency distribution can be analyzed through a number of statistical indices and measures. Mean value (μ), which is used as an indicator for the wind behaviour of the study area can be calculated as

$$\mu = \frac{1}{N}\sum_{i=1}^{N} x(i) \qquad (2\text{-}8)$$

where *x* denotes the parameter under study and *N* the size of the sample. For a more comprehensive analysis, a fundamental task would be the description of wind speed distribution characteristics using the skewness and the kurtosis of the variable under study. Skewness (g_1) defines the lack of symmetry and consequently the tendency of the value to get greater or smaller values (skewed to the right or left respectively). At the same time, kurtosis (g_2) is a measure of the peakedness and the tail weight of the distribution. The combination of these statistical indexes provides useful information about the occurrence and the potential impact of non-frequent values in the wind park operation. Skewness and Kurtosis are calculated, based on the sample mean (μ) and standard deviation (σ), using the equations

$$g_1 = \frac{\frac{1}{N}\sum_{i=1}^{N}(x(i)-\mu)^3}{\sigma^3} \qquad (2\text{-}9)$$

and

$$g_2 = \frac{\frac{1}{N}\sum_{i=1}^{N}(x(i)-\mu)^4}{\sigma^4} - 3 \qquad (2\text{-}10)$$

At the same time, the wind speed variability can be critical for various applications. For this reason, a fourth statistical parameter, namely the index of variation is introduced to depict its temporal variation. Index of variation is equal to the standard deviation:

$$\sigma = \sqrt{1/N \sum_{\iota=1}^{N} (x(\iota) - \mu)^2)} \qquad (2\text{-}11)$$

This is divided by the sample mean to obtain a dimensionless outcome.

2.3.2 Wind averaging and variability

The wind speed as can vary in throughout different temporal and spatial scales from micro-turbulence to synoptic level and even higher. The variability of each scale is correlated to the time averaging performed for the estimation of mean wind speed. For the typical 10-min averaging, variability exceeding the timeframe of 10 minutes can be studied beginning from the diurnal and reaching multiannual cycles.

Wind speed averaging in general is preformed historically, with a variety of averaging times ranging from three seconds to an hour depending on the use of the outcome. The conversion of mean wind speed to among different averaging times can be done through the use of the Durst Curve (Figure 2-4). The last defines the relation between probable maximum wind speed averaged over t seconds (V_t) and mean wind speed over one hour (V_{3600}).

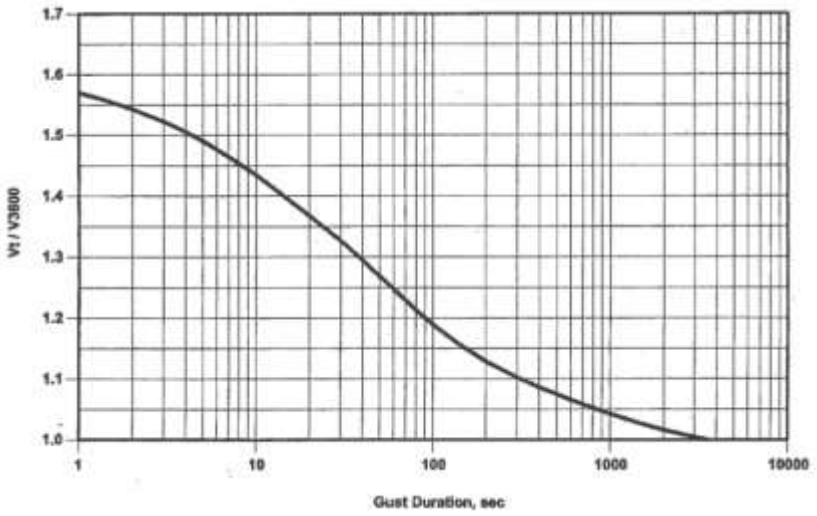

Figure 2-4: Durst curve.

A typical selection is a 10-min average at a 10m height. 30-min and hourly averages are also widely used as well as wind speed in different heights depending on the application. These time periods fall within the spectral gap mentioned earlier. This is quite helpful as in this way the effects of turbulence are excluded.

As mentioned earlier, one critical parameter for this type of analysis is the presence and magnitude of surface wind gusts, which is defined as the maximum observed wind speed over a period of time (World Meteorological Organization, 1987; Friedrichs et al., 2009). More than one gust definitions are proposed in the literature for wind gusts. For example, Extreme Operating Gust (EOG) and Extreme Coherent Gust (ECG) are described within the IEC 61400 standard for wind energy (TC88 WG1. IEC 61400-1, 2005). Moreover, several parameterizations and formulas are applied for their description and estimation.

2.3.3 Low wind speed conditions

The existence and the frequency of low wind speed events are positively correlated with the existence of high-pressure systems. These systems are characterized by light winds at the surface, cover large areas and can last up to several days depending on the local climate. This

form of extreme conditions can cause several problems in electricity networks since several wind turbines are affected simultaneously leading to a low productivity for long periods. At the same time it can lead to extreme atmospheric pollution events since the dispersion of pollutants is slower. Low wind speed events have been studied alongside their persistence at measurement locations in the UK for the estimation of plume dispersion following accidental releases of airborne pollutants (Deaves and Lines, 1998; 1997). These studies resulted that completely calm conditions are rather rare. Low wind speeds at the surface that did not exceed the 2.4 m/s had a frequency of occurrence of around 20-30%.

Actually, there are more than one definitions of calm conditions related to light winds. It should be noted that different authors use various ways to define it and refer to a range of conditions. A characteristic example is the definition implied by Smith (1993). According to this, calm conditions are specified when the mean wind speed is comparable to or less than the root-mean-square turbulent horizontal velocity. Within the present work, the impact of low wind speed events will be tested in energy applications. The cut in speed of a wind turbine has values normally around 3 m/s, depending on its type. For this reason, the threshold of 3 m/s is employed for a low wind event definition. However, the methodologies discussed in the following sections can be applied for different values.

2.3.4 Extreme wind speed conditions

Extreme winds can cause several problems in buildings, bridges, wind turbines, nuclear power plants, trees, plantation while they may pose a threat to life. This is why several industries affected directly or indirectly from the effects of extreme wind speed in structures explore and try to mitigate its impact through risk analysis reports and studies. The construction, the insurance, reinsurance and energy industries are among the most affected. Regarding the first, for example, a design wind speed is accepted by most building codes in the United States. This design value is often referred to as a "3-second gust" (the highest sustained gust over a 3-second period) with a recurrence interval (see chapter 3.1) of 1 in 50 years.

It has been already discussed that wind speed is well described by the Weibull distribution (Hennessey, 1977). Its extremes in an annual base are often approached by the first type of GEV

(Cook, 1985). More details will be presented in the General Methodology and the Extreme Value Theory chapters.

2.3.5 Frequency Distribution of Wave Parameters

The random nature of ocean waves often requires a statistical description for their representation. The shape, the scale and the tails of the distribution can give important information regarding the nature and characteristics of the wave field. Before, however, preceding to the probability distributions most suitable for the data some basic wave parameters often used should be outlined.

- The significant wave height (SWH or H_s or H1/3) is the mean of the highest third of the waves representing practically the sea state.
- The mean wave period (T_m) is the mean of all wave periods in a time-series representing a certain sea state.
- The peak wave period (T_p) is the wave period with the highest energy.
- The mean wave direction (θ_m) is defined as the mean of all the individual wave directions in a time-series representing a certain sea state.

Observed wave heights often follow the Rayleigh distribution. The Rayleigh distribution does not put a limit on the wave height leading to overestimation of the highest waves. Therefore often the Weibull distribution is used instead of the Rayleigh distribution accurately describing the full distribution (Arena et al., 2015). The Weibull distribution has an additional parameter (m) that allows suppression of the highest waves and an optimum adjustment to the observed wave data. This is the case for shallow-water waves that are truncated due to depth-induced wave breaking.

The three-parameter Weibull distribution is found to better describe the upper tail of the distribution and not the full dataset. The Rayleigh distribution also describes well the highest waves, H1/100. On the other hand, the two-parameter Weibull describes better the lower tail of the distribution. As in the wind, the distribution fit is case sensitive and it is affected from the area characteristics (depth, fetch etc.) and climate.

A wave state can further be characterized through its frequency spectrum. This can be extracted by applying a Fourier transform to a wave record.

2.3.6 Wave variability and mean conditions

Waves are a continuous and random variable. Therefore as in wind, sampling (averaging) periods are required for their measurement. This should be defined according to the characteristics of the area of interest and the sea state. A widely used methodology is based on the 100 cycles of the longest expected wave which practically means 100 times the expected wave period. A common procedure is to study the sea state by applying statistical measures directly derived from a wave record. In this way the wave field is characterized in terms of height, period and direction.

As mentioned earlier, the significant wave height is a description of the wave height widely used, being quite representative to the visually observed one (Bouws et. al., 1998; Holthuijsen, 2007). A similar approach can be used to define the height of different fractions of the wave field. Regarding the wave period, a commonly used statistical output is the average zero-crossing period (T_z). The last represents the average time between two sequential crests. Other approaches the peak wave period and the mean wave period described above or the average period of the highest one-third of waves T1/3 (Bouws et. al., 1998; Holthuijsen, 2007).

These parameters, however, give only a portion of the behavior regarding the sea state. This limited description can be deceptive in complex situations (Semedo et al., 2011, Holthuijsen, 2007). This is the reason why a more detailed analysis is also needed. Such an analysis can be performed through the full spectrum of wave energy since it has the extra information regarding the distribution of energy in different frequencies and distributions. In this way it is easier and safer to distinguish the characteristics of the waves such as swells from wind driven local waves.

This is highly associated to the variability of waves, which follow the variability of the wind field that generated them. Differences in the nature of the field have effect in the variability. The water is denser meaning that the response in potential changes in the atmospheric

conditions is slower. At the same time ocean waves can travel away from the place they were generated. Therefore, the simultaneous presence of local waves and swell increases the complexity and the level of difficulty in defining their variability.

In general, offshore wave conditions do not vary significantly within distances of a few hundreds of km in large open sea areas. The spatial variability of waves is more evident in nearshore locations and coastal water. The topographic formations, the depths and the shoreline highly affect the wave characteristics and several physical processes like wave refraction, diffraction and reflection, bottom friction and breaking are taking place. Under such conditions the spatial variability of wave state seems to be higher.

2.3.7 Extreme wave conditions

Extreme wave conditions mainly occur during major storms at sea under the effect of surface winds and the nonlinear wave interaction. Offshore infrastructure such as offshore wind turbines and oil platforms and activities like fishing and shipping are widely affected by the presence of rough and high sea states. In coastal areas extreme waves have the potential to cause extensive damage to the shoreline environment and landforms as well to human infrastructure while they may pose threat to life. As a result, their impact on coastal communities and environment has led a range of mitigation and adaptation strategies to cope with these hazards. Among them, better coast defenses and early warning systems based on numerical modeling, weather forecasting and climatology have been adopted.

In general, a risk assessment regarding the structural design and survivability of nearshore and offshore structures is based on the different descriptions of wave height. In operations and forecasting apart from the SWH, the maximum wave height (H_{max}) and the mean value of the highest 10% of waves (H_{10}) are often used to describe the existence of extremes in an intense state of the sea. However, it should be noted that the estimation of maximum wave height may lead to overestimations as derived from the wave spectrum. In climatological approaches, used for risk assessment in infrastructures, the concept of return periods is adopted. In this way the probability of an event with a particular SWH to occur is defined and used to adapt the design limits of a potential installation.

2.4 A brief summary of the wind and wave climatic characteristics of offshore Europe

A brief summary of the climatological characteristics associated to extreme events in the areas of interest will be addressed. In Europe offshore, near shore and coastal activities are associated with a great part of the socioeconomic activities, while in 2011, 40.8 % of the EU-27 population lived in coastal regions covering the 40.0 % of EU-27 territory (Figure 2-5).

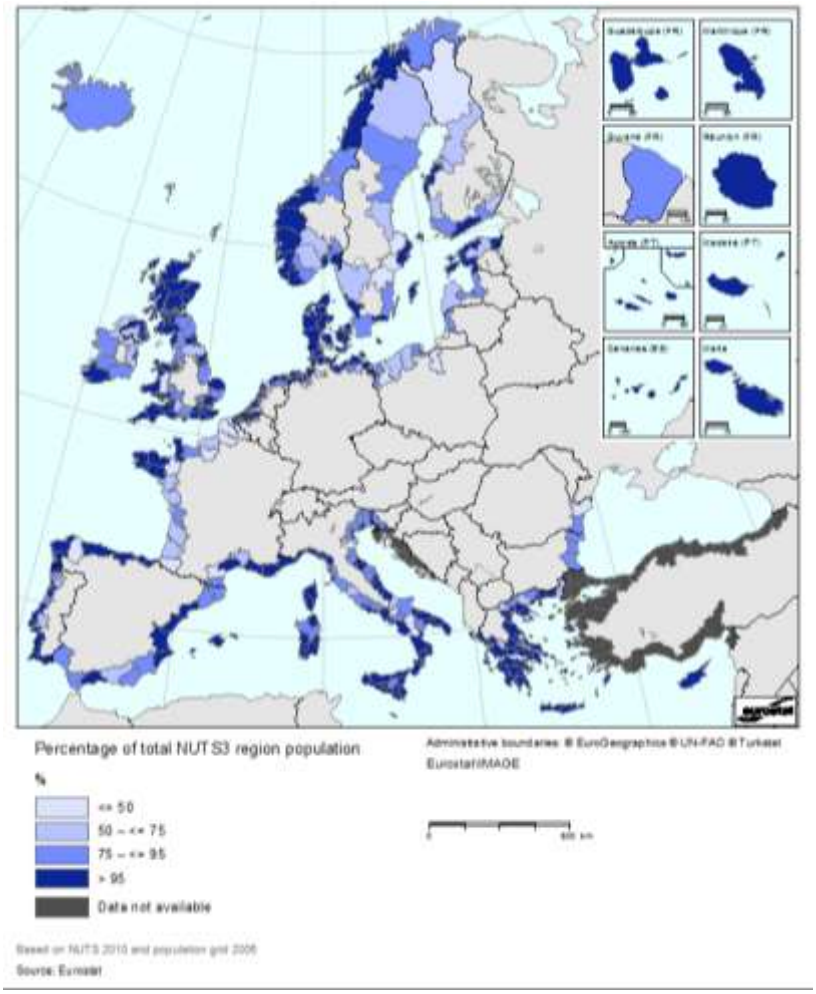

Figure 2-5: Share of population in coastal regions living within 50km from the coastline by NUTS3 regions (source: Eurostat - www.ec.europa.eu)

These regions are associated with offshore activities and are exposed to direct impacts from coastal storms and sea-level rise (Neumann et al., 2015). The exceptional severity of cyclonic activity is a prominent feature of the European climate (Della-Marta et al, 2009; Schiesser et al, 1997). The present study will focus on two major sub-regions, North Sea and

Mediterranean Sea. The first one is selected due to the high interest in offshore wind energy production (high energy potential, Figure 2-6) and the second mainly due to offshore and nearshore activities associated to tourism, shipping and energy.

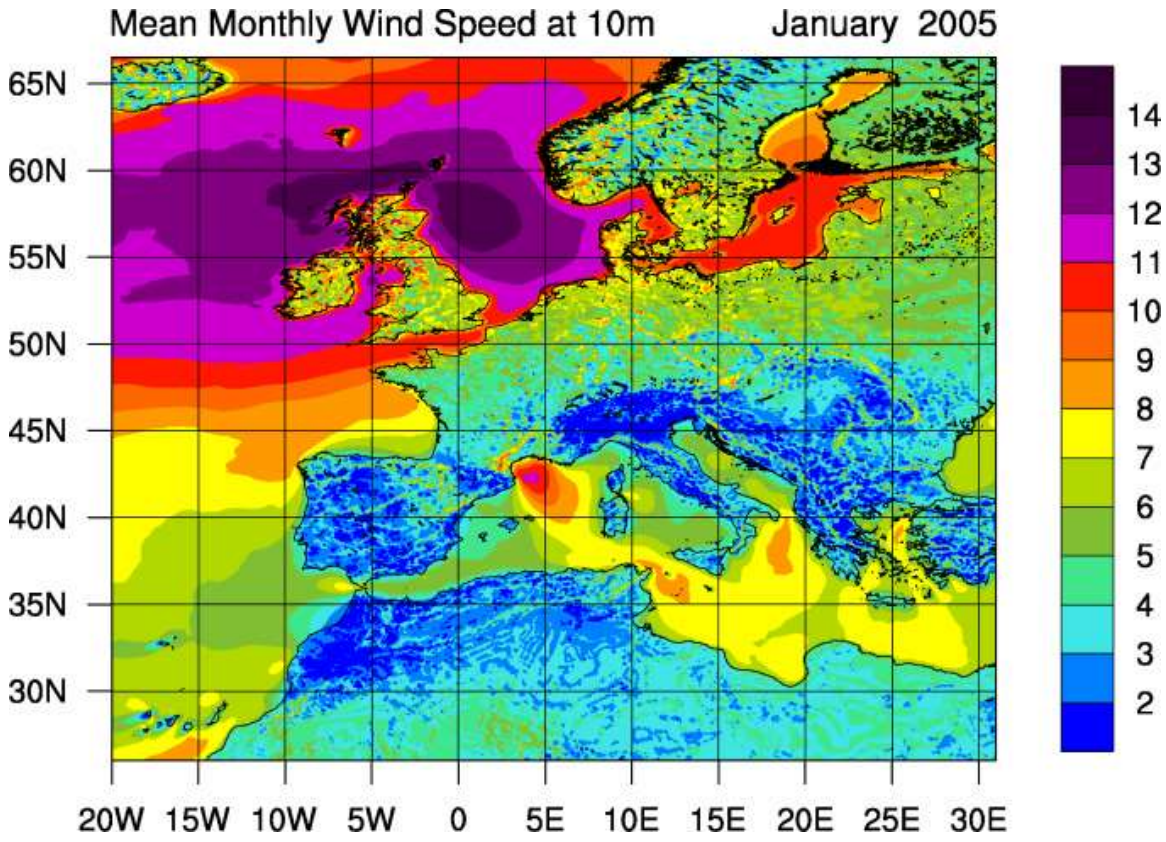

Figure 2-6: Mean monthly wind speed at 10m of the January of 2015 (Marina Database).

Beginning with the North Sea, its climate can be categorized in a transition between the maritime climate of the northeastern North Atlantic and the continental climate of Europe. It is characterized by high variability covering several time scales from days to decades. The wind climate of North Sea is influenced by the "Westerlies" and characterized by relatively high winds due to polar lows (low-pressure systems) and extra tropical cyclones moving from West to East. These storms can lead to an intense state of the sea and high waves considering also that the fetch and the characteristics of the area support it.

There exist several studies regarding the storm climatology affecting North Sea and the potential changes throughout the years. Schmidt and von Storch (1993) found pronounced decadal variability but no significant long-term trend through an analysis of geostrophic wind speeds beginning in 1876. These findings were further supported in later years by numerous authors such as Alexandersson et al. (1998), Alexandersson et al. (2000) and Matulla et al. (2008). They resulted that storm activity was more intense at the end of the 19th century and in the mid-1990s decreasing again from then. Similar findings are obtained through the observation and the analysis of extreme conditions in various parameters such as sea level height (Dangendorf et al., 2013) or regional (atmospheric and wave) hindcast simulations (Beate et al., 2015; Weisse and Günther, 2007; Weisse et al., 2005)

The Mediterranean Sea in particular is a region with complex terrain being characterized by local winds (Chinook winds, Mistral, Etesians etc.) and by intense cyclonic activity. Mediterranean cyclones on a climatological basis have been extensively studied during the last two decades (e.g. Trigo et al. 1999, 2002; Maheras et al. 2001; Bartholy et al. 2009; Campins et al. 2010; Flocas et al. 2010, 2013). Additional climatological research in explosive cyclones (Kouroutzoglou et al., 2011, 2014) and medicanes (Cavicchia et al., 2014; Miglietta et al. 2015) have been performed especially during the latest years.

Mediterranean cyclones frequently cause events of extreme and adverse weather, often having high social and economic impact (Lionello et al. 2006). Many cases have been recorded in the past decades, which have caused extended destructions and even loss of lives (Jansa ` et al. 2001; Nissen et al. 2010). Heavy precipitation and hail, flooding, intense waves, storm surge and gale-force winds can severely affect coastal and agricultural areas, ports and shipping. Therefore, their meteorological and climatic characteristics are of great importance with implications in many sectors.

2.5 Medicanes: characterization and identification

One of the most interesting type of cyclones present in the area is the Mediterranean tropical-like cyclones (TLCs) known also as medicanes. Their name, a combination of the term Mediterranean hurricanes, resembles their nature. Medicanes are mesoscale low-pressure systems with characteristics of tropical cyclones such as a warm core, spiral cloud coverage and a central cloud-free “eye” (Figure 2-7).

Figure 2-7: Satellite imagery of Medicane Ianos (September 17, 2020). Its spiral cloud coverage and a central cloud-free “eye” can be seen.

Medicane creation is different from hurricanes. They often develop from existing cut-off, cold-core low pressure systems. Therefore, a vast amount of Medicanes are accompanied by upper-level troughs. In order for their development to take place favorable conditions are needed. Among these, low wind shear and atmospheric instability induced by incursions of cold air are often required. Although the sea surface temperature (SST) does not have a prime role in their transition it can affect their development and impact (Stathopoulos et al., 2020b). The characteristics of the Mediterranean basin alongside the limited capability of heat fluxes in the case of medicanes, lead to events with diameters, typically, not greater than 300 km. It is also quite often that the tropical characteristics are only achieved for some hours as the system dissipates and loses its energy. Fita and Flaounas (2018) highlighted, among other things, the hybrid nature of TLCs as they may exhibit both tropical and extratropical cyclonic features.

Medicanes have drawn the attention of the scientific community with a range of studies focusing on their genesis (Chaboureau et al, 2012; Emanuel, 2005; Raveh-Rubin & Flaounas, 2017) and their evolution (Claud et al, 2010; Flaounas et al, 2015; Pytharoulis et al, 2000). Concerning the last, many analyze the air-sea interactions and their impact on the evolution of the systems (Akhtar et al, 2014; Emanuel, 2005; Fita et al, 2007; Miglietta et al, 2011; Pytharoulis et al, 2018; Stathopoulos et al, 2020a; Tous et al, 2013).

From a climatological point of view, a further analysis was performed by Nastos et al. (2018) who studied the climatic features of medicanes pointing out the existence of significant interannual variability in their number. Cavicchia et al. (2014) investigated the environmental factors affecting medicanes as well as their spatial distribution and frequency. It is quite clear that despite the rarity of medicanes, their extreme characteristics include intense winds, heavy precipitation, tornadoes, lightning activity and high waves (Cavicchia et al, 2014; Miglietta et al, 2013; Tous et al, 2013; Winstanley, 1970). The last combined to their presence in a basin surrounded by intense coastal activities may lead to severe natural, social and financial implications. Towards this direction a risk-oriented analysis is more than necessary. In fact, there is a limited number of works focusing on the spatial and temporal variability of large-scale parameters associated to the presence of medicanes (Tous & Romero, 2013) and detecting the centers or tracking the paths of the warm core systems (Cavicchia et al, 2014; Gaertner et al, 2007). In their work, Gaertner et al. (2007) used an ensemble of Regional Climate Models to estimate the risk of tropical cyclone development over the Mediterranean Sea, based on

anthropogenic climate change scenarios. Additionally, to the definition of areas with potential threat, the estimation of the return periods of cyclones is a key component on risk assessment. Emanuel and Jagger (Emanuel & Jagger, 2010) estimated hurricane return periods for several highly populated regions while Parisi and Lund (Parisi & Lund, 2008) used another approach for the estimation of the recurrence interval of Continental Hurricanes in the United States. A similar concept regarding Mediterranean cyclones is presented by Romero and Emanuel (2013). Their approach generates thousands of synthetic storms employed for the estimation of the spatial distribution of their tracks and the return periods for extreme winds.

The identification of the systems was performed qualitatively using satellite images. In this concept, different identification methodologies have been proposed (Tous & Romero, 2013). A quantitative approach for cyclone characterization has been issued by Hart (2003) and used in a variety of studies (Cavicchia et al, 2014; Picornell et al, 2014; Pytharoulis et al, 2018; Stathopoulos et al, 2020a). These studies are atmospheric-modeling oriented and the structural evolution of the cyclones during their lifespan is made in terms of the thermal core structure and thickness asymmetry. The description of these features is made employing phase diagrams.

Their construction is based on the thermal symmetry (B), the upper thermal wind $(-|V_T^U|)$ and the lower thermal wind $(-|V_T^L|)$. Parameter B is calculated for the layer 900–600 hPa. It represents the difference of the layer mean thickness of the right side minus that of the left side of the cyclone, defined according to its direction of movement. $B \gg 0$, refers to thermally asymmetric or frontal nature cyclones with/and extratropical type, matured or conventionally intensified. Values of $\cong 0$, denote matured tropical cyclones, with non-frontal nature or thermally symmetric. A threshold between the tropical and extratropical type has been set close to 10m. Regarding the thermal winds, the upper focuses on the middle/upper atmosphere (between the 300-600 hPa) while the lower one refers to the lower/middle atmosphere (between the 600-900 hPa). Both expressions in positive values indicate a warm-core structure and a cold-structure otherwise. These are calculated within a radius of 200 km around the minimum mean sea level pressure of the cyclonic center.

A cyclone, using the described criteria, is considered as a medicane when simultaneously the thermal symmetry factor is smaller than 10 and the thermal winds are both positive.

3 General Methodology

The main objective of the present thesis is the quantification of the extremity and the associated uncertainty of different environmental parameters and weather events. Towards this way, novel techniques and approaches are proposed and applied in large areas in the North Sea and the Mediterranean basin. The concept is to test the proposed methodologies in gridded timeseries, summary measures and weather patterns. It is clear, therefore, that all these different processes have substantial differences that are discussed in detail within each chapter. They all start, however, from a common basis. All the analysis is based on atmospheric and wave modeling hindcast simulations. The model output is employed for the extreme value analysis which is performed under the principles of the Extreme Value Theory.

Beginning with the last, the theory is characterized as one of the most essential statistical disciplines for a variety of sectors. Extreme value techniques are widely used in various disciplines such as constructions and insurance industry, risk assessment and financial markets or telecommunications. The distinguishing feature in extreme value analysis applications is the quantification of the stochastic behavior of a process such as the estimation of the probability of occurrence of events based on smaller samples. This statistical measure is very important as an indication of the possibility of potential extreme values to take place even they far exceed the values of the sample. The extreme value theory is highly dependent in fitting probability distributions in the extreme values as these defined in each approach.

Thus, the next sub-chapters are devoted in describing the different extreme value analysis techniques alongside a brief probabilistic theoretical overview, followed by the description of the atmospheric and wave models used, the model development and the evaluation procedure.

3.1 Extreme Value Analysis

Risk can be expressed through the concept of return period that is a statistical estimator for extreme phenomena reoccurrence based on data of shorter range. There are different approaches proposed for the estimation of the magnitude and reoccurrence interval of extreme events. Annual Maxima and Peaks Over Threshold methods (Coles, 2001) meet great acceptance for their effectiveness followed by the Method of Independent Storms and an extension of the classical method to take into consideration the r-largest values (Palutikof et al., 1999).

Beginning with the Annual Maxima method, Cook (1985) suggested that extreme wind speed is often well represented by Gumbel distribution. The same author (1982) used the dynamic pressure to achieve a faster convergence and better distribution fitting. A more recent study was held by Larsén et al. (2011) where an extreme wind speed atlas is created based on the principles of Generalized Extreme Value (GEV) theory and the Annual Maxima (AM) method.

3.1.1 Block (Annual) Maxima method

The Block Maxima method uses the GEV theory (Jenkinson, 1955). For this application the time series are divided in same-size blocks and the maximum value of each block is used to create the dataset for the application (Figure 3-1).

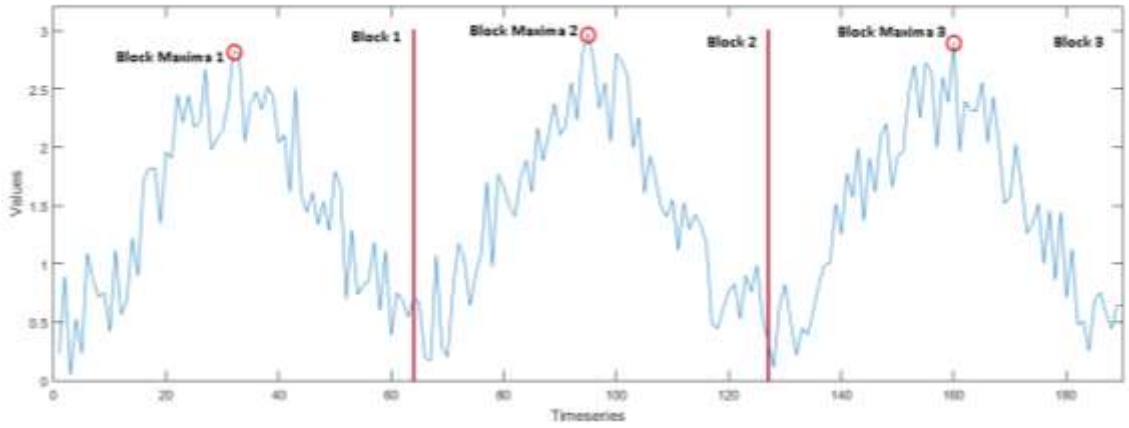

Figure 3-1: The Block Maxima approach.

The choice of the block size is of major importance since a very small can lead to overestimation and increased bias. On the other hand, very large blocks will lead to smaller datasets, large variability (Coles, 2001) and rather unreliable estimation. These reasons led to the use of annual blocks (Annual Maxima) because shorter periods may violate the principles of the GEV theory (Coles, 2001). The sample created by selecting the annual maximum values, is used to fit a distribution that belongs to the GEV family.

It is widely accepted that wind speed is well described by the Weibull distribution (Hennessey, 1977), while the extremes (AM) are often approached by the first type of GEV (Cook, 1985). The later, combined with the fact that Gumbel's Probability Density Function requires the estimation of only two parameters, led to this selection.

The estimation of the parameters of the fitting distribution is based on two methods. The first one is the Maximum Likelihood (ML) Method (Cramér, 1946; Hazewinkel, Michiel, 2001) and the second is the Method of Moments (MoM) (Cramér, 1946; Kendall & Stuart, 1987). Using the ML Method, the location (β) and the scale (α) parameter can be estimated through the numerical solution of the following equations simultaneously:

$$\tilde{x} - \frac{\sum_{t=1}^{n} x_t \exp(-x_t/a)}{\sum_{t=1}^{n} \exp(-x_t/a)} - a = 0 \quad \text{and} \quad -a \cdot log[\frac{1}{n}\sum_{i=1}^{n} \exp(-\frac{x_i}{a})] - \beta = 0 \qquad (3\text{-}1)$$

Where x_1, ..., x_n is a random sample, $\tilde{x}$ is the sample mean and α, β the scale and location parameter respectively.

Using the MoM, the location (β) and the scale (α) parameters can be calculated by:

$$\alpha = \frac{s \cdot \sqrt{6}}{\pi} \ , \ \beta = \tilde{x} - 0.57721 \cdot a \qquad (3\text{-}2)$$

Where $\tilde{x}$ and s are the sample mean and standard deviation, respectively.

In order to verify the appropriateness of the distribution selection, the raw data under study (modeled or observed) is compared with the corresponding values of the theoretical distribution. There are different approaches either graphical or analytical such as Probability plots (P-P plots), Quantile plots (Q-Q plots) (Coles, 2001) and the Kolmogorov-Smirnov test (Marsaglia et al., 2003).

The next step is to estimate extreme wind speed (UT) with the preferred return period (T) through the relation F(UT) = 1 – (1/T) leading to the following results (Palutikof et al., 1999):

$$U_T = \begin{cases} \beta + \frac{\alpha}{k}\left\{1 - \left[-ln\left(1 - \frac{1}{T}\right)\right]^k\right\} & k \neq 0 \\ \beta - \alpha ln\left[-ln\left(1 - \frac{1}{T}\right)\right] & k = 0 \end{cases} \quad (3\text{-}3)$$

Where α, β and k are the scale, location and shape parameter respectively.

The extreme wind speed uncertainty is normally distributed and expressed through the 95% confidence interval that equals to 1.96·σ(U_T), where $\sigma(U_T) = \pi \cdot \alpha\sqrt{\frac{1+1.14k_T+1.10{k_T}^2}{6n}}$, n is the number of maxima, $k_T = \frac{\sqrt{6}\,(\ln T - \gamma_E)}{\pi}$ and γ_E is the Euler's constant.

For the successful implementation with respect to the principles of Extreme Value theory, events should be independent and identically distributed (Palutikof et al., 1999). It is also assumed that a stationary extreme wind speed climate characterizes the study area. The main disadvantage regarding the AM method is that only one value per year is used. This reduces the amount of the analyzed data significantly. For this reason, the original time series must be large enough. Cook (1985) suggests the use of 20 years of data for reliable results and argues that the method cannot be applied to time series of less than 10 years.

Continuing, the Peaks Over Threshold (POT) methodology is employed for studies based on smaller time series and the use of exponential is supported (Abild et al., 1992). As in the first case, the wind speed square is found to fit better, especially in areas with low wind speeds and in cases where the wind speed distribution is not skewed enough for an exponential quick convergence to the distribution tail (Caires και Sterl, 2004; Galambos, 1987; Cook, 1982). These extreme value analysis methods are also used to more targeted studies of extremes based on similar characteristics such as the year season or the direction (Cook, 1982).

3.1.2 Peaks Over Threshold method

To overcome the above-mentioned shortcomings, a second approach for the estimation of return periods has been used through the Peaks Over Threshold method that is based on the Generalized Pareto Distribution (GPD) that is used to estimate the values exceeding a threshold.

The great advantage of POT method is the utilization of more data for the application that can be achieved also by smaller time series. For this reason, in contrast to AM, a period of 5-6 years is statistically adequate (Coles & Walshaw, 1994).

The first step for creating the dataset is to apply a high threshold to form wind speed clusters above it (Figure 3-2). The problem that arises with the selection of the threshold is similar to the block selection for the Block Maxima. Low thresholds may lead to violation of the asymptotic behavior of the distribution, while high will create fewer exceedances and will lead to an increase of variance. Therefore, the threshold should be high enough so as to converge to GPD and avoid the coexistence of different populations of extremes. At the same time, it must be sufficiently low in order to create a dataset big enough for a better distribution parameters estimation (Abild et al., 1992).

The climatic characteristics of the study area are of major importance for the application and should be taken into consideration before the selection of the threshold (Caires and Sterl, 2004). Independence between the events is critical and even high thresholds cannot ensure it. This is the reason why minimum separation time between the events should be established. For European climates the separation time can be set at 48 hours (Cook 1985, Gusella 1991) while Walshaw (1994) uses 60 hours for Sheffield wind data.

The next step is to select the peaks of the clusters and subtract these values from the threshold (Figure 3-2). The created data (exceedances) is used to simulate the distribution. For high thresholds, the number of exceedances per year (crossing rate) is low and Poisson distributed while the total dataset is well approximated by the Exponential distribution (Palutikof et al., 1999).

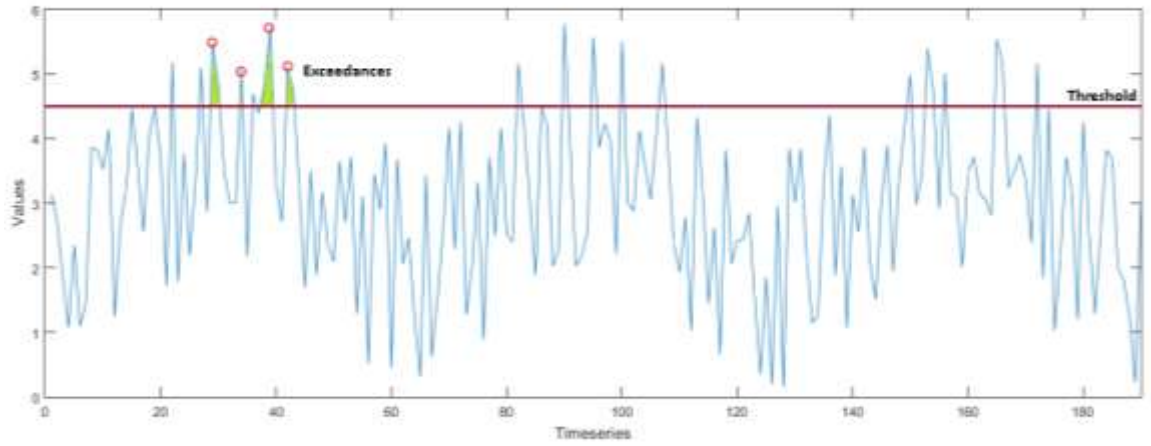

Figure 3-2: The Peaks Over Threshold (POT) approach

The exponential distribution fit to the exceedances is obtained with the same techniques (ML and MoM) in order to achieve comparable outcome. However, in this case the two methodologies converge.

At this point a goodness-of-fit test is necessary for checking the suitability of threshold selection in line with the parameters estimation techniques. A graphical technique is the so called Conditional Mean Exceedance (CME) graph that is also known as residual life graph (Davison, 1984; Ledermann et al., 1990). Walshaw (1994) proposed a different approach of CME named re-clustered excess graph. Another approach is the use of the Multiple-Threshold Model by the (Northrop & Coleman) NC diagnostics. According to Northrop & Coleman (2014), the diagnostics fit piecewise equality of the shape parameter using score and likelihood ratio tests (Tsalis et al., 2020). Theoretically, the output of the tests (p-values) should increase together with the threshold and vice versa. However, at some point stabilization is achieved and this is considered to be the best value to select as a threshold for the analysis. Another approach is to select the threshold at the sharpest p-value increase (Tsalis et al., 2020). An analytical way to determine the appropriate threshold is by comparing the created exceedances to a theoretical distribution through the well-known Kolmogorov-Smirnov test (Marsaglia et al., 2003).

For the calculation of the extreme wind event UT with return period of T years (T-year event) the threshold crossing rate is necessary. The T-year event can be calculated for different values of the shape parameter (k) and rate parameter (α) (Abild et al., 1992):

$$U_T = \begin{cases} \xi + \left(\frac{a}{k}\right)[1 - (\lambda T)^{-k}] & , \quad k \neq 0 \\ \xi + a ln(\lambda T) & , \quad k = 0 \end{cases} \qquad (3\text{-}4)$$

Assuming that the crossing rate (λ) follows the Poisson distribution, it can be calculated by λ=n/M where n is the total number of exceedances above threshold ξ, and M is the length of data in years. For a Poisson simulation, uncertainty can be determined using the variance:

$$\sigma(U_T) \approx \left(\frac{a}{\sqrt{\lambda L}}\right)\sqrt{1 + ln^2(\lambda T)} \qquad (3\text{-}5)$$

where L is the length of data in years.

The T-year event can be assumed to be normally distributed (Kite, 1975). Thus, the 95% confidence interval can be estimated as $1.96 \cdot \sigma(U_T)$ as in the AM method.

The necessity for bigger datasets that do not violate the principles of Extreme Value (EV) theory led to the introduction of other methodologies such as the Method of Independent Storms (MIS) (Harris, 1998) and the EV theory based on the r largest annual events (Smith, 1986). At the same time different approaches are proposed by Lopatoukhin et al. (2000) for the estimation of extreme wind wave heights such us the Initial Distribution Method (IDM). Breivik et al. (2014) studied wind and wave extremes using large ensembles and computed a non-parametric Direct Return Estimate (DRE) from the tail of the fitted distribution function. This was used for the estimation of the 100-year marine wind speed over the Globe.

3.1.3 Extension of the block maxima method to the r-largest values approach

The method (Weissman, 1978) is based on taking into consideration the r-largest values (X1>X2>…>Xr) in a block (eg. year – Figure 3-3).

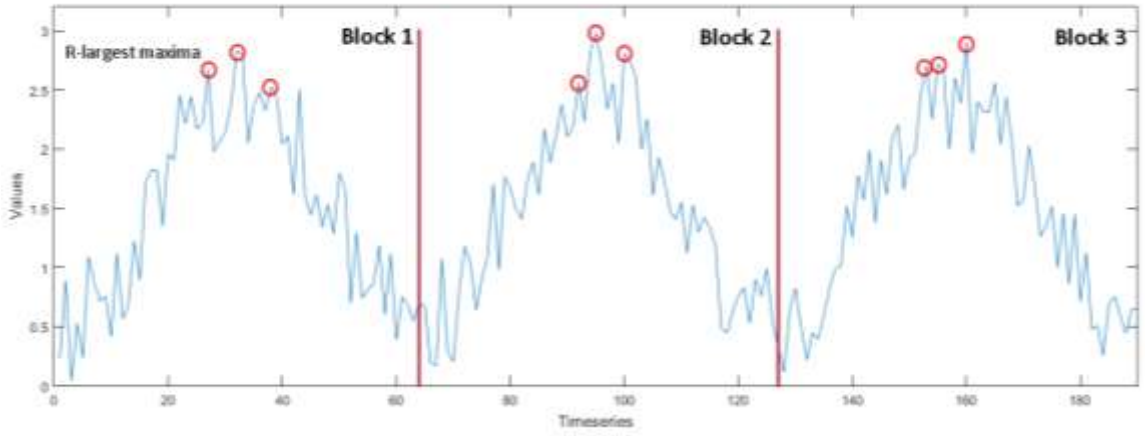

Figure 3-3: The r-largest values approach.

The joint probability density function for this sample is given by:

$$F(x_1 \dots x_r) = \begin{cases} a^{-r} exp\left[-(1-kZ_r)^{\frac{1}{k}} + \left(\frac{1}{k}-1\right)\sum_{j=1}^{r}\ln(1-kZ_j)\right] & ,k \neq 0 \\ a^{-r} exp\left[-\exp(-Z_r) - \sum_{j=1}^{r} Z_j\right] & ,k = 0 \end{cases} \quad (3\text{-}6)$$

The likelihood functions are given by Smith (1986) and the estimates of a and b can be computed numerically using ML methods. The application of this method requires the independence of extremes and the size of r (Tawn, 1988). This problem is of the same concept as the threshold selection in POT. The extremes are more likely to be independent if r is kept small (Smith, 1986). However, the reason of utilizing this procedure is the larger amount of extreme values to process and thus, r should be the maximum possible having in mind the restrictions. Coles & Walshaw (1994) applied the r-largest method in a six-year wind gust data with the number of values per year set to 10. In order to ensure the independency, they added a minimum separation time between the events equal to 60 hours.

3.1.4 The method of independent storms (MIS)

Another approach aiming at increasing the number of extremes available for the application is the method of independent storms (MIS – Cook, 1982; 1985). The independence between the extremes is ensured by separating the initial dataset into clusters – independent storms. Subsequently, the selection of the highest value from each storm is the final step for the creation of the dataset for the extreme value analysis. The storm "clustering" is achieved by applying a long-duration low-pass filter to the timeseries. Through the up- and downward crossings of the selected threshold, the storms are defined (Figure 3-4). These can be considered independent for quite low thresholds.

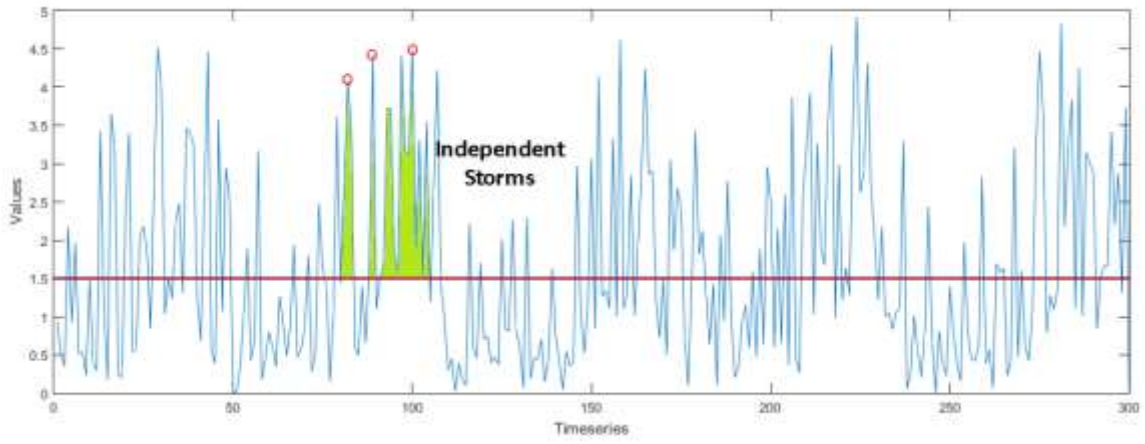

Figure 3-4: The method of independent storms (MIS)

Cook (1982) uses GEV Type I (Gumbel) distribution to fit the selected extremes. The best-fit line is found using the best linear unbiased estimators (BLUE) method (Lieblein, 1974; Cook, 1985). Through different sensitivity tests, he finds that threshold leading to an annual rate of 10 events/year gives a reliable recurrence interval estimate. More improvements in the method were introduced by Harris (1998) with a highlight the substitution of the BLUE method with his own (Harris, 1996). This way the need for data reduction is eliminated, leading to larger input datasets and smaller uncertainties.

In many cases the description of the extremity of the parameter under study should be associated to the duration of the event. This would be valuable information for a variety of environmental parameters as persistent extreme events could cause much more implications. Towards this way the Intensity, Duration and Frequency analysis tries to capture all the potential extreme characteristics of a variable under study. This methodology was firstly adopted in hydrology studies since for example not only the intensity but also the duration of a potential rainfall event would have a crucial role in flooding. The same methodology is adopted in the first and second part of this PhD thesis.

3.2 Probability distributions used in the study

The behavior of an atmospheric parameter is often described employing a probability distribution function. The same is the case in exploring the characteristics of the extremes. For this reason, several probability distributions are employed in different parts of this thesis mainly (but not only) during the application of the Extreme Value Theory. The use of each one is explained thoroughly within the chapters. However, a brief introduction regarding the characteristics of each distribution used here is presented in the following lines.

3.2.1 Generalized extreme value (GEV) distribution

GEV is a family of continuous distributions developed under the principles of the extreme value theory, combining Gumbel, Fréchet and Weibull families. The last are well known as type I, II and III extreme value distributions respectively. According to the extreme value theorem the GEV distribution is the only possible limit distribution of properly normalized maxima of a sequence of independent and identically distributed random variables (IID criterion). Thus, the GEV distribution is often used to model the maxima of long timeseries.

The cumulative distribution function is:

$$F(x) = e^{-(1-kz)^{1/k}} \qquad k\neq 0 \qquad (3\text{-}7)$$

$$F(x) = e^{-e^{-z}} \qquad k=0 \qquad (3\text{-}8)$$

Where k=shape parameter, $z=\frac{x-\beta}{\alpha}$, β=location parameter, α=scale parameter

GEV takes the form of Type 1 (Gumbel) when the shape parameter is equal to zero. Type II has a negative value of k will in Type III k is positive. Type I and Type II are unbounded at the upper end with Type II to be characterized by a thicker tail. On the other hand, Type III is bounded at the upper end (Figure 3-5).

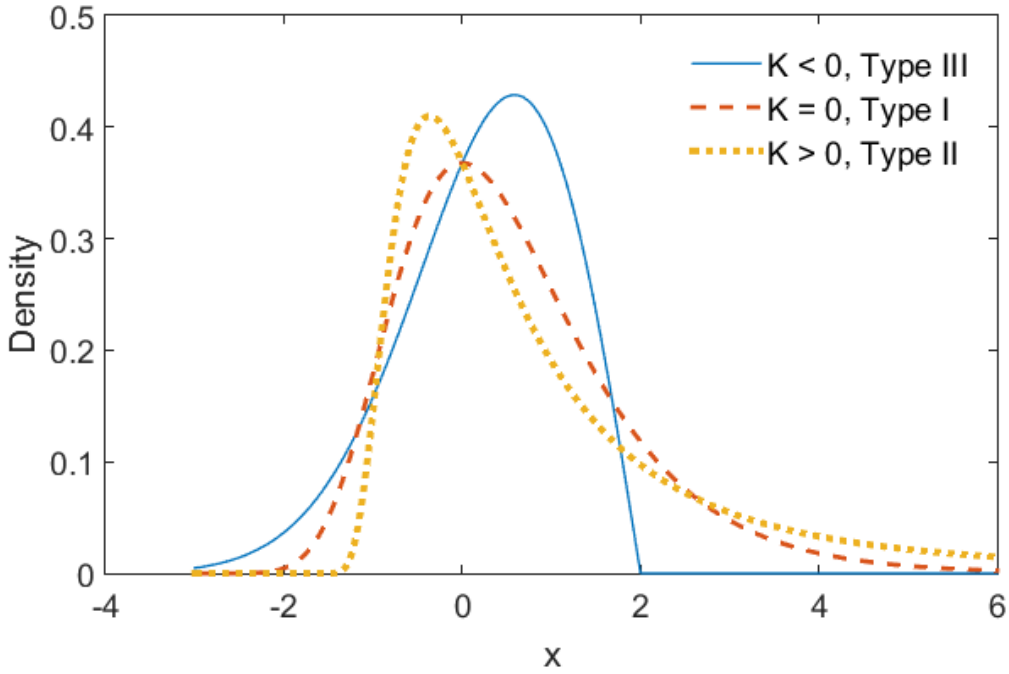

Figure 3-5: All types of GEV with β=0, α=1 and ξ={-0.5, 0, 0.5}

The type of GEV distribution is determined by the form of the parent distribution. The parent distributions of Type I extremes (i.e., with k = 0) include the Weibull distribution.

3.2.2 Weibull Distribution

The Weibull distribution is a continuous probability distribution. It is widely accepted that the Weibull probability density function is a good model for wind speed distributions (Hennessey, 1977). The probability density function of a Weibull random variable is:

$$F(x) = \frac{k}{\alpha}\left(\frac{x}{\alpha}\right)^{k-1} e^{-(\frac{x}{\alpha})^k} \qquad x \geq 0 \qquad (3\text{-}9)$$

$$F(x) = 0 \qquad x < 0 \qquad (3\text{-}10)$$

Where k=shape parameter, α=scale parameter.

Its complementary cumulative distribution function is a stretched exponential function. The Weibull distribution is related to a number of other probability distributions; in particular, it interpolates between the exponential distribution (k = 1) and the Rayleigh distribution.

3.2.3 Rayleigh Distribution

The Rayleigh distribution is continuous and suitable for nonnegative-valued random variables. A characteristic example for its application is the representation of wind velocity when analyzed in two dimensions, assuming that each component is uncorrelated, normally distributed with equal variance and zero mean. The probability density function of a Rayleigh random variable is:

$$F(x) = \frac{k}{\alpha^2} e^{-\frac{x^2}{2\alpha^2}} \qquad x \geq 0 \qquad (3\text{-}11)$$

Where k=shape parameter, α=scale parameter.

3.2.4 Generalized Pareto Distribution (GPD)

The generalized Pareto distribution (GPD) is a family of continuous probability distributions. As an asymptotic distribution, GPD is used to describe and model the tails of another distribution. Similarly, to the GEV distribution, the GPD has a shape and a scale parameter. The maximum values of samples from the GPD distribution are GEV distributed. Their shape parameter is equal to the one of the parent GPD (Palutikof et al., 1999).

The probability density function for the distribution with shape parameter $k \neq 0$, scale parameter σ, and threshold parameter θ, is (Figure 3-6):

$$F(x) = \frac{1}{\alpha}\left(1 + k\frac{x-\theta}{\alpha}\right)^{-1-\frac{1}{k}} \qquad (3\text{-}12)$$

For $\theta < x$, when $k > 0$, or for $\theta < x < \theta - \alpha/k$ when $k < 0$

For k = 0, the density is:

$$F(x) = \frac{1}{\alpha} e^{-\frac{x-\theta}{\alpha}} \qquad (3\text{-}13)$$

If k =0 and ϑ =0, the generalized Pareto distribution is equivalent to the exponential distribution:

$$F(x) = \frac{1}{\alpha} e^{-\frac{x}{\alpha}} \qquad (3\text{-}14)$$

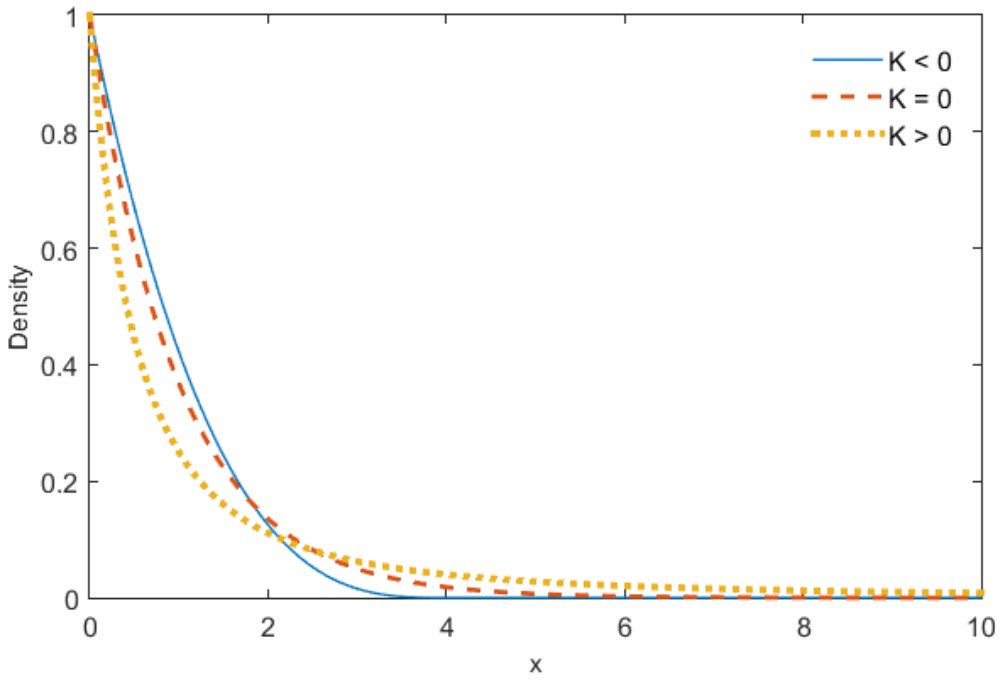

Figure 3-6: Generalized Pareto Distributions with shape parameter k = { -0.25, 0, 1} respectively.

3.3 Intensity, Duration and Frequency analysis

The methodology is based on the principles of the Extreme Value Theory described in the General Methodology. However, the technical part of and the tools applied in this chapter are described in the following lines.

3.3.1 Intensity Given Duration

The application of this methodology requires the selection of a range of different durations/windows from 2 to 480 hours (20 days, as a safe limit ensuring a big range of durations (Leahy & McKeogh, 2012)). More specifically, maximum values mv_d of wind speed v_t are estimated over moving windows for each year (Figure 3-7):

$$max\{v_t \dots v_{t+d}\} = mv_d \text{ , where } t=\{1\dots \text{total annual hours} - d\} \text{ ; } d=2,\dots,480 \qquad (3\text{-}15)$$

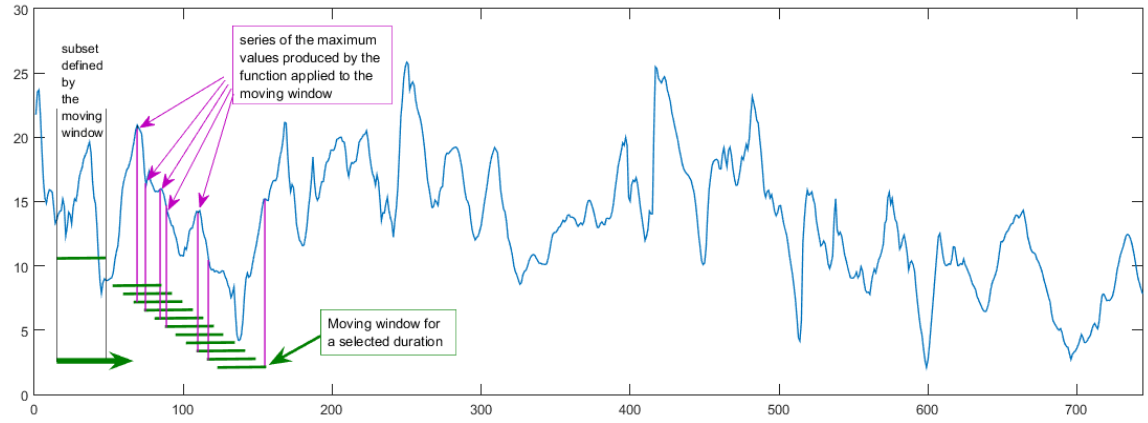

Figure 3-7: Data creation through the moving window graphical explanation.

As a result, a new array (mv_d) with *n-d+1* components per year is obtained with Cumulative Distribution Function (CDF) $F_u(u|d)$ and Probability Density Function (PDF) $f_u(u|d)$, where *u* is the variable under study (here wind speed), *n* equals the total hours (of each year) and *d* represents the window length (in hours).

The next step is the adoption of a representative distribution for the extrapolation in time. The PDF and the CDF of the data will be denoted as $F_u(u|d;a,b,c,\dots)$ and $f_u(u|d;a,b,c,\dots)$ respectively. The parameters *a, b, c,…* are highly dependent on the given duration, the characteristics of the selected distribution and the method used for the distribution fit. The relation between the intensity, the duration and the frequency (return period- T_u) of the event is the following:

$$1 - \frac{\Delta t}{T_u} = F_u(u|d; a, b, c, \dots) \qquad (3\text{-}16)$$

where Δt is the time interval of the data to be fitted

The extrapolation will be based on the principles of Extreme Value Theory and the use of Annual Maxima Method as it is considered straight forward and no decisions have to be made for its application (Palutikof et al., 1999). The fitting distribution selected is Gumbel (minimum) as the desired outcome is the lowest value for a defined return period (Leahy & McKeogh, 2012). For this reason, there is the need for a new dataset, created by selecting the lowest value of the vector mv_d for each particular year. Since the database is 10-year long, the dataset will be constituted of 10 values in total. The new PDF and CDF are set as $F_u'(u|d;\alpha,\beta)$ and $f_u'(u|d;\alpha,\beta)$ respectively where α is the scale and β is the location parameter. At the same time, Δt in equation 3-16 is equal to one as the values are annual. The above equation is transformed into the following:

$$1 - \frac{1}{T_u} = F_u'(u|d; \alpha, \beta) \qquad (3\text{-}17)$$

The application of this method can be done by using different tools for the parameters estimation such as Method of Moments (MoM) (Cramér, 1946; Kendall & Stuart, 1979) and Maximum Likelihood (ML) Method (Cramér, 1946; Hazewinkel, 2001). Using these as well as the CDF of Gumbel (minimum) and equation (3-17), the maximum value of a low wind speed event (U) of a given duration (D) can be extracted from:

$$U_D(T_u) = \alpha * \left(\ln\left(-\ln\left(1 - \frac{1}{T_u}\right)\right)\right) + \beta \qquad (3\text{-}18)$$

(Variable U corresponds to the wind speed threshold as defined in the following lines in Duration Given Intensity methodology.)

Applying different time windows will result to a matrix of the wind speed (*U*), the total duration (d) and the return period of the event (T_u) (all combined). The graphical representation of this matrix is made through the use of Intensity-Duration-Frequency (IDF) curves.

The wind speed maximum intensity for a given return period can be related to the duration of the event by fitting a curve to the results. This curve is a function of the duration which is found to be well represented by a second-degree polynomial (eq. 3-19) or a logarithm function (Leahy & McKeogh, 2012) (eq. 3-20):

$$U(D)=b\,D^2+c\,D+d \qquad (3\text{-}19)$$

$$U(D)=d+c\,\ln(D) \qquad (3\text{-}20)$$

In both cases the parameters (*b, c* and/or *d*) are estimated using least squares method. In this study and for the selected area, polynomials were found to be more representative concerning lower speeds.

Regarding extreme winds, there are two basic differences. The first one is the application of the moving window and the extrapolation in time (eq. 3-15). The window will filter the lower values as it moves. Then the highest of them for each year will be chosen and Gumbel (max) will be used for the return period estimation. Additionally, the final output fit will be based on a logarithm function (eq. 3-20) as it was found to be a better option.

3.3.2 Duration Given Intensity

This approach, applied for low wind speed events, is based on the definition of a threshold. This threshold is set at 3 m/s, based on the cut-in wind speed for energy generators. The time windows that wind speed is constantly below the selected threshold are characterized as low wind (no production) periods. These cases can be identified by taking into consideration the threshold crossovers. The application of this methodology required the largest period of each year to be selected (annual maximum) for the creation of the dataset needed to apply Annual

Maxima Method. The distributions used for the dataset fit vary, while the parameter estimation method tested is ML. For the estimation of low wind speed periods with return period T_d years the following relationship was used:

$$1 - \frac{1}{T_d} = F_d(d|u; \alpha, \beta, \gamma) \qquad (3\text{-}21)$$

where α is the scale parameter, β the location parameter and γ the shape parameter

Equation 3-21, combined with the CDF of the distributions under study, leads to the relationships for the estimation of the T-year Duration of a low wind speed event.

The selected distributions belong to the Generalized Extreme Distribution family. The use of them is common for the estimation of return periods but it depends on the dataset characteristics (eg. skewness) and the desired degrees of freedom (parameters of the distribution). The distributions used alongside with the equations for the estimation of the durations are:

Gumbel (Maximum) distribution:

$$D_u(T_d) = \beta - \alpha ln\left[-ln\left(1 - \frac{1}{T_d}\right)\right] \qquad (3\text{-}22)$$

Generalized Extreme Value (G.E.V.) distribution:

$$D_u(T_d) = \beta + \frac{a}{\gamma}\left\{1 - \left[-ln\left(1 - \frac{1}{T_d}\right)\right]^{\gamma}\right\} \qquad (3\text{-}23)$$

Weibull distribution:

$$D_u(T_d) = \alpha ln(T_d)^{1/\gamma} \qquad (3\text{-}24)$$

Rayleigh distribution:

$$D_u(T_d) = \sqrt{2\alpha^2 \ln(T_d)} \qquad (3\text{-}25)$$

3.4 Extreme wind and wave indices

In order to be able to define the behavior of an area under consideration and apply the extreme value theory, a summary measure is needed. This is practically a scalar index summarizing the characteristics of a region into one value for each timestep, creating a corresponding timeseries. These timeseries describe the evolution of a storm and include information regarding its magnitude and spatial extent in terms of wind and wave parameters. They are computed employing the gridded data derived from the Marina Database (chapter 3.5.6). In the lines to follow a short description of each index used, alongside their characteristics and the mathematical calculations for their description are presented.

3.4.1 The maximum value

This measure is apparently the maximum value of the selected region for each hour. This index is a measure of the storms extremity with a rather local and highly sensitive character.

3.4.2 Mean value

Mean value index is the time series of the mean calculated variable over the given area. This is a simple index but the most robust and a good starting point for the analysis. The index is rather sensitive to both the event severity and spatial extent.

3.4.3 The spatial 95^{th} quantile

It is retrieved by using the already selected grid-points for each subdomain. These values are ranked and the empirical 95% quantile is chosen as the value for this index. Therefore, this index is concentrated on measuring only the windiest parts of the storm-affected areas at any given time. This particular index describes the severity of the storm and it is a more sensitive

extremity factor than the mean values. At the same time, it is less sensitive than the maximum values described above.

3.4.4 The spatial 99th quantile

This is quite similar to the 95th quantile. However, it is concentrated to the highest part of the wind speed (or wave) distribution tail. In terms of sensitivity it is somewhere between the 95th quantile and the maximum values.

3.4.5 The cube root of the sum of variable, cubed above the domain climatological 90% quantile (Sw3q90)

It somehow resembles the Power Dissipation Index (Emanuel, 2005) which is expressed in nondimensional units. This index needs the absolute 90% quantile to be calculated. The term absolute is used to show that the quantile is calculated from all grid points of the domain and all the temporal coverage. The values exceeding this threshold (exceedances) are cubed and summed in order to make a timeseries. The cube root is then taken as a final step to help make the index less skewed. This index is targeting at grid point extremes and this is why it is highly sensitive to areas of high absolute magnitude of the environmental parameters.

3.4.6 The sum of the fraction of the variable divided by the grid-point climatological 95% quantile (Sfq95)

The present index has similarities in its concept to the above mentioned. It is derived through the sum of the fraction of the variable divided by the grid-point climatological 95% quantile. In contrast to the Sw3q90, this index describes the extremity of the variable under consideration in relation to the local climate. The reason is because it is based on the 95th percentile of each grid point instead of the 90th of the whole dataset. Then, for each timestep, the fraction of the values above the selected percentile is selected for each grid point and summed. This index is rather characterized by sensitivity in smaller scale climatic features.

3.4.7 The sum of the fraction of the extreme value divided by the length of the distribution tail (Sfq95q99)

This index is similar to index Sfq95 in terms of sensitivity. However it includes a normalizing factor. It requires the estimation of the 95^{th} and the 99^{th} percentile. Then, for each timestep and grid point, in cases where the values are larger than the 95^{th} quantile the fraction of the difference between the value and the quantile above the difference between the two quantiles is calculated. Subsequently, the outcome is summed for each timestep. This index should be also sensitive to the relative extremity of local wind speed and waves.

3.5 Atmospheric Models employed for the study

The study is numerical modeling oriented. The great advantage of this approach is the spatial and temporal capabilities of the models. They can provide with the environmental parameters needed for the application in scales observations are not capable of. So, despite their disadvantage in accuracy, the need for dense spatial and temporal information led to their adoption. Several atmospheric and wave models were used in this study and were chosen against global datasets already existing in the literature due to their fine resolution. The first one described in short in the following line is SKIRON model, followed by the atmospheric model RAMS/ICLAMS and the wave model WAM.

3.5.1 Atmospheric model SKIRON

SKIRON is a non-hydrostatic modeling system developed at the University of Athens from the AM&WFG (Kallos et al., 1997; 2006) within the framework of the nationally and European Union (EU)-funded projects SKIRON, Mediterranean Dust Experiment (MEDUSE), Atmospheric Deposition and Impact on the Open Mediterranean Sea (ADIOS), and recently Climate Change and Impact Research (CIRCE).

The dynamical core of the model is based on the ETA/ National Centers for Environmental Prediction (NCEP) limited-area model, which was originally developed by Mesinger (1984) and Janjic (1994, 1984). It utilizes for the horizontal grid, the semi-staggered Arakawa E grid to simulate the large- and synoptic-scale features of the atmospheric processes, while for the vertical grid it uses the eta coordinates.

The physical part of the model is able to properly represent atmospheric processes that are not resolved explicitly due to various sophisticated parameterization schemes. The Betts-Miller-Janjic deep and shallow cumulus convection scheme is used for excessive precipitation events. The moist atmospheric processes of stratiform clouds are simulated through the large-scale condensation scheme. Regarding the surface processes the Oregon State University (OSU) scheme and a corresponding set of high-resolution ground conditions (soil and vegetation types,

topography, SST) is used. The Rapid Radiative Transfer Model (RRTM) is used for the estimation of the radiative atmospheric effects. The vertical turbulent mixing between the free atmosphere levels is estimated by using mixing coefficients of the modified Mellor-Yamada 2.5 level turbulence. Vertical mixing in the surface layer is performed by a Monin-Obukhov similarity model.

SKIRON also includes a dust production sub-model. The predicted atmospheric and hydrological conditions and the soil characteristics are used in order to calculate the effective rates of the injected dust concentration. The dust module (Nickovic et al., 2001) includes the effects of the particle size distribution in order to simulate size-dependent processes more accurately.

3.5.2 Atmospheric model RAMS/ICLAMS

The second of the two atmospheric modeling systems used in this thesis is the integrated modeling system RAMS/ICLAMS (Cotton et al, 2003; Kallos et al, 2014; Kushta et al, 2014; Solomos et al, 2011). The model has been developed by the Atmospheric Modeling & Weather Forecasting Group (AM&WFG) at the University of Athens as an enhanced version of RAMS 6.0 (Pielke et al., 1992; Cotton et al., 2003).

It has two-way interactive nesting capabilities, allowing a sufficient representation of atmospheric processes at resolutions ranging from tens of kilometers down to a few meters. The model also incorporates a two-moment bulk microphysical parameterization for the description of the cloud processes for seven categories of hydrometeors (rain droplets, pristine ice, snow, aggregates, graupel, hail and vapor), taking into consideration both the mixing ratio and the number concentration of each one (Meyers et al., 1997). Additionally, RAMS/ICLAMS includes an explicit cloud droplet nucleation parameterization scheme (Nenes and Seinfeld, 2003; Fountoukis and Nenes, 2005). The last provides a comprehensive microphysical link between aerosols and clouds. More specifically, soil dust and sea salt contribute to the CCN population that is expressed as a function of supersaturation using Kohler theory (Kohler, 1936; Nenes and Seinfeld, 2003). Regarding the dust particles, they are considered to follow a lognormal size distribution at source regions, with properties (number mean diameter and

geometric dispersion) expected to change throughout aging. It should be noted that these properties are explicitly calculated and resolved at every model step based on the predicted dust concentration (Schulz et al., 1998). Dust particles are well known ice nuclei especially when they are not aged (Pruppacher and Klett, 1997; DeMott et al., 2003; Levin et al., 2005). In the model, the insoluble fraction of dust contributes to the prognostic ice-forming nuclei (IFN) following the formulation of Meyers et al. (1992; Astitha et al., 2010). The direct effects of mineral dust and sea-salt are calculated within the model in the RRTMG scheme for both SW and LW bands (Mlawer et al., 1997; Iacono et al., 2000). The module used pre-calculated look-up tables for the simulation of the impact of clouds and aerosols in the radiation along the atmosphere. Moreover, the final version includes a new gust module based on the physical surface gust parameterization described by Brasseur (Brasseur, 2001; Patlakas et al, 2017a).

3.5.3 Wind gust sub model

The processes leading to gust formation vary among boundary-layer turbulence, deep convection, mountain waves and wake phenomena (Sheridan, 2011). It is well known that these phenomena are difficult to be properly resolved by NWP systems (Sheridan, 2011; Orrell et al., 2001) without the need of considerable computational resources. In addition, the subscale interactions are not always sufficiently described and generate errors or uncertainties. In general, gust forecasting is based on semi-empirical formulas derived from experimental studies (Weggel, 1999; Schulz & Heise, 2003; Simon et al., 2011), statistical models (using observations, ex. MOS - Model Output Statistics - Glahn & Dallavalle, 2006; Barrett & Short, 2008) and physical parameterizations that take into account atmospheric conditions in the processes of gust formation.

The gust forecasting scheme adopted for the needs of this thesis is the WGE method as suggested by Brasseur (2001). According to this approach, the turbulent wind fields of the boundary layer can be considered as an overlay of a large number of eddies with different sizes. Larger eddies have the scale of the depth of the boundary layer, while the smaller ones rapidly dissipate through friction.

This leads to momentum transportation both upwards and downwards. Under specific conditions, air parcels within eddies may deflect toward the surface, leading to gusty type wind fluctuations (Goyette et al., 2003). The estimation of its values is performed by assuming that a parcel flowing at a given height will be able to reach the surface if the average turbulent kinetic energy of the corresponding large turbulent eddy is greater than the buoyant energy between the surface and the height of the parcel as it is displayed in the following equation.

$$\frac{1}{z_p}\int_0^{z_p} E(z)dz \geq \int_0^{z_p} g\frac{\Delta\theta_\upsilon(z)}{\Theta_\upsilon(z)}dz \qquad (3\text{-}26)$$

where z_p is the height of the parcel, g is gravitational constant, $\Theta_\upsilon(z)$ is the virtual potential temperature, and $\Delta\theta_\upsilon$ (z) is the variation of virtual potential temperature over a given layer. The right part of the equation coincides to the potential energy of buoyancy, while the local turbulent kinetic energy is considered as E(z). A graphical representation is shown in Figure 3-8.

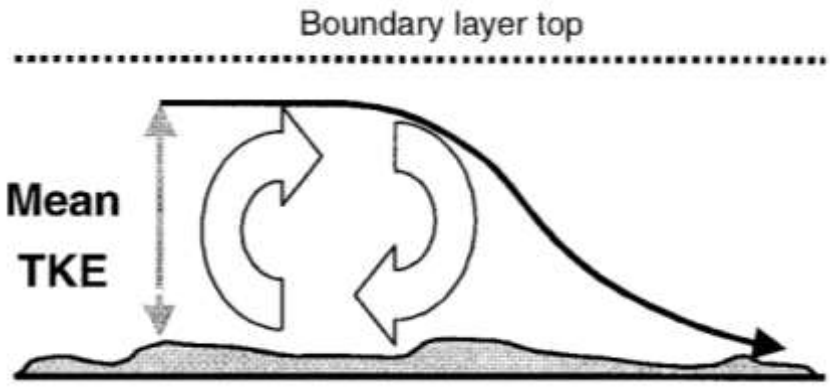

Figure 3-8: Determination of the wind gust estimate based on turbulent kinetic energy averaged over a given depth (from the surface) in the boundary layer (Image taken from Brasseur, 2001)

Considering that z_p refers to different heights that the equation 3-26 is satisfied, the gust estimate is selected as the maximum wind speed between all parcels in these heights:

$$W_g = max\left(\sqrt{U^2(z_p) + V^2(z_p)}\right) \qquad (3\text{-}27)$$

These processes have been incorporated in the RAMS/ICLAMS modeling framework, allowing the estimation of wind gusts at the surface. A further evaluation regarding the gust

output has been performed showing acceptable results (see Appendix – Wind gust model evaluation).

3.5.4 Wave model WAM

The wave model used in this study is based on the Wave Analysis Model (WAM) which comprises of a third generation wave spectral model (The Wamdi Group, 1988). In particular, the version WAM CY33R1 is employed (Bidlot and Janssen, 2003), enhanced with several features. The model simulates the distribution of wave variance in different frequencies and propagation directions based on the two-dimensional wave spectrum. Energy source derives from the surface wind speed forcing. The basic transport equation describes the evolution of the spectrum and interpreted without assumptions in respect to the spectral shape. With the solving of the wave spectrum equation the calculation of wave properties from the integral of the estimated spectrum is achieved. This includes parameters such as significant and swell wave height, peak frequency and directional spread. The current version utilizes explicit source functions to describe white-capping dissipation and bottom friction. Additional features are the consideration of depth induced wave breaking and shallow water effects by modifications in the non-linear source term expressions. An example of the model used in the Mediterranean Sea can be found in Galanis et al. (2012).

3.5.5 Online coupling of RAMS/ICLAMS and WAM

In the last chapter of the thesis a coupled atmospheric-wave modeling system is utilized based on RAMS/ICLAMS and WAM model (Stathopoulos et al., 2020a, b). This has been established in order to achieve a continuous feedback of information between the atmospheric and wave environment. The two model components operate in parallel and synchronously under the OASIS-MCT (Valcke, 2013) coupling module. The OASIS-MCT coupler allows the online transfer of information between numerical codes supporting the interface of any number of model components, the interpolation of data between the different model components grids as

well as the parallel transfer of data among them. In this context, the exchange of parameters between the atmospheric and wave model, occurs in time intervals proportional to the time step of each model component.

With respect to the transferred parameters, the surface wind speed, wind direction and air density are passed by the atmospheric model to the wave model. Wind speed is the energy source in the wave model, while surface air density is used in the computation of ocean surface stress. One the other hand, the ocean surface roughness Z_{oc} is transferred by the wave model to the atmospheric model. In order to consider explicitly the wave surface influence, ocean surface roughness is parameterized by wave parameters such as the significant wave height (SWH) and the wave slope (the ratio of SWH and wavelength L_p), given in Taylor & Yelland (2001).

$$z_{oc} = 1200\mathrm{SWH}(\mathrm{SWH}/L_p)^{4.5} \qquad (3\text{-}28)$$

3.5.6 Marina Database

The atmospheric database used in chapters 5 and 6 was created under the framework of the Marina Platform Project (Figure 3-9). One of the most important effects accounted for, was the coupling between wind- and wave-induced processes using state-of-the-art modeling systems. More specifically, the regional atmospheric model SKIRON (Spyrou et al., 2010; Kallos et al., 2007; 1998) is used for wind, the third-generation ocean wave model WAM (Galanis et al., 2011; Hasselmann et al., 1988) is used for wave and HYCOM (Chassignet, 2003) for currents. Moreover, Kalogeri et al. (2017) used the database to identify the main features of the available offshore wind and wave energy resource of Europe.

The coupled system, used for the Marina Database is a well-established model and successfully evaluated in various research works (Galanis et al., 2012; Janeiro et al., 2012; Dykes et al., 2009; Louka et al, 2008; Zodiatis et al., 2003; Korres et al., 2002; Papadopoulos et al., 2002).

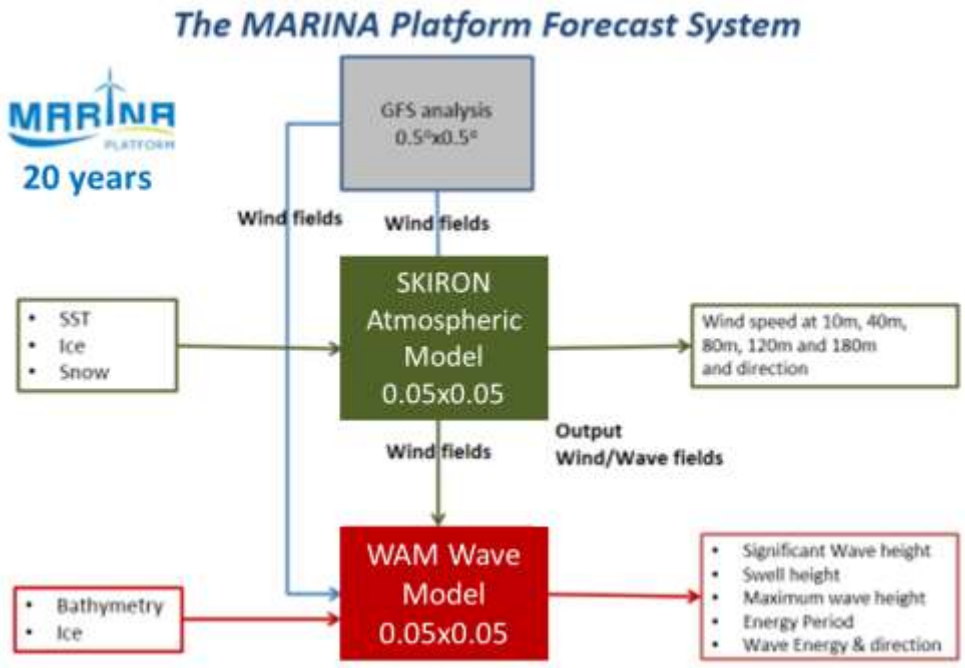

Figure 3-9: Graphical description of Marina Database construction.

The models have been run at a relatively high spatial resolution of 0.05° x 0.05° latitude/longitude covering a large part of Europe, North Atlantic and Mediterranean region (Figure 3-10).

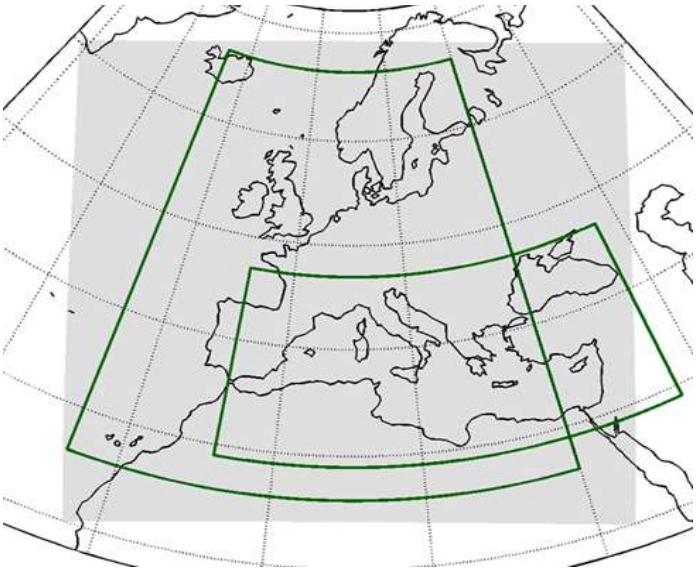

Figure 3-10: Domains used for the development of the MARINA Database.

SKIRON uses 45 levels in the vertical on a telescopic distribution (from surface to 50 hPa with more layers near the ground), and a time step of 15 seconds. The outputs of the models are co-located and stored with time frequency of one hour, initially covering the period 2001-2010 and now an extended period from 1996 to 2015.

3.5.7 Medicane Database

The analysis performed for chapter 5 is event oriented. Since the weather events selected for the analysis are medicanes, a great number of them is required in order to have a substantial amount of data to process. This data is the product of a large number of high-resolution hindcast numerical simulations while each event was treated as a separate case study.

The simulations were performed employing the coupled atmospheric-wave modeling system based on RAMS/ICLAMS and WAM model, taking advantage of all its benefits described extensively in chapter 3.5.5. The model was also developed in order to calculate a characteristic factor for the description of the extremity of wind and potential risk and that is gustiness (see chapter 3.5.3).

Multiple cases (52) have been found and simulated with this coupled system during the period 1994-2018 (25 years). Two nests have been used with a spatial resolution of 24 and 6 km for the outer and inner domain of the atmospheric model respectively. The inner domain covers the mid and southern Europe as well as the northern parts of Africa (Figure 3-11). The outer one is much larger in order to keep the lateral boundary conditions far from the area of interest. Vertically, both domains stretch up to 20 km with 39 vertical levels. The time step is set to 24 and 6 seconds for the coarse and the fine domain respectively. The initial and lateral boundary conditions, used for the model runs, are retrieved from the ERA-Interim dataset (Dee et al, 2011). ERA-Interim is a global atmospheric reanalysis dataset produced by the European Centre for Medium-Range Weather Forecasts (ECMWF), beginning from 1979 and updated continuously in real time. A significant advantage of the reanalysis product compared to the operational analyses is the consistency in terms of model outputs. For studies like the present one, which span across several decades, it is essential to rely on datasets that are not affected by changes that took place in the operational setup throughout the years. Daily Sea Surface

Temperature (SST) gridded data (with a resolution of 0.083o) provided by NCEP has been used. The soil texture and properties were derived from the Food and Agriculture Organization of the United Nations (FAO). The elevation dataset used is of high resolution (90x90 mxm) in order to obtain a detailed topography representation in the model. The vegetation and landuse were acquired by the United States Geological Survey (USGS) and are based on the Olson Global Ecosystem categorization. The horizontal resolution of the datasets is 30 arcsec (~900 m).

Regarding the wave model, the resolution is set to 6 km, while 30 frequencies and 24 wave directions are applied. The bathymetry is ETOPO1 at a resolution of 1 minute obtained from NOAA's National Centers for Environmental Information (NCEI). The model time step is 120 sec and the parameter exchange between the two models is updated every 360 sec. The output for both the atmospheric and the wave component has a temporal resolution of 1 hour.

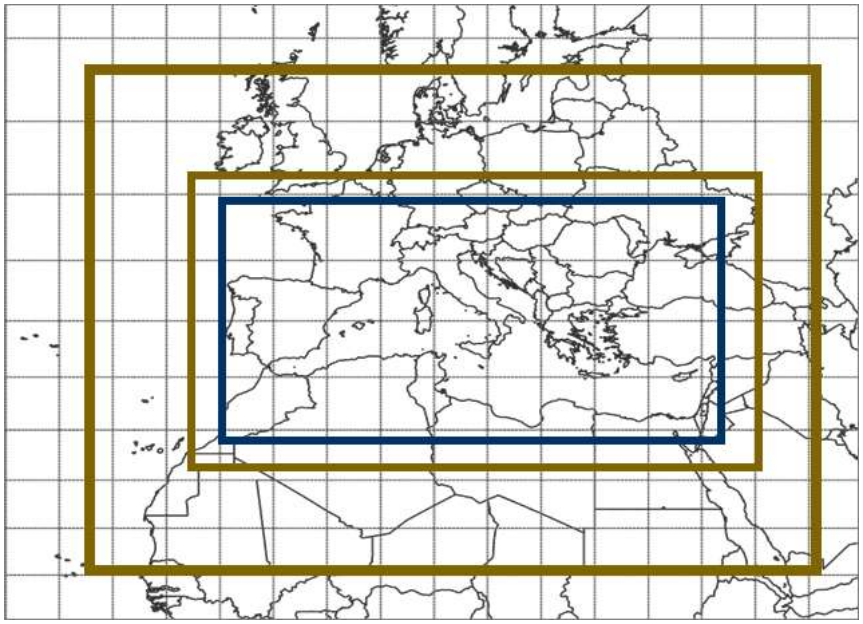

Figure 3-11: Model domain for RAMS/ICLAMS (2nests-gold line) and WAM (blue line)

Regarding the cases employed for the study, 52 events (Table 3-1) were simulated out of an analytic list of medicane events provided by (Nastos et al, 2018), enriched by a few more reported cases (McTaggart-Cowan et al, 2009; Stathopoulos et al, 2020a). The modeled cyclones cover all (or a vast majority of) the events (to the best of our knowledge) of a 25-year period.

For each cyclone, phase diagrams have been derived in order to define whether it has tropical characteristics at least for a single moment during its life span. These were applied employing a constant radius of 200km. It should be noted here that it is already proved in other studies that the lateral and boundary conditions, the model physics and the parameterizations used have a significant effect on the evolution of cyclones (Pytharoulis et al, 2018, Stathopoulos et al, 2020a). This is the reason why each cyclone was examined thoroughly and independently but also why there is also a small amount of cases included that do not cover strictly the criteria (e.g. B values close but not greater than 10).

Cyclone Qendresa for example for most of its lifetime presents a symmetric formation and gradually a weak warm-core structure (Figure 3-12). A transition to TLC behavior is found for the day 07/11 at around 18:00 UTC, where also the minimum surface pressure appears. After a short period it loses its warm core structure and its energy and it is characterized by extra-tropical features.

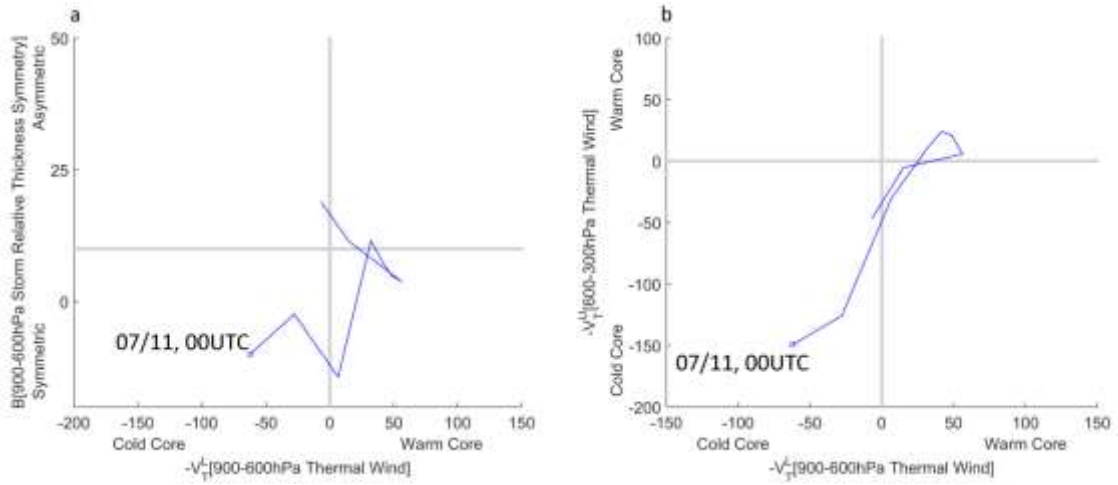

Figure 3-12: Phase space diagrams of (a) − V_T^L / B for 900–600 hPa and (b) − V_T^L (900–600 hPa) / − V_T^U (600–300 hPa) for Medicane Qendresa with a 6hours time interval.

The process followed to create the dataset employed for the analysis resulted to the exception of some case studies as the cyclone characterization or the selected wind and wave criteria were not covered (Table 3-1).

Table 3-1: List of all the simulated events including those that were not finally used for the analysis as they did not fit the criteria.

Case No	Date	Criteria fit	Case No	Date	Criteria fit
1	21–25/10/1994	✓	27	2–5/11/2004	✗
2	14–18/1/1995	✓	28	15–16/9/2005	✓
3	27–29/9/1995	✓	29	22–23/10/2005	✗
4	11–13/9/1996	✓	30	26–29/10/2005	✗
5	3–6/10/1996	✓	31	13–16/12/2005	✓
6	6–10/10/1996	✓	32	31/1-3/2/2006	✗
7	8–11/12/1996	✓	33	25–28/9/2006	✓
8	24–28/9/1997	✓	34	19–23/3/2007	✗
9	30–31/10/1997	✓	35	16–18/10/2007	✓
10	5–8/12/1997	✓	36	25–27/10/2007	✓
11	25–27/1/1998	✓	37	14-16/11/2007	✗
12	18–21/3/1999	✓	38	4/12/2008	✓
13	27–29/3/1999	✓	39	27–29/1/2009	✗
14	13/9/1999	✓	40	28/1/2010	✓
15	10/12/1999	✓	41	4–9/11/2011	✓
16	7–11/9/2000	✓	42	13–17/4/2012	✓
17	7–10/10/2000	✓	43	17–22/11/2013	✓
18	7/8/2001	✗	44	19–22/1/2014	✓
19	10–12/11/2001	✓	45	7–9/11/2014	✓
20	18/2/2002	✓	46	1–4/12/2014	✓
21	6/7/2002	✗	47	30/09 -02/10	✓
22	25–28/5/2003	✓	48	22/10/2015	✗
23	15–19/9/2003	✗	49	21-22/11/2015	✓
24	27–29/9/2003	✗	50	26/10- 01/11/2016	✓
25	17–19/10/2003	✓	51	15-20/11/2017	✓
26	19/9/2004	✓	52	27/09-01/10/2018	✓

The simulated medicanes are generated mainly in 4 regions shown in Figure 3-13. The topography of each subsector highly impacts the cyclone development and tracking as well as the areas affected. In order to assess the quality and performance of the model-derived parameters an evaluation was performed.

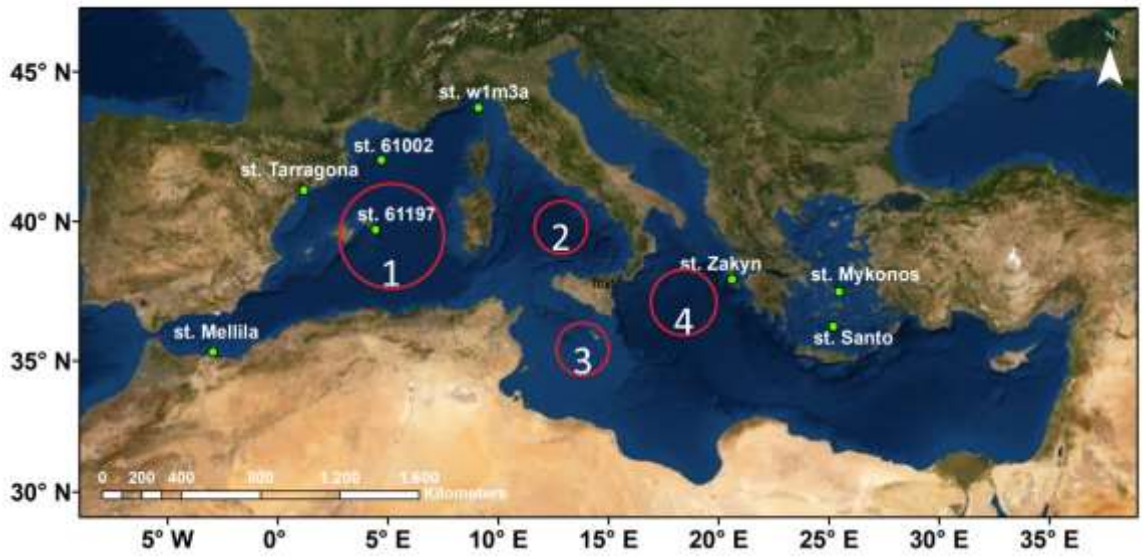

Figure 3-13: List of buoys used for the evaluation and main formation areas of the simulated medicanes (in circles).

3.6 Statistical analysis and Evaluation

The study of the return periods of extreme events will be based on the outputs of atmospheric and wave modeling systems. Therefore, a statistical analysis and a comparison between the model output and observations will provide useful information regarding the model behavior and support to the final results. For this reason, different statistical indexes and graphs are used within the study.

The Coefficient of Determination (R^2 - eq. 3-29) is a number indicating the fit of the modeled data and the measurements, being calculated by:

$$R^2 = 1 - \frac{\sum_i^k [obs(i) - for(i)]^2}{\sum_i^k [obs(i) - \frac{1}{n}\sum_i^k obs(i)]^2} \qquad (3\text{-}29)$$

Where “for” denotes the modeled values, “obs” the corresponding observations and “k” is the size of the sample.

The Pearson correlation coefficient (r - eq. 3-30) is used to measure the strength of a linear association between two variables, where the value r = 1 means a perfect positive correlation and the value r = -1 means a perfect negative correlation.

$$r = \frac{\sum_{i=1}^k (for(i) - \overline{for})(obs(i) - \overline{obs})}{\sqrt{\sum_{i=1}^k (for(i) - \overline{for})^2}\sqrt{\sum_{i=1}^k (obs(i) - \overline{obs})^2}} \qquad (3\text{-}30)$$

Bias (eq. 3-31) and Normalized Bias (eq. 3-32) provide information about the systematic deviations between the two data sets while the Root Mean Square Error (RMSE - eq. 3-33) takes also into consideration non-systematic errors. Following the same terminology, these indexes are estimated by the relations:

$$Bias = \frac{1}{k}\sum_{i=1}^k [for(i) - obs(i)] \qquad (3\text{-}31)$$

$$Normalized\ Bias = \frac{1}{k}\sum_{i=1}^k \left|\frac{for(i) - obs(i)}{obs(i)}\right| \qquad (3\text{-}32)$$

$$RMSE = \sqrt{\frac{1}{k}\sum_{i=1}^k [for(i) - obs(i)]^2} \qquad (3\text{-}33)$$

Scatter Index, which is also used, is the RMS value normalized by the mean measured value.

A more sophisticated index used is the Nash-Sutcliffe model efficiency coefficient (NSE - eq. 3-34 - Nash et al., 1970; Wilks, 2006). The index varies from -∞ to 1, where 1 indicates the perfect match between observations and model predictions. A zero value suggests that the accuracy of the model is as good as the accuracy of the mean value of observations.

$$NSE = 1 - \frac{\sum_{i=1}^{k}[obs(i) - for(i)]^2}{\sum_{i=1}^{k}[obs(i) - \overline{obs}]^2} \qquad (3\text{-}34)$$

4 Intensity Duration and Frequency analysis: a gridded approach

Wind farm siting is approached today by generally accepted standards. High wind potential and site sustainability are among the most important requirements. However, these cannot always be compatible and this is the reason why, risk assessment techniques are needed. These techniques usually take into consideration various parameters including the impact of wind speed in a wind power project. The study of the wind speed probability distribution main body and upper tail is used for the estimation of the energy potential and the extreme wind events that characterize the area under consideration. A more sophisticated analysis on the behavior of the wind would require additional information. For example, persistent low wind speed events could cause several issues in electricity networks since several turbines are affected simultaneously.

Towards this way this chapter will focus on analysis of the Intensity and the Duration of non-frequent events focusing on the wind speed probability distribution lower and upper tail. The main objective is to define the probability of occurrence of such events in terms of return periods and quantify the associated uncertainties. This estimation can be approached by using the principles of Extreme Value Theory. Beginning with the investigation of the duration and the frequency of low wind speed events two approaches were followed, “Intensity Given Duration” (IGD) and “Duration Given Intensity” (DGI) method. At the same time, the intense wind speed events are studied through the first approach. Different tools and probability distributions are tested in order to quantify the uncertainties employed from the use of these methodologies. The convergence of the final results is discussed and the application in wider areas is tested. In the following lines, the basic facts and tools are discussed.

IGD provides more information simultaneously if compared with DGI, as the results are expressed through intensity–duration–frequency (IDF) curves (Durrans, 1998). The last are widely used in hydrology for the study of extreme precipitation events (Koutsoyiannis et al., 1998) or the frequency and the duration of droughts (Halwatura et a., 2015). IDF curves can be used also in wave climate characterization describing the relationship between sea state intensity, sea state duration and frequency (Sobey and Orloff, 1999). Considering wind, there is a variety of studies describing the upper tails of wind speed distribution in terms of return

periods (Palutikof et al., 1999; Larsén et al., 2015; Patlakas et al., 2015). Studies about low wind speed events are quite few. Deaves and Lines (1998) studied the frequency of low wind speed conditions oriented for risk assessments for hazardous installations. More specifically, they studied the effect of low winds on the dispersion of toxic or flammable gases. Continuing this work, Lines defined guidelines for the inclusion of low wind speed conditions into risk assessment techniques (Lines et al., 2001). Gadian focuses on the directional persistence of low wind speed that can affect the dispersion of pollutants (Gadian et al., 2004). Another approach, introduced by Leahy and McKeogh (2012), is focused on the implications of low wind speed persistence in wind power and contains the concept of both IGD and DGI methodologies.

In the present study, for the application of DGI and IGD, annual maxima/minima (AM) method (Cook, 1985) was used for the extrapolation in time. The area under consideration is a part of the North Sea and different regions in the Mediterranean Basin with rather high interest in offshore activities and energy applications.

The data employed in this work consists mainly of modeled time series, extracted from a database created by the Atmospheric Modeling and Weather Forecasting Group (AM&WFG—University of Athens) under the framework of Marina Renewable Integrated Application Platform (MARINA—Platform, http://forecast.uoa.gr/proj_marina.php,15). The use of the database has the advantage that wind speed values are available at different model levels/heights and cover a large area without missing values. At the same time, the spatial coverage allows neighboring points on the spatial grid to be used to test elements of the methodology. More information about this database is provided in a following section (data used).

The provided output forms alternative information concerning the climatology of the study area that is not widely used. Such information can be included in risk assessment techniques and can be applied among others for energy activities.

4.1 Data used

The data employed for the analysis is derived from the MARINA Platform database (see chapter 3.5.6). Wind speed of the third vertical level (80 m) of the atmospheric model used for the hindcast analysis is the quantity under consideration regarding the low wind speed events. The choice of this level is based on the fact that this is a computational layer of the model (no interpolation needed) and corresponds to the height used in most of offshore wind generators. Regarding the intensity duration and frequency of extreme wind speed events wind speed at 10m was chosen as this is a reference height in risk assessment.

The Intensity-Duration-Frequency methodology was applied both on the lower and upper tail of the wind speed probability distributions showing interesting results.

4.2 Low wind speed events

Regarding the behavior of low wind speed events, an explicit analysis will be performed and applied in a great part of the North Sea. Additional analysis will be performed in the offshore area on the South of France in order to test the robustness of the proposed methodology in a region with different climatic and microclimatic characteristics (it is affected both by cyclogenesis and by local winds - Mistral). Beginning with the first, the domain (51^{o}-60^{o}N, 5^{o}W-15^{o}E) is illustrated in Figure 4-1 (marked by a red box).

Figure 4-1: The Skiron –WAM coupling domain (grey box) and study area (red box).

4.2.1 Statistical Analysis - Evaluation

The main objective of this study is to present different approaches for the estimation of low wind speed periods based on modeled data. The length of observational time series in the area is not statistically adequate for the evaluation of the methodology. However, similar studies support the use of measurements for such applications (Leahy & McKeogh, 2012). So, despite the fact that the evaluation of the model is not the first priority of this work (it has been performed in other works – Kalogeri et al., 2017), a short statistical analysis is included to support the use of it for extreme persistence statistics. Therefore, the purpose of this chapter is not to discuss the model performance in detail but to illustrate some local characteristics and how they are recorded in the model output and observations. In particular, measurements are derived from three different sources. The first is the offshore research platform FINO 1 used for

studying environmental conditions for wind power applications in the German North Sea. The second is the meteorological mast at the site of the Docking Shoal Farm. The third source of measured data is the Greater Gabbard offshore wind farm located around 22 km east of Suffolk coast. The quantity to be evaluated is the 80 m wind speed. The locations of the stations are presented in Figure 4-2.

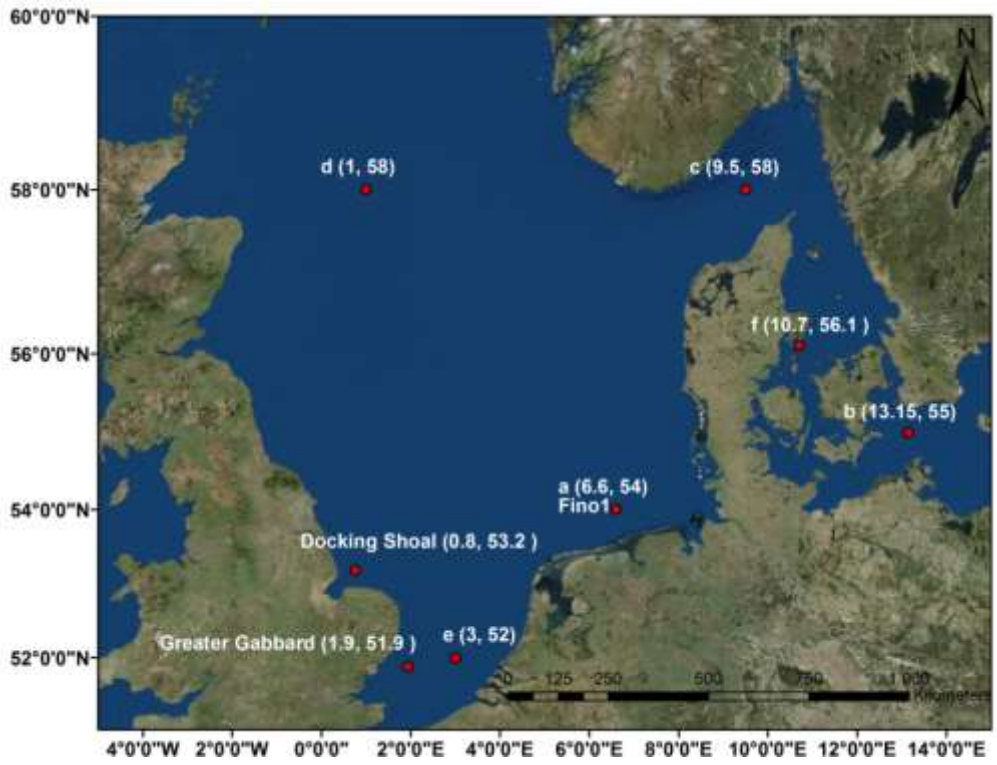

Figure 4-2: The area of interest and the coordinates of the five selected locations for the application (a, b, c, d, e), the test location for the estimator selection (f) and the offshore platforms FINO 1, Docking Shoal, and Greater Gabbard.

It should be noted that modeled parameters are smoothed, during the integration procedure, over the corresponding timestep (15 sec. in our case). From these values the model provides/stores outputs on an hourly basis without any further smoothing or averaging. In addition, the observations used are 10-minute wind speed averages paired with the modeled data.

Different statistical indexes and graphical analyses were utilized such as Coefficient of Determination (R^2), Bias and Normalized Bias and Root Mean Square Error. The results of the

statistical analysis reveal a rather good agreement between the model and the station for all three cases. In Table 4-1, these basic statistical indexes are provided for the station under consideration.

Table 4-1: Statistical analysis of the Modeled wind speed against FINO 1, Docking Shoal and Greater Gabbard platforms

	Fino 1	**Docking Shoal**	**Greater Gabbard**
RMSE (m/s)	2.7965	2.613	2.568
Correlation Coefficient	0.799	0.821	0.826
R^2	0.638	0.674	0.6823
Bias (m/s)	-0.044	-0.453	-0.472
Normalized Bias	0.113	0.052	0.054

The low Bias indicates the non-existence of systematic errors. Higher values (within acceptable limits though) of the other indexes are associated with system noise. The deviation of the two datasets is a result of the smoothing effects associated with the atmospheric model temporal and spatial resolution and physical parameterization. RMSE is always high in such model analysis. It is affected by temporal variations and high values and can be attributed among others to phase errors (Ardhuin et al., 2006). Such errors are not considered as crucial in our analysis since we focus mainly on the climatic characteristics. The last is the reason why a comparison regarding the probability distribution of the samples is also needed. It is found that the model compares quite well, focusing on low wind speeds, giving acceptable response (Figure 4-3).

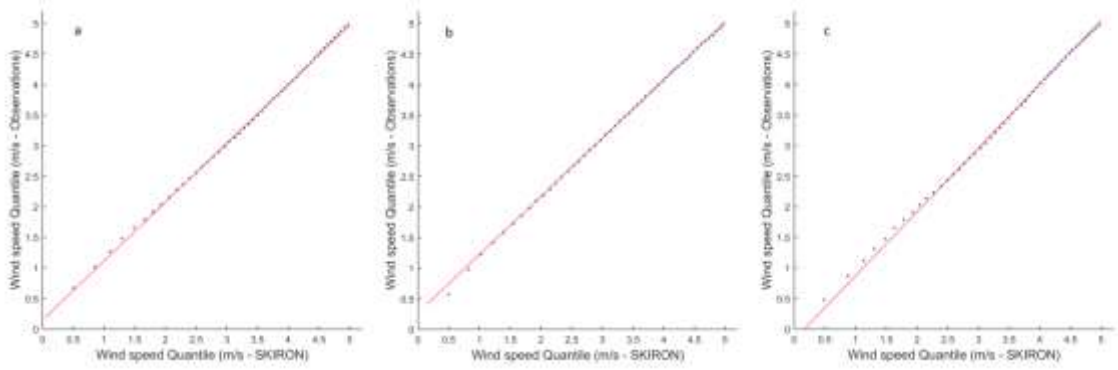

Figure 4-3: Q-Q plots between Marina database (wind speed – 80m) and FINO 1 (a), Docking Shoal (b), and Greater Gabbard (c) platforms.

Issues associated with the modeling capabilities of wind speed in general are well known. The main purpose of this work is not to study wind speed variability but to identify periods of low wind speeds. In order to define the durations of low wind speed events, the wind speed of 3 m/s was selected because this is the operational threshold for many wind turbines. The total annual events with wind speed below this threshold are presented with respect to their duration (from 2 hours to the longest duration) in Figure 4-4. The year of 2006 of FINO 1 data is chosen as an indicative example because in this case the missing values of the observations are limited.

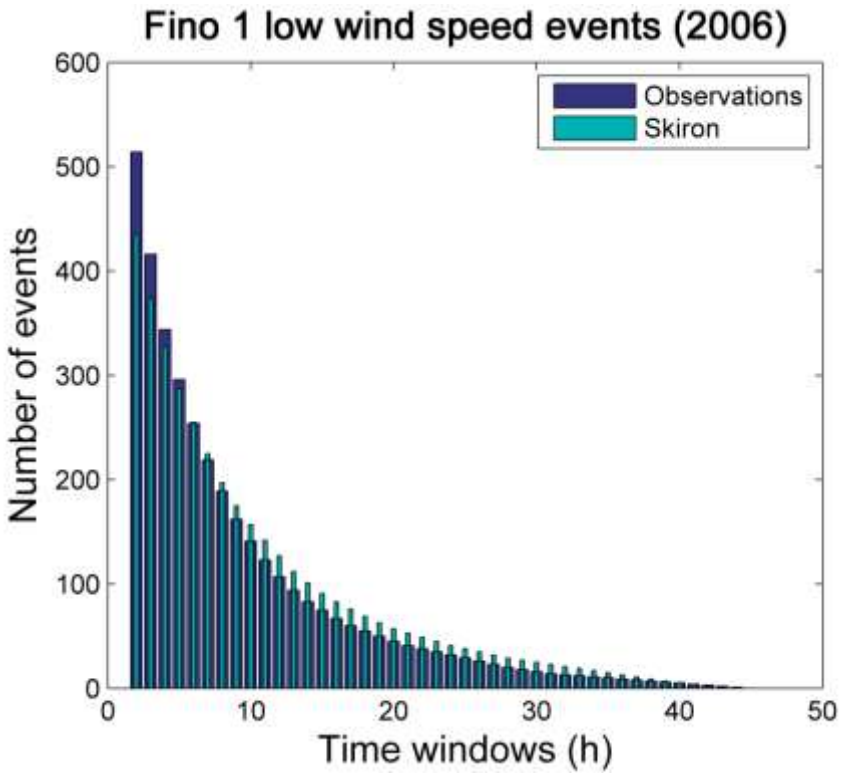

Figure 4-4: Duration of low wind speed events (<3m/s) based on the dataset of Skiron-Marina and the measurements of Fino1 for the year of 2006.

It is observed that for the low wind speed events between the modeled timeseries and the observations show a good agreement. At the same time an underestimation of the model concerning the short period events is clear, while for longer periods there is a slight overestimation. The existence of large amounts of missing measurements creates difficulties in this type of comparison as the wind speed down- and up- crossings of the selected threshold is a

precondition for the definition of low wind speed events. It should also be noted that some types of anemometers face problems measuring such low wind speeds. At the same time, the sampling rate can affect the estimation of the duration of low wind speed events as considered here. However, the errors imported from it are not significant since it is well known that light wind conditions show consistency in terms of intensity.

The lack of availability of at least 10-year measurements with no (or small amount of) missing data, causes significant problems in the application of the methodology. This combined with the fact that the atmospheric models provide the needed parameters in multiple grid points (giving a spatial distribution of them), supports the use of modeled results. So, despite the already mentioned differences, the study is based on a mesoscale modeling system database since in the present work the main objective is to discuss different methodologies and approaches for estimating low wind speed events.

4.2.2 Intensity Given Duration approach

Intensity Duration Frequency probability plots

Low wind speed conditions are always associated with weak pressure gradients encountered often in anticyclonic systems over NE Atlantic and Northern Europe. In addition to the above, the area under consideration is offshore and rather homogeneous. These facts can lead to the assumption for similar behavior over relatively large regions. Therefore, it is expected that the outcome of the applied methodology from neighboring model grid points should be similar. In this study, five different characteristic areas have been identified and used for further analysis. The selected areas have been chosen according to the mean wind speed, the distance from the coast and the fetching range. For each of these areas, a square consisting of three consequent points for each side was used (nine points in total).

Using this dataset, probability Intensity Duration Frequency analysis was performed. This analysis can be used to estimate the robustness of different techniques for the estimation of the distribution parameters. This can be achieved through the spread of the raw outcome (before the fit of the second-degree polynomial), among the nine neighboring grid points as illustrated

via probability plots. The methodology is used for the selection of the better estimator for this area among the Method of Moments (MoM) and Maximum Likelihood (ML). An example of a near-shore location (location f in Figure 4-2) is depicted in Figure 4-5. In this case, MoM shows a slightly higher deviation concerning the outcome of neighboring points. Apart from the graphical comparison, the values under study have been fitted to a 2nd degree polynomial and the corresponding spread is quantified by standard statistical measures (R^2). The above reveal a slightly better behavior of ML (0.83 /0.80), but with a small difference.

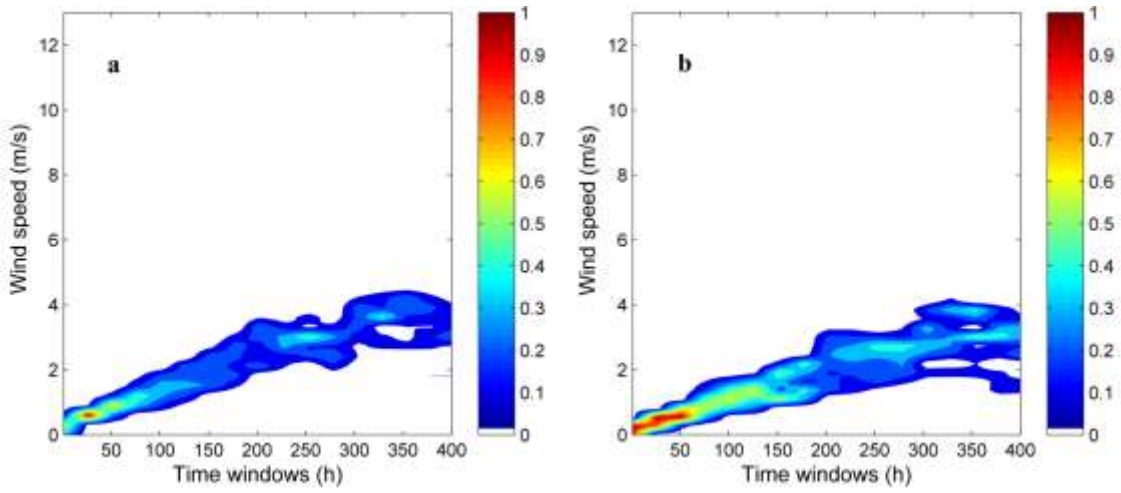

Figure 4-5: Intensity Duration Frequency Probability plots using ML (a) and MoM (b) methodologies (20-year return period) for a nearshore location (10.7 E, 56.1 N – location f in Figure 4-2).

In general, bigger differences were found in locations surrounded by land. Considering this, the result could be that MoM may face problems when applied in areas with lower winds. It is known that in light winds, geostrophic control becomes weak and the land-water distribution becomes relatively more important in determining the wind field. The last can lead to the conclusion that the local climate of near-shore areas may affect the fitting capabilities of MoM and lead to different behavior of neighboring locations. All these come into agreement with previous work (Zhang et al., 2004; Katz et al., 2002; Smith, 1989) suggesting that ML method is easily adaptable to include effects of covariates, or other influencing factors. For this reason and

after a number of corresponding sensitivity tests, it was decided that the Maximum Likelihood method is more suitable for this study.

Another important use for the IDF probability graphs would be to quantify uncertainties associated with the spatial distribution of low wind speed events. In this way, the area of interest is described combining the wind speed threshold with the total duration of the event and the probability distribution as confidence interval limits. The probability plots are applied in the fitting curves for the five preselected areas and displayed in Figure 4-6.

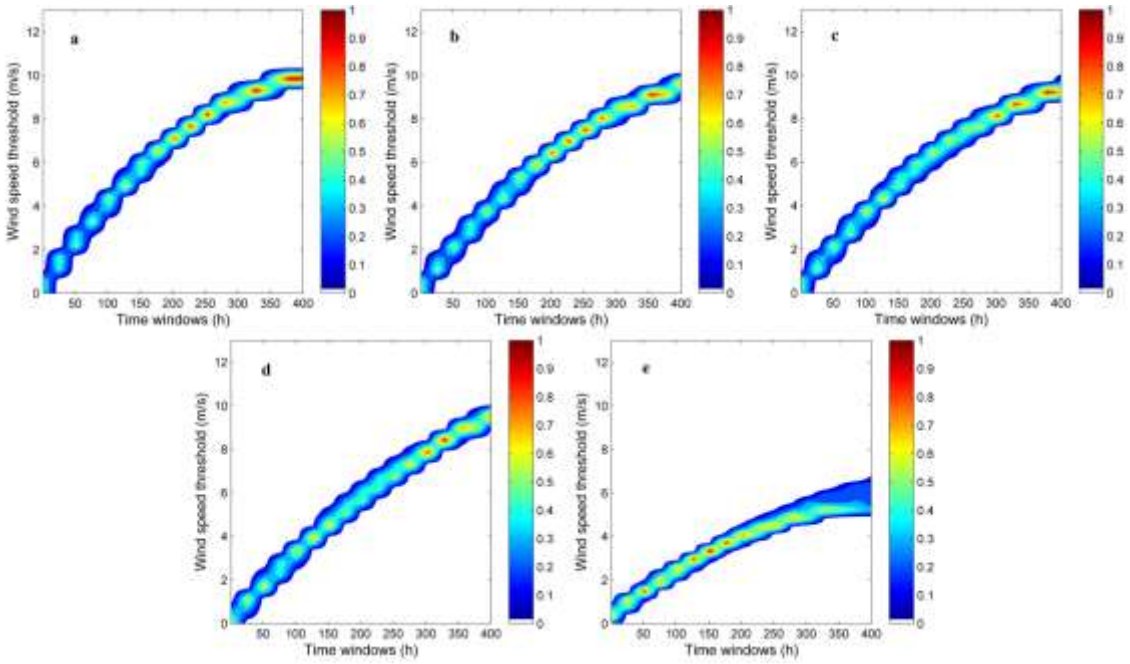

Figure 4-6: Intensity Duration Frequency Probability plots for the five selected locations (20-year return period).

A conclusion that could be reached by taking a closer look to these probability plots is that in case e (the location is shown in Figure 4-2) there is a relatively large spread that corresponds to a wider confidence interval mainly in higher durations. The reason for this behavior is the location of this area and the specific climatic characteristics as mentioned before. The position is surrounded by land with an open to the North. The land blocks high winds and therefore the mean wind speed has smaller values as compared with North Sea in general. At the same time

local winds dominate the location. As mentioned earlier, in light wind conditions, land-sea interaction becomes considerable and affects the large-scale flow. The influence is more obvious in higher return periods. However, higher deviations are observed in longer durations that correspond to stronger winds. This does not affect the analysis presented in this thesis, as lower winds are the main interest. Concluding, it should be noted that a similar procedure could be used for larger areas and more grid points depending on the needs of the study.

Intensity Duration Frequency curves

The establishment of the relation between the duration, the intensity and the frequency of occurrence of a low wind speed event is represented through the IDF curves. The IDF curves of events associated with wind speed probability distribution lower tail for 20 years return period and the corresponding confidence interval are illustrated in Figure 4-7. The confidence intervals have been calculated by utilizing the corresponding intervals of the PDF parameters as estimated by the fitting procedure (ML). The curves tend to bend asymptotically, something that was rather expected. For larger time windows, the highest observed speed should be higher but with a decreasing rate. It is also observed that, for point e, the IDF curves reach a maximum value considerably smaller than the other test cases. A conclusion that can be reached is that this area is characterized by low wind speed events that show persistence and/or higher frequency of occurrence as compared with the other test cases. The comparison of the four remaining cases revealed a consistent pattern despite the different local characteristics. However, location d is characterized by a lower curvature. This can be attributed to the fact that it is a deep offshore area, and because there are not land barriers, it is highly exposed to the synoptic systems passage. The synoptic systems of North Atlantic are well known for moving fast and formatting sharp pressure gradients. Locations a, b and c show similar behavior, although it would be expected to observe larger deviations due to the local climate conditions and particularly the sea–land interaction. This shows a persistence in the characteristics of the IDF curves in near shore locations.

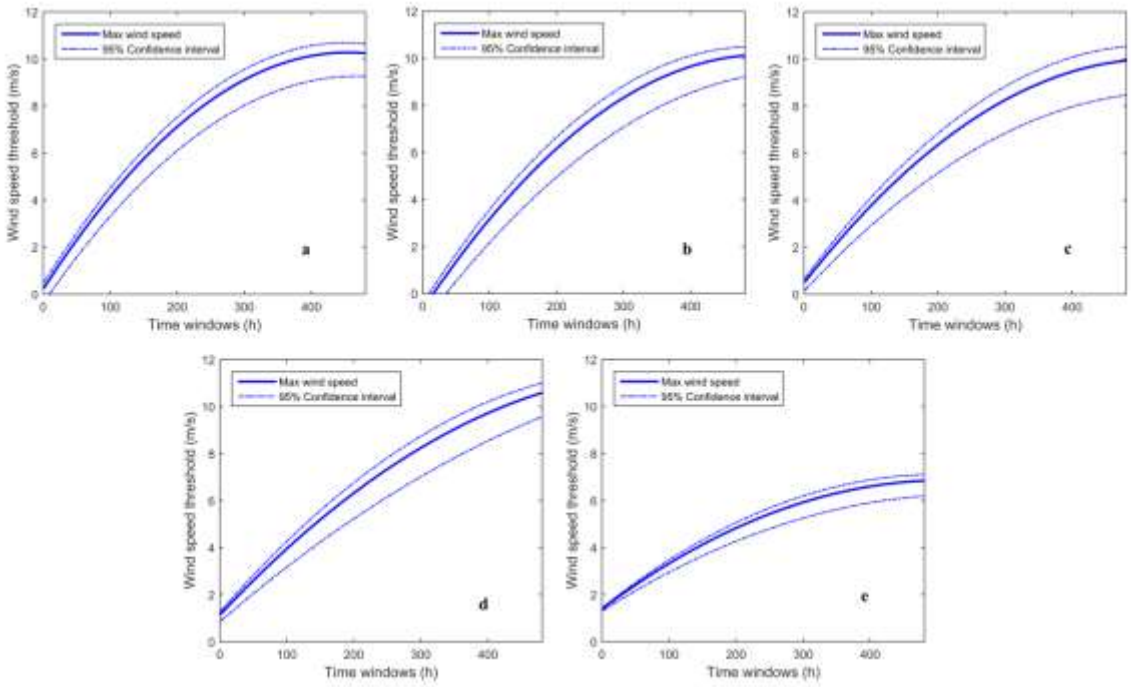

Figure 4-7: Intensity Duration Frequency curves and the associated confidence intervals for the five selected locations (20-year return period). The confidence intervals have been calculated by utilizing the corresponding intervals of the PDF parameters as estimated by the fitting procedure (Maximum Likelihood). The maximum expected wind speed over a low wind speed event is referred here as wind speed threshold to be in conjunction with DGI method.

The IDF curves for the fourth and fifth test case for different return periods (2, 5, 10, 20 and 50 years) are shown in Figure 4-8. As expected, the relative positions of the curves with different return periods lead to the conclusion that low wind speed events are less likely to happen for higher durations. From another point of view, such events are expected to last more for higher return periods. At the same time, wind characteristics seem to affect the shape of the IDF curves as the low-wind-speed-event probability of occurrence is obviously higher in the second case (location e).

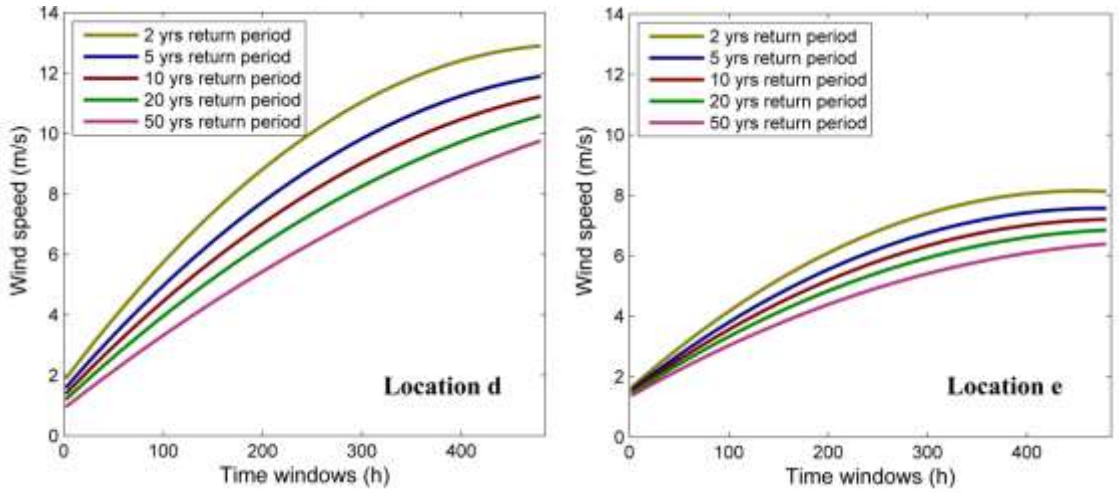

Figure 4-8: Intensity Duration Frequency curves for Locations d (left) and e (right) and different return periods.

Spatial distribution of low wind events

The application of the procedure introduced in the previous steps to the whole area of study led to a series of maps describing the spatial distribution of the three parameters (see eq. 4.1-5) used for the IDF curves. The coefficient of x^2 (α) can take negative values and in some cases, values close to zero. In these cases, the parabolic curve part used for the fit of IDF curves is open downward. In some single cases, mainly near shore the value of α is close to zero and the curve tends to become linear. The linear coefficient of x (β) takes some negative and more positive values. When the coefficient takes positive values, the line will shift towards the left-bottom and vice versa. The combination of the linear and the nonlinear terms shows how fast the curve will bend and determines the point where the upper wind speed threshold will not change dramatically for larger time windows. More precisely, the coefficient γ determines whether the curve shifts upward or down. The value of γ is in fact the value where the curve intersects the y-axis. It is obvious that everywhere it is below the selected threshold of 3 m/s used for the definition of low wind speed events, which means that such events are more than likely to happen. The negative values mean that the curve will intersect the positive part of x-axis and wind speed will be constantly close to zero for several hours (for the defined return period). These parameters can be used for the creation of IDF curves throughout the used domain. Their spatial distribution supports the above discussion and is depicted in Figure 4-9.

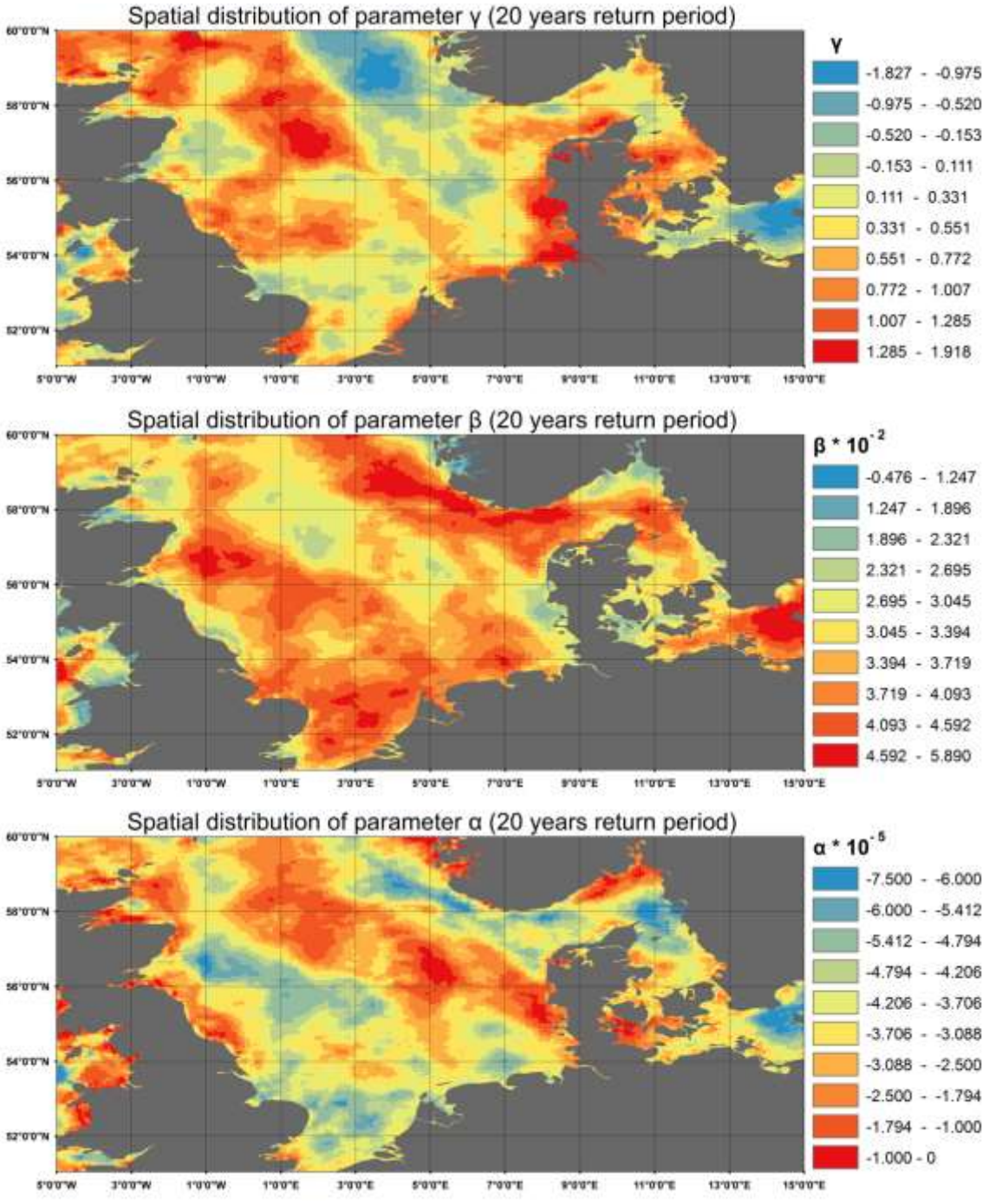

Figure 4-9: Spatial distribution of the three parameters used for the Intensity Duration Frequency curves.

The noticeable spatial distribution of the parameters will change the shape and the characteristics of the IDF curves. These parameters can be used for the solution of the 2nd

degree polynomials for 3 m/s (f(x)=3), for each point. The outcome is the maximum (statistically) consequent no-energy production period with a recurrence interval of 20 years (Figure 4-10). It can be easily observed that in the open sea, a low wind speed event can last up to 4-5 days with a recurrence interval set to 20 years. The values rise near shore and reach to more than ten-day periods. This increase is generally expected in gulfs and areas where the wind shadow effect of land affects the wind intensity overseas. At the same time there are some single cases where low wind speed events can last up to 20 days. This is caused by the interaction of complex terrain (with high altitude variations near the shore, especially in the Scandinavian Peninsula) with the atmosphere and the effects of this in the configuration of the model. On one side, the flow near the coast and especially in areas with significant topographic barriers or complex coastline is rather complicated due to dynamical and thermodynamical effects (eg. channeling, sea-land barriers, boundary layers). On the other side, the mesoscale models fail to reproduce such details in flow structure due to the model resolution used and in general due to the configuration. In this case the observed discrepancies can be attributed to both.

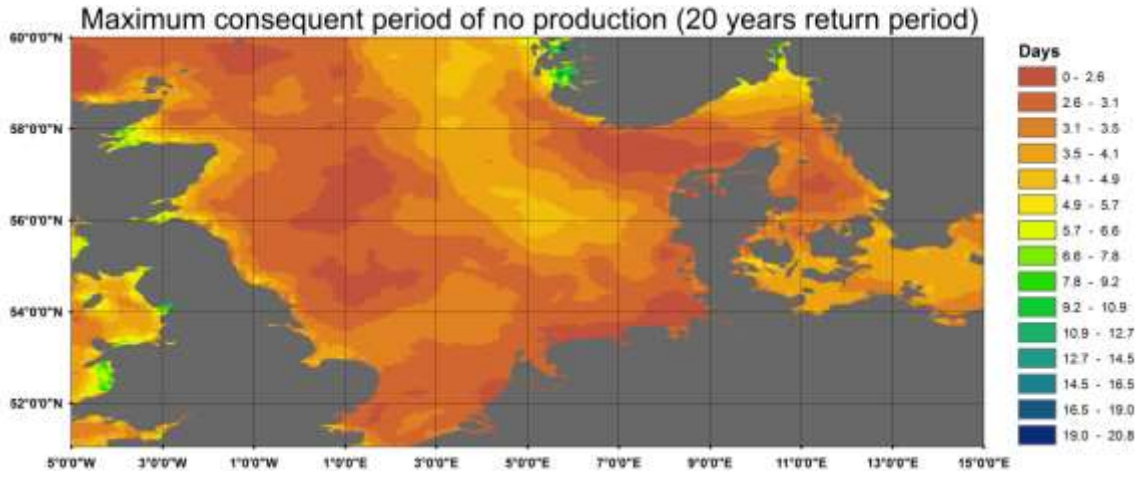

Figure 4-10: Maximum consequent hours of no energy production with 5% annual probability of occurrence.

4.2.3 Duration Given Intensity approach

For the Duration Given Intensity (DGI) approach, multiple distributions such as Gumbel, Generalized Extreme Value, Weibull and Rayleigh, were used for the extrapolation of the low wind event duration. The application was made for the five preselected areas used previously. The outcome of Intensity Given Duration (IGD) approach for the threshold of 3 m/s is used as a measure for comparison. The results for different return periods are shown in Table 4-2.

Table 4-2: DGI and IGD results (duration in hours) for the selected locations (20, 30, 40 and 50 years return period).

	Duration Given Intensity								**Intensity Given Duration**			
	Gumbel				**G.E.V.**							
	20 yrs	***30 yrs***	***40 yrs***	***50 yrs***	***20 yrs***	***30 yrs***	***40 yrs***	***50 yrs***	***20 yrs***	***30 yrs***	***40 yrs***	***50 yrs***
a	61.4	65.5	68.4	70.6	58.9	62.5	65	67.1	68.1	75.7	81.3	85.9
b	90.5	97	101.5	105.1	97.3	105.7	111.8	116.5	95	106	114	121
c	67	71.1	74	76.3	61	63.1	65.2	66.1	74	84	91	97
d	52.4	55.3	57.4	59	76.5	87.6	96.6	104.3	64.4	73.3	80	86.3
e	55.6	57.5	58.8	59.8	108.7	134.8	157.2	177.7	81.7	88.6	94	98.5
	Weibull				**Rayleigh**							
	20 yrs	***30 yrs***	***40 yrs***	***50 yrs***	***20 yrs***	***30 yrs***	***40 yrs***	***50 yrs***				
a	59.5	62	63.6	64.8	68.1	72.6	75.6	77.9				
b	85.3	89.1	91.6	93.5	96.1	102.4	106.6	109.8				
c	68	70.8	72.7	74	78.3	83.4	86.9	89.5				
d	46.8	48	48.7	49.3	61.5	65.6	68.3	70.3				
e	50.6	51.2	51.5	51.8	76.9	82	85.4	87.9				

For a better understanding of the behavior of the DGI approaches, a normalization based on the intensity given duration methodology was employed and presented in Table 4-3. More specifically, the result is derived as:

$$p = \frac{k_2 - k_1}{k_1} \cdot 100\% \qquad (4\text{-}1)$$

where k_2 stands for DGI method and k_1 for IGD. It is obvious that both the use of Gumbel and Weibull distribution lead to a constant underestimation as compared to IGD method. This underestimation tends to become more significant in greater return periods and shows a lower exponentiality. Concerning the application of G.E.V. distribution there is not a particular pattern

on the behavior of the results. The major issue to be mentioned though, is that the analysis resulted to up to 80% higher values for the fifth case study. This is a result of the fact that the shape parameter in this case (one of the three parameters to be estimated) is not limited. This is in contrast with Gumbel, for example, where the shape parameter is equal to zero. This can lead to a "bad" distribution behavior in some cases, depending on the characteristics and the size of the sample. At this point it should be noticed that in this application, only ten values were used (annual maxima) that is the lowest limit of the input size recommended for such applications (Cook, 1985).

Table 4-3: Normalized differences between DGI and IGD results for five locations (20, 30, 40 and 50 years return period).

Duration Given Intensity								
	Gumbel				**G.E.V.**			
	20 yrs	***30 yrs***	***40 yrs***	***50 yrs***	***20 yrs***	***30 yrs***	***40 yrs***	***50 yrs***
a	-9.8 %	-13.5 %	-15.9 %	-17.8 %	-13.5 %	-17.4 %	-20.0 %	-21.9 %
b	-4.7 %	-8.5 %	-11.0 %	-13.1 %	2.4 %	-0.3 %	-1.9 %	-3.7 %
c	-9.5 %	-15.4 %	-18.7 %	-21.3 %	-17.6 %	-24.9 %	-28.4 %	-31.9 %
d	-18.6 %	-24.6 %	-28.2 %	-31.6 %	18.8 %	19.5 %	20.78 %	20.9 %
e	-32.0 %	-35.1 %	-37.4 %	-39.3 %	33.0 %	52.1 %	67.2 %	80.4 %
	Weibull				**Rayleigh**			
a	-12.6 %	-18.1 %	-21.8 %	-24.6 %	0.0 %	-4.1 %	-7.0 %	-9.3 %
b	-10.2 %	-15.9 %	-19.6 %	-22.7 %	1.2 %	-3.4 %	-6.5 %	-9.3 %
c	-8.1 %	-15.7 %	-20.1 %	-23.7 %	5.8 %	-0.7 %	-4.5 %	-7.7 %
d	-27.3 %	-34.5 %	-39.1 %	-42.9 %	-4.5 %	-10.5 %	-14.6 %	-18.5 %
e	-38.1 %	-42.2 %	-45.2 %	-47.4 %	-5.9 %	-7.4 %	-9.1 %	-10.8 %

Another important issue, that is worth mentioning, is the better results obtained with the use of Rayleigh distribution. The highest difference reaches 18.5%, while for Gumbel (that is a more popular distribution used in AM method and similar applications) it reaches 39.3%. At the same time in most of the cases, the difference is lower than 10% and within the confidence intervals of both methodologies namely IGD and DGI. It should be mentioned also that the exponentiality in DGI method is higher if compared to IGD since for higher return periods the growing ratio is obviously smaller in the first case. Despite the acceptable results, the method is case sensitive and the use in other areas (with different climatic characteristics) requires a prior analysis similar to the one performed here.

4.2.4 Robustness test in an area with different characteristics

The same methodology was followed for a second area (Figure 4-11) with slightly lower winds and specific wind patterns. The selection of this particular region for the study is done due to the high wind energy potential and the strong interest for sustainable energy investments. It is characterized by intense anthropogenic activity, biodiversity and a variation concerning the sediment characteristics, factors that may affect a potential installation of wind turbines. In terms of wind climatology, the selected area is highly affected by cyclogenesis and local winds (Mistral). This additional application is performed in order to test the robustness of the methodology and potential differences among the two cases studies.

Figure 4-11: Study area and location of the points used in the study.

In the following lines the results will be presented briefly as everything was analyzed extensively above. Beginning with the behavior of the IDF curves (Figure 4-12), three selected locations with different characteristics were utilized. In the first two locations the tendency for bending is quicker, which is associated with the climatology of the area. Low winds can be

associated with weak pressure gradients, often encountered in anticyclonic systems. Location 3 is highly affected by local winds (mistral) that cause a lower probability of persistent low wind events appearance.

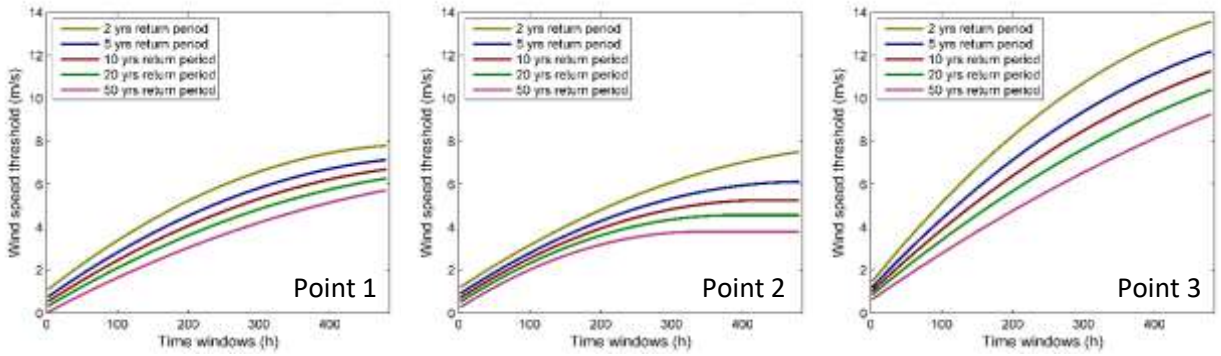

Figure 4-12: Low wind speed events IDF curves for the three selected locations.

Noticeable spatial variability concerning the parameters for the IDF curves is also observed in this area leading to variations in the duration of low wind speed events (Figure 4-13).

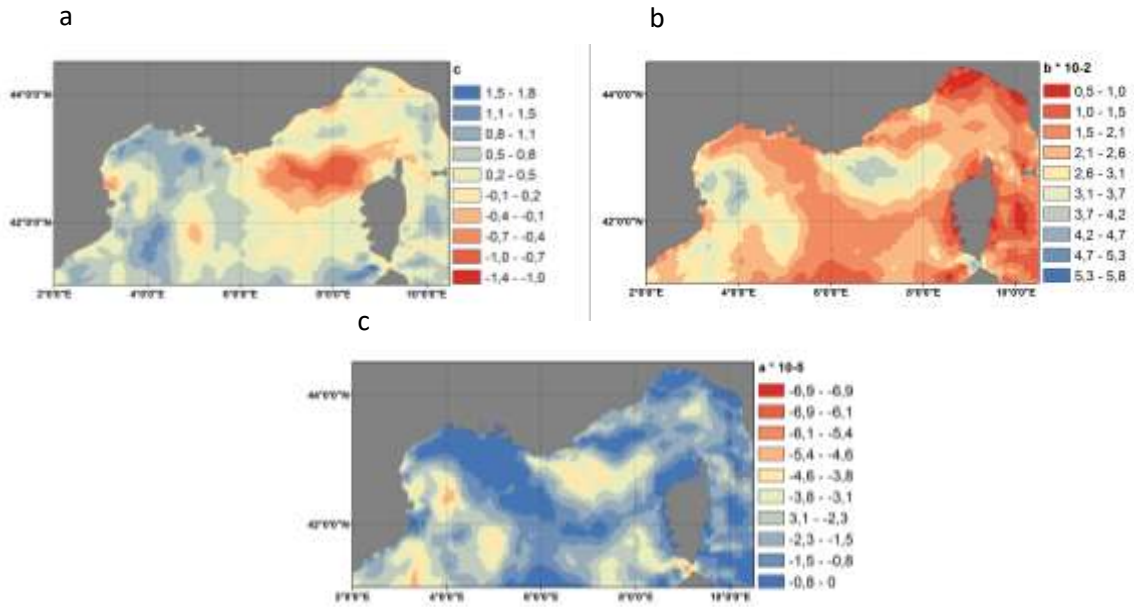

Figure 4-13: Spatial distribution of the three parameters used for the Intensity Duration Frequency curves

In order to keep a consistency with the previous results, the second-degree polynomials are solved for the value of three leading to the estimation of the duration of an event where wind speed remains constantly below 3 m/s (Figure 4-14).

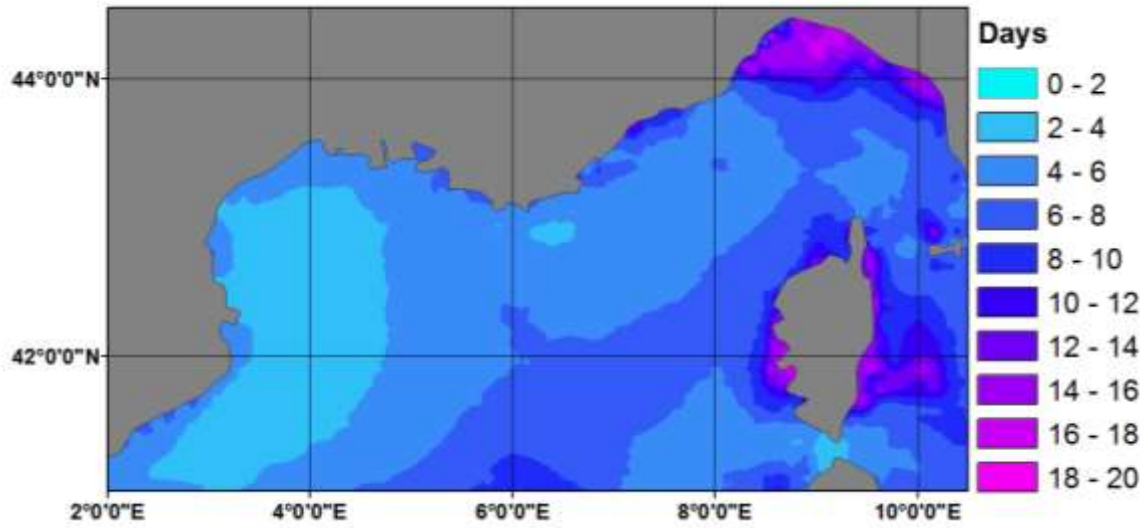

Figure 4-14: Duration of low wind speed events (wind speed <3 m/s) with a probability of occurrence equal to 5%.

Among the results it is quite obvious that low wind speed events may last up to 4-5 days in the open sea with a return period equal to 20 years. These values rise near shore to ten-day periods due to wind shadow effect. The last is related with complex terrain and the corresponding effects in the model configuration. Near the Gulf of Lion or in the straight between Corsica and Sardinia low wind speed events are less likely to happen due to the effect of mistral and wind channeling effects.

Following the same procedure, the DGI methodology is tested against the IGD using thee different probability distribution functions for the fit, Gumbel, Weibull and Rayleigh (Table 4-4).

Table 4-4: DGI and IGD results (duration in hours) for the selected locations.

	2 yrs	5 yrs	10 yrs	20 yrs	50 yrs	2 yrs	5 yrs	10 yrs	20 yrs	50 yrs
	DGI - Gumbel					DGI – Weibull				
1	45.1	51.8	56.8	61.8	64.5	44.8	50.5	53.1	55.1	57.3
2	85.5	101.7	114	126.3	142.6	83.1	102.9	112.7	120.4	128.9
3	88.2	109	124.8	140.6	161.4	85.6	106.3	116.5	124.6	133.5

	DGI - Rayleigh					IGD				
1	37.2	56.7	67.8	77.3	88.3	40.8	55.3	68	83.4	110.3
2	71.3	108.7	130	148.3	169.5	90.9	111.7	128	146.7	178.8
3	73.6	112.2	134.2	153.1	175	81.9	108.9	131	156.1	195.7

It is found that Gumbel and Weibull distribution lead to significant differences up to 70% for Gumbel and 90% for Weibull respectively while good results obtained with the use of Rayleigh distribution. The differences are significantly lower mainly in cases 2 and 3, which supports the use of it. In any case it is proven that the method is case sensitive and the use in other areas requires a corresponding prior analysis.

This particular region will also be used for the discussion of wind speed distribution upper tail in relation with the duration and the frequency of the events.

4.3 Extreme wind speed events

Extreme wind speed events may cause several problems in different sectors and even pose threat to life. The frequency and intensity of such events alongside their duration may affect various sectors such as civil protection, construction, tourism, offshore and coastal applications, insurance and reinsurance, shipping and transport. Similar applications are widely performed for other environmental parameters. The intensity, duration and frequency of precipitation is used in hydrometeorological applications both from a scientific perspective and a practical one. It can lead to the application of targeted mitigation measures in order to minimize the likelihood of floods to occur. Another application is in heatwaves where extreme temperatures may persist for several days. The application in extreme winds is not quite common and therefore the duration of extreme wind speeds is discussed thoroughly in the following pages.

The analysis is performed by adopting similar methodologies as in low wind speed events. The intensity, duration and frequency of extreme wind speed events are discussed through the “intensity given duration” approach.

4.3.1 Intensity Given Duration approach

Following the same steps with some differentiations as these were described in the beginning of the chapter, the Intensity Duration and Frequency curves of extreme winds were studied. The same area as in the application of low wind speed events was also used here (Figure 4-11). This was mainly selected for its high wind energy potential. Additionally it would be interesting to be able to compare the results among the low and extreme wind speed events. This additional information can be useful in risk analysis for offshore installations.

Beginning with the IDF curves (Figure 4-15), extreme winds reach 35 m/s for Locations 1 and 2, something obviously affected by wind channeling. In the 3rd case, higher values were expected due to the impact of Mistral. However, due to the land interaction the local winds effects are not obvious nearshore.

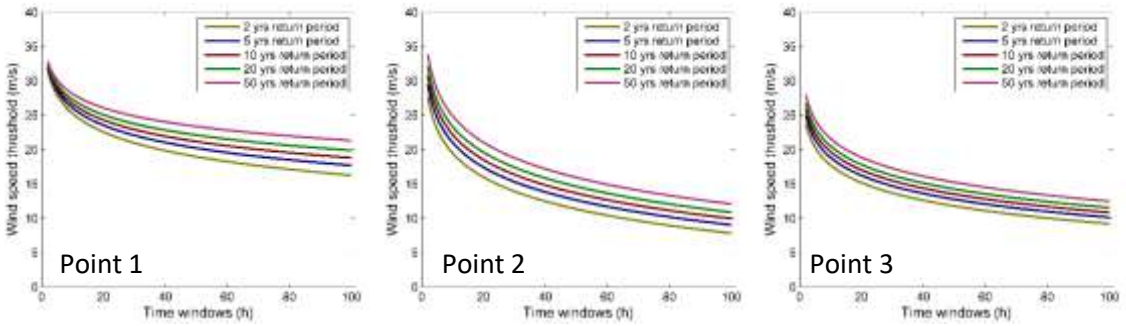

Figure 4-15: Extreme wind speed events IDF curves for the three selected locations.

The selection of a duration that is equal to 1 will lead to the classical approach of AM that is used for the estimation of an extreme event occurrence interval. Additionally, the selection of a particular return period can lead to an extreme wind atlas for the area under consideration. This is performed here for the return period set to 20 years (Figure 4-16) while the results are compared against the other widely used methodology, POT (Figure 4-17).

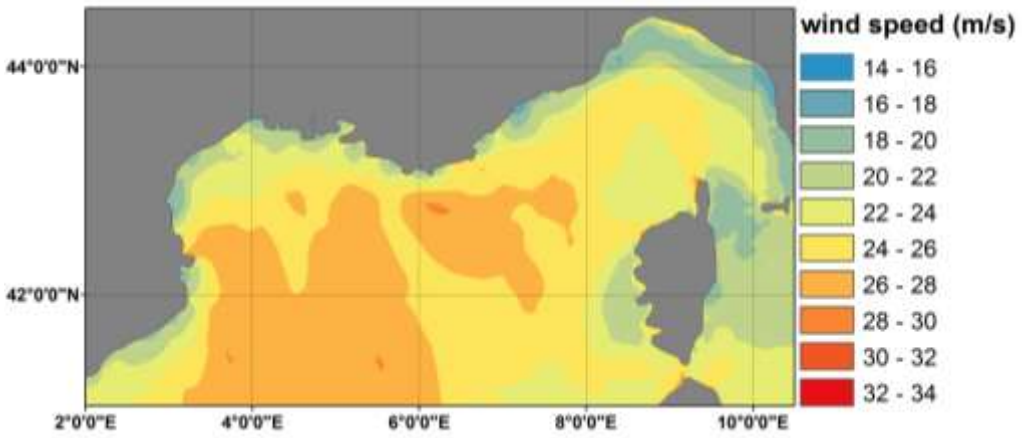

Figure 4-16: Extreme wind speed Atlas based on AM methodology (20 years return period)

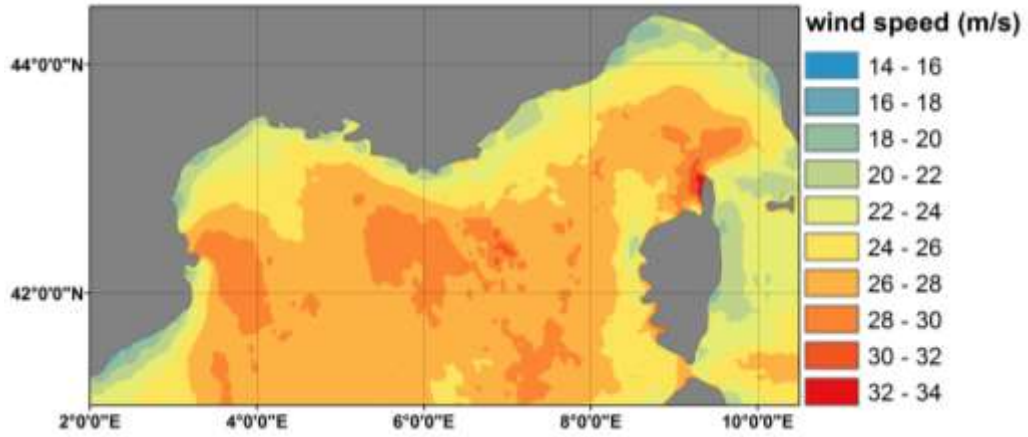

Figure 4-17: Extreme wind speed Atlas based on POT methodology (20 years return period)

Values up to 34 m/s are observed mainly in the open sea while smaller values are found nearshore as expected. The extreme wind speed spatial distribution is quite similar among the two methods. At the same time there is an obvious underestimation of the extreme values using AM method as compared to POT. This is due the fact that only 10 values are used (10-year dataset). On the other hand, POT takes into consideration also the secondary maxima, which leads in a thicker distribution tail in contrast to AM. From another perspective, information about wind speed characteristics of an area can be extracted (Patlakas et al., 2015). The climate of the area is influenced by both synoptic and local conditions and is characterized by strong

winds under certain circumstances. The Mediterranean region on the South of France and Spain is characterized by intense cyclogenesis while a strong and frequent wind pattern is often developed on the south coasts of France affecting a wide offshore area, the Mistral winds. These winds are channeling along the valleys of continental France and end up at the Gulf of Lion. Once they meet the ocean, they accelerate due to the smaller drag values and at the same time they produce big waves that travel for kilometers towards the South. These wind systems of this region form general conditions characterized of moderate to high frequency of appearance. These characteristics lead to the conclusion that the use of POT method will produce higher extreme wind speed values as compared to AM for this area. This comes also into agreement with Figures 4-16 and 4-17.

An attempt to test the same methodologies in an onshore location was made. The effect of the topography, the local climate and the air-land-sea interaction can affect the analysis. This is the reason why the proposed methodology was applied in an area covering the island of Crete, Greece. For the in-situ analysis, one onshore and two offshore locations were selected (Figure 4-18).

Figure 4-18: Study area and locations used.

The results are found to be similar as before. Higher values are observed over the sea with extreme events to last for several hours for all return periods (Figure 4-19). For example, 20 m/s may persist for more than 10 hours with a repeatability of 50 years. 80% lower winds are observed in the onshore location compared to the other two.

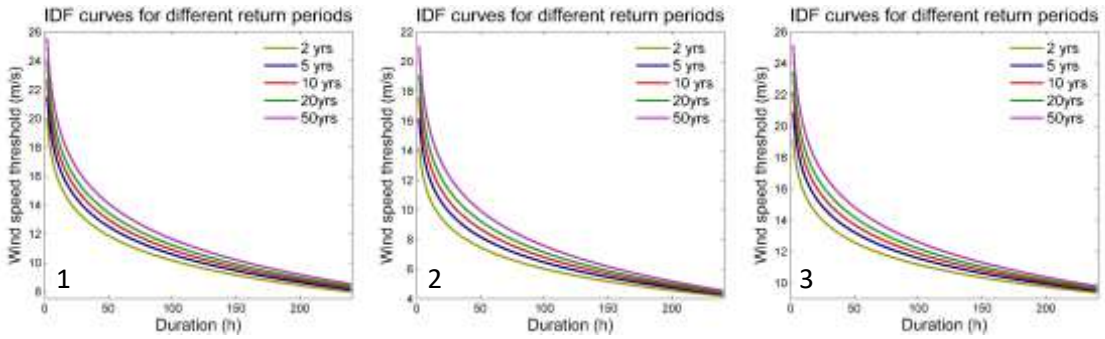

Figure 4-19: Extreme wind speed events IDF curves for the three selected locations.

Towards an application regarding the whole domain, the parameters for the IDF curves are characterized by similar patterns while there is an increased spatial variability especially over land (Figure 4-20). The last can be attributed to the interaction with land and complex terrain in general.

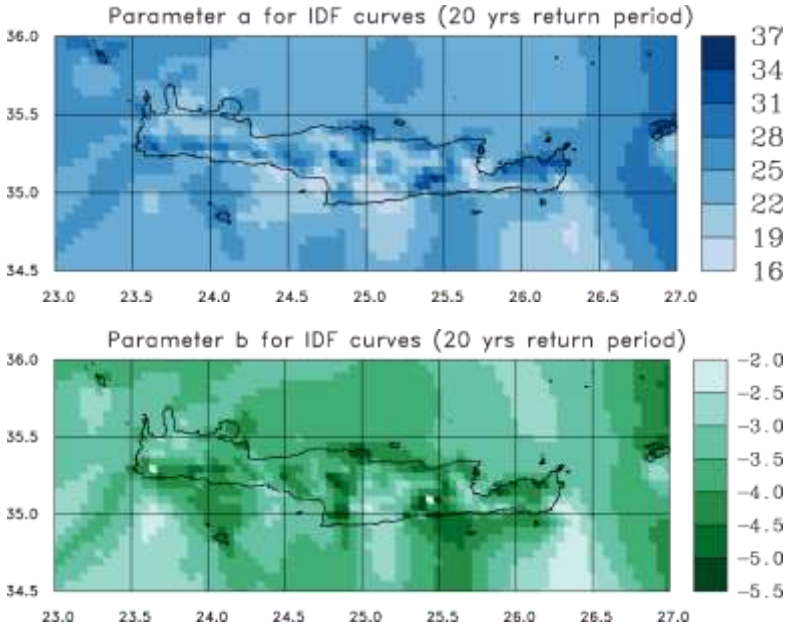

Figure 4-20: Parameters of the logarithm function applied in the IDF output.

Solving the equation for duration equal to 1 and selecting a particular return period can lead to the production of an extreme wind Atlas (Figure 4-21). Extreme wind speed varies from 17 to 35 m/s for the area under study for both methods. At the same time POT results seem to overestimate extreme values as compared to AM method results something also discussed earlier.

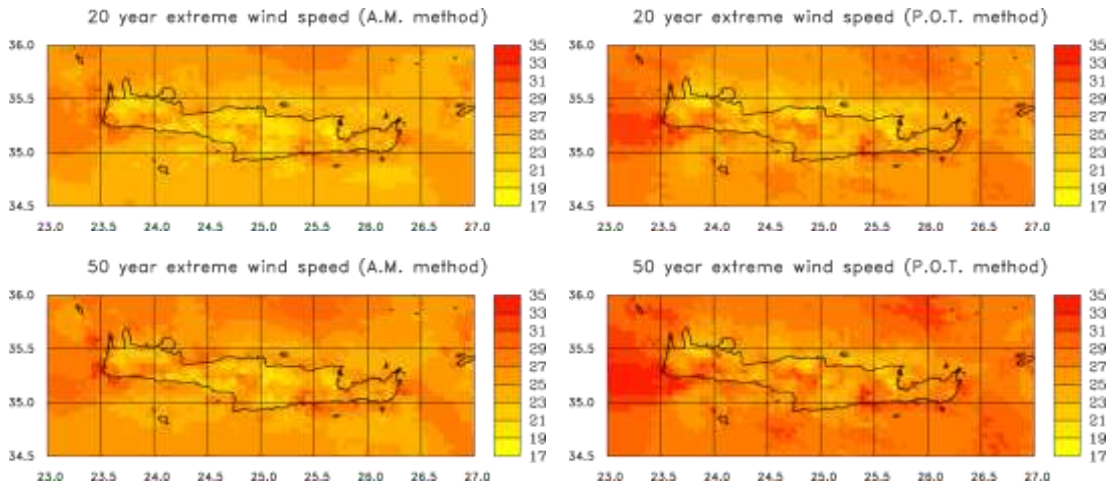

Figure 4-21: Extreme wind speed Atlas based on a) AM methodology (20 years return period), b) AM methodology (50 years return period), c) POT methodology (20 years return period), d) POT methodology (50 years return period),

4.4 Concluding remarks

The main objective of this work was to study the duration of both low and extreme wind speed events and quantify the associated uncertainties. Special focus was given in low wind speed events as they are not extensively studied in the literature. Two approaches for the quantification were applied and discussed: Intensity Given Duration (IGD) and Duration Given Intensity (DGI). These methods combine the intensity of such events with their duration and their likelihood of occurrence (in terms of return periods). The application of these techniques has as prerequisite the analysis of the suitability of the proposed tools defining their optimum implementation.

The suitability of two different techniques for the distribution parameters estimation, namely MoM and ML method was tested alongside with IGD method. The performed tests were based on the assumption that the outcome of the method in neighboring grid points, exhibit similar behavior. The results depict the spread of the two methodologies and support the preference of ML.

The relationship between the magnitude and the duration of wind speed for different return periods is made by using IDF curves. The upper and lower bounds are defined using the corresponding parameter estimation confidence intervals and provide a measure of the uncertainties employed in the estimation. These are highly dependent on the estimators and the length of the dataset used for the application. In addition, a quantification study of the uncertainties associated with the spatial distribution of the results of the IGD method was attempted by utilizing a probability analysis, based on the IDF curves of neighboring grid points. These results provided the necessary information for the application of IGD method uniformly in a large area. The illustration was made through different maps that depict the spatial distribution of the variables characterizing the IDF curves as well as the consequent hours of no energy production (wind speed below 3m/s) with a statistical repeatability that was set to be 20 years long. The main outcomes can be summarized as follows:

- In the open seas, such low wind speed events can last up to 4-5 days.
- Near shore these periods can reach up to 10 days and in certain cases even more.

Subsequently, the presented study was focused on the examination of the performance of the DGI methodology by using four different theoretical probability distributions. The comparison of the results with that of the IGD method revealed that:

- A constant underestimation is observed when using Gumbel and Weibull distribution.
- The application of G.E.V. distribution led to outcome of no particular pattern and large deviations.
- The best results were achieved by using the Rayleigh distribution.

It is worth mentioning that the exponentiality in DGI is higher as compared to IGD method, because for higher return periods the growing ratio is obviously smaller in the first case.

Regarding the wind speed probability distribution upper tail, the IDF curves were found to be highly affected by the topography. Especially over land there is an increased spatial variability of the parameters of logarithm function used for the fit. Setting the duration equal to one would lead to the classic approach of AM that is used for the estimation of an extreme event occurrence interval. The predefinition of a return period can lead to the construction of an extreme wind Atlas. The results of AM are tested against another widely used approach, POT.

Extreme wind speed values up to 35 m/s are found mainly in the open sea for both domains. At the same time POT results seem to overestimate extreme values compared to AM method results. This can be attributed to the fact that POT takes into consideration also the secondary maxima, which leads in a thicker distribution tail in contrast to AM in particular regions. This is the case in both tests as there are significant wind patterns affecting their wind climatology, Mistral and Etesians.

As a concluding remark, it should be noticed that the use of each method and the analysis provided for their comparison give valuable information concerning the local climatic characteristics. The outcome of similar studies could be used to define the probability of occurrence alongside the duration regarding wind speed events and their effects in various sectors such as wind energy applications. The impact of such cases in an economy based on wind energy could be critical. Other renewable energy sources, jointly exploited with wind energy, may support the minimization of potential drawbacks.

5 Return periods of extreme weather events in the Mediterranean Sea: a summary measure approach

The exceptional severity of storms is a characteristic feature of the European climate (Della-Marta et al, 2009; Schiesser et al, 1997). Hazardous conditions including strong winds and a rough state of the sea are responsible for many disasters in coastal regions and the shipping industry (Lamb, 1991). Therefore, studying their probability of occurrence and their characteristics is of great importance with implications in many sectors. Towards this direction, in this chapter, an alternative approach based on a regional summary measure is proposed. The return periods of storms can be addressed through this summary measure, which can be applied in various atmospheric and wave parameters.

The extreme indices used here, take into account several characteristics of the meteorological storminess such as the location, path, spatial extent and the duration and all these in five different predefined subregions. The summary measures can help to identify the case studies selected and support an overall risk assessment from selected scenarios. So, the demand for regional-scale Return Period estimation derives primarily from the straightforward use in practical applications. It should be noted that the uncertainties associated to the measure's creation and the misrepresentativity of local features need to be further investigated in applications.

Following this approach an analysis of the extreme wind and wave characteristics of storms in the Mediterranean Sea is taking place. The basin is separated in five sub-regions depending on the behavior of the extremes. In each of these domains several extreme indices are applied. The repeatability of their extremes is discussed through the application of AM and POT method.

The main objective of this chapter is to move from the gridded approach discussed earlier into one based on a summary measure. Therefore, most of the methods and tools used for the extreme value analysis have already been analyzed. The extreme wind and waves that are used as a summary measure for the area of interest are discussed thoroughly in the following lines.

5.1 Data used / Study area

The data used is derived from the Marina database (chapter 3.6.6). The variables under consideration are wind speed at 10m and significant wave height. The study domain is the offshore area covering the entire Mediterranean Sea. The selection of a such an extended area can lead to generalized conclusions of a basin characterized by intense cyclonic activity and extreme local winds. It should be noted that there is an intense socioeconomic activity in the region that may be affected by these extreme events.

5.2 Spatial clustering

The study area for the test of the proposed methodologies is the Mediterranean Sea. The region will be separated in sub-regions in order to have more representative outcome based on a criterion. Since the objective of this thesis is the study of extreme events a criterion associated to the extreme behavior of the sample is adopted. Hence, in order to divide the domain into spatial clusters only the extreme parts of the variables into consideration were taken into account. Therefore, a high threshold was applied and the exceedances were used as a subsample in a process quite similar to the clustering procedure in POT method. The threshold was set to the 98^{th} quantile for each grid point and variable. The five subregions are therefore defined based on their extreme characteristics while each one of them contains equal number of grid-points (Figures 5-1, 5-2). Other approaches, such as through the application of Principal Component Analysis, could be quite useful and planned to be tested in the future.

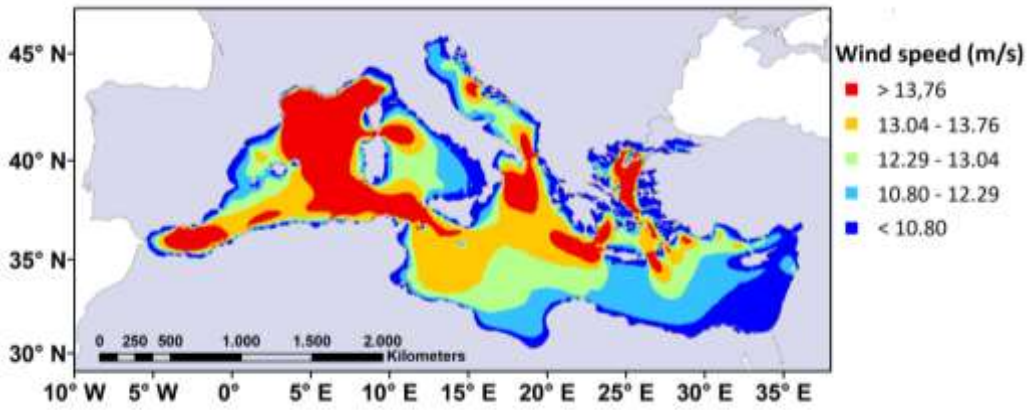

Figure 5-1: Area clustering based on wind speed 98th quantile.

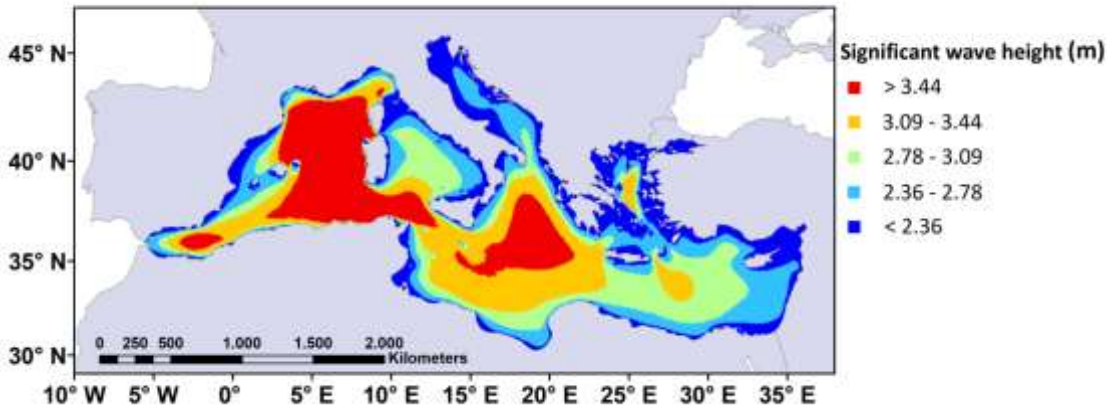

Figure 5-2: Area clustering based on significant wave height 98th quantile.

5.3 Extreme indices

The main objective of this chapter is to move from the gridded approach discussed earlier into one based on a summary measure. This is achieved through several extreme indices applied in the different sub-regions both for wind speed and significant wave height. The maximum and the mean value for each time interval and the 95th - 99th percentiles are among the simplest ones. The “mean value” index is the most robust while the others focus on the extreme parts of the spatial distribution and are highly sensitive. Some more sophisticated analysis is performed employing more indices.

- **Sw3q90** is the cube root of the sum of wind cubed above the domain climatological 90% quantile. Here the 90th percentile is calculated to be equal to 8.3, 8.2, 8.1, 8.0 and 7.1 m/s for the five sub-regions starting from the windiest. Regarding significant wave height the corresponding values are equal to 2.4, 2.1, 1.8, 1.6 and 1.2 m respectively.
- **Sfq95** is derived through the summary of the fraction of the variable divided by the grid-point climatological 95% quantile.
- Finally, **Sfq95q99** corresponds to the sum of the fraction of the extreme value divided by the length of the distribution tail. It takes into consideration both the 95th and the 99th percentiles of the wind/wave timeseries of each grid-point.

The calculated quantiles are quite similar to that of 98th. They can provide additional information regarding the extreme climate of the area. More specifically the windiest part of the Mediterranean basin, the Gulf of Lion is highlighted alongside with some secondary maximums located in the Alboran Sea, the Ionian/Adriatic Sea and the Aegean Sea (Figures Ap-4, Ap-5). A similar, though smoother, distribution is observed regarding the significant wave height quantiles (Figures Ap-6, Ap-7).

In general the mean values, Sfq95 and Sfq95q99 should be employed when more focus is needed to local characteristics compared to their climatology or in regions with low frequency of extremes. On the other hand Sw3q90 should be used if more weight of the absolute magnitude of the extreme event is needed. The extreme indices RPs are highly sensitive to the domain over which they are calculated and this should be also taken into consideration

The extreme wind and waves that are used as a summary measure for the area of interest are discussed thoroughly in the following lines.

5.4 Extreme value analysis

The return periods of storms in the basin will be performed in terms of wind speed and significant wave height. In order to obtain an indicative value for each subregion, several extreme indices will be applied. The probability of occurrence of a hypothetical event will be then calculated based on the principles of the Extreme Value Theory. One key aspect in estimating the return periods of storms in the Mediterranean Basin is the appropriate methodology for the extrapolation in time. For the needs of the study and for a more comprehensive analysis two methodologies will be used, the Annual Maxima and the Peaks Over Threshold. The first one is a more straightforward approach but the second can be more reliable in smaller size samples.

The greatest issue to deal with the POT approach as discussed in the methodology, is the selection of the appropriate threshold as it contains a subjectivity. To cope with it, two tools were applied at the same time. The selection of the threshold is primarily based in NC diagnostics and secondarily in a Kolmogorov-Smirnov test. Regarding the first one, the threshold model is applied in daily maxima time series. The threshold value is estimated at a range between 60 and 99.5 quantile with a 0.5 increment and the p-values are calculated at the significance level of 0.05. The threshold is selected where a sharp increase in the p-values is observed in the NC diagram (Figure 5-3, see also Appendix for the whole analysis).

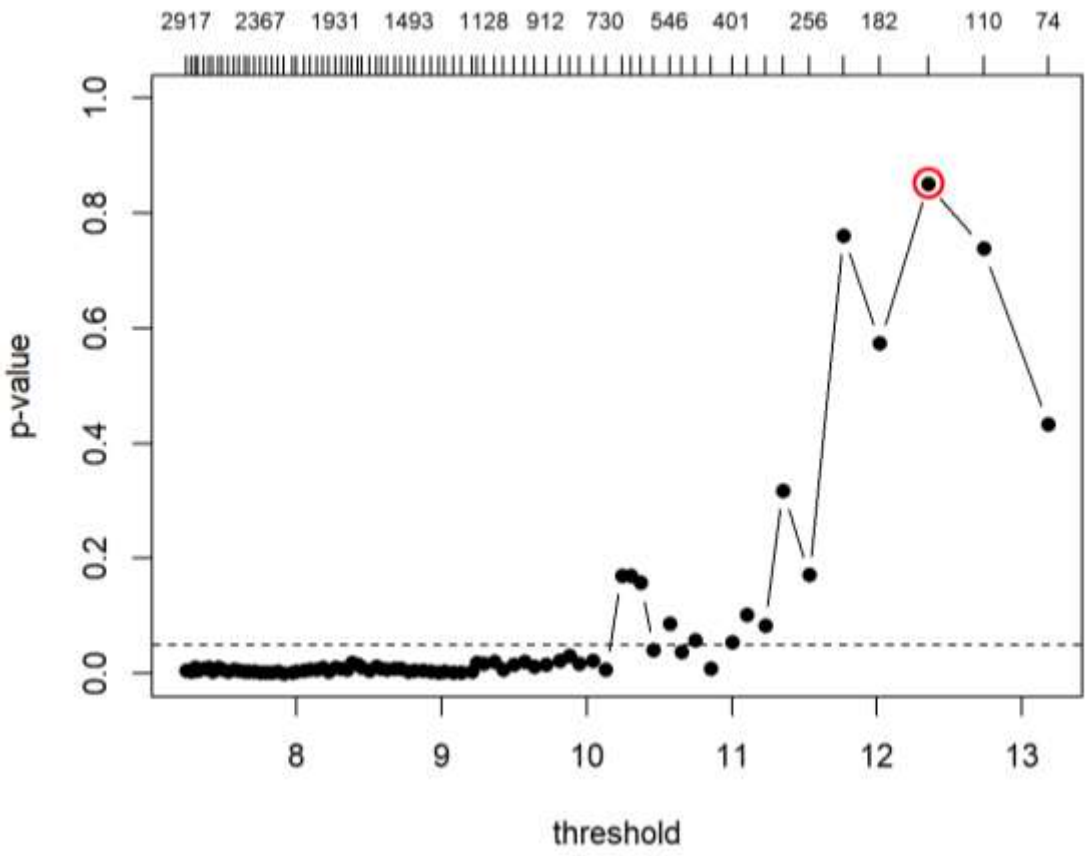

Figure 5-3: Score test for shape parameter over multiple thresholds - NC diagram.

This increase however is not the only factor to take into consideration. Although a sharp increase in lower thresholds could be considered desirable as the sample size would be greater, there is also the issue of the extreme values independence. Lower thresholds would probably compromise the independence criterion as defined by the extreme value theory. Moreover, the threshold should be selected in a way that the total events are not fewer than 50 totally, (Jonathan and Ewans, 2013) and non-more than 5-10 events/year (Tsalis et al., 2020; Palutikof et al., 1999). This is the reason why in some cases a second peak is selected. Also, in cases that the p-values show an early increase and a persistent stability, a threshold is selected in higher values. The decision for the appropriate threshold selection in such cases is assisted through the use of a Kolmogorov-Smirnov test leading to different thresholds for each sub-domain, extreme index and parameter as depicted in Tables 5-1, 5-2.

Table 5-1: Wind speed thresholds for each location and extreme index.

	Area 1	Area 2	Area 3	Area 4	Area 5
Mean value	12.35	9.97	10.29	8.47	6.86
Maximum value	23.24	21.23	23.24	22.66	20.44
Spatial 95th quantile	19.16	16.44	17.11	16.64	14.73
Spatial 99th quantile	19.99	17.87	17.46	17.51	15.01
Sw3q90	730.91	783.41	752.13	788.99	711.16
Sfq95	12258.83	11564.39	9898.1	11548.00	9687.72
Sfq95q99	10052.91	7668.75	9945.00	7362.00	5244.89

Table 5-2: Significant wave height thresholds for each location and extreme index.

	Area 1	Area 2	Area 3	Area 4	Area 5
Mean value	3.14	2.77	1.36	1.65	1.40
Maximum value	7.37	6.21	6.68	5.49	6.32
Spatial 95th quantile	5.49	5.08	4.71	3.91	3.10
Spatial 99th quantile	6.86	5.569	5.24	4.86	3.93
Sw3q90	445.27	388.36	351.59	270.82	168.29
Sfq95	18509.49	18715.00	13921.77	11558.60	11900.04
Sfq95q99	11812.86	12993.00	8870.92	5030.58	6256.95

5.5 Return periods in terms of wind speed

The application of the two methodologies was performed for the estimation of the extreme values of wind speed for return periods ranging from one to one hundred years. A general remark is that POT tends to overestimate the extreme values compared to AM. This can be attributed to the fact that it takes into consideration more secondary extremes leading to a thicker distribution tail. Another point is that almost in all extreme indices the area with the highest values of wind speed 98th quantile (area 1) resulted in higher extreme values as well.

More specifically, regarding the mean spatial value (Figure 5.4) a quicker convergence is observed in the AM output. This leads to an underestimation compared to POT in all cases.

However, the differences are not considered to be substantial and are within the confidence intervals (Figure 5-11). For the first area the 100-year extreme value is found to be equal to 20 m/s and 17 m/s for the POT and the AM respectively. The second sub-region faces slightly lower winds reaching values around 18 and 16 m/s while the third shows a convergence among the two methods with values around 15-16 m/s. The fourth and the fifth areas as defined earlier are characterized by a spatial averaged wind of 14-16 m/s and 12-13 m/s respectively.

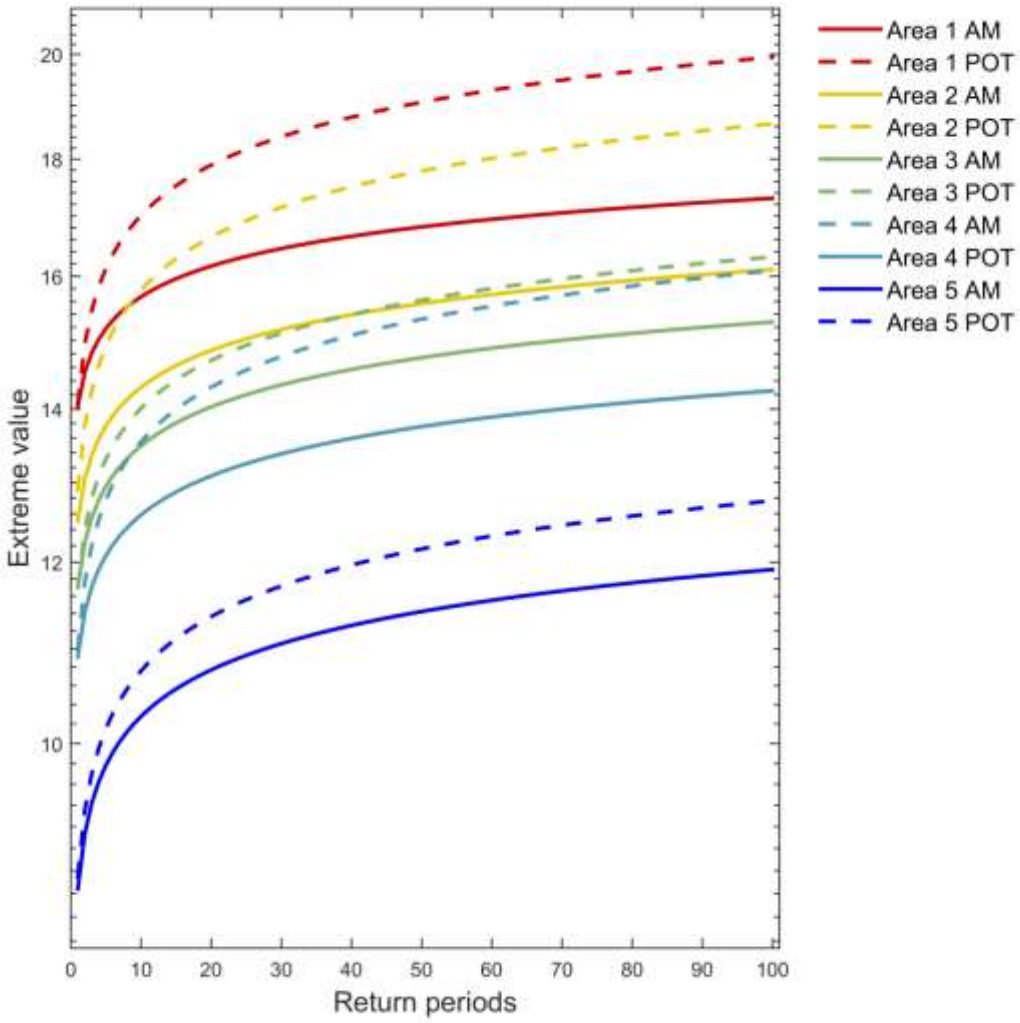

Figure 5-4: Extreme values for the wind speed spatial mean and return periods ranging between 1 and 100 years.

The same procedure applied in the spatially maximum values for each timestep and each domain resulted in some unpredicted outcome. Regarding the AM, the areas characterized by stronger winds produce extreme values not as strong as expected, surpassed by the other sub-regions (Figure 5-5). This however is not the case with POT. These results can be used to make some good arguments.

Employing the spatial maximum value as an extreme index over a so large domain is not suggested as this index is characterized by volatility and potential misrepresentation. The selection of the maximum values leads to no smoothing at all and the sample will also include potential outliers and even values that could be attributed to model misbehavior. The employment of each other extreme index for this analysis will lead to a smoothing and a better representation of the features of each domain. Additionally, even if an index like that will be used is should be accompanied with POT. Taking more extremes into consideration can smooth the results and depreciate potential non-representative outliers.

In each case however the observed behavior is something that should not be considered as rare. The area clustering based on the distribution of each grid point should not be confused with the extreme indices used and are based on a spatial analysis. It is not rare that a local or a smaller scale event to produce higher values regarding the extreme indices in Area 3 compared to Area 1. This is associated to the correlation of the timeseries in the sub-regions. Therefore, an additional principal component analysis may be useful in the future.

All the above resulted in remarkable differences among the extreme value methodologies. More specifically regarding the first region the 100-year wind speed is found to be equal to 35 m/s and 32 m/s for POT and AM respectively. Similar results are obtained regarding the second area of interest with values around 34 and 30 for the two methodologies. Regarding the third domain the AM methodology reaches 33.5 m/s about 1m/s higher than POT. The fourth sub-region is characterized by robustness and consistency as both methodologies have similar behavior while regarding the last one an underestimation of the AM is traced for a recurrence interval equal to 100 years.

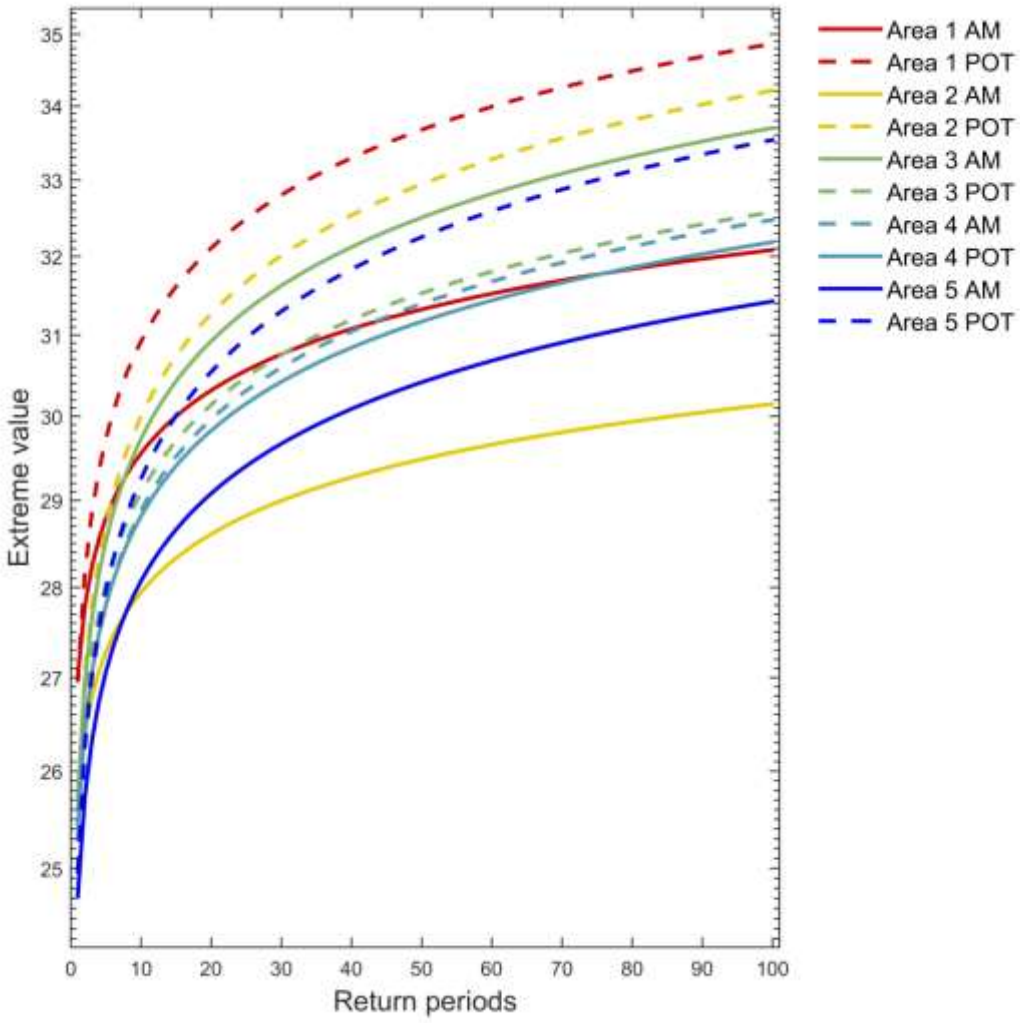

Figure 5-5: Extreme values for the wind speed maximum value and return periods ranging between 1 and 100 years.

The 95th and 99th percentiles resulted in a rather expected outcome. The index Sw3q90 is targeting at grid point extremes within each sub-region and this is why it is highly sensitive to areas of high wind speed. It is expressed in non-dimensional units. The rank of the RPs of Sw3q90 are most highly correlated with the rank of the RPs from the grid point analysis over offshore areas. Areas 1, 2 and 3 behave similarly regarding AM while areas 2, 3 and 4 for POT (Figure 5-6). The characteristic tendency of POT to result in higher values is depicted here as well.

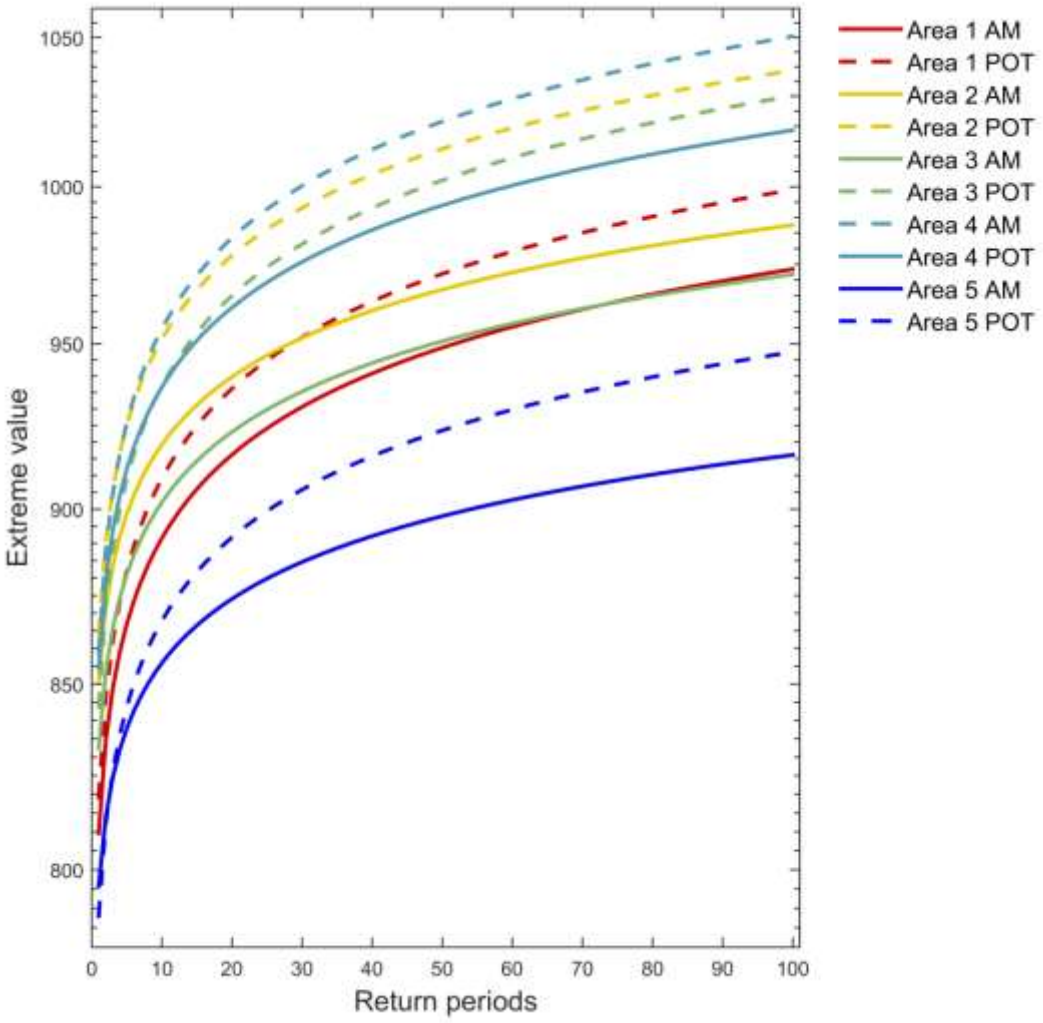

Figure 5-6: Extreme values for the cube root of the sum of wind speed cubed above the domain climatological 90% quantile (Sw3q90) and return periods ranging between 1 and 100 years.

Index Sfq95 describes the extremity of the variable under consideration in relation to the local climate for each sub-region. Index Sfq95q99 is similar to index Sfq95 in terms of sensitivity including, however a normalizing factor. This index is sensitive to the relative extremity of local wind speeds for each sub-domain. Sfq95 and Sfq95q99 are highly correlated not only with each other but also with the mean spatial values. A similar behavior is also observed regarding the estimated return periods especially using the AM method. Differences in the POT method could

be attributed to the normalization of the second index. For an easier to follow manuscript most of the figures supporting the aforementioned analysis can be traced in the Appendix.

Regarding the confidence, POT resulted generally in narrower confidence values (Figure 5-7) something that can be attributed to the larger sample taken into consideration for the extreme value analysis. In some cases, the opposite is observed. However, the estimation of the confidence intervals takes into consideration information about the absolute value of the extreme value analysis output and such a behavior is totally expected. As a rule of thumb, here the 100-year confidence intervals regarding POT are about half the ones obtained by AM.

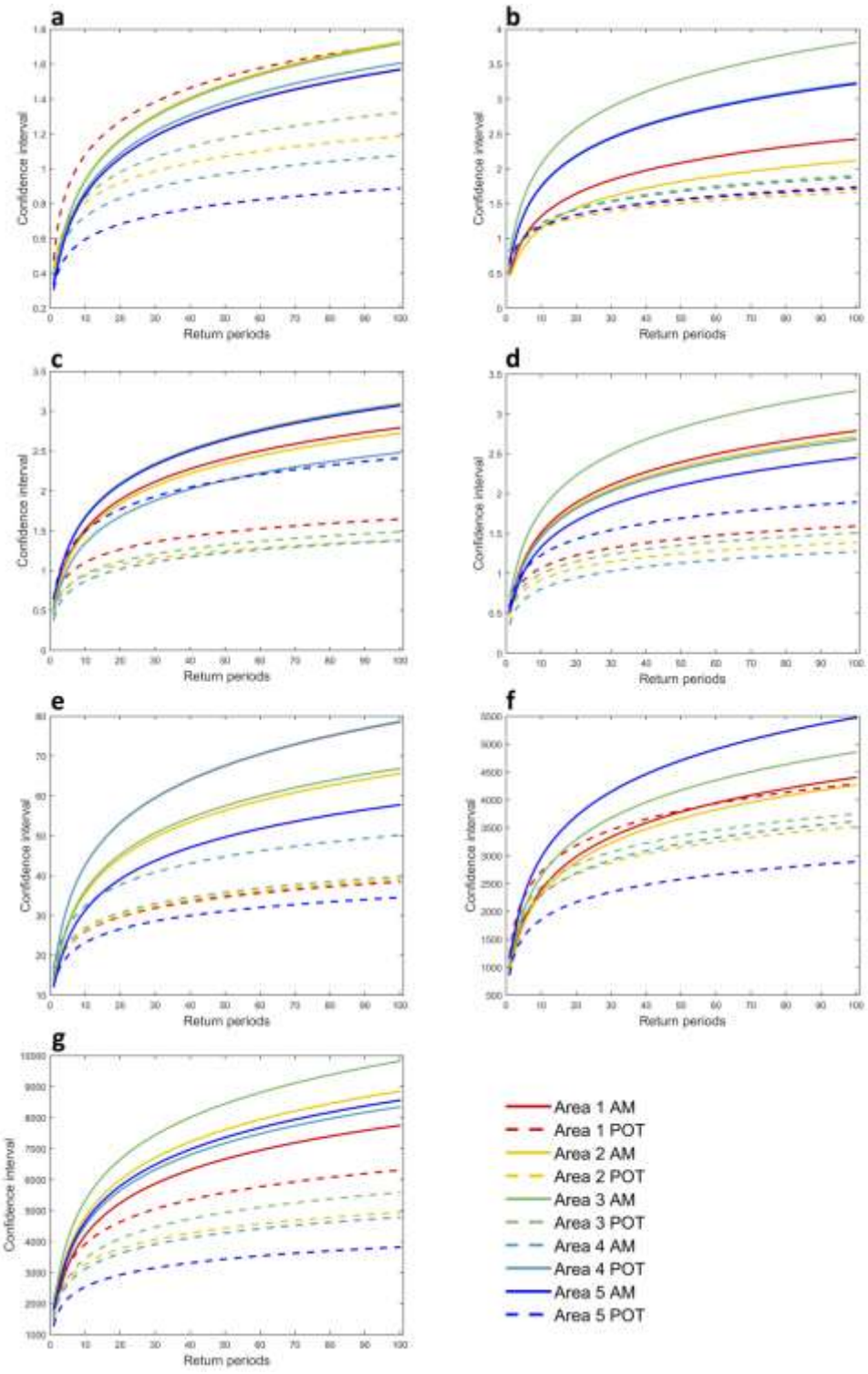

Figure 5-7: Confidence intervals for the wind speed extreme indices that correspond to the a) mean, b) maximum, c)95th quantile, d) 99th quantile e) Sw3q90, f) Sfq95 and g) Sfq95q99 and return periods ranging between 1 and 100 years.

5.6 Return periods in terms of significant wave height

A similar concept as with wind speed is followed in the case of significant wave height. Although wind speed is highly correlated to wind-driven waves, the impact of swell can be critical in extreme conditions. Therefore, the estimation of a potential extreme weather event severity in terms of significant wave height can provide useful information especially when used alongside the wind speed perspective analyzed earlier.

The results show a convergence between AM and POT in many cases. Even when a substantial difference is observed, it is quite frequent that the confidence intervals of each methodology cover it (Details on the figures can be found in Appendix, Figures Ap-26 – Ap-30). Beginning with the mean spatial value, regions 2 and 5 present a similar behavior between the two approaches while for the rest, POT seems to result in higher values. Regarding the application of the methodology in the spatially maximum values, the results are more robust compared to these of wind speed, further indicating the more local nature of the second. However, 100-year significant wave heights of up to 14 m are rather unrealistic. As stated earlier this index is highly sensitive and should only be used in limited areas with similar climatic characteristics.

There is not something worth commenting regarding the 95^{th} and 99^{th} percentiles. The index Sw3q90 is characterized by a convergence between POT and AM with the exception of the first zone. The index is sensitive to areas of high absolute magnitude of significant wave height. Having this in mind it makes sense that the bigger differences are observed in the region with the higher waves. It should be mentioned that these regions are characterized by the presence of swell. Similar behavior is observed with Sfq95 and Sfq95q99.

The confidence intervals for the corresponding return periods are quite wider in the application of the AM methodology (Figure 5-8). This is due to the larger amount of data used for the analysis and it is observed even in cases where POT resulted in higher extreme values than AM.

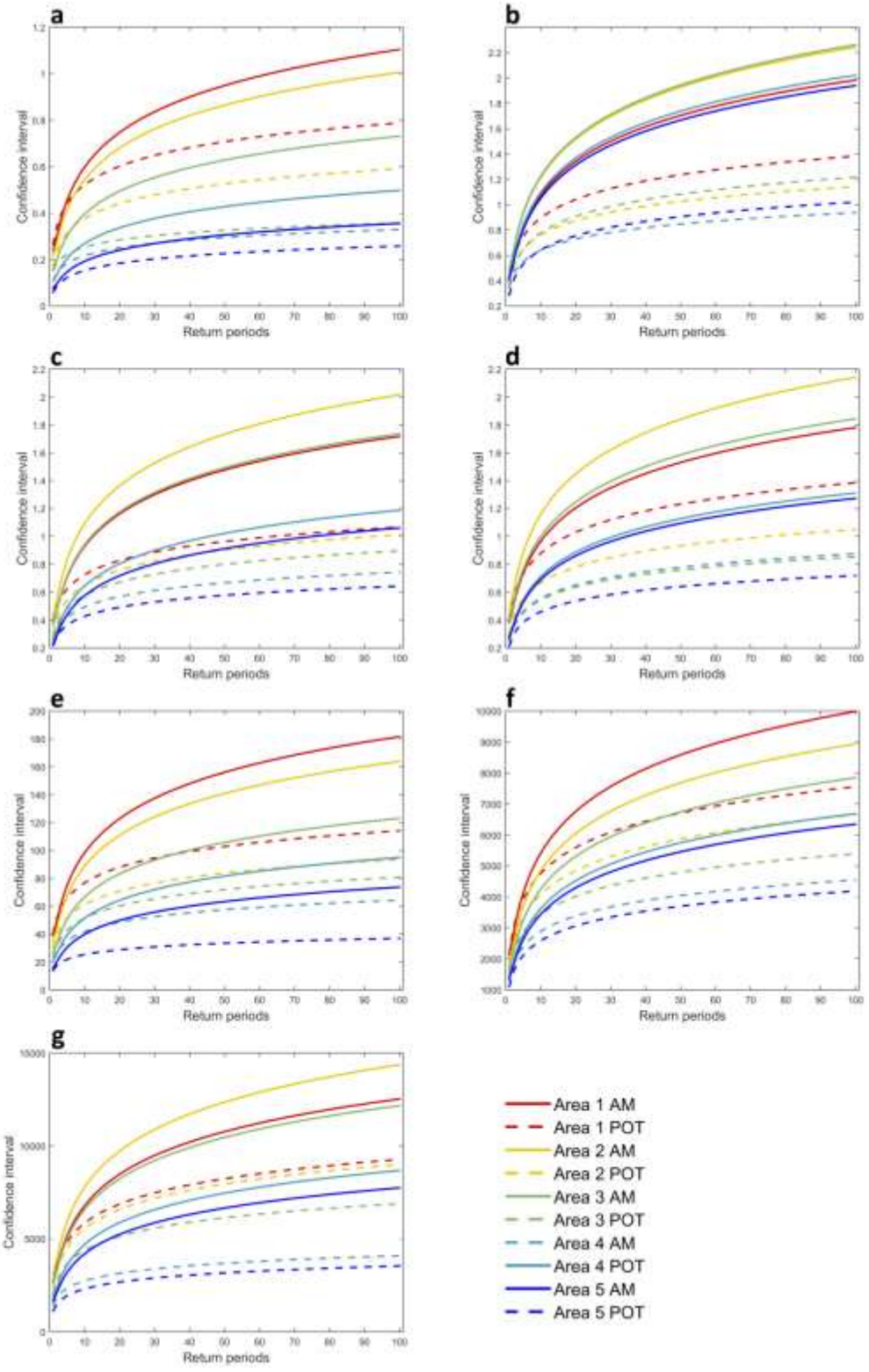

Figure 5-8: Confidence intervals for the significant wave height extreme indices that correspond to the a) mean, b) maximum, c)95th quantile, d) 99th quantile e) Sw3q90, f) Sfq95 and g) Sfq95q99 and return periods ranging between 1 and 100 years.

5.7 Application of the analysis in past cases

The different approaches were tested against various weather patterns in the Mediterranean basin. These tests were performed in order to better understand how to use the results of the methodologies in real life scenarios. The first application was that of an intense cyclonic activity in Mediterranean and North Europe lasting for more than two days causing extreme weather in several sub-regions at the same time (Figure 5-9).

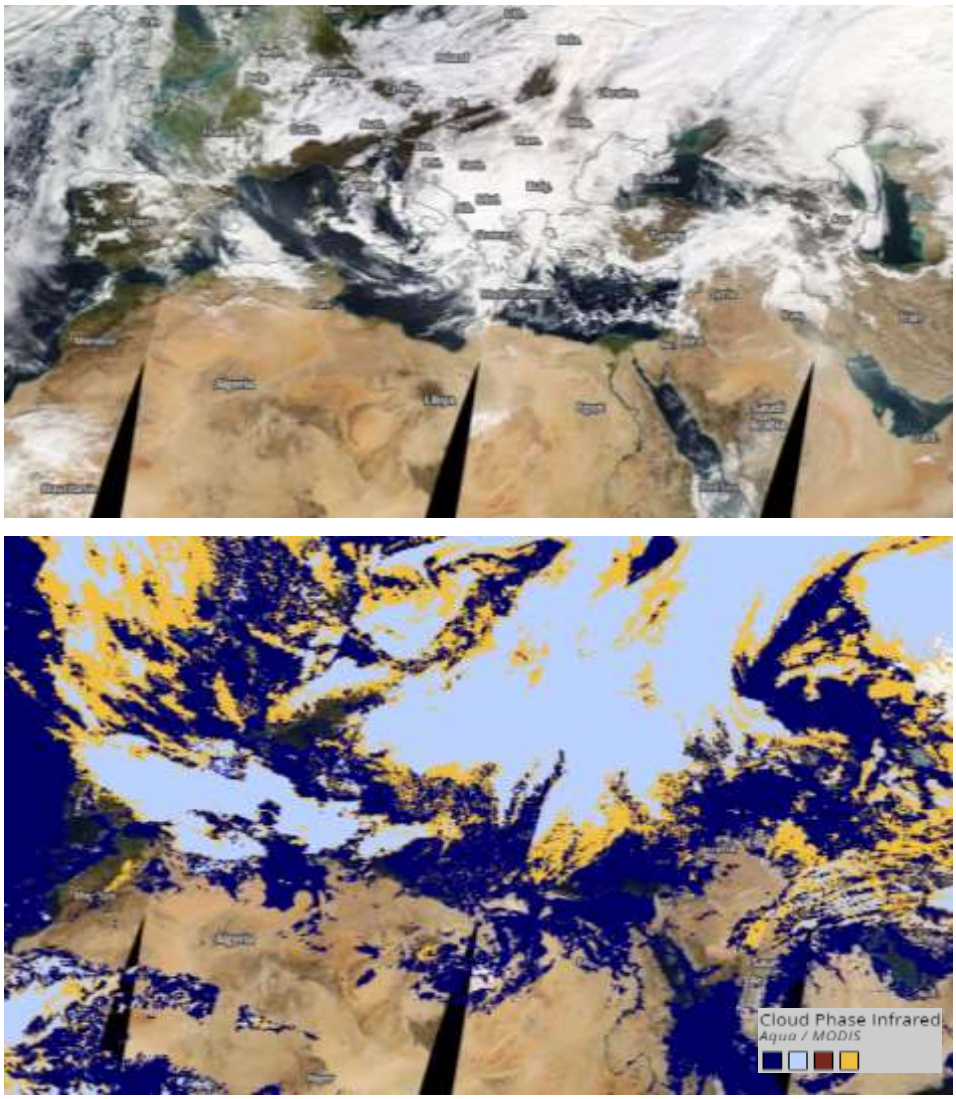

Figure 5-9: Aqua Modis Visual image (top) and Cloud Phase Infrared (bot) of the bad weather that hit Europe in the sixth of January, 2012. In the bottom image blue represents liquid water, cyan represents the ice and yellow is not specified.

The event affected at an enormous scale the Mediterranean basin with extreme winds covering an area from the Gulf of Lion to the south of Peloponnese (Greece). Wind speed exceeded the 25 m/s several times during the evolution of the event (Figure 5-10). A similar pattern is observed regarding significant wave height with values up to ten m found near the shore of Corsica and Sardinia.

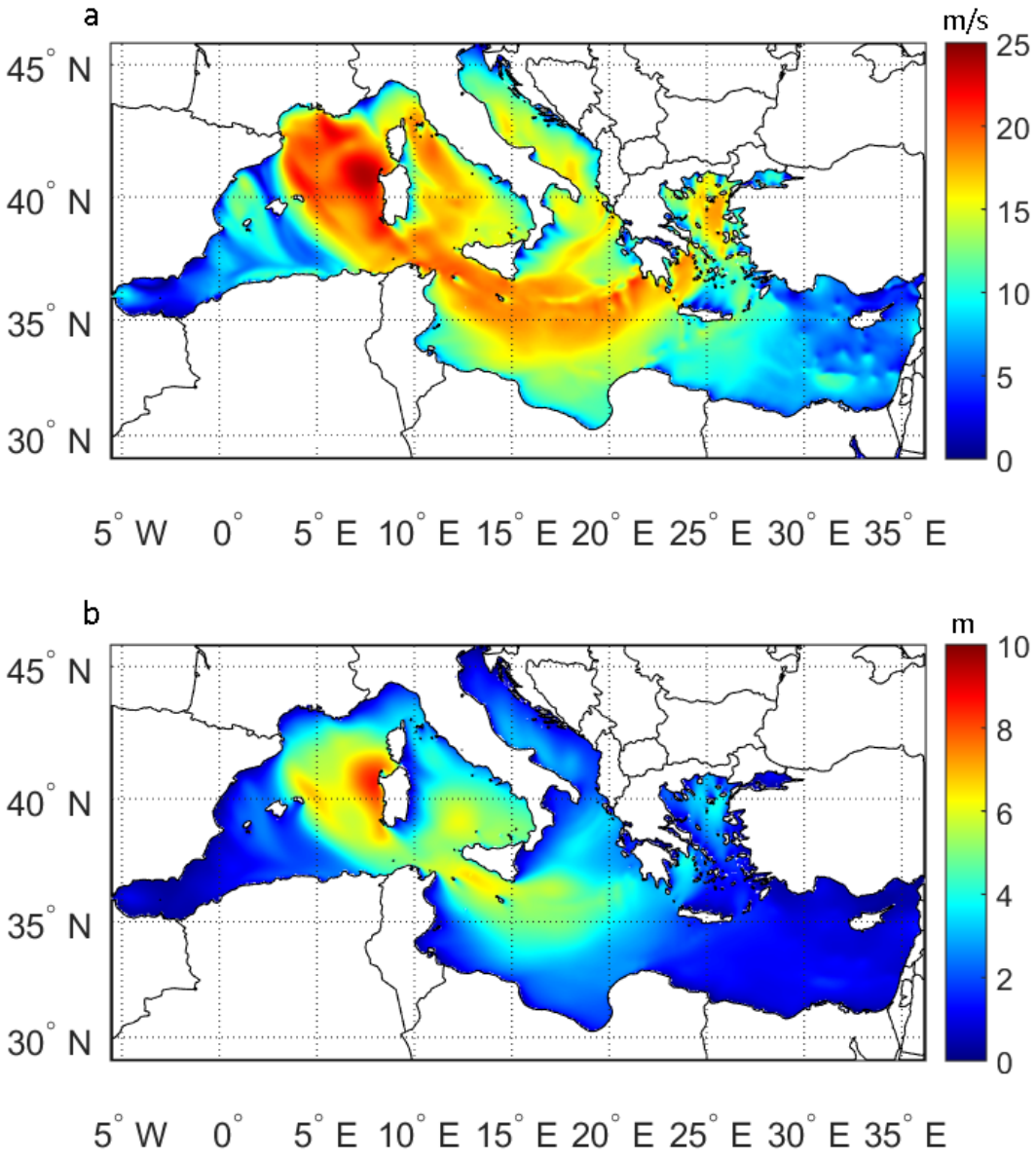

Figure 5-10: Wind speed (a) and significant wave height (b) for extreme weather affected the Mediterranean region, 06/01/2012, 09UTC.

A first result is something observed in all case studies. The extreme indices of maximum values and the spatial quantiles do not seem to work properly as in all cases they produce very small return periods meaning that these extreme values are rather common in the domain. This can be associated to the fact that the region is highly affected by cyclonic activity and several wind systems like the Etesians (not so extreme), tramontane winds and the Mistrals. So these quantiles or the maximum values may be found frequently during a year period. However, these approaches are not so sophisticated and the analysis should be performed employing the rest indices.

Regarding wind, for the first region the return periods span between 17 and 29 years for AM and 5 to 9.5 years for POT. The same probability of occurrence is observed in the second region regarding AM while POT categorized the event as one with frequency 4 to 11 years depending to the index. Regarding the third sector values between 17.5-19.5 and 12-24 years for AM and POT respectively. It is quite clear according to POT that the event affected the third region more than it did in the first two. The recurrence interval for the fourth area is 7.5-8.5 and 3.5-7.5 years for AM and POT respectively. Negligible was found to be the effect in the fifth region as this was defined above. In POT Sfq95q99 resulted in higher RPs in all regions while in AM there was no particular pattern with quite similar values in areas three to five. In the first two cases Sfq95 showed an overestimation as compared to the rest extreme indices.

The return periods of this extreme weather activity in terms of significant wave height are generally lower. The first region is affected by waves with a return period from 3.5 to 6 and from 2 to 4.5 years for AM and POT respectively. In the second region the impact was more intense, met once in 7-10 years based on the AM approach and once in 5.5-11 based on the POT one. The third area was affected in a similar way as the first one. Values between 3 and 6 years emerge from the AM methodology while values between 2.5 and 4.5 are produced through POT. In the fourth region the impact was quite low with the event to be characterized by a probability of occurrence equal to 50-60 % annually. The fifth sector is highly affected with recurrence intervals reaching the 6-7 years. This is quite important as this sub-region is generally closer to the coast meaning that extreme weather there may cause several issued in human activities.

In general, the extremity of this particular event is lower if analyzed in terms of swh. At the same time in swh smaller differences are found between AM and POT and in most of the cases both approaches tend to overlap. More case studies are selected to further understand the behavior of the proposed methodology.

A characteristic wind pattern observed in Greece and more specifically in the Aegean Sea are the Etesians. These are strong, dry north winds, which blow from about mid-May to mid-September. A selected case that took place during August of 2009 was studied for the estimation of its frequency of occurrence (Figure 5-11).

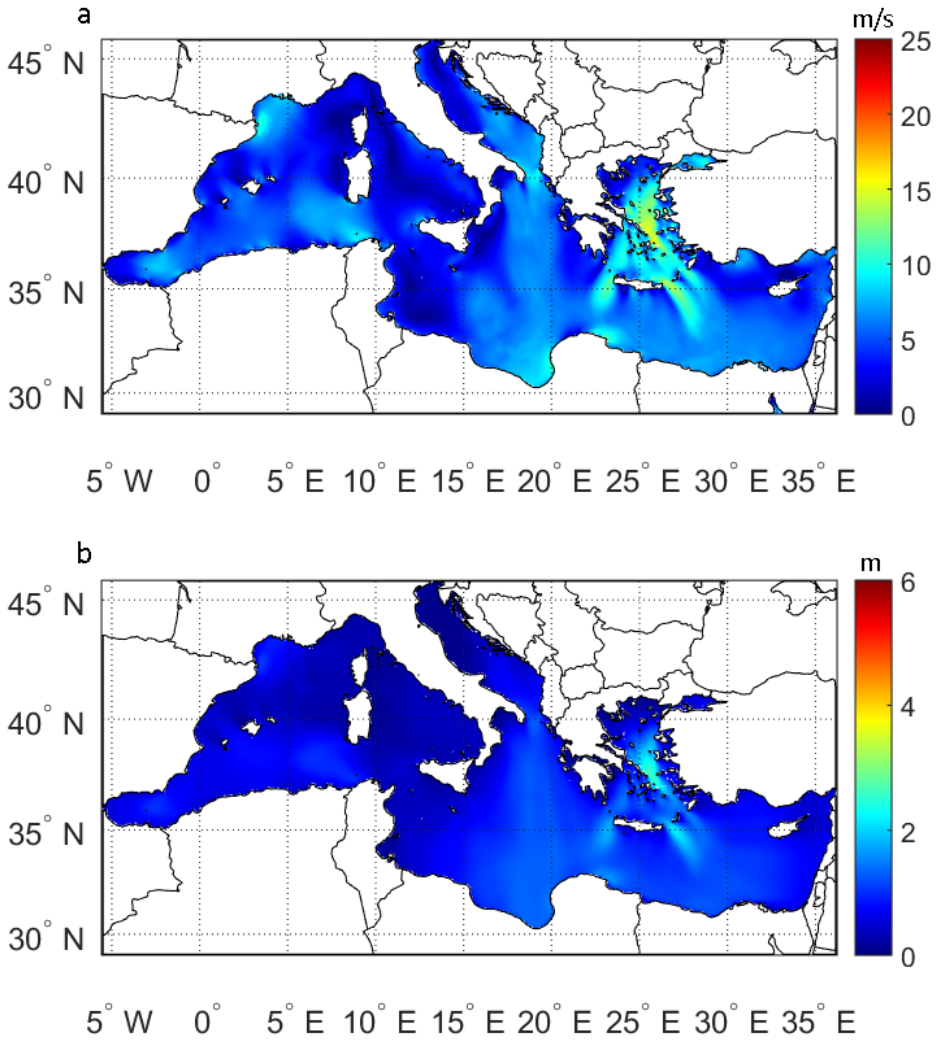

Figure 5-11: Wind speed (a) and significant wave height (b) for an Etesian event, 02/08 2009, 13UTC.

Values for all areas, indices, extreme value methodologies and both parameters span in a range between 0.02 and 0.1 years which means practically that such conditions more than common in the Mediterranean basin.

Moving on, another weather system with district characteristics that highly affect the region is selected as a case study. The so called “Medicanes” are Mediterranean cyclones that gain tropical features at some point during their evolution. Two cases were selected for this. The first one is the Medicane Qendresa (Figure 5-12). This cyclone resulted in three reported deaths and $250 million estimated damages. It affected South Italy, Malta, North Tunis, North Libya and the island of Crete in Greece.

Figure 5-12: Medicane Qendresa - 07-08/11/2014 (Modis)

During the evolution of the event, wind speeds of more than 22 m/s and significant wave heights of up to 6 m affected the southern parts of Italy (Figure 5-13).

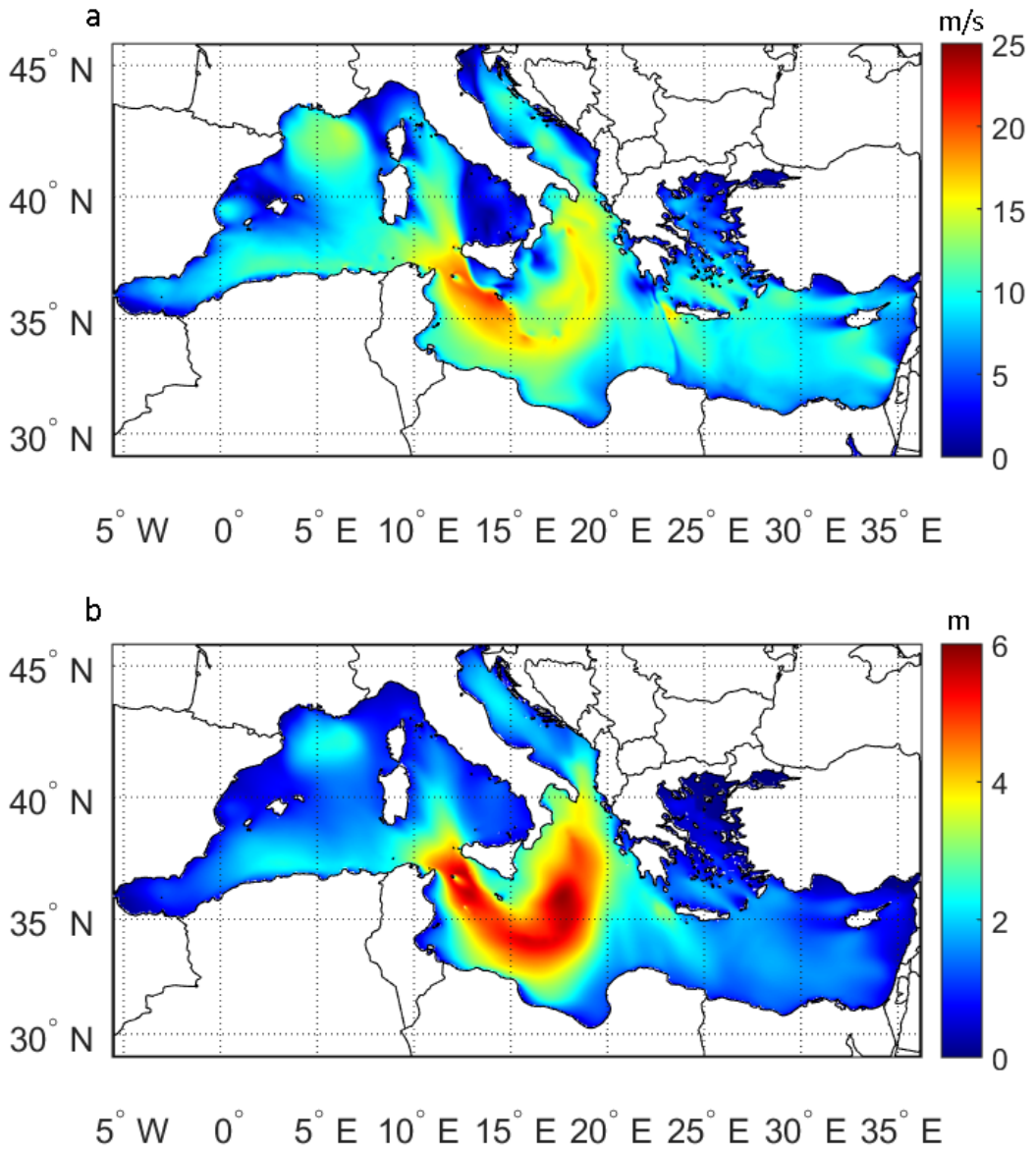

Figure 5-13: Modeled wind speed (a) and significant wave height (b) during the evolution of Medicane Qendresa, 08/11/2014, 00UTC.

In this case, values for all areas, indices, extreme value methodologies and both parameters span in a range between 0.09 and 0.4 years which means that such conditions may be encountered more than 10 times per year in the basin. In all cases the wave analysis resulted in lower return periods.

.

5.8 Concluding remarks

The Mediterranean Basin is highly affected by extreme wind and waves originating both from the cyclonic activity in mid-latitudes and local wind patterns. The estimation of extreme weather probability of occurrence in characteristic Mediterranean sub-regions is vital for several sectors such as reinsurance. Therefore, the Basin is categorized in 5 sub-regions based in wind characteristics and five more based on the wave climate. For each one of these sub-regions several extreme indices were selected. These extreme indices summarize the behavior of each area taking into consideration the location, path, spatial extent and the duration of the potential storm activity.

An extreme value analysis was performed in these extreme indices for the production of regional-scale Return Periods in terms of wind and waves. Two methodologies were employed for this part, AM and POT. Beginning with the second a major issue is the selection of the appropriate threshold. This was primarily based in NC diagnostics and secondarily in a Kolmogorov-Smirnov test resulting in thresholds ranging mainly between 92th and 97th percentile.

The application of the two methodologies in extreme winds resulted in higher values when applying POT compared to the results employing AM. This can be attributed to the fact that it takes into consideration more secondary extremes leading to a thicker distribution tail. In most of the cases, however, the differences are not considered to be substantial and are within the confidence intervals. A strange behavior is observed in the application in the spatially maximum values for each timestep and each domain that resulted in remarkable differences among the two extreme value methodologies. The selection of the maximum values leads to no smoothing at all and the sample will also include potential outliers and even values that could be attributed to model misbehavior and should not be used as an extreme index in such large domains.

A similar concept as in wind speed is followed in the case of significant wave height. This resulted in a convergence between AM and POT in many cases. Even when a substantial difference is observed, it is quite frequent that the confidence intervals of each methodology overlap. Regarding the application of the methodology in the spatially maximum values, the results are more robust compared to these of wind speed, indicating the local nature of the

second. The 100-year significant wave heights of up to 14 m however, may be unrealistic setting this index highly sensitive suitable only in limited areas with similar climatic characteristics.

The confidence intervals for the estimated return periods are quite wider in the application of the AM methodology. This is due to the larger data set used for the analysis. This is observed even in cases where POT resulted in higher extreme values than AM.

The application of the proposed methodology in selected case studies revealed that the extreme indices of maximum values and the spatial quantiles do not work properly as in all cases they produce very small return periods in contrast with the rest indices. Therefore, for such analyses more sophisticated extreme indices are needed. In general, the selected events are characterized by lower recurrence interval values in terms of significant wave height. A notable outcome however is that in some cases extreme events with high winds that caused serious damages are not considered so rare. It should be stated that this is a regional-oriented approach and can be useful for studies with a similar orientation. For example, in reinsurance it is important to know the return periods of extreme values in wide areas simultaneously.

In order to further analyze the impact of a potential extreme event there are two options. The first one is to add more environmental variables into the analysis. An important factor is for example the precipitation or the storm surge. Another way to address the extremity of a rare weather event is to adopt an event-oriented approach. The last is discussed widely in the next chapter of the thesis.

6 Return periods of extreme weather events in the Mediterranean Basin: an object-oriented approach

The Mediterranean Sea is a region characterized by intense cyclonic activity, something studied extensively in the past (Bartholy et al, 2009; Flaounas et al, 2018a; b; Flocas et al, 2010; Lionello et al, 2006; Maheras et al, 2001; Trigo, 2006; Trigo et al, 1999; 2002). There is a great variety of genesis mechanisms and different evolution characteristics, intensities and depths (Kouroutzoglou et al, 2014; Lionello et al, 2016). The last can be attributed to the latitude of the basin resulting in warm waters and its geomorphological characteristics including complex topography with intense orographic structures and many islands. One of the most interesting type of cyclones present in the area is the Mediterranean tropical-like cyclones (TLCs) known also as medicanes. The last are extensively analyzed in chapter 2.5 and will be used as an example for the presentation of the proposed methodology.

The purpose of this chapter is to define the risk-exposed regions and developing a summary measure of the storminess of TLCs in the Mediterranean. The first is expressed through the spatial distribution of the affected regions during all stages of their life while the second utilizes extreme indices that summarize storm intensity and spatial extent. The point is to be able to describe the extremity of the event by using just one value, utilizing the results of these indices and the concept of return periods (RP). The RP of medicanes can be a valuable measure in comparing actual and past events and in determining their socioeconomical impact. The analysis is based both on wind and wave parameters and particularly on wind speed at 925 hPa, wind speed at 10m, surface gust and significant wave height. For the needs of the study a high resolution coupled atmospheric-wave system was employed for the modeling of 52 case studies during a 25 year-period. The coupled modeling system supports the direct communication of the atmospheric and wave component resulting in more reliable outcome, especially under storm conditions (Stathopoulos et al., 2020 a, b).The results are post processed in order to quantify the risk exposed areas based on wind and wave intensity. At the same time three extreme indices are used for the estimation of the return periods of medicanes through two different approaches corresponding to the Annual Maxima methodology and the Method of Independent Storms.

6.1 Data used / Study area

The analysis performed is basically composed of two parts. The first one is the quantification of the wind and wave affected areas associated directly or indirectly with the evolution of medicanes. The second follows and utilizes the results from the first part, targeting on the estimation of the recurrence interval of these cyclones employing the Extreme Value Theory principles. The data used from the analysis is the product of many high-resolution numerical simulations – the Medicane Database described extensively in chapter 3.6.7.

The simulated medicanes are generated mainly in 4 regions shown in Figure 6-1. In order to assess the quality and performance of the model-derived parameters an evaluation was performed. The evaluation consists of two parts, a quantitative and a qualitative one. Beginning with the first part, the evaluation was based on multiple buoys. Buoys were selected because the wind field over land is strongly affected by the topographic features. The available parameters that were evaluated are wind speed and significant wave height. Although, these observations do not cover spatially and temporally at a desired extent the Mediterranean Basin, they can give us a first idea regarding the behavior of the model during the simulations.

The data is retrieved from the European Marine Observation and Data Network (EMODnet - http://www.emodnet-physics.eu/Map/). The utilized buoys are limited to the ones that frequently collect and supply continuous data during the modeled events. The evaluation period differs depending on the station and the observational data availability. Their names and exact locations are displayed subsequently in Figure 6-1.

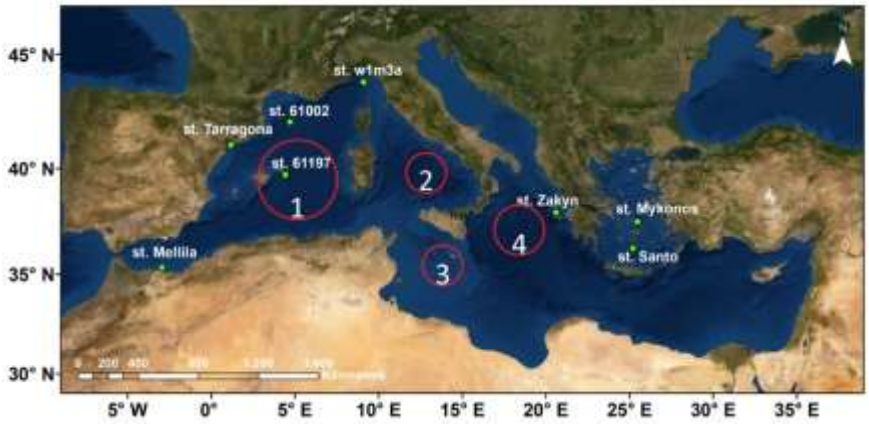

Figure 6-1: List of stations used for the evaluation and main formation areas of the simulated medicanes (in circles).

Overall, the results summarized in Table 6-1, show a good model agreement with the recorded values both in surface wind speed and SWH. The statistical indicators used are the mean BIAS error (BIAS) between modeled and observed values, the Mean Absolute Error (MAE), the Root Mean Absolute Error (RMSE), the Scatter Index (RMS value normalized by the mean measured value) and the Correlation Coefficient. In wind speed, a small tendency for underestimation is evident from the negative BIAS. The results in MAE, RMSE and Scatter Index that indicate the error variability between modeled and observed values show a moderate spread between them. On the other hand, the results in the correlation coefficient metric do not denote a significant linear relationship between modeled and observed wind speed values. For the SWH, BIAS errors are close to zero, so as a concrete conclusion concerning a regular overestimation or underestimation cannot be derived. With respect to the other statistical metrics of performance, decreased error variability and a well-established correlation can be traced.

Table 6-1: Wind speed and significant wave height evaluation indices

	Wind speed					Significant Wave Height				
	BIAS	**MAE**	**RMSE**	**Scatte**	**Correlation**	**BIAS (m)**	**MAE**	**RMSE**	**Scatter**	**Correlation**
61197	-0.176	2.13	2.81	0.39	0.691	0.241	0.555	0.735	0.368	0.848
Melilla	-	-	-	-	-	0.37	0.465	0.561	1.06	0.489
Tarragona	-	-	-	-	-	0.087	0.262	0.364	0.599	0.603
W1M3A	-0.888	2.39	3.3	0.501	0.363	-	-	-	-	-
ZAKYN	1.2	2.58	3.22	0.733	0.485	-0.035	0.32	0.425	0.325	0.714
61002	-0.31	2.07	2.72	0.271	0.849	-	-	-	-	-
MYKON	-1.43	2.36	3.02	0.443	0.63	-0.127	0.325	0.508	0.523	0.695
SANTO	-1.06	2.11	2.79	0.503	0.618	0.0	0.262	0.355	0.374	0.842

Additionally, the behavior of the wind speed and significant wave height probability distributions have been tested against the same observations (Figure 6-2). Both seem to perform quite well with their best fit line to be close to a 45o degrees line (1-1 line). More specifically, regarding wind, there is a slight overestimation in the distribution upper and lower tail and a good agreement for the rest of it. The modeled significant wave height has a good agreement to the observations for the first half of the probability distribution while moderate to high waves are slightly overestimated and the extremes slightly underestimated.

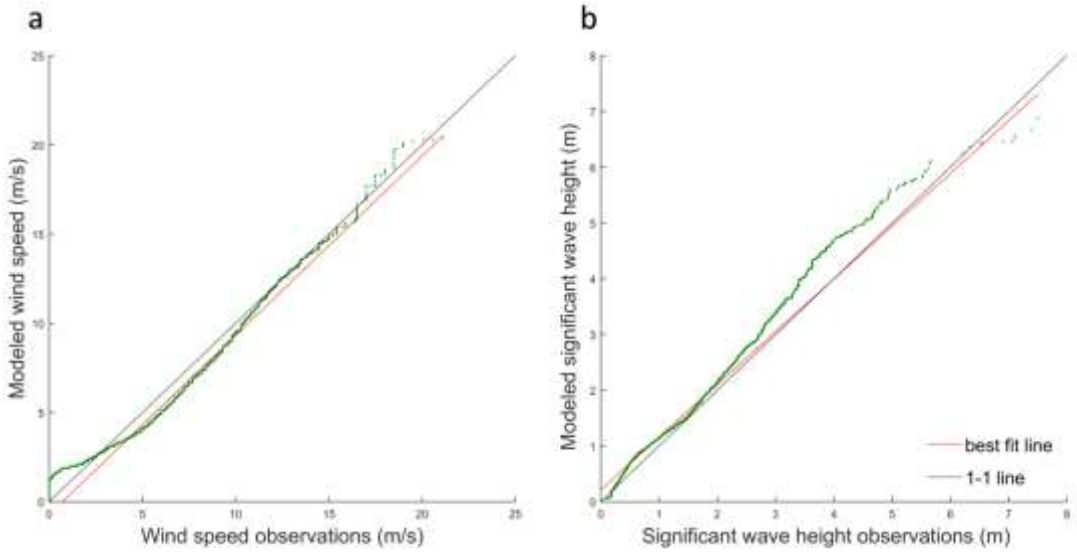

Figure 6-2: Q-Q plots for the modeled (a) wind speed and (b) significant wave height against the observations.

A qualitative evaluation has also been performed employing the dataset of Blended Sea Winds (Zhang et al, 2006). This product was utilized in order to compare the medicane tracks between the model and the processed satellite data where such data was available. A characteristic case displayed here is Medicane Qendresa. The model was able to capture quite well the path of the cyclone with a deviation of relatively few kilometers (5-40 km) performing well both temporally and spatially, something clearly illustrated in Figure 6-3.

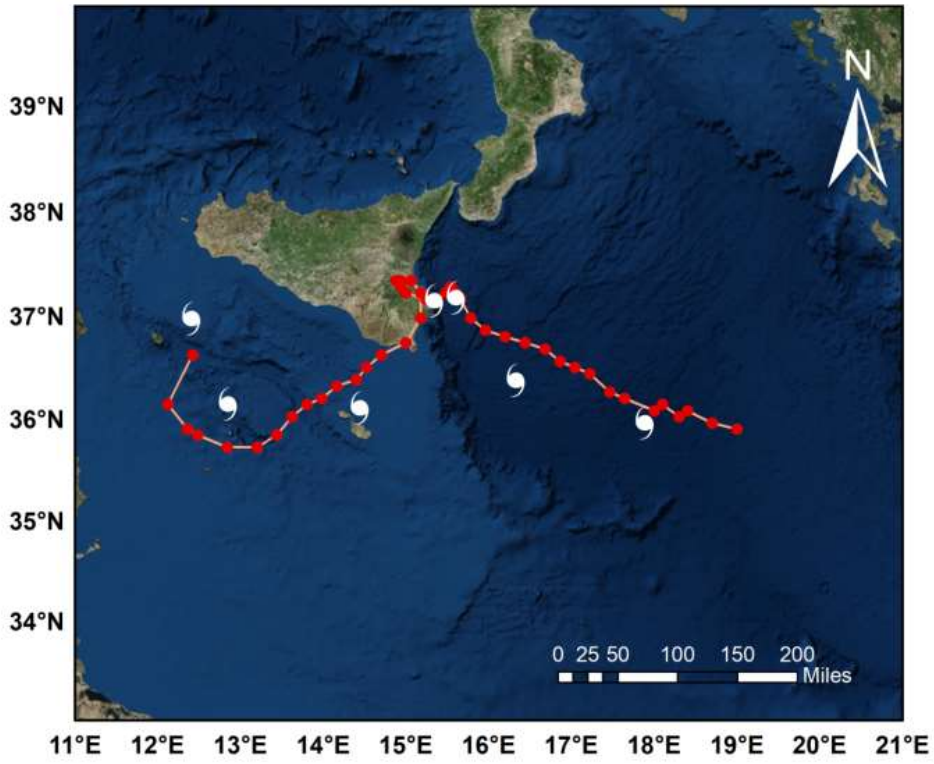

Figure 6-3: Modeled cyclone path (red dots – 1h time interval) and cyclonic path emerged from Blended Sea Winds (white cyclone symbol – 6h time interval). In both cases there is an eastward direction of the system.

It should be noted, however, that satellite data was not used for a point to point evaluation of wind and wave values. This choice was taken based on the fact that the coverage was limited but mainly because it is a post-process product and in the case of utilizing it for the evaluation of the magnitude of these parameters would add additional noise to the procedure.

6.2 Risk analysis methodology, de-clustering and dataset creation

The main scope of this study is to estimate areas highly affected by medicanes as well as their frequency and intensity in terms of both wind and wave parameters. The spatial extent of the affected regions is determined employing two different reference values regarding the wind and wave component respectively. Concerning wind, the reference value for the definition of the affected area is the Gale Speed (17.2 m/s) at 925 hPa. The reason that the 925 hPa level was selected is to reduce the effect of the Mediterranean complex topography in the index. The application of this procedure in a selected medicane (Medicane “Qendresa”) that took place in November 2014 is depicted in Figure 6-4. For consistency, the same event will be used as an example, demonstrating the following steps of the applied methodology.

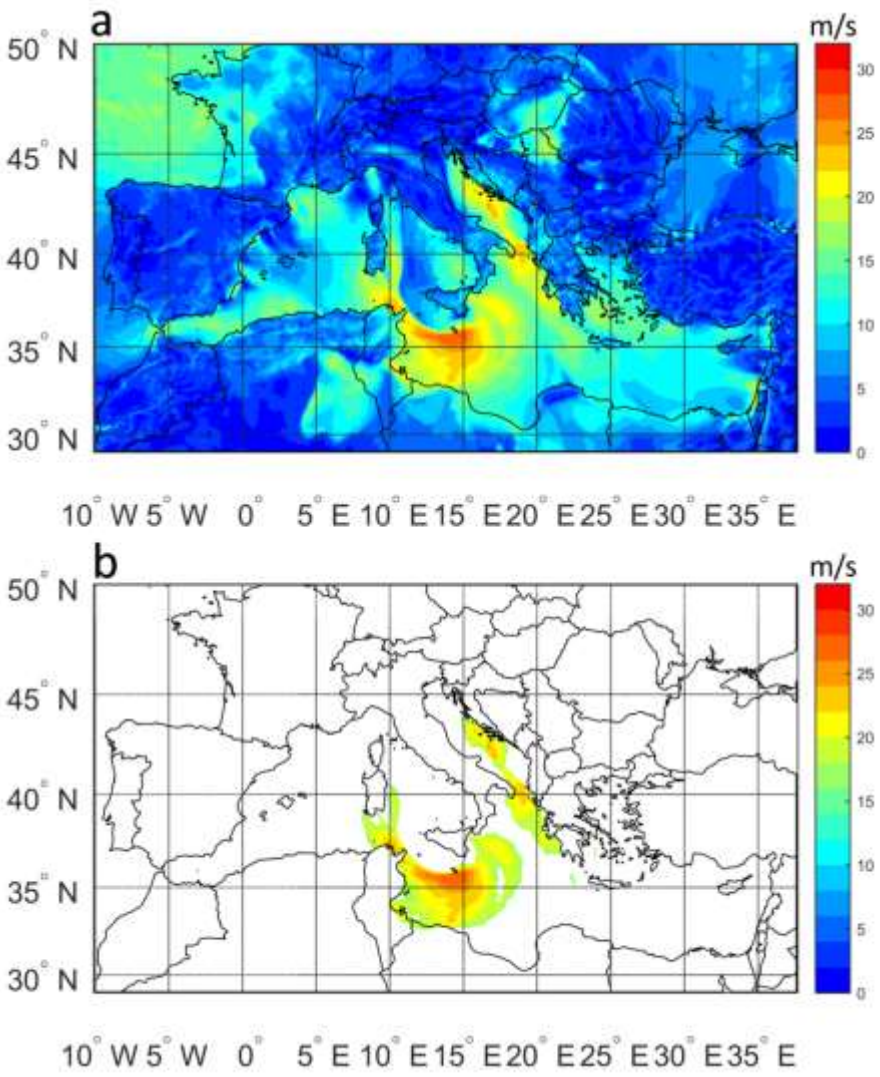

Figure 6-4: Wind speed at 925hPa (a) and wind affected areas/data used (b) of Medicane Qendresa (07 November 2014, 17:00 UTC).

The proposed definition for the influenced areas results into the inclusion of the directly affected ones (within the cyclone radius) but also of locations that are rather indirectly affected. One of the main goals of this study is to quantify areas of high potential impact even if these are not found within the strict limits of the estimated cyclone radius.

Accordingly, the definition of the wave affected areas is based on the status of the Very Rough State of the sea that corresponds to a Significant Wave Height (SWH) of 4 m in the Douglas scale (Figure 6-5).

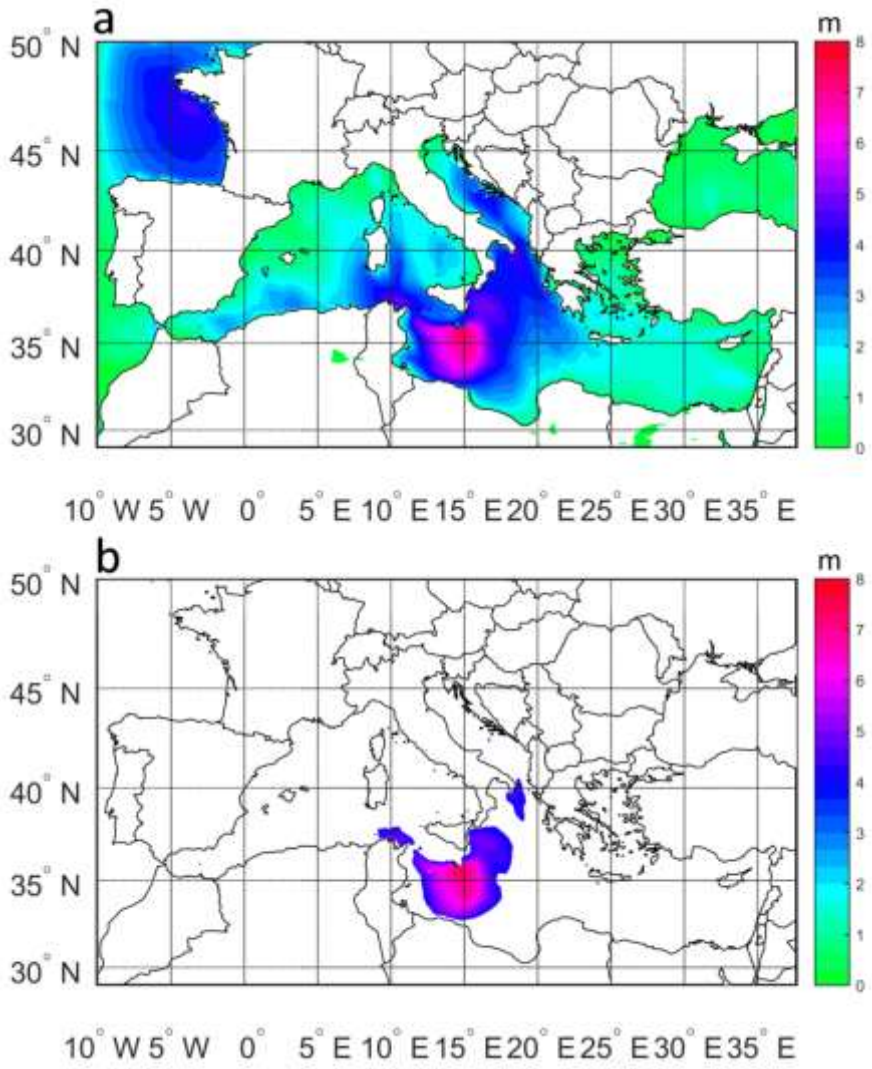

Figure 6-5: Significant wave height (a) and wave affected areas/data used (b) for Medicane Qendresa (07 November 2014, 17:00 UTC).

The result regarding the region affected by Medicane "Qendresa" during its lifespan for wind, wave and wind-wave combined is presented in Figure 6-6. Obviously the most affected region is the southern parts of Central Mediterranean Sea for all parameters and most parts of the Adriatic Sea regarding wind. This is associated to the cyclonic path, the fetch, the channeling effect in Adriatic and topography in general. Moreover, a characteristic effect during the evolution of this cyclone is the shading emanating from Sicily and Etna. The thresholds described above are crossed for more than 35 hours in all three approaches. In the description of the affected regions in general, all these outcomes from the simulated medicanes will be combined.

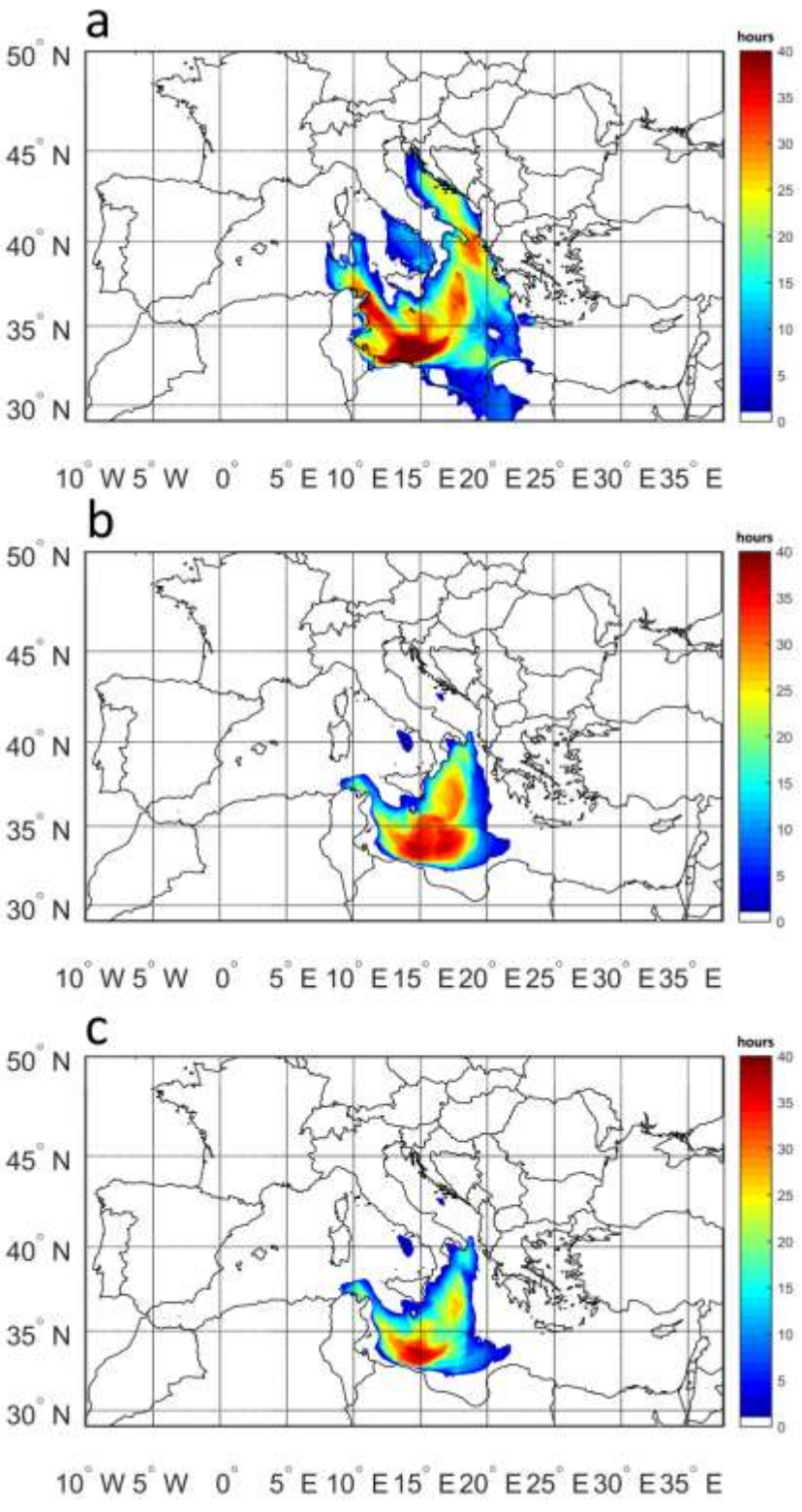

Figure 6-6: Wind (a), wave (b) and wind-wave (c) affected areas by Medicane "Qendresa".

Beginning with wind speed and the frequency of occurrence of values above the predefined threshold, the risk exposed regions are located mainly in the central and the western Mediterranean (Figure 6-7). These areas are positively associated to the regions of medicane genesis and their tracking, affected by the westerly flow at these latitudes. Regions 1, 3 and 4 (see Figure 6-1) have a larger fetch and are associated to higher winds while region 2 is surrounded by land and the created medicanes often dissipate in the coasts of Italy, thus not been able to deepen and induce more severe winds. It should be noted that the general pattern is consistent with the tropical-like cyclones climatology as provided by literature. Cavicchia et al. (2014) showed that the medicane genesis density has two maxima, one in the South of the Gulf of Lion and a second in the South of Sicily. The track density has also a pattern that is positively correlated to the outcome presented here with the cyclonic tracks to lie mainly between 34^{o}-41^{o} N and 3^{o}-19^{o} E. As stated earlier, the main objective of the study is the identification of the affected areas and the estimation of the return periods of medicanes and not the analysis of the meteorological conditions and paths during their development and evolution. Regarding this, areas that are indirectly affected are also taken into consideration. This is the case in many locations, for example in the Adriatic Sea or near the straits of Gibraltar. At the same time, regarding the maximum observed in the South of France, the particular area is directly affected by medicanes developed in Region 1 (Figure 6-1) and indirectly by the ones found mainly in Region 2 and secondary in Region 3. This is due to the fact that in our study all stages of the cyclonic life are taken into consideration. The initial phases of the low-pressure systems in these areas are often associated to the passage of a trough leading to atmospheric conditions that enhance a north wind flow over the Gulf of Lion. These, high density cold air masses accelerate as they move from land to water where the drag is considerably smaller resulting in the pattern displayed in Figure 6-7.

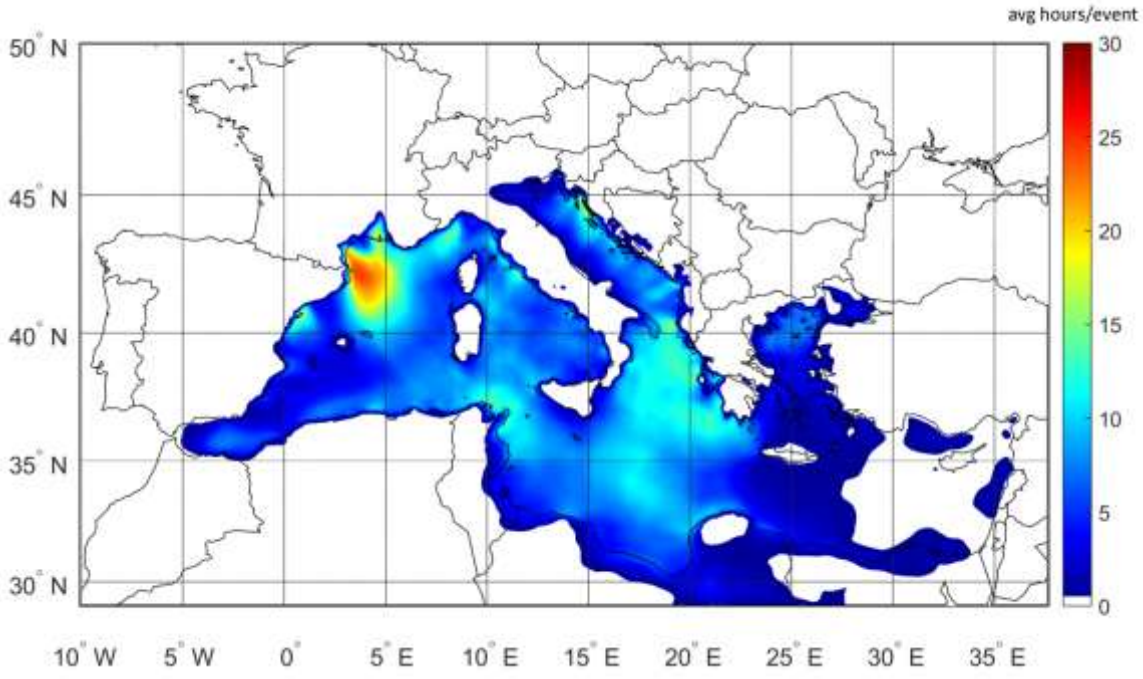

Figure 6-7: Wind affected (risk exposed) areas

While the areas affected from the TLC activity as defined above show consistency with previous research, the intensity of the winds in these regions is highly important for the characterization of risk exposed areas. Therefore, wind speed at 10m and surface gusts are further analyzed. Beginning with wind speed, the 90th and 97th quantiles regarding the outcome of all the modeled cyclones is presented in Figure 6-8. In both cases, the maximum values are positively correlated to the areas affected most. In the 90th percentile (Figure 6-8a), values reaching the 20 m/s are found in the South of the Gulf of Lion while in the rest of Mediterranean Sea the spatial variability is smoother with wind speed values around 10 m/s. Concerning the 97th quantile (Figure 6-8b), more local maximums and a greater variability are observed. The most characteristic can be attributed to the northwestern flow over the Gulf of Lion in cases where low pressure systems enhance this type of weather patterns and atmospheric circulation. Values greater than 23 m/s are found there while values reaching 19 m/s are observed all over the domain creating a similar pattern to that of Figure 6-7.

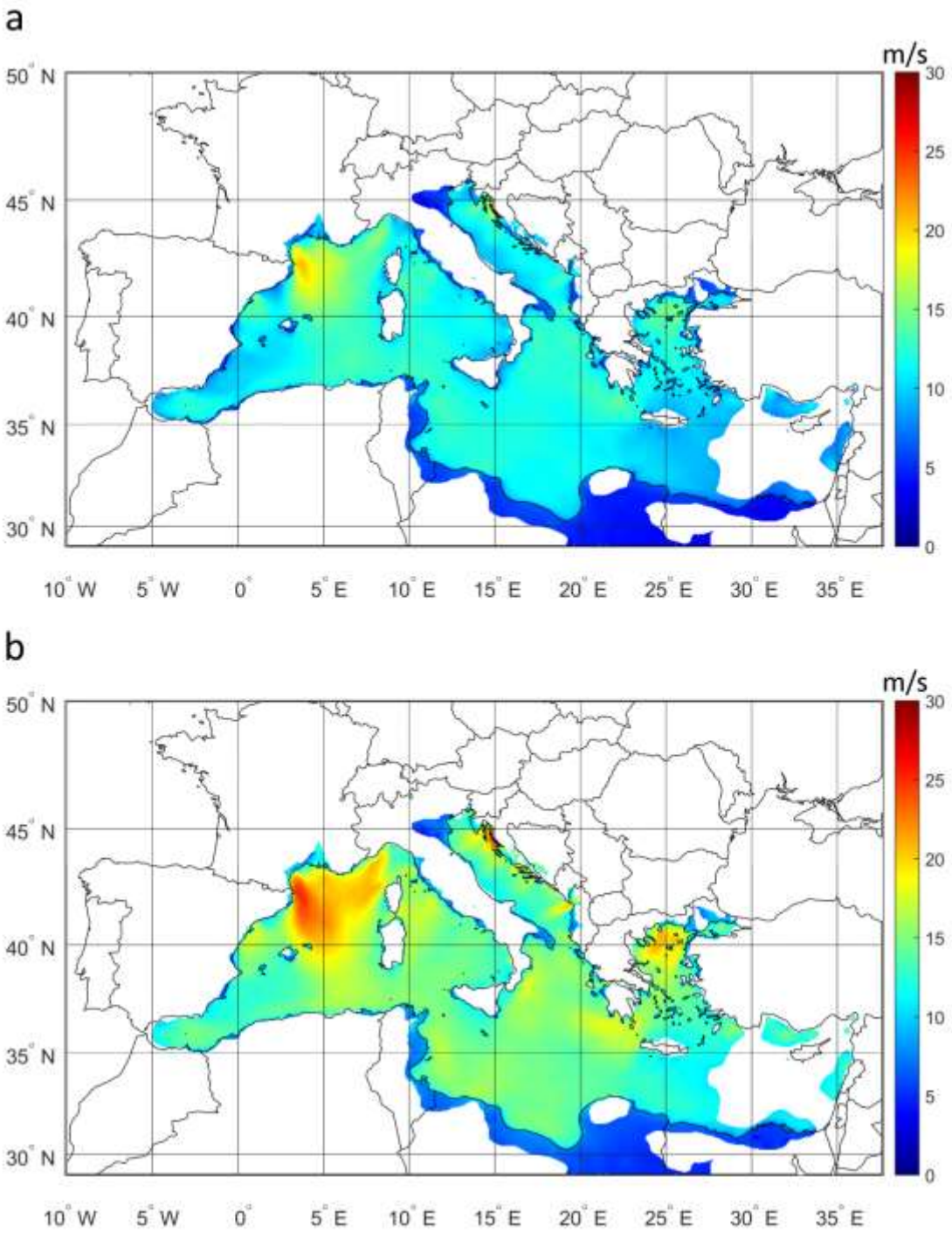

Figure 6-8: 90th (a) and 97th (b) quantile of 10m wind speed.

An additional variable to measure the potential losses and the impact of extreme events is the surface gust. Following the same principles, a greater spatial variability is observed in this

parameter as compared to wind speed at 10m. The areas with maximum values coincide to that of wind speed but with a greater extend. Values around 27 m/s and over 30 m/s are observed in the marine area on the south of France regarding the 90^{th} and the 97^{th} quantile of surface gust, respectively (Figure 6-9). Higher values are found in areas where air-land-sea interaction is present, with the complex terrain and the local climate to have a major role in this more intense gustiness. Having this in mind, a conclusion could be that populated areas face a higher threat and their exposure in extreme conditions is something that should be considered. The aforementioned pattern is found along the Valencian and Catalonian coasts in Spain, the east coasts of the Adriatic and the Ionian Sea as well as the North Aegean. It is noteworthy, however, that this is also associated to the frequency of the storm occurrence in particular areas as it affects the thickness of the distribution tail and thus the presented quantiles.

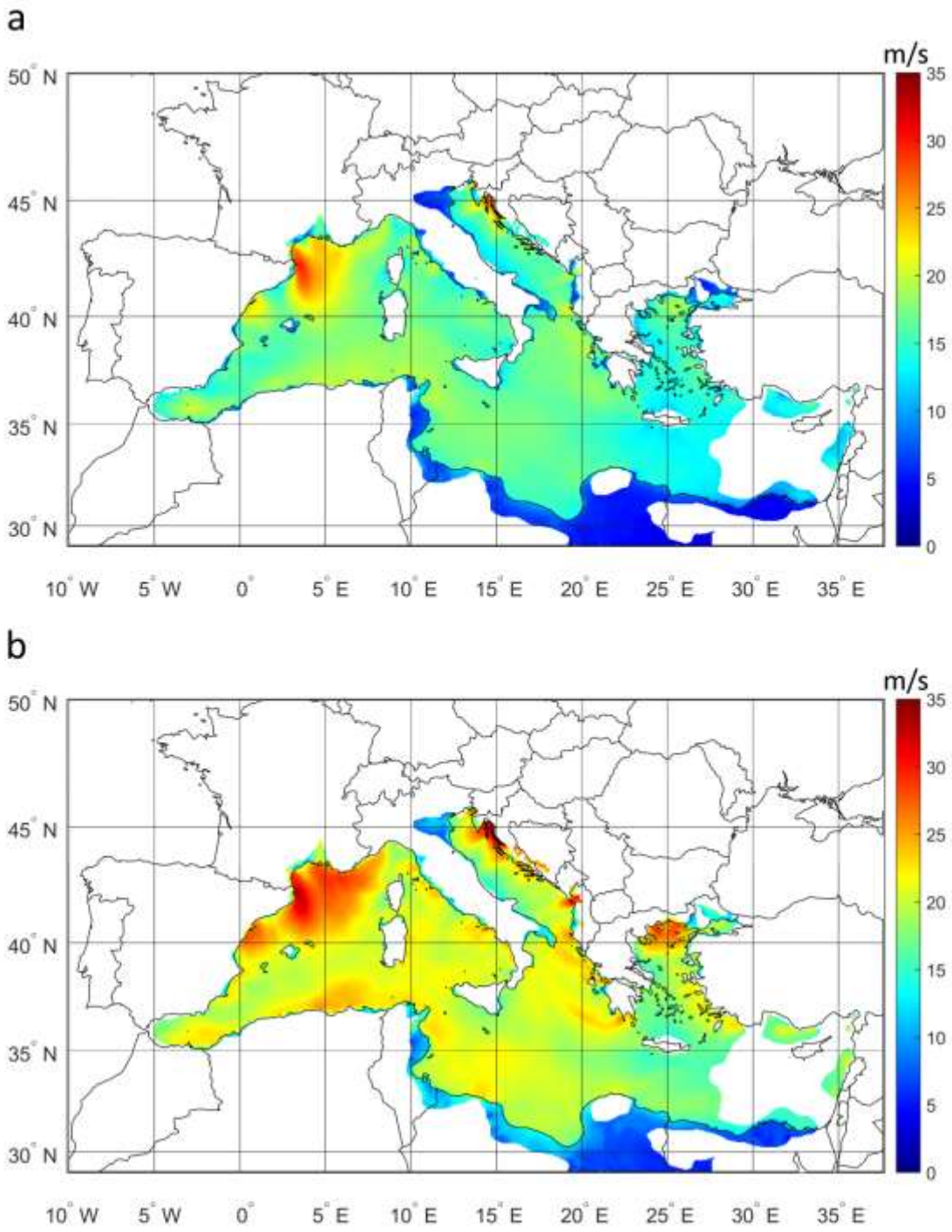

Figure 6-9: 90th (a) and 97th (b) quantile of surface wind gust.

Concerning the waves generated in these extreme conditions, the frequency of significant wave height qualified for the characterization of a Very Rough State of the sea (Figure 6-10) has

a similar pattern to the one of wind speed. This is rather expected since the generated waves surpassing the threshold are driven by the extreme winds during the cyclonic activity. At the same time the wave distribution is also smoother due to the complex interactions of wave frequencies and the presence of swell. The last is further highlighted through the differences between the spatial distribution of the wave (Figure 6-10) and the wind-wave (Figure 6-12) affected regions. It is quite interesting to notice the shadowing in the South of the Balearic Islands (Figure 6-10). This comes into agreement with what stated above regarding prevailing atmospheric conditions. It is getting clearer that in this area, northerly winds prevail, generating swell towards the South and therefore forming strip zones with lower waves at the wakes of the islands. Finally, a reduced rate of the wave threshold exceedances is observed as compared to the wind distribution above. However, this is just a matter of the employed definition and the selected threshold, something that can be subjective. For this reason, more attention should be given to the spatial distribution rather to the actual frequency values.

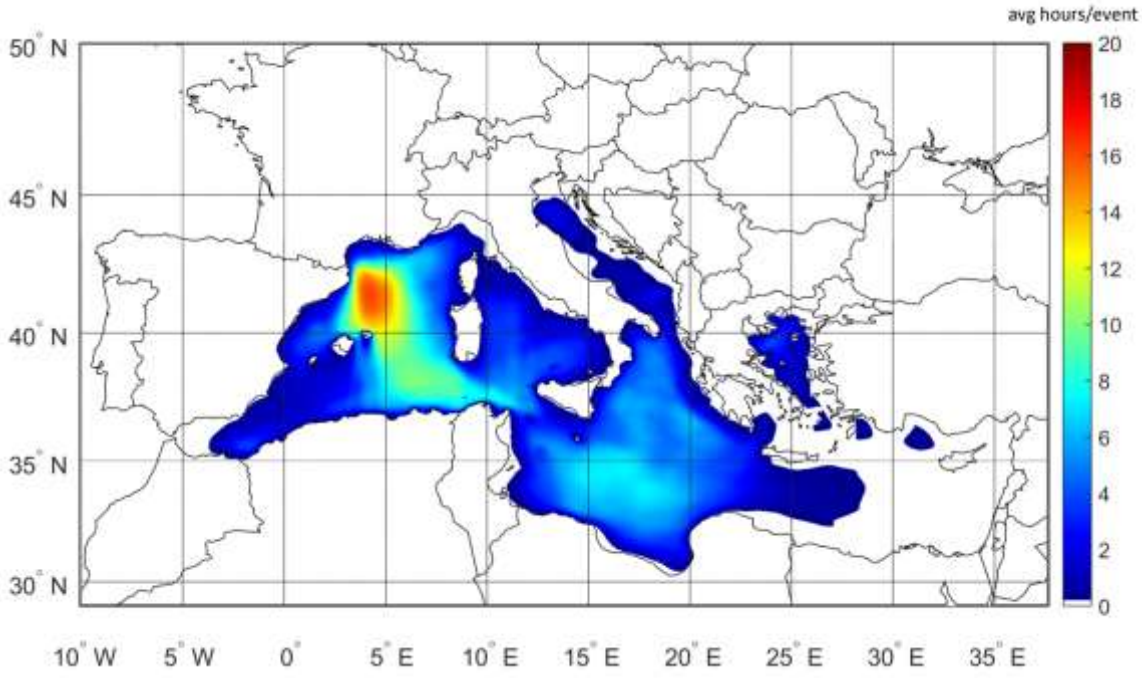

Figure 6-10: Wave affected (risk exposed) areas

Following the same concept to that of wind parameters, the 90th quantile of SWH follows the same spatial distribution to that of 10m wind speed (Figure 6-11). The values reach 5 meters

in the South of the Gulf of Lion while regarding the 97th quantile, values of around 6 m are observed. In contrast to the spatial distribution of wind parameters and especially to that of surface gust, higher values are observed in the open sea. This can be attributed to the larger fetch associated to the development of swell. Concluding, the maximum values are found in the western and secondary in the central Mediterranean Sea, where the medicane presence is more frequent.

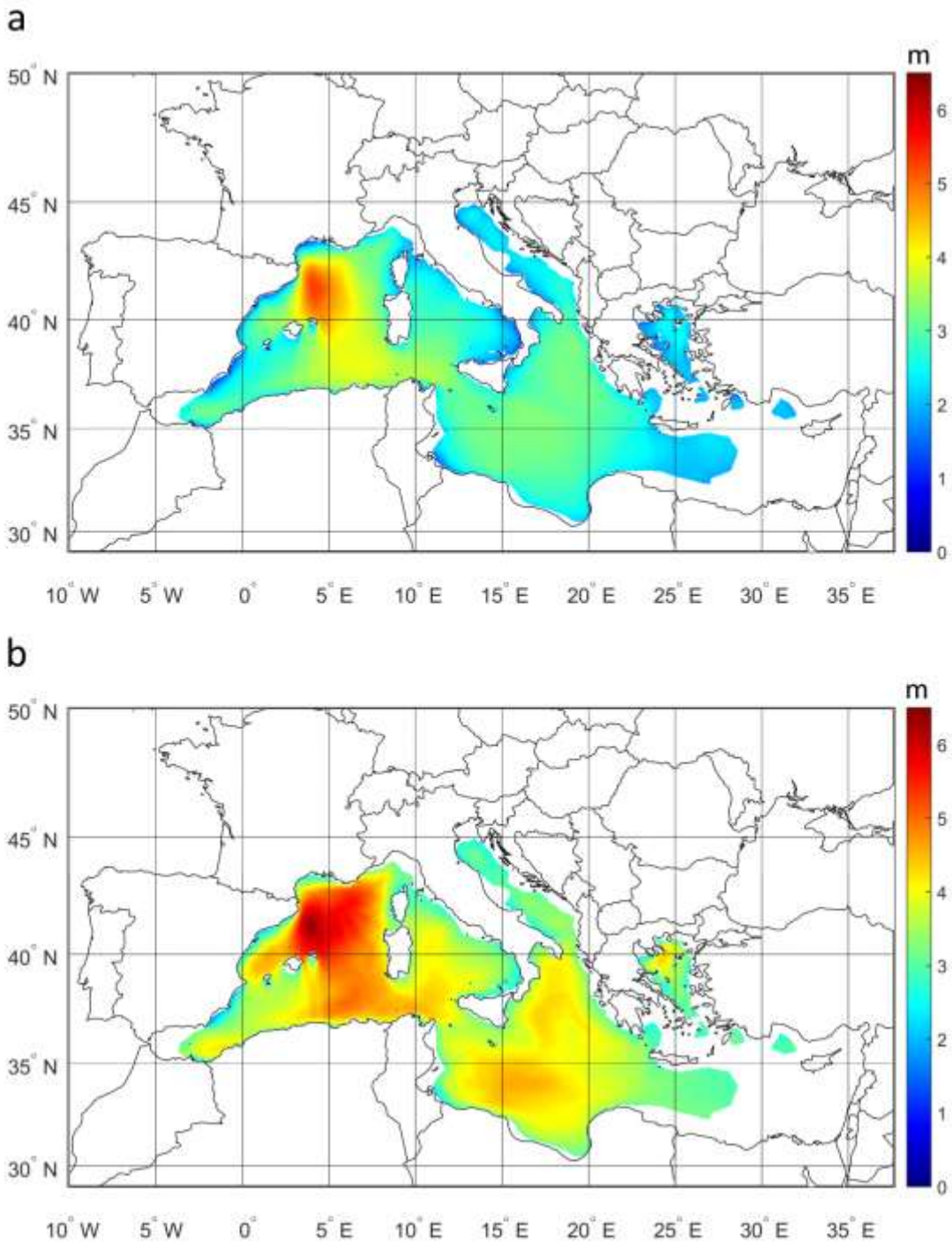

Figure 6-11: 90th (a) and 97th (b) quantile of significant wave height.

Continuing to the wind-wave affected areas, as expected the pattern (Figure 6-12) is quite similar to Figure 6-10 and the wave affected ones. The intercomparison of the wave and wind-

wave results can be used to define areas where intense waves are present without strong winds. These swell affected areas can be found throughout the whole domain but mainly on the north of Tunis (affected from cyclones generated in Region 1, 2 and 3 – Figure 6-1) and Algeria (affected mainly from cyclonic activity in Region 1– Figure 6-1). Despite this fact, in many cases the swell generated is not quite important due to the small life span of the cyclones and the limited fetch of the basin.

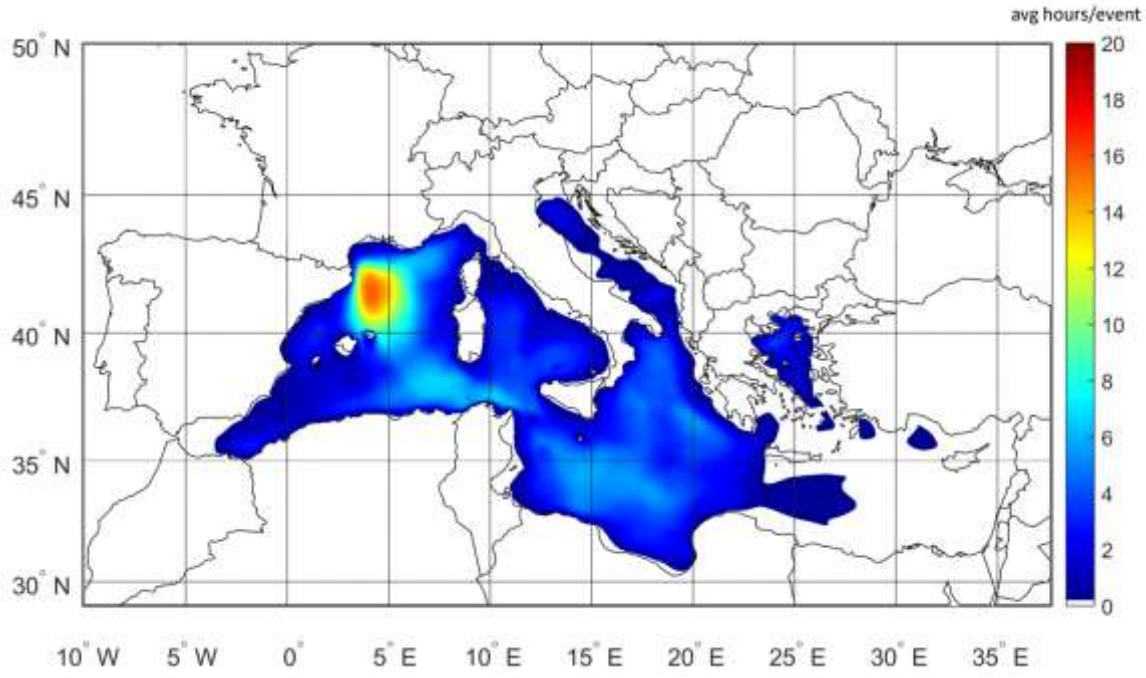

Figure 6-12: Wind-wave (combined) affected (risk exposed) areas

6.3 Return periods of medicanes

This chapter focuses on developing a summary measure of the storminess of TLCs in the Mediterranean. Towards this way, extreme indices that summarize storm intensity and spatial extent are used. The point is to be able to describe the extremity of the event by using just one value, utilizing the results of these indices and the concept of return periods (RP). The RP of medicanes can be a valuable measure in comparing actual and past events and in determining their socioeconomical impact. Actually, a similar concept is adopted by reinsurance companies

that often need a singular estimate of the frequency of an event to estimate the expected frequency of an aggregated loss over a portfolio (Della-Marta et al, 2009).

The first step is to employ the same domains defined from the wind process for the dataset creation needed for the application of the Extreme Value Theory. The return periods of medicane intensity will be estimated in terms of 10m wind speed, surface gustiness, wind speed at 925 hPa and significant wave height. This is the reason why the same areas defined by wind speed at 925 hPa (Figure 6-6b) are also employed for the 10m wind speed and surface gust (Figure 6-13 a, b).

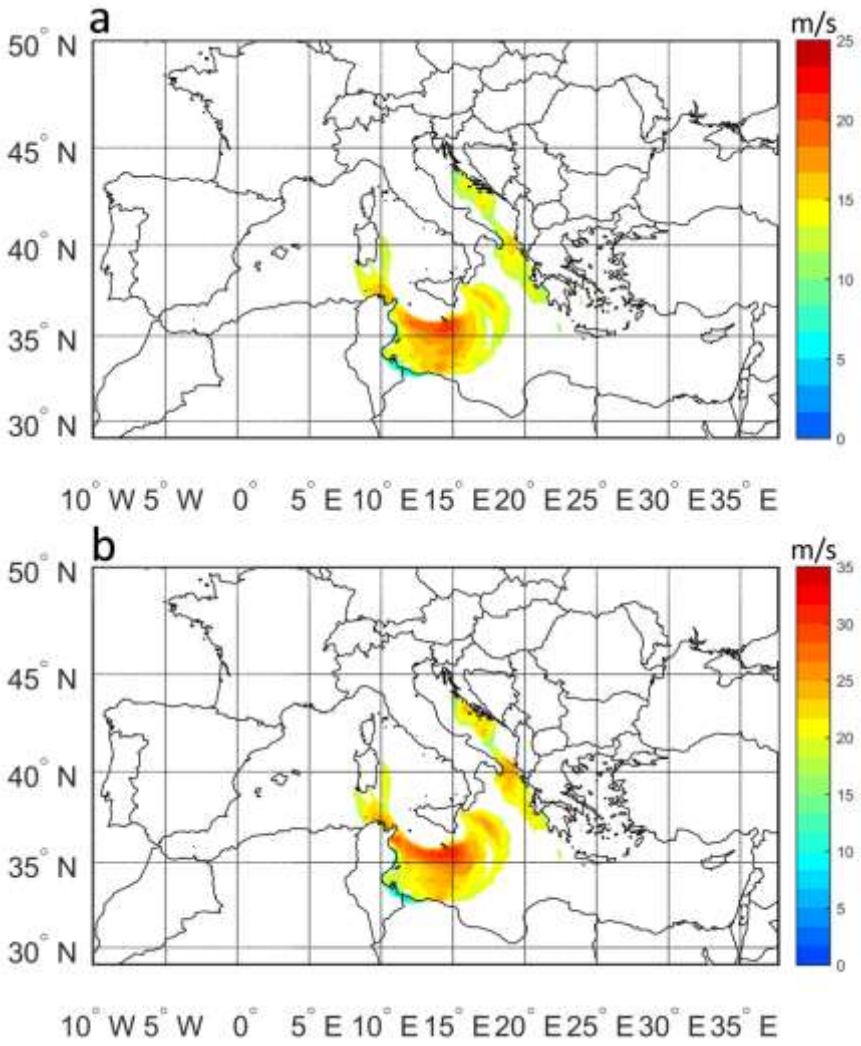

Figure 6-13: Data used regarding wind speed at 10m (a) and surface gust (b) for Medicane Qendresa (07 November 2014, 17:00 UTC).

In order to create the scalar values to be used for the estimation of the return periods of the medicanes, three different extreme indices were employed (Della-Marta et al, 2009), mean value, the spatial 95th quantile and the maximum value (see chapter 3.4).

The created sequences can be an indication of the evolution of each medicane (Figure 6-14), while their maximum values (shown with dots) are used for the extreme value analysis application.

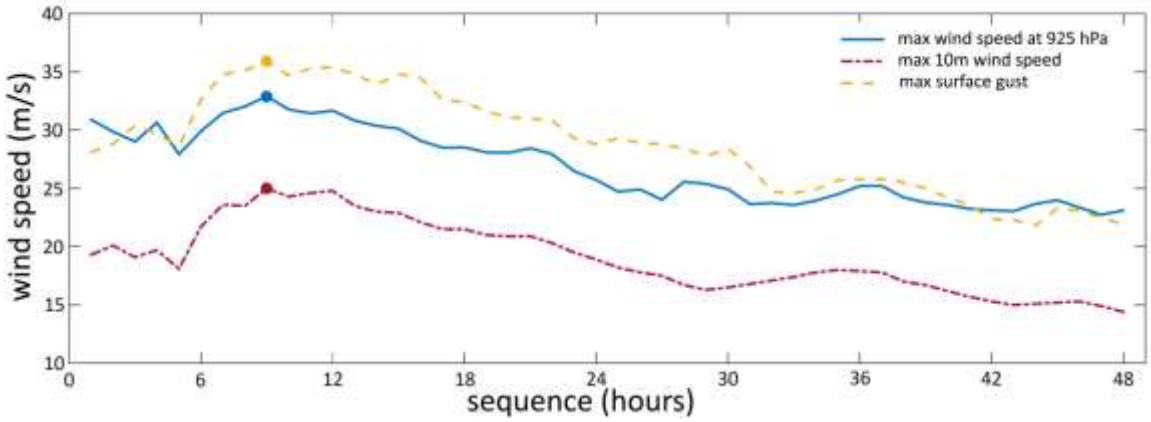

Figure 6-14: The maximum value index evolution through time for the Medicane Qendresa (starting at 07 November 2014, 00UTC)

One basic restriction for the application of the Extreme Value Theory is the need of independence between the utilized values (Patlakas, 2016). It should be noted that these values are considered to be independent here, since they belong to different events. The independency is ensured using a physical approach describing the existence and development of an event (here medicanes) and not a statistical one.

The three extreme indices are created from the parameters used for the study while the maximum values for each event were picked to create the Event Maxima, covering a 25-year period.

Two different approaches are followed for the estimation of the return levels of medicanes in terms of wind speed and wave height. The first approach requires the maximum value for each year to be selected for the creation of the Annual Maxima (AM) and the application of the homonymous methodology for the estimation of their return periods (RP) (Patlakas et al, 2016;

Patlakas et al, 2017b). The second approach takes all the available events into account and is similar to the Method of Independent Storms (MIS) (Cook, 1982; Cook, 1986; Palutikof et al, 1999). In our case, the independence of the storms is guaranteed from the nature of the event and the dataset creation methodology.

Beginning with the wind variables, the AM curve has a higher starting point, with differences varying in a range between 1-5 m/s depending on the variable and the index applied (Figures 6-15 - 6-17). This fact can be attributed to the greater values taken into consideration in the AM methodology. In general, the differences between the two approaches are insignificant and within the confidence intervals. It should be also mentioned that the confidence intervals emerged from the MIS methodologies are more limited as compared to the AM ones. The last is something expected due to the fact that in MIS more values are utilized leading to smaller uncertainty. Additionally, a highlight would be the slightly faster convergence of the AM methodology in almost all cases. This can be attributed to the fact that in MIS approach more extreme values are taken into consideration leading to larger distribution spread and larger scale parameters after the distribution fit. The same pattern is evident moving from the mean values to the 95^{th} quantiles and the maximum ones. The exponentiality consecutively grows and the reason is that the spatial averaging leads to smooth results and small differences thus small spread. This is weaker in 95^{th} percentile and not present at all when it comes to the application in the maximum values.

The 50-year mean wind speed at 10 m is around 19-20 m/s while the 95^{th} percentile is around 29 m/s with the AM to present slightly higher values (Figure6-15). Regarding the maximum winds, the 50-year extreme value is about 33-35 m/s. In this case the MIS curve manages to overtake the AM one quite early in terms of return periods due to the fast convergence of the second. This outcome is quite common in the maximum values of the wind related parameters as a faster curve crossing is observed.

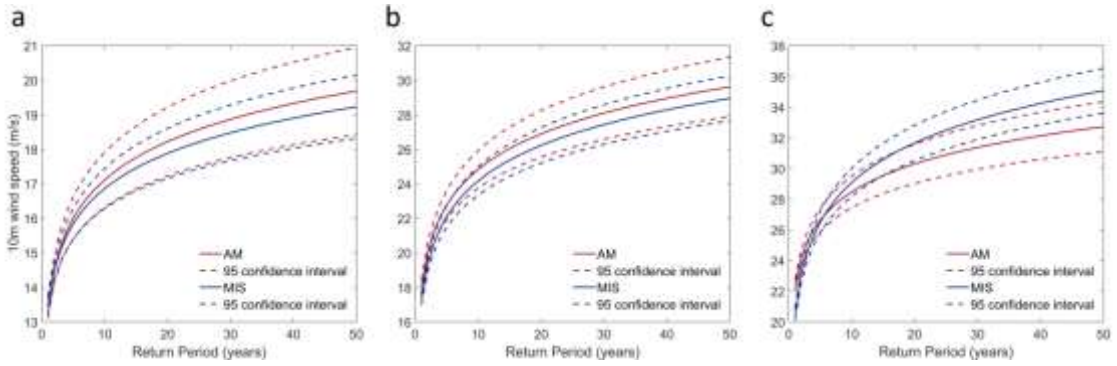

Figure 6-15: Return periods of medicanes in terms of wind speed at 10m regarding the mean (a), the 95th quantile (b) and the maximum (c) values.

Wind speed at 925 hPa has, more or less, a similar behavior with the one of 10m. The 50-year values for the mean, the 95th percentile and the maximum wind speed is around 25, 38 and 45 m/s respectively (Figure 6-16). Something rather expected, is the obvious reduction in the wind speed field values as we move from 925 hPa to 10m. This is attributed to drag as lower winds are found near the surface.

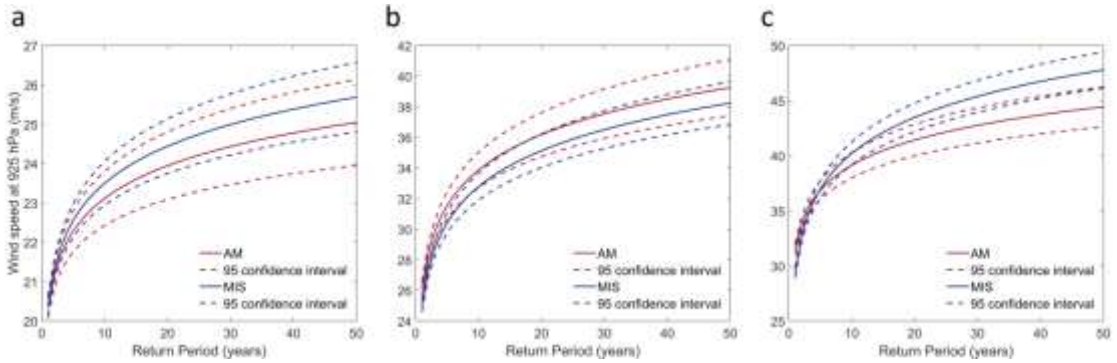

Figure 6-16: Return periods of medicanes in terms of wind speed 925 hPa regarding the mean (a), the 95th quantile (b) and the maximum (c) values.

Surface gust values (Figure 6-17a-c) have the widest range regarding all indices up to now. A fifty-year return period mean surface gust is expected to reach 31 m/s while regarding the 95th percentile the estimation is around 44-45 m/s. Regarding the maximum surface gust, values around 50 m/s have a chance of 2% to happen. Despite the high estimated intensity, these values can be realistic in extreme events especially in complex environment. At the same time,

although it is not obvious at a first glance, surface gust presents the highest deviation among the three extreme indices, which comes as a result of its local nature.

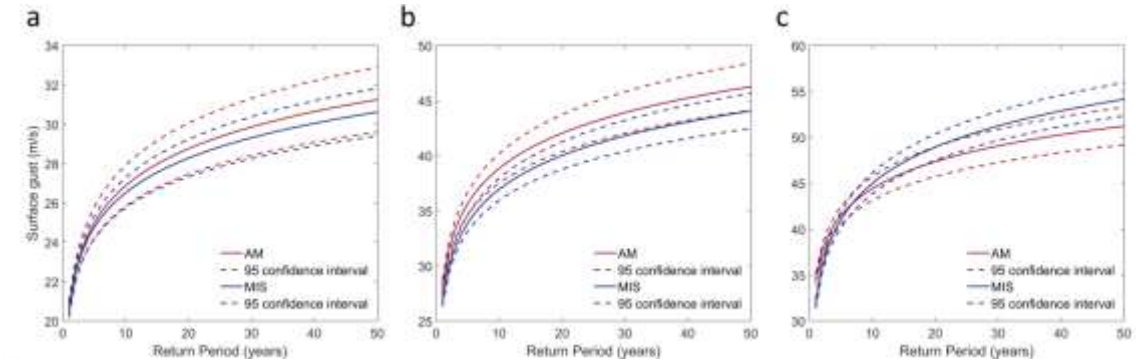

Figure 6-17: Return periods of medicanes in terms of surface gust regarding the mean (a), the 95th quantile (b) and the maximum (c) values.

Moving to the wave perspective and significant wave height, the convergence is similar for both AM and MIS (Figure 6-18). Smaller confidence intervals are present for MIS, something explained earlier. The fifty-year average spatial SWH reaches the 6.5 m while the spatial 95th percentile ranges around 9-10 m. At the same time, the maximum SWH is around 10-11 m for the same recurrence interval. This magnitude is quite high for a closed basin like the Mediterranean but can be found under specific conditions, fetch type and event duration.

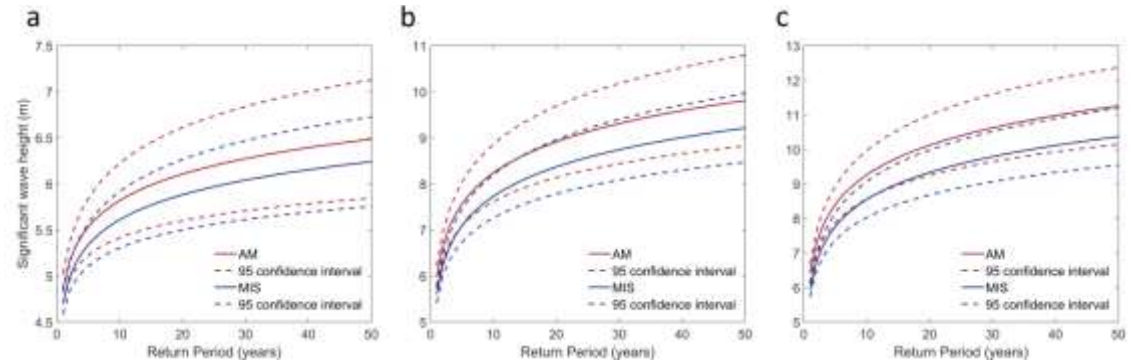

Figure 6-18: Return periods of medicanes in terms of significant wave height regarding the mean (a), the 95th quantile (b) and the maximum (c) values.

6.4 Concluding remarks

The Mediterranean basin is strongly affected by cyclonic events with different characteristics. Medicanes form a category of Mediterranean cyclones characterized by tropical characteristics at least at one point during their lifespan.

The spatial extent of the regions affected by these events was addressed employing two different reference values, one for wind at 925 hPa and one for significant wave height. Concerning wind, the risk exposed regions are located mainly in the central and the western Mediterranean. A maximum on the affected areas is observed in the Gulf of Lion. The 90^{th} percentile values reach the 20 m/s in the south of the Gulf of Lion while in the rest of Mediterranean Sea they are lower. Higher values as expected are found regarding the wind speed 97^{th} quantile, accompanied however with more local maximums and a greater variability. Continuing with surface gusts, the pattern is similar to that of wind speed at 10m with greater values and variability. Higher values are traced in areas where air-land-sea interaction is present.

The wave affected areas, defined through a threshold that corresponds to the Very Rough State of the sea, are like the ones of wind speed. This is something expected since the generated waves are mainly wind driven. The 90^{th} quantile of SWH follows the same spatial distribution to that of 10m wind speed with values of 5 meters in the South of the Gulf of Lion. Concerning the 97^{th} quantile, values of 6 m are observed. As expected, higher values are observed in the open sea. This can be attributed to the larger fetch associated to the development of swell. A similar state is observed regarding the wind-wave affected areas. The intercomparison of the last two datasets can be used to define areas where swell is present. These areas can be found in the straights between Majorca and Menorca and in larger domains on the area north of the coasts Tunis and Algeria.

In addition to the definition of the risk exposed regions, the return periods of medicanes are studied in terms of wind and wave parameters. For this reason, three extreme indices (mean value, 95^{th} percentile and maximum values) alongside with two different extreme value theory approaches (AM and MIS) were employed. Beginning with the wind variables, the differences between the two approaches are insignificant and within the confidence intervals. MIS produced smaller confidence intervals compared to AM due to the fact that it takes into account

more values. Additionally, AM is characterized by a faster convergence, something also found moving from the mean values to the 95th quantiles and the maximum ones. The exponentiality grows and the reason can be found in the spatial averaging leading to smoother results. Regarding the significant wave height, the convergence is similar for both AM and MIS. Smaller confidence intervals are also present for MIS.

The proposed methodology is useful from a climatological point of view as information can be derived regarding the risk exposed areas and the return periods of medicanes in terms of wind and wave parameters. The extremity of the event is environmental parameter depended; thus, it could help towards employing targeted measures. The last, associated to the losses these events could result to, can be of great assistance to the reinsurance sector and civil protection as well as to other industries such as platform exploitation (oil and gas energy activities), coastal management, tourism, transportation fisheries and other offshore and coastal economic activities.

7 General Conclusions – Future Work

In this dissertation, extreme weather events are studied through various approaches. The main objective was to propose ways of expressing the repeatability of such events by taking into consideration different environmental parameters and other factors such as their duration. This is achieved through the concept of return periods, a statistical estimate for the frequency of extreme phenomena based on limited data. The analysis is performed under the principles of Extreme Value Theory employing different methodologies, tools and datasets.

The Thesis moves gradually from a gridded approach for the estimation of the potential extreme values towards a sub-regional one and finally to an object-oriented methodology. The gridded approach is the most complete as it contains all the raw information in all grid points considered and it is suitable for making extreme value Atlases. The outcome can be used to define the probability of occurrence alongside the duration regarding extreme events and their effects in various sectors such as wind energy applications. Here, the methodology was applied focusing both on extreme and low winds. The impact of such cases in an economy based on wind energy could be critical. However, there are several sectors (e.g. reinsurance) that apart from the most common approaches like this, require additional information on a regional basis. This can be achieved employing an extreme index that summarizes the behavior of the area through a single value. There are cases, though, whose destructivity is not reflected in the estimated return periods from this approach. Therefore, an attempt to address the extremity adopting an event-oriented approach is performed. To test this scenario a particular weather pattern was selected; medicanes. The last form a category of Mediterranean cyclones characterized by tropical characteristics at least at one point during their lifespan.

A general remark regarding the outcome is that the POT method seems to result in higher values compared to AM. This can be attributed to the fact that the first takes into consideration also the secondary maxima, which leads in a thicker distribution tail in contrast to AM in particular regions. Also, the confidence intervals for the estimated return periods are wider in the application of the AM methodology due to the larger data used for the analysis.

When focusing on low wind speed events and their duration, the Maximum Likelihood method for the parameter-fitting was found to better perform regarding the Intensity Given Duration approach. The study was also focused on the examination of the performance of the

Duration Given Intensity approach by using four different theoretical probability distributions in the application of AM method. This revealed a constant underestimation when using Gumbel and Weibull distribution. The application of G.E.V. distribution led to outcome of no particular pattern and large deviations while the best results were achieved by using the Rayleigh distribution. Regarding the wind speed probability distribution upper tail, the intensity, duration and frequency of the events were found to be highly affected by the topography. Especially over land there is an increased spatial variability in their behavior.

In the sub-regional analysis, the spatially maximum values or high spatial quantiles should not be selected as extreme indices for large areas. This is supported by the fact that they resulted in remarkable differences among AM and POT methodologies and/or the rest indices. In general, the events are characterized by lower return periods in terms of significant wave height. It should be also noted that there are cases with impact that was not reflected in the estimated extremity from this approach.

Regarding the object-oriented analysis, the medicane affected regions are mainly in the central and the western Mediterranean. The most affected area is the Gulf of Lion. The wave affected areas are similar to the ones of wind speed. This is something expected since the generated waves are mainly wind-driven. A similar state is observed regarding the wind-wave affected areas. In addition to the definition of the risk exposed regions, the return periods of medicanes are studied in terms of wind and wave parameters using AM and MIS. The differences between the two methodologies used are insignificant and within the confidence intervals. AM is characterized by a faster convergence, something also found moving from the mean values to the 95^{th} quantiles and the maximum ones. The exponentiality grows and the reason can be found in the spatial averaging leading to smoother results.

The proposed approaches are useful from a climatological perspective and could be helpful towards employing more targeted measures. The last, associated to the losses of these events can be of great assistance to the reinsurance sector and civil protection as well as to other industries such as platform exploitation (oil and gas energy activities), coastal management, tourism, transportation fisheries and other offshore and coastal economic activities.

Plans for future work based on the findings of this work can be summarized as follows:

This work can be enriched with additional analysis in the definition of extremes and the affected regions and the development of stochastic processes for a more comprehensive outcome. It this context some future work could be focused in the following:

Employ another approach for the separation of the domain in zones such as through Principal Component Analysis.

Use bivariate approaches in the Extreme Value Analysis studying for example the effects of extreme wind speed under particular circumstances such an intense precipitation.

Add other important parameters affecting the destructivity of extreme events such as precipitation and storm surge.

Expand the object-oriented approach so as to include other extreme weather systems.

Utilize the developed approach in climate change studies.

References

1. Abild, J., Andersen, E. Y. & Rosbjerg, D., 1992. The climate of extreme winds at the Great Belt, Denmark. J. Wind Eng. Ind. Aerodyn., 41–44: 521–532.
2. Adams, N., 2004. A numerical modeling study of the weather in east antarctica and the surrounding southern ocean. Wea. Forecast., 19, 653–672.
3. Akhtar, N.; Brauch, J.; Dobler, A.; Béranger, K.; Ahrens, B., 2014. Medicanes in an ocean–atmosphere coupled regional climate model. Nat. Hazards Earth Syst. Sci. 2014, 14, 2189-2201, doi:10.5194/nhess-14-2189-2014.
4. Albers, S.C., 1995. The LAPS wind analysis. Weather Forecast., vol. 10, no. 2, pp. 342–352.
5. Alexander LV, Tett SFB, Jonsson T., 2005. Recent observed changes in severe storms over the United Kingdom and Iceland. Geophysical Research Letters 32(13): L13 704.
6. Alexandersson H, Schmith T, Iden K, Tuomenvirta H., 1998. Long term variations of the storm climate over NW Europe. Global Atmospheric and Ocean Systems 6: 97–120.
7. Alexandersson, H., Tuomenvirta, H., Schmith, T., Iden, K., 2000. Trends of storms in NW Europe derived from an updated pressure data set Clim. Res., 14 (2000), pp. 71-73
8. Aliabadi, A.A., Staebler, R.M., de Grandpré, J., Zadra, A. and Vaillancourt, P.A., 2016. Comparison of Estimated Atmospheric Boundary Layer Mixing Height in the Arctic and Southern Great Plains under Statically Stable Conditions: Experimental and Numerical Aspects, Atmosphere-Ocean, 54:1, 60-74, DOI: 10.1080/07055900.2015.1119100
9. Astitha, M., G. Kallos, C. Spyrou, W. O'Hirok, J. Lelieveld, and H. A. C. Denier van der Gon, 2010. Modelling the chemically aged and mixed aerosols over the eastern central Atlantic Ocean – potential impacts, Atmos. Chem. Phys., 10(13), 5797– 5822, doi:10.5194/acp-10-5797-2010.
10. Barrett, J. H., and D. A. Short, 2008. Peak wind tool for general forecasting. nasa contractor report nasa/cr-2008-214743. Technical report, NASA Applied Meteorology Unit, Kennedy Space Center, Florida.
11. Barring L, von Storch H., 2004. Scandinavian storminess since about 1800. Geophysical Research Letters 31(20): L20 202.
12. Bartholy, J.; Pongrácz, R.; Pattantyús-Ábrahám, M., 2009. Analyzing the genesis, intensity, and tracks of western Mediterranean cyclones. Theoretical and Applied Climatology 2009, 96, 133-144, doi:10.1007/s00704-008-0082-9.
13. Beate Geyer, Ralf Weisse, Peter Bisling, Joerg Winterfeldt, 2015. Climatology of North Sea wind energy derived from a model hindcast for 1958–2012, Journal of Wind Engineering and Industrial Aerodynamics, Volume 147, 2015, Pages 18-29, ISSN 0167-6105, https://doi.org/10.1016/j.jweia.2015.09.005.
14. Bidlot J.-R., 2012. Present status of wave forecasting at ECMWF. Proceedings from the ECMWF Workshop on Ocean Waves, 25-27 June 2012. ECMWF, Reading, United Kingdom.
15. Bidlot, J. and Janssen, P.,2003. Unresolved bathymetry, neutral winds and new stress tables in WAM. Tech. Rep. ECMWF Research Department Memo R60.9/JB/ 0400, ECMWF.
16. Bidlot, J., Janssen, P., Abdalla, S., Hersbach, H., 2007. A revised formulation of ocean wave dissipation and its model impact. ECMWF Tech. Memo. 509. ECMWF, Reading, United Kingdom, 27pp. available online at: http://www.ecmwf.int/publications/.

17. Bouwer, L. M., 2010. Have disaster losses increased due to anthropogenic climate change? Bulletin of the American Meteorological Society, 92(1), 39–46. https://doi.org/10.1175/ 2010BAMS3092.1
18. Bouws, E., Draper, L., Shearman, E.D.R., Laing, A.K., Feit, D., Mass, W., Eide, L.I., Francis, P., Carter, D.J.T. and Battjes, J.A., 1998. Guide to Wave analysis and forecasting. WMO-No. 702. World Meteorological Organization.
19. Brasseur, O.,2001. Development and Application of a Physical Approach to Estimating Wind Gusts. Monthly Weather Review 2001, 129, 5-25, doi:10.1175/1520-0493(2001)129<0005 :daaoap>2.0.co;2.
20. Breivik, Ø., Aarnes, O.J., Abdalla, S., Bidlot, J.-R. and Janssen, P.A.E.M., 2014. Wind and wave extremes over the world oceans from very large ensembles. Geophys. Res. Letters, Volume 41, Issue 14, pages 5122–5131.
21. Caires, S., and A. Sterl., 2004. 100-Year Return Value Estimates for Ocean Wind Speed and Significant Wave Height from the ERA-40 Data. J. of climate vol.18
22. Campins, J., Genovés, A., Picornell, M.A., Jansà, A., 2011: Climatology of Mediterranean cyclones using the ERA-40 dataset. Int J Climatol 31:1596–1614.
23. Cavicchia, L.; Storch, H.v.; Gualdi, S., 2014. Mediterranean Tropical-Like Cyclones in Present and Future Climate. Journal of Climate 2014, 27, 7493-7501, doi:10.1175/jcli-d-14-00339.1.
24. Chaboureau, J.-P.; Pantillon, F.; Lambert, D.; Richard, E.; Claud, C., 2012. Tropical transition of a Mediterranean storm by jet crossing. Quarterly Journal of the Royal Meteorological Society 2012, 138, 596-611, doi:10.1002/qj.960.
25. Chan, P. W., C. C. Lam, and P. Cheung, 2011. Numerical simulation of wind gusts in intense convective weather and terrain-disrupted airflow. Atmsfera, 24, 287–309.
26. Chang, H., & Franczyk, J., 2008. Climate change, land-use change, and floods: Toward an integrated assessment. Geography Compass, 2(5), 1549–1579. https://doi.org/10.1111/j.1749-8198.2008.00136.x
27. Chassignet E.P., Smith L.T., Halliwell G.R. and Bleck R., 2003. North Atlantic simulations with the Hybrid Coordinate Ocean Model (HYCOM): impact of the vertical coordinate choice, reference pressure, and thermobaricity, J. Phys. Oceanog., 33, 2504–2526.
28. Cheung, P., C. C. Lam, and P. W. Chan, 2008. Numerical simulations of wind gusts in terrain-disrupted airflow at the Hong Kong international airport. P2.34, 13th Conference on Mountain Meteorology, Whistler, BC, Canada, AMS.
29. Claud, C.; Alhammoud, B.; Funatsu, B.M.; Chaboureau, J.-P., 2010. Mediterranean hurricanes: large-scale environment and convective and precipitating areas from satellite microwave observations. Natural Hazards and Earth System Sciences 2010, 10, 2199-2213, doi:10.5194/nhess-10-2199-2010.
30. Clough, S.A., Shephard, M.W., Mlawer, E.J., Delamere, J.S., Iacono, M.J., Cady-Pereira, K., Boukabara, S., Brown, P.D., 2005. Atmospheric radiative transfer modeling: a summary of the AER codes. J. Quant. Spectrosc. Radiat. Transfer., 91, 233-244, 2005
31. Coles, S. G. & Walshaw, D., 1994. Directional modelling of extreme wind speeds. Appl. Stat., 43: 139–157.
32. Coles, S., 2001. An Introduction to Statistical Modeling of Extreme Values. Springer-Verlag, 208 pp.
33. Cook, N. J., 1985. The Designer's Guide to Wind Loading of Building Structures. Part 1: Background, Damage Survey, Wind Data and Structural Classification. Building Research Establishment, Garston, and Butterworths, London, 371 pp.

34. Cook, N.J., 1982. Towards better estimation of extreme winds. Journal of Wind Engineering and Industrial Aerodynamics 1982, 9, 295-323, doi:https://doi.org/10.1016/0167-6105(82)90021-6.
35. Cotton, W.R.; Pielke Sr., R.A.; Walko, R.L.; Liston, G.E.; Tremback , C.J.; Jiang, H.; McAnelly, R.L.; Harrington, J.Y.; Nicholls , M.E.; Carrio, G.G., et al., 2003. RAMS 2001: Current status and future directions. Meteorology and Atmospheric Physics 2003, 82, 5-29, doi:10.1007/s00703-001-0584-9.
36. Cramér, H., 1946. Mathematical Methods of Statistics. Princeton New Jersey: Princeton Uni. Press.
37. Dafka, S., Toreti, A., Luterbacher, J., Zanis, P., Tyrlis, E., Xoplaki, E., 2018. Simulating extreme etesians over the Aegean and implications for wind energy production in Southeastern Europe. (2018) Journal of Applied Meteorology and Climatology, 57 (5), pp. 1123-1134.
38. Dangendorf, S., Mudersbach, C., Wahl, T., Jensen J., 2013. Characteristics of intra-, inter-annual and decadal sea-level variability and the role of meteorological forcing: the long record of Cuxhaven. Ocean Dyn., 63 (2013), pp. 209-224 http://dx.doi.org/10.1007/s10236-013-0598-0
39. Davidson, P., 2013. Elementary properties of turbulence. In Turbulence in Rotating, Stratified and Electrically Conducting Fluids (pp. 197-219). Cambridge: Cambridge University Press. doi:10.1017/CBO9781139208673.011
40. Davison, A. C., 1984. Modelling excesses over high thresholds, with an application. In Statistical Extremes and Applications (J. Tiago de Oliviera, Editor), 461–482, Reidel, Dordrecht.
41. Deaves DM, Lines IG., 1997. On the fitting of low mean wind speed data to the Weibull distribution. Journal of Wind Engineering and Industrial Aerodynamics 1997; 66(3): 169–178, DOI: 10.1016/S0167-6105(97)00013-5.
42. Deaves, D.M., and Lines, I.G., 1998. The nature and frequency of low wind-speed conditions, J. Wind Eng. Ind. Aerodyn., 73(1), pp. 1-29
43. Dee, D. P., Uppala, S. M., Simmons, A. J., Berrisford, P., Poli, P., Kobayashi, S., Andrae, U., Balmaseda, M. A., Balsamo, G., Bauer, P., Bechtold, P., Beljaars, A. C. M., van de Berg, L., Bidlot, J., Bormann, N., Delsol, C., Dragani, R., Fuentes, M., Geer, A. J., Haimberger, L., Healy, S. B., Hersbach, H., Hólm, E. V., Isaksen, L., Kållberg, P., Köhler, M., Matricardi, M., McNally, A. P., Monge-Sanz, B. M., Morcrette, J.-J., Park, B.-K., Peubey, C., de Rosnay, P., Tavolato, C., Thépaut, J.-N. & Vitart, F., 2011. The ERA-Interim reanalysis: configuration and performance of the data assimilation system. Quarterly Journal of the Royal Meteorological Society 2011, 137, 553-597, doi:doi:10.1002/qj.828.
44. Della-Marta, P.M.; Mathis, H.; Frei, C.; Liniger, M.A.; Kleinn, J.; Appenzeller, C., 2009. The return period of wind storms over Europe. International Journal of Climatology 2009, 29, 437-459, doi:10.1002/joc.1794.
45. DeMott, P. J., K. Sassen, M. R. Poellot, D. Baumgardner, D. C. Rogers, S. D. Brooks, A.J. Prenni, and S. M. Kreidenweis, 2003. African dust aerosols as atmospheric ice nuclei, Geophysical Research Letters, 30(14), 251, doi:10.1029/2003GL017410.
46. Dordrecht R., 1987. Encyclopaedia of mathematics : an updat. and annotat. transl. of the Soviet mathematical encyclopaedia.
47. Dukes MDG, Palutikof JP., 1995. Estimation of extreme wind speeds with very long return periods. Journal of Applied Meteorology 34(9): 1950–1961.

48. Durrans, S. R., 2010. Intensity-Duration-Frequency Curves, in Rainfall: State of the Science (eds F. Y. Testik and M. Gebremichael), American Geophys. Union, Washington, D. C.. doi: 10.1029/2009GM000919
49. Dykes, J. D., Wang, D. W., & Book, J. W., 2009. An evaluation of a high-resolution operational wave forecasting system in the Adriatic Sea. J. Marine Systems, 78(SUPPL. 1), S255-S271.
50. Emanuel KA., 2005. Increasing destructiveness of tropical cyclones over the past 30 years. Nature 436: 686–688.
51. Emanuel, K., 2005. Genesis and maintenance of "Mediterranean hurricanes". Advances in Geosciences 2005, 2, 217-220.
52. Emanuel, K.; Jagger, T., 2010. On Estimating Hurricane Return Periods. Journal of Applied Meteorology and Climatology 2010, 49, 837-844, doi:10.1175/2009jamc2236.1.
53. Fiedler, F. and Panofsky, H.A., 1970. Atmospheric scales and spectral gaps. Bulletin of the American Meteorological Society, 51(12), pp.1114-1120.
54. Fita, L.; Flaounas, E., 2018. Medicanes as subtropical cyclones: the December 2005 case from the perspective of surface pressure tendency diagnostics and atmospheric water budget. Quarterly Journal of the Royal Meteorological Society 2018, 144, 1028-1044, doi:10.1002/qj.3273.
55. Fita, L.; Romero, R.; Luque, A.; Emanuel, K.; Ramis, C., 2007. Analysis of the environments of seven Mediterranean tropical-like storms using an axisymmetric, nonhydrostatic, cloud resolving model. Nat. Hazards Earth Syst. Sci. 2007, 7, 41-56, doi:10.5194/nhess-7-41-2007.
56. Flaounas, E.; Kelemen, F.D.; Wernli, H.; Gaertner, M.A.; Reale, M.; Sanchez-Gomez, E.; Lionello, P.; Calmanti, S.; Podrascanin, Z.; Somot, S., et al., 2018. Assessment of an ensemble of ocean–atmosphere coupled and uncoupled regional climate models to reproduce the climatology of Mediterranean cyclones. Climate Dynamics 2018, 51, 1023-1040, doi:10.1007/s00382-016-3398-7.
57. Flaounas, E.; Kotroni, V.; Lagouvardos, K.; Gray, S.L.; Rysman, J.-F.; Claud, C., 2018. Heavy rainfall in Mediterranean cyclones. Part I: contribution of deep convection and warm conveyor belt. Climate Dynamics 2018, 50, 2935-2949, doi:10.1007/s00382-017-3783-x.
58. Flaounas, E.; Raveh-Rubin, S.; Wernli, H.; Drobinski, P.; Bastin, S., 2015. The dynamical structure of intense Mediterranean cyclones. Climate Dynamics 2015, 44, 2411-2427, doi:10.1007/s00382-014-2330-2.
59. Flocas, H.A., Kountouris P., Kouroutzoglou J., Hatzaki, M., Keay, K., Simmonds, I., 2013. Vertical characteristics of cyclonic tracks in eastern Mediterranean during the cold period of the year. Theor. Appl. Climatol. DOI: 10.1007/s00704-012-0737-4,112, 375-388
60. Flocas, H.A.; Simmonds, I.; Kouroutzoglou, J.; Keay, K.; Hatzaki, M.; Bricolas, V.; Asimakopoulos, D., 2010. On Cyclonic Tracks over the Eastern Mediterranean. Journal of Climate 2010, 23, 5243-5257, doi:10.1175/2010jcli3426.1.
61. Fountoukis, C., and A. Nenes, 2005. Continued development of a cloud droplet formation parameterization for global climate models, Journal of Geophysical Research D: Atmospheres, 110(11), 1–10, doi:10.1029/2004JD005591.
62. Friedrichs, P., M. Gober, S. Bentzien, A. Lenz, and R. Krampitz, 2009. A probabilistic analysis of wind gusts using extreme value statistics. Met. Zeit., 18, 615–629.

63. Gadian, A., Dewsbury, J., Featherstone, F., Levermore, J., Morris, K., Sanders C., 2004. Directional persistence of low wind speed observations. J. Wind Eng. Ind. Aerodyn. 92 (2004) 1061–1074.
64. Gaertner, M.A.; Jacob, D.; Gil, V.; Domínguez, M.; Padorno, E.; Sánchez, E.; Castro, M., 2007. Tropical cyclones over the Mediterranean Sea in climate change simulations. Geophysical Research Letters 2007, 34, doi:10.1029/2007gl029977.
65. Galambos, J., 1987: The Asymptotic Theory of Extreme Order Statistics. 2d ed. Krieger, 414 pp.
66. Galanis G., Chu P.C., Kallos G., 2011. Statistical post processes for the improvement of the results of numerical wave prediction models. A combination of Kolmogorov-Zurbenko and Kalman filters. J. Operat. Ocean., 4 (1), 23-31.
67. Galanis G., Emmanouil G., Kallos G., Chu P. C., 2009. "A new methodology for the extension of the impact in sea wave assimilation systems," Ocean Dynamics, 59 (3), 523-535.
68. Galanis, G., Hayes D., Zodiatis, G., Chu P.C., Kuo, Y.H., and Kallos, G., 2012. Wave height characteristics in the Mediterranean Sea by means of numerical modeling, satellite data, statistical and geometrical techniques. Marine Geophys. Research 33, 1–15.
69. Galanis, G., Louka, P., Katsafados, P., Pytharoulis, I. and Kallos, G., 2006. Applications of Kalman filters based on non-linear functions to numerical weather predictions. Ann. Geophys., 24, 2451-2460.
70. Glahn, B., and J. P. Dallavalle, 2006. Gridded mos–techniques, status, and plans. 18th Conference on Probability and Statistics in the Atmospheric Sciences, Atlanta, AMS.
71. Goyette, S., O. Brasseur, and M. Beniston, 2003. Application of a new wind gust parameterization: Multiscale case studies performed with the canadian regional climate model. J. Geophys. Res., 108, D13, 4374., doi:10.1029/2002JD002646, 2003.
72. Gusella, V., 1991. Estimation of extreme winds from short-term records. J. Struct. Eng., 117: 375–390.
73. Halwatura, D., Lechner, A. M. and Arnold, S, 2015. Drought severity–duration–frequency curves: a foundation for risk assessment and planning tool for ecosystem establishment in post-mining landscapes. Hydrol. & Earth System Sciences, 19 2: 1069-1091. doi:10.5194/hess-19-1069-2015
74. Harris, R.I., 1998. Improvements to the 'Method of Independent Storms'. J. Wind Eng. Ind. Aerodyn.
75. Hart, R.E., 2003. A Cyclone Phase Space Derived from Thermal Wind and Thermal Asymmetry. Monthly Weather Review 2003, 131, 585-616, doi:10.1175/1520-0493(2003)131 <0585:acpsdf>2.0.co;2.
76. Hasager, C.B., Astrup, P., Christiansen, M.B., Nielsen, M., and Barthelmie, R., 2006. Wind resources and wind farm wake effects offshore observed from satellite, Proceedings European Wind Energy Association (EWEA).
77. Hasselmann, S., Hasselmann, K., Bauer, E., Bertotti, L., Cardone, C.V., Ewing, J.A., Greenwood, J.A., Guillaume, A., Janssen, P., Komen, G., Lionello, P., Reistad, M., Zambresky, L., 1988. The WAM Model - a third generation ocean wave prediction model, J. Physical Ocean. 18 (12), 1775–1810.
78. Hazewinkel, Michiel, ed., 2001. Maximum-likelihood method, Encyclopedia of Mathematics, Springer, ISBN 978-1-55608-010-4
79. Hennessey, J. P. Jr., 1977. Some aspects of wind power statistics. J. Appl. Meteorol., 16: 119–128.

80. Holthuijsen, L.H., 2007. Waves in Oceanic and Coastal Waters. Cambridge University Press, 387 pp.
81. Holton, J. 2004. An Introduction to Dynamic Meteorology, Volume 88, 4th Edition. eBook ISBN: 9780080470214.
82. Hu, X.-M., 2015. BOUNDARY LAYER (ATMOSPHERIC) AND AIR POLLUTION | Air Pollution Meteorology, Encyclopedia of Atmospheric Sciences (Second Edition), Academic Press, 2015, Pages 227-236, ISBN 9780123822253.
83. Iacono, M. J., E. J. Mlawer, S. A. Clough, and J.-J. Morcrette, 2000. Impact of an improved longwave radiation model, RRTM, on the energy budget and thermodynamic properties of the NCAR community climate model, CCM3, Journal of Geophysical Research: Atmospheres, 105(D11), 14873–14890, doi: 10.1029/2000JD900091.
84. Iacono, M.J., Delamere, J.S., Mlawer, E.J., Clough, S.A., 2003. Evaluation of upper tropospheric water vapor in the NCAR community climate model (CCM3) using modeled and observed HIRS radiances. J. Geophys. Res.,108(D2),4037, doi:10.1029/2002JD002539, 2003
85. Intergovernmental Panel on Climate Change, 2012. Managing the risks of extreme events and disasters to advance climate change adaptation. In C. B. Field, V. Barros, T. F. Stocker, D. Qin, D. J. Dokken, K. L. Ebi, et al. (Eds.), A Special Report of Working Groups I and II of the Intergovernmental Panel on Climate Change. Cambridge, England/New York, NY: Cambridge University Press.
86. Janeiro, J., Martins, F., & Relvas, P., 2012. Towards the development of an operational tool for oil spills management in the Algarve coast. J. Coastal Conserv, 16(4), 449-460.
87. Janjic, Z.I., 1994. The Step-Mountain Eta Coordinate Model: Further Developments of the Convection, Viscous Sublayer, and Turbulence Closure Schemes. Monthly Weather Review, 122, 927-945.http://dx.doi.org/10.1175/1520-0493(1994)122<0927:TSMECM>2.0.CO;2
88. Janjic, Z.I. and F. Mesinger, 1984: Finite-difference methods for the shallow water equations on various horizontal grids. Numerical Methods for Weather Prediction, Vol. 1, Seminar, ECMWF, 1983, Reading, U.K. Shinfield Park, Reading, Berkshire RG2 9AX, U.K., 29-101.
89. Jansa, A., Alpert, P., Buzzi, A., Arbogast, P., 2001: MEDEX, cyclones that produce high impact weather in the Mediterranean, available at http://medex.inm.uib.es
90. Jenkinson, A.F., 1955. The Frequency Distribution of the Annual Maximum (or Minimum) of Meteorological Elements. Quarterly J. of the Royal Meteor. Society, 81, 158-171.
91. Jonathan, P., Ewans, K., 2013, "Statistical modelling of extreme ocean environments for marine design: A review", Ocean Engineering, vol. 62, pp. 91-109.
92. Kaas E, Li TS, Schmith T., 1996. Statistical hindcast of wind climatology in the North Atlantic and northwestern European region. Climate Research 7: 97–110.
93. Kallos, G., Galanis, G., Spyrou, C., Kalogeri, C., Adam A. and Athanasiadis P., 2012. Offshore Energy Mapping for Northeast Atlantic and Mediterranean: MARINA PLATFORM project. Geophys. Research Abstracts Vol. 14, EGU2012-10767.
94. Kallos, G., Kotroni, V., Lagouvardos, K., and Papadopoulos, A., 1998. On the long-range transport of air pollutants from Europe to Africa. Geophys. Research Letters. 25, No 5, 619-622.
95. Kallos, G., M. Astitha, P. Katsafados and C. Spyrou, 2007. Long-Range Transport of Anthropogenically and Naturally Produced particulate matter in the Mediterranean and

North Atlantic: Current State of Knowledge. J. of Applied Meteorology and Climatology 46, (8): 1230-1251. DOI 10.1175/JAM2530.1.

96. Kallos, G., Nickovic, S., Papadopoulos, A., Jovic, D., Kakaliagou, O., Misirlis, N., Boukas, L., Mimikou, N., Sakellaridis, G., Papageorgiou, J., Anadranistakis, E., and Manousakis, M, 1997. The regional weather forecasting system Skiron: An overview. Proceedings of the Symposium on Regional Weather Prediction on Parallel Computer Environments, 15–17 October 1997, Athens.
97. Kallos, G.; Solomos, S.; Kushta, J.; Mitsakou, C.; Spyrou, C.; Bartsotas, N.; Kalogeri, C., 2014. Natural and anthropogenic aerosols in the Eastern Mediterranean and Middle East: Possible impacts. Science of The Total Environment 2014, 488-489, 389-397, doi:https://doi.org/10.1016/j.scitotenv.2014.02.035.
98. Kalman R.E., 1960. A New Approach to Linear Filtering and Prediction Problems. Transactions of the ASME – Journal of Basic Engineering, 82 (Series D): 35-45,1960 by ASME
99. Kalnay,E., 2002. Atmospheric Modeling, Data Assimilation and Predictability. Cambridge, Cambridge University Press,p.341 2003.
100. Kalogeri, C., Galanis, G., Spyrou, C., Diamantis, D., Baladima, F., Koukoula, M., Kallos, K., 2017. Assessing the European offshore wind and wave energy resource for combined exploitation, Renewable Energy, Volume 101, 2017, Pages 244-264, ISSN 0960-1481 https://doi.org/10.1016/j.renene.2016.08.010.
101. Katz, R.W., Parlange, M.B. and Naveau, P., 2002. Statistics of extremes in hydrology. Advances in Water Resources, 25, 1287–1304.
102. Kendall, M.G. & Stuart, A., 1987. The advanced theory of statistics Oxford University Press, Inc. New York, NY, USA. ISBN:0-195-20561-8
103. Kite, G.W., 1975. Confidence limits for design events. Water Resources Research 11, 48-53.
104. Köhler, H. 1936. The nucleus in and the growth of hygroscopic droplets, T. Faraday Soc., 32, 1152–1161
105. Korres, G., Lascaratos, A., Hatziapostolou, E., & Katsafados, P., 2002. Towards an ocean forecasting system for the Aegean Sea. Global Atmosph. and Ocean System, 8(2-3), 191-218.
106. Kouroutzoglou, J., Flocas, H.A., Keay, K., Hatzaki, M., D. 2011. Climatological aspects of explosive cyclones in the Mediterranean. Int. J. Climatol., 31, 1785-1802, doi: 10.1002/joc.2203
107. Kouroutzoglou, J.; Flocas, H.A.; Hatzaki, M.; Keay, K.; Simmonds, I., 2014. A high-resolution climatological study on the comparison between surface explosive and ordinary cyclones in the Mediterranean. Regional Environmental Change 2014, 14, 1833-1846, doi:10.1007/s10113-013-0461-3.
108. Koutsoyiannis. D, Kozonis, D., Manetas, A., 1998. A mathematical framework for studying rainfall intensity-duration-frequency relationships. J. of Hydrol. 206 118-135
109. Kristensen L, Rathmann O, Hansen SO., 1999. Extreme winds in Denmark, Technical report, Riso National Laboratory.
110. Kushta, J.; Kallos, G.; Astitha, M.; Solomos, S.; Spyrou, C.; Mitsakou, C.; Lelieveld, J. 2014.Impact of natural aerosols on atmospheric radiation and consequent feedbacks with the meteorological and photochemical state of the atmosphere. Journal of Geophysical Research: Atmospheres 2014, 119, 1463-1491, doi:10.1002/2013jd020714.
111. Lamb, H.H., 1991. Historic storms of the North Sea, British Isles and Northwest Europe. Cambridge University Press, Cambridge, England 1991.

112. Larsén, X.G., Badger, J., Hahmann, A., Ott, S., 2011. Extreme wind atlas from the selective dynamical downscaling method. EWEC 2011.
113. Larsén, X.G., Kalogeri, C., Galanis, G. and Kallos, G., 2015. A statistical methodology for the estimation of extreme wave conditions for offshore renewable applications. Renewable Energy, pp. 205-218 DOI information: 10.1016/j.renene.2015.01.069.
114. Leahy, P., and McKeogh, E., 2012. Persistence of low wind speed conditions and implications for wind power variability. Wind Energy doi: 10.1002/we.1509.
115. Ledermann, W., Lloyd, E., Vajda, S. & Alexander, C., editors., 1990. Handbook of Applicable Mathematics Volume 7: Supplement. Wiley-Interscience, Chichester, 479 pp.
116. Levin, Z., A. Teller, E. Ganor, and Y. Yin, 2005. On the interactions of mineral dust, sea-salt particles, and clouds: A measurement and modeling study from the Mediterranean Israeli Dust Experiment campaign, Journal of Geophysical Research: Atmospheres, 110(D20), 75, doi:10.1029/2005JD005810.
117. Lines, I.G., Daycock, J.H., and Deaves, D.M., 2001. Guidelines for the inclusion of low wind speed conditions into risk assessments, J HAZARD M, 83(3), pp. 153-179
118. Lionello, P.; Bhend, J.; Buzzi, A.; Della-Marta, P.M.; Krichak, S.O.; Jansà, A.; Maheras, P.; Sanna, A.; Trigo, I.F.; Trigo, R., 2006. Chapter 6 Cyclones in the Mediterranean region: Climatology and effects on the environment. In Developments in Earth and Environmental Sciences, Lionello, P., Malanotte-Rizzoli, P., Boscolo, R., Eds. Elsevier: 2006; Vol. 4, pp. 325-372.
119. Lionello, P.; Trigo, I.F.; Gil, V.; Liberato, M.L.R.; Nissen, K.M.; Pinto, J.G.; Raible, C.C.; Reale, M.; Tanzarella, A.; Trigo, R.M., et al. 2016. Objective climatology of cyclones in the Mediterranean region: a consensus view among methods with different system identification and tracking criteria. Tellus A: Dynamic Meteorology and Oceanography 2016, 68, 29391, doi:10.3402/tellusa.v68.29391.
120. Liu, W.T., K.B. Katsaros, and J.A. Businger, 1979: Bulk Parameterization of Air-Sea Exchanges of Heat and Water Vapor Including the Molecular Constraints at the Interface. J. Atmos. Sci., 36, 1722–1735.
121. Lopatoukhin, L.J., Rozhkov, V.A., Ryabinin, V.E., Swail, V.R., Boukhanovsky, A.V. and Degtyarev, A.B., 2000. Estimation of extreme wind wave heights. LCOMM Tech. Rep. No9, World Meteor. Organization.
122. Louka, P., Galanis, G., Siebert, N., Kariniotakis, G., Katsafados, P., Pytharoulis, I., Kallos, G., 2008. Improvements in wind speed forecasts for wind power prediction purposes using Kalman filtering. J. Wind Eng. Ind. Aerodyn., 96, pp. 2348-2362.
123. Maheras, P.; Flocas, H.A.; Patrikas, I.; Anagnostopoulou, C., 2001. A 40 year objective climatology of surface cyclones in the Mediterranean region: spatial and temporal distribution. International Journal of Climatology 2001, 21, 109-130, doi:10.1002/joc.599.
124. Marsaglia, G., W. Tsang, and J. Wang., 2003. Evaluating Kolmogorov's Distribution. J. Statistical Software. Vol. 8, Issue 18.
125. Mason, P.J. and Thomson, D.J., 2015. BOUNDARY LAYER (ATMOSPHERIC) AND AIR POLLUTION | Overview, Encyclopedia of Atmospheric Sciences (Second Edition), Academic Press, 2015, Pages 220-226, ISBN 9780123822253.
126. Matulla, C., Schöner, W., Alexandersson, H., von Storch, H., Wang X., 2008. European storminess: late nineteenth century to present Clim. Dyn., 31 (2008), pp. 1125-1130, 10.1007/s00382–007–0333–y

127. McPhillips, L. E., Chang, H., Chester, M. V., Depietri, Y., Friedman, E., Grimm, N. B., Kominoski, J. S., McPhearson, T., Méndez-Lázaro, P., Rosi, E. J., & Shafiei Shiva, J., 2018. Defining Extreme Events: A Cross-Disciplinary Review. Earth's Future, 6, 441–455. https://doi.org/10.1002/ 2017EF000686
128. McTaggart-Cowan, R.; Galarneau, T.J.; Bosart, L.F.; Milbrandt, J.A., 2009. Development and Tropical Transition of an Alpine Lee Cyclone. Part I: Case Analysis and Evaluation of Numerical Guidance. Monthly Weather Review 2009, 138, 2281-2307, doi:10.1175/2009MWR3147.1.
129. Meehl, G.A.; Arblaster, J.M.; Fasullo, J.T.; Hu, A.; Trenberth, K.E., 2011. Model-based evidence of deep-ocean heat uptake during surface-temperature hiatus periods. Nature Climate Change 2011, 1, 360, doi:10.1038/nclimate1229
130. Mesinger, F., 1984. A blocking technique for representation of mountains in atmospheric models, Riv. Meteor. Aeronaut., 44, 195–202, 1984.
131. Meyers, M. P., P. J. DeMott, and W. R. Cotton, 1992. New Primary Ice-Nucleation Parameterizations in an Explicit Cloud Model, Journal of Applied Meteorology, 31(7), 708–721, doi:10.1175/1520-0450(1992)031<0708:NPINPI>2.0.CO;2.
132. Meyers, M. P., R. L. Walko, J. Y. Harrington, and W. R. Cotton, 1997. New RAMS cloud microphysics parameterization. Part II: The two-moment scheme, Atmospheric Research, 45(1), 3–39, doi:10.1016/S0169-8095(97)00018-5.
133. Miglietta, M.M.; Laviola, S.; Malvaldi, A.; Conte, D.; Levizzani, V.; Price, C. 2013. Analysis of tropical-like cyclones over the Mediterranean Sea through a combined modeling and satellite approach. Geophysical Research Letters 2013, 40, 2400-2405, doi:10.1002/grl.50432.
134. Miglietta, M.M.; Moscatello, A.; Conte, D.; Mannarini, G.; Lacorata, G.; Rotunno, R., 2011. Numerical analysis of a Mediterranean 'hurricane' over south-eastern Italy: Sensitivity experiments to sea surface temperature. Atmospheric Research 2011, 101, 412-426, doi:https://doi.org/10.1016/j.atmosres.2011.04.006.
135. Miller C. 2003. A once in 50-year wind speed map for Europe derived from mean sea level pressure measurements. Journal of Wind Engineering and Industrial Aerodynamics 91(12–15): 1813–1826.
136. Mlawer, E. J., S. J. Taubman, P. D. Brown, M. J. Iacono, and S. A. Clough, 1997. Radiative transfer for inhomogeneous atmospheres: RRTM, a validated correlated-k model for the longwave, Journal of Geophysical Research D: Atmospheres, 102(14), 16663–16682.
137. Monahan AH., 2006. The probability distribution of sea surface wind speeds. part 1: Theory and seawinds observations. Journal of Climate 19(4): 497–520.
138. Morcrette, J.-J. 2001. Impact of the radiation-transfer scheme RRTM in the ECMWF forecasting system. ECMWF Newsletter No. 91, 2001
139. MunichRe, 2000. Winter storms in Europe (II)—analysis of 1999 losses and loss potentials. Münchener Rückversicherungs-Gesellschaft 2000.
140. Nash, J. E. and J. V. Sutcliffe, 1970. River flow forecasting through conceptual models part I — A discussion of principles. Journal of Hydrology, 10 (3), 282–290.
141. Nastos, P.T.; Karavana Papadimou, K.; Matsangouras, I.T., 2018. Mediterranean tropical-like cyclones: Impacts and composite daily means and anomalies of synoptic patterns. Atmospheric Research 2018, 208, 156-166, doi:https://doi.org/10.1016/j.atmosres.2017.10.023.

142. Nenes, A., and J. H. Seinfeild, 2003. Parameterization of cloud droplet formation in global climate models, Journal of Geophysical Research, 108(D14), 6837, doi: 10.1029/2002JD002911.
143. Neumann, B., Vafeidis, A. T., Zimmermann, J., & Nicholls, R. J., 2015. Future coastal population growth and exposure to sea-level rise andcoastal flooding—A global assessment. PLoS One, 10(3), e0118571. https://doi.org/10.1371/journal.pone.0118571
144. Nickovic, S., Kallos, G., Papadopoulos, A., and Kakaliagou, O., 2001. A model for prediction of desert dust cycle in the atmosphere, J. Geophys. Res., 106(D16), 18113–18129, doi:10.1029/2000JD900794.
145. Nilsson, C., S. Goyette, and L. Bärring, 2007. Relating forest damage data to the wind field from high- resolution rcm simulations: Case study of anatol striking Sweden in December 1999. Global and Planetary Change, 57, 161–176.
146. Nissen, K.M., Leckebusch, G.C., Pinto, J.G., Renggli, D., Ulbrich, S., Ulbrich, U., 2010. Cyclones causing wind storms in the Mediterranean: characteristics, trends and links to large-scale patterns. Nat Hazard Earth Syst Sci 10:1379–1391. doi:10.5194/nhess-10-13792010
147. Orrell D., L. Smith, J. Barkmeijer, and T. N. Palmer, 2001. Model error in weather forecasting, Nonlinear Processes in Geophysics. (2001) 8: 357–371.
148. Palutikof, J.P.; Brabson, B.B.; Lister, D.H.; Adcock, S.T., 1999. A review of methods to calculate extreme wind speeds. Meteorological Applications 1999, 6, 119-132, doi:10.1017/s1350482799001103.
149. Papadopoulos, A., Kallos, G., Katsafados, P., and Nickovic, S., 2002. The POSEIDON weather forecasting system: An overview, The Global Atmosph. & Ocean Systems, 8, 219-237
150. Parisi, F.; Lund, R., 2008. Return Periods of Continental U.S. Hurricanes. Journal of Climate 2008, 21, 403-410, doi:10.1175/2007jcli1772.1.
151. Patlakas, P.; Drakaki, E.; Galanis, G.; Spyrou, C.; Kallos, G., 2017. Wind gust estimation by combining a numerical weather prediction model and statistical post-processing. Energy Procedia 2017, 125, 190-198, doi:https://doi.org/10.1016/j.egypro.2017.08.179.
152. Patlakas, P.; Galanis, G.; Barranger, N.; Kallos, G., 2016. Extreme wind events in a complex maritime environment: Ways of quantification. Journal of Wind Engineering and Industrial Aerodynamics 2016, 149, 89-101, doi:10.1016/j.jweia.2015.11.006.
153. Patlakas, P.; Galanis, G.; Diamantis, D.; Kallos, G., 2017. Low wind speed events: persistence and frequency. Wind Energy 2017, 20, 1033-1047, doi:10.1002/we.2078.
154. Petersen, E.L., Mortensen, N.G., Landberg, L., Højstrup, J. and Frank, H.P., 1998. Wind power meteorology. Part II: siting and models. Wind Energy, 1(2), pp.55-72.
155. Picornell, M.A.; Campins, J.; Jansà, A., 2014. Detection and thermal description of medicanes from numerical simulation. Nat. Hazards Earth Syst. Sci. 2014, 14, 1059-1070, doi:10.5194/nhess-14-1059-2014.
156. Pielke, R.A., Cotton, W.R., Walko, R.L. et al., 1992. A comprehensive meteorological modeling system—RAMS. Meteorl. Atmos. Phys. 49, 69–91 (1992). https://doi.org/10.1007/BF01025401
157. Pinto, J. G., C. P. Neuhaus, A. Kruger, and M. Kerschgens, 2009. Assessment of the wind gust estimate method in mesoscale modelling of storm events over west Germany. Met. Zeit., 18, 495–506.

158. Pruppacher, H. R. and Klett, J. D., 1997. Microphysics of Clouds and Precipitation, Second Revised and Enlarged Edition with an Introduction to Cloud Chemistry and Cloud Electricity, Kluwer Academic Publishers, Dordrecht, 954 pp.
159. Pytharoulis, I.; Craig, G.C.; Ballard, S.P., 2000. The hurricane-like Mediterranean cyclone of January 1995. Meteorological Applications 2000, 7, 261-279, doi:10.1017/s1350482700001511.
160. Pytharoulis, I.; Kartsios, S.; Tegoulias, I.; Feidas, H.; Miglietta, M.M.; Matsangouras, I.; Karacostas, T., 2018. Sensitivity of a Mediterranean Tropical-Like Cyclone to Physical Parameterizations. Atmosphere 2018, 9, 436.
161. Raveh-Rubin, S.; Flaounas, E., 2017. A dynamical link between deep Atlantic extratropical cyclones and intense Mediterranean cyclones. Atmospheric Science Letters 2017, 18, 215-221, doi:10.1002/asl.745.
162. Romero, R.; Emanuel, K., 2013. Medicane risk in a changing climate. Journal of Geophysical Research: Atmospheres 2013, 118, 5992-6001, doi:10.1002/jgrd.50475.
163. Sacre C., 2002. Extreme wind speed in France: the '99 storms and their consequences. Journal of Wind Engineering and Industrial Aerodynamics 90(10): 1163–1171.
164. Schiesser, H.H.; Pfister, C.; Bader, J., 1997. Winter storms in Switzerland North of the Alps 1864/1865–1993/1994. Theoretical and Applied Climatology 1997, 58, 1-19, doi:10.1007/bf00867428.
165. Schinke H., 1993. On the occurence of deep cyclones over Europe and the North Atlantic in the period 1930–1991. Beitr¨age zur Physik der Atmosphare 66: 223–237.
166. Schmidt, H. and von Storch, H. 1993. German Bight storms analysed, Nature, 365 (1993), p. 791
167. Schmith T, Kaas E, Li TS. 1998. Northeast Atlantic winter storminess 1875–1995 re-analysed. Climate Dynamics 14: 529–536.
168. Schulz, J.-P., and E. Heise, 2003. A new scheme for diagnosing near-surface convective gusts. COSMO Newsletter No. 3.
169. Schulz, M., Y. Balkanski, F. Dulac, W. Guelle, 1998. Treatment of aerosol size distribution in a global transport model: Validation with satellite-derived observations for a Saharan dust episode, J. Geophys. Res., 103, 10589–10592, 1998.
170. Semedo, A., SušElj, K., Rutgersson, A., Sterl, A. 2011. A global view on the wind sea and swell climate and variability from ERA-40 (2011) Journal of Climate, 24 (5), pp. 1461- 1479.
171. Sheridan, P., 2011. Review of techniques and research for gust forecasting and parameterization. Forecasting Research Technical Report 570, Met Office, 2011.
172. Simon, A., A. Kann, M. Nestiak, I. Meirold-Mautner, A. Horvath, K. Csirmaz, O. Ulbert, and C. Gruber, 2011. Nowcasting and very short range forecasting of wind gusts generated by deep convection." General Assembly 2011, Vienna, Austria, EGU.
173. Smith, F.B. 1993. Low wind speed meteorology, for Cambridge Atmospheric Dispersion Modelling Course, 6/7 July 1993 - based on the paper presented at Riso in May 1992 and at ECCOMAS, September 1992.
174. Smith, R. L., 1986. Extreme value theory based on the r largest annual events. J. Hydrol., 86: 27–43.
175. Smith, R.L., 1989. Extreme value analysis of environmental time series: An application to trend detection in ground-level ozone. Statistical Science, 4, 367–393.
176. Smits A, Tank AMGK, Konnen GP., 2005. Trends in storminess over the Netherlands, 1962–2002. International Journal of Climatology 25(10): 1331–1344.

177. Sobey R.J., Orloff. L. S., 1999. Intensity-duration-frequency summaries for wave climate. Coastal Engineering Volume 36, Issue 1, February 1999, Pages 37–58. doi:10.1016/S0378-3839(98)00048-9
178. Solomos, S.; Kallos, G.; Kushta, J.; Astitha, M.; Tremback, C.; Nenes, A.; Levin, Z., 2011. An integrated modeling study on the effects of mineral dust and sea salt particles on clouds and precipitation. Atmos. Chem. Phys. 2011, 11, 873-892, doi:10.5194/acp-11-873-2011.
179. Spyrou, C., Kallos, G., Mitsakou, C., Athanasiadis, P., Kalogeri, C., Iacono, M. J., 2013. Modeling the radiative effects of desert dust on weather and regional climate. Atmos. Chem. Phys., 13, 5489–5504, doi:10.5194/acp-13-5489-2013, 2013.
180. Spyrou, C., Mitsakou, C., Kallos, G., Louka, P., and Vlastou, G., 2010. An improved limited area model for describing the dust cycle in the atmosphere. J. Geophys. Res., 115, D17211, doi:10.1029/2009JD013682, 2010.
181. Stathopoulos, C., Kaperoni, A., Galanis, G. & Kallos, G., 2013. Wind power prediction based on numerical and statistical models. J. Wind Eng. Ind. Aerodyn., 112, 25-38.
182. Stathopoulos, C., Patlakas, P., Tsalis, C., Kallos, G., 2020. The Role of Sea Surface Temperature Forcing in the Life-Cycle of Mediterranean Cyclones. Remote Sensing 12 (5), 825
183. Stathopoulos, C., Galanis, G., Kallos, G., 2020. A coupled modeling study of mechanical and thermodynamical air-ocean interface processes under sea storm conditions. Dynamics of Atmospheres and Oceans, 2020, 91, 101140.
184. Stull, R.B., 2012. An introduction to boundary layer meteorology (Vol. 13). Springer Science & Business Media.
185. Stull, Roland B. 1988. An Introduction to Boundary Layer Meteorology. Springer. ISBN 978-94-009-3027-8
186. SwissRe., 2000. Storm Over Europe – An Underestimated Risk. Swiss Reinsurance Company: Zurich 2000.
187. Taylor, P.K.; Yelland, M.J., 2001. The Dependence of Sea Surface Roughness on the Height and Steepness of the Waves. Journal of Physical Oceanography 2001, 31, 572-590, doi:10.1175/1520-0485(2001)031<0572:tdossr>2.0.co;2.
188. TC88 WG1., 2005 IEC 61400-1 Wind turbines : Design requirements. (2005)
189. The Wamdi Group., 1988. The WAM Model—A Third Generation Ocean Wave Prediction Model. Journal of Physical Oceanography, 18(12), 1775-1810.
190. Tous, M.; Romero, R., 2013. Meteorological environments associated with medicane development. International Journal of Climatology 2013, 33, 1-14, doi:10.1002/joc.3428.
191. Tous, M.; Romero, R.; Ramis, C., 2013. Surface heat fluxes influence on medicane trajectories and intensification. Atmospheric Research 2013, 123, 400-411, doi:https://doi.org/10.1016/j.atmosres.2012.05.022.
192. Trigo, I. F., Davies, T. D. & Bigg, G. R., 1999. Objective Climatology of Cyclones in the Mediterranean Region. Journal of Climate, 12(6), 1685-1696.
193. Trigo, I.F., 2006. Climatology and interannual variability of storm-tracks in the Euro-Atlantic sector: a comparison between ERA-40 and NCEP/NCAR reanalyses. Climate Dynamics 2006, 26, 127-143, doi:10.1007/s00382-005-0065-9.
194. Trigo, I.F.; Bigg, G.R.; Davies, T.D., 2002. Climatology of Cyclogenesis Mechanisms in the Mediterranean. Monthly Weather Review 2002, 130, 549-569, doi:10.1175/1520-0493(2002)130<0549:cocmit>2.0.co;2.

195. Tsalis, C., Patlakas, P., Stathopoulos, C., Kallos, G., 2020. Optimizing a new De-clustering approach for relatively small samples of wind speed with an application to offshore design conditions. Under review, Ocean Engineering.
196. United Nations Office for Disaster Risk Reduction., 2013. From Shared Risk to Shared Value- The Business Case for Disaster Risk Reduction. Global Assessment Report on Disaster Risk Reduction. Geneva, Switzerland: UNISDR.
197. Valcke, S., 2013. The OASIS3 coupler: a European climate modelling community software. Geosci. Model Dev. 2013, 6, 373-388, doi:10.5194/gmd-6-373-2013.
198. Van der Hoven, 1957. Power spectrum of horizontal wind speed in the frequency range from 0.0007 to 900 cycles per hour. Journal of Meteorology, 14, 160-164
199. Walshaw, D., 1994. Getting the most from your extreme wind data: a step by step guide, J. Res. Natl. Inst. Stand. Technol., 99: 399–411.
200. Walter A, Keuler K, Jacob D, Knoche R, Block A, Kotlarski S, Muller-Westermeier G, Rechid D, Ahrens W. 2006. A high resolution reference data set of German wind velocity 1951–2001 and comparison with regional climate model results. Meteorologische Zeitschrift 15(6): 585–596.
201. Weggel, J. R., 1999. Maximum daily wind gusts related to mean daily wind speed. J. Struct. Eng., 125, 465– 468, 1999.
202. Weisse, R., von Storch, H., Feser, F. 2005. Northeast Atlantic and North Sea storminess as simulated by a regional climate model during 1958–2001 and comparison with observations J. Clim., 18 (2005), pp. 465-479
203. Weisse, R., Günther, H. 2007. Wave climate and long-term changes for the Southern North Sea obtained from a high-resolution hindcast 1958–2002. Ocean Dyn., 57 (June (3)) (2007), pp. 161-172, 10.1007/s10236-006-0094-x
204. Wilks, Daniel S., 2006. Statistical Methods in the Atmospheric Sciences, Second Edition. Academic Press, London. ISBN 13: 978-0-12-751966-1.
205. Winstanley, D., 1970. THE NORTH AFRICAN FLOOD DISASTER, SEPTEMBER 1969. Weather 1970, 25, 390-403, doi:10.1002/j.1477-8696.1970.tb04128.x.
206. World Meteorological Organization, 1987. The Measurement of Gustiness at Routine Wind Stations: A Review (A.C.M. Beljaars). (Instruments and Observing Methods Report No. 31), Geneva.
207. Yan Z, Bate S, Chandler RE, Isham V, Wheater H., 2006. Changes in extreme wind speeds in NW Europe simulated by generalized linear models. Theoretical And Applied Climatology 83(1–4): 121–137.
208. Yan ZW, Bate S, Chandler RE, Isham V, Wheater H., 2002. An analysis of daily maximum wind speed in northwestern Europe using generalized linear models. Journal of Climate 15(15): 2073–2088.
209. Zhang, H.-M.; Bates, J.J.; Reynolds, R.W., 2006. Assessment of composite global sampling: Sea surface wind speed. Geophysical Research Letters 2006, 33, doi:10.1029/2006gl027086.
210. Zhang, X., Zwiers, F.W., and Li, G., 2004. Monte Carlo experiments on the detection of trends in extreme values. J. Climate, 17, 1945–1952.
211. Zodiatis, G., Lardner, R., Georgiou, G., Demirov, E., Manzella, G., & Pinardi, N., 2003. An operational European global ocean observing system for the eastern mediterranean levantine basin: The Cyprus coastal ocean forecasting and observing system. Marine Technology Society J., 37(3), 115-123.

212. Trigo, I.F.; Davies, T.D.; Bigg, G.R., 1999. Objective Climatology of Cyclones in the Mediterranean Region. Journal of Climate 1999, 12, 1685-1696, doi:10.1175/1520-0442(1999)012<1685:ococit>2.0.co;2.

Web references (10/09/2015)

1. http://forecast.uoa.gr/proj_marina.php
2. http://forecast.uoa.gr/oldproj.php
3. http://www.eurocodes-online.com
4. http://portal.tee.gr/portal/page/portal/SCIENTIFIC_WORK/scient_typopoiisi/eurocodes
5. https://ec.europa.eu/eurostat/statistics-explained/index.php/Archive:Coastal_regions_-_population_statistics
6. https://earthobservatory.nasa.gov/blogs/earthmatters/tag/hadley-cells/
7. https://www.nhc.noaa.gov/aboutsshws.php
8. http://www.eurometeo.com/english/read/doc_douglas
9. https://www.spc.noaa.gov/faq/tornado/beaufort.html
10. www.ec.europa.eu

Appendix

Wind gust model evaluation

In order to evaluate the model estimated wind gust, a series of test runs were carried out. The model was integrated for a period of four months (July and October of 2014 and January and March of 2015) over an area covering a large part of the West Coast of the American continent and the neighboring part of the Pacific Ocean. The testing period was selected with two criteria: 1) including a month from each season, so to check potential deviations and 2) ensuring availability of data from the buoys. The computational domain is shown in Figure Ap-1. The horizontal grid increment was 0.09 degrees (approximately ~9km) while on the vertical 45 levels were used, stretching from the surface up to 20 km. Daily NCEP GFS operational fields (horizontal resolution of 0.5 degrees) were used for initial and lateral boundary conditions. The main reason reanalysis fields were not used in this study is that we needed to evaluate the capabilities of a gust forecasting system in operational mode.

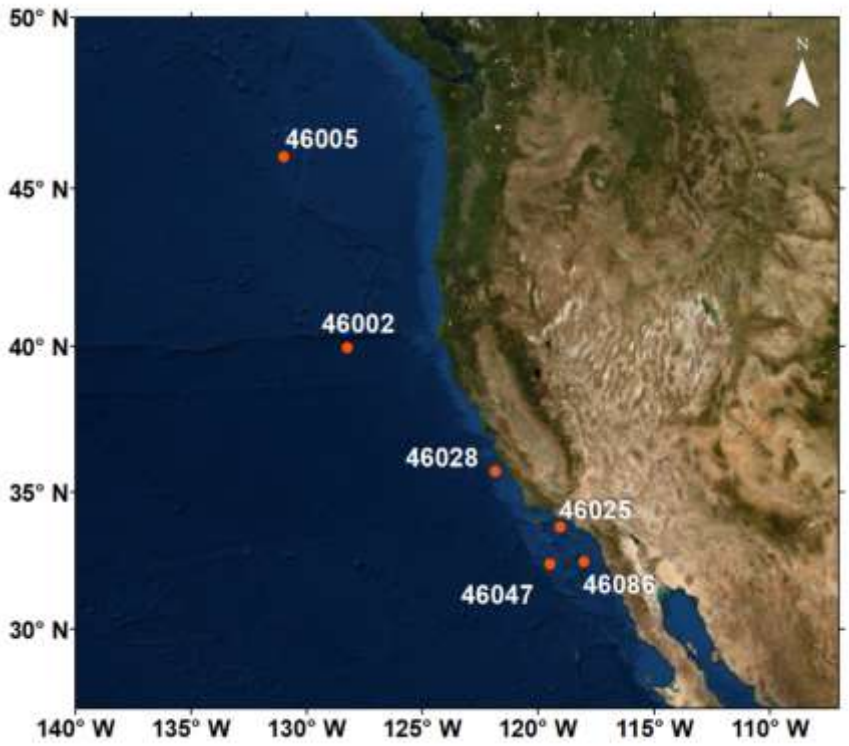

Figure Ap-1: Model domain and the location of the six selected stations of the NOAA's National Data Buoy Center with code numbers 46002, 46005, 46025, 46028, 46047, 46086.

The model was modified to provide outputs every 10 minutes to correspond with the actual data available (as explained below) running in operational mode: For each day under study the model provided 72-hours forecasts. This allowed us to further examine the capabilities of the method applied for different forecasting horizons (24h, 48h and 72h forecasts).

For evaluating the wind gust parameterization scheme, observations from NOAA's National Data Buoy Center were used. The location of the buoys is illustrated in Figure Ap-1. These stations provide wind gust data as the maximum 5-second peak gust during the measurement hour, reported at the last hourly 10-minute segment. The specific buoys were selected according to data availability for the months under consideration.

Using the model output and the wind gust data for the testing period (July and October of 2014, January and March of 2015) wind gust time series were evaluated against corresponding observations. An indicative example is presented in Figure Ap-2 for January 2015 for station 46002, (24h, 48h and 72h forecasts).

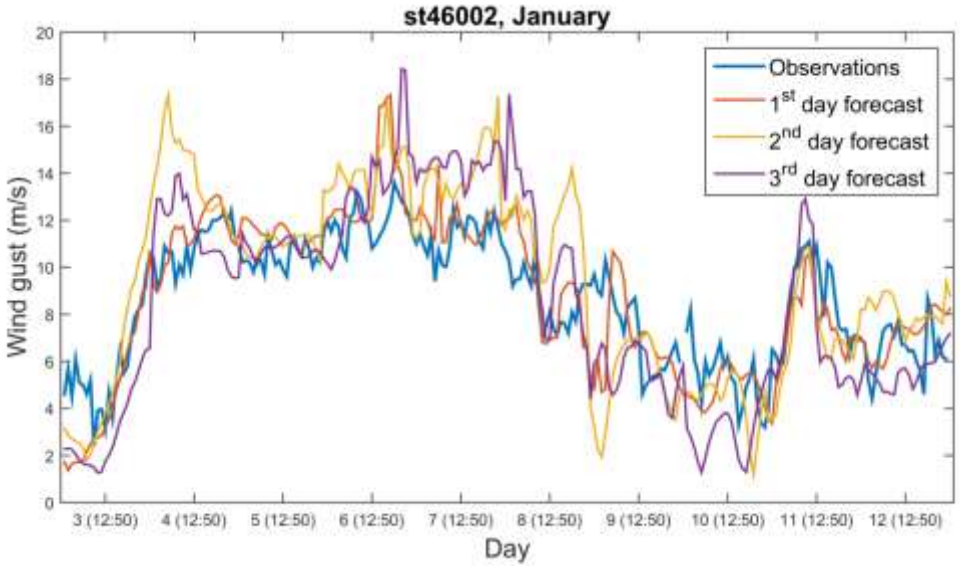

Figure Ap-2: Time-series of buoy data (blue line) and model forecasts for 24h (red line), 48h (yellow line) and 72h (purple line) forecasts.

It is apparent that the 1st day forecasts exhibits the best agreement between model results and data. The 2nd and 3rd day forecasts deviate from the measured gusts, especially the minimum and maximum values. This is something that was expected since the errors in NWP forecasts usually grow with the length of the forecasting horizon. This example is a first indication that the methodology applied in the RAMS/ICLAMS model for wind gust calculations

is solid and provides acceptable results. However, in order to reach more clear and consistent evaluation results of the applied parameterization, the distributions of the number of wind gust occurrences are presented in Figure Ap-3 (a-f).

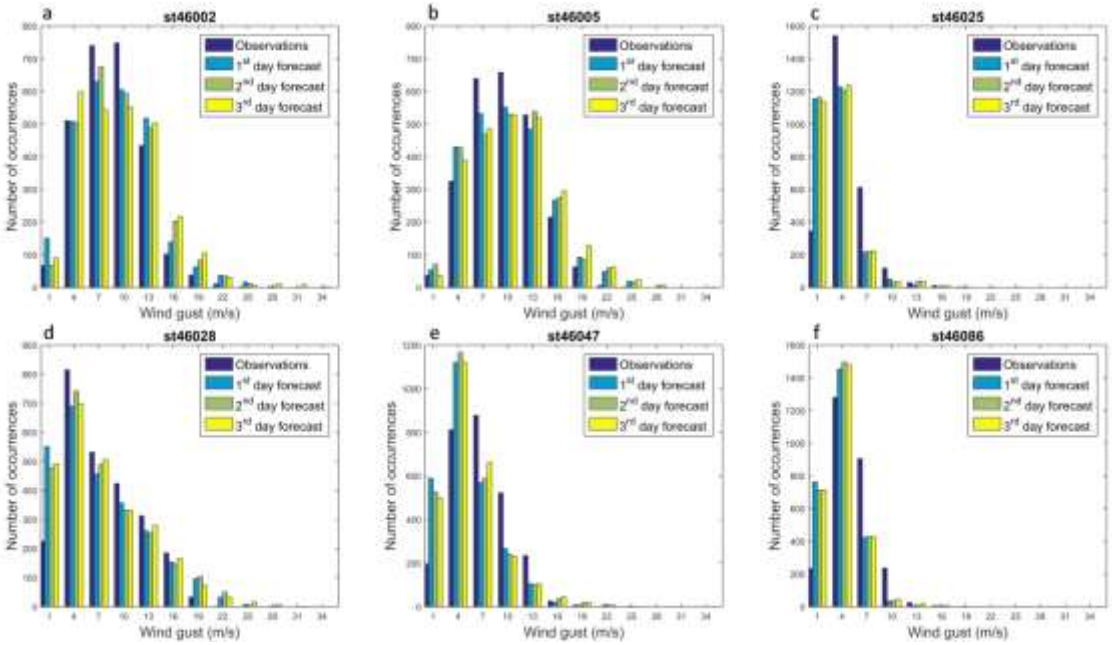

Figure A-3: Histograms for the number of occurrences of each wind gust bin for the observations (purple) and the corresponding model results for 24h (blue), 48h (green) and 72h (yellow) forecasts.

Moreover, a number of statistical scores were calculated for the entire simulation period and for the three forecasting days. The results are presented in Table Ap-1. This analysis proves that the model manages to capture the wind gust distributions in most of the cases. RAMS/ICLAMS performs well for the first forecasting day, with all statistical scores deviating as the forecasting horizon increases. For the second- and third-day forecasts it is increasingly difficult to accurately describe wind gusts due to truncation and parameterization errors. Generally, in operational forecasting the model accuracy is limited both by the rapid divergence of nearby initial conditions and by deficiencies in the core model (Orrell et al., 2001), thus deviating more from the actual conditions, as the forecasting horizon increases.

The best statistical scores for the first day forecasts are reached in Stations 46002 and 46028 with Bias and RMSE around -0.5 and 2.5 respectively. The Normalized Bias is also close to 0. The Nash-Sutcliffe coefficient is closer to the ideal value of 1 only in Station 46028 (0.628) while for 46002 it remains slightly negative. This indicates that the model was able to properly capture the atmospheric parameters needed for the wind gust parameterization leading to

acceptable results. At the same time, the model forecasts that correspond to the offshore Station 46005, exhibit a satisfactory performance according to the statistical indices of Bias (-1.84) and RMSE (3.28). The Normalized Bias and Nash-Sutcliffe coefficient have values of -0.112 and 0.273 respectively for the 1st day of forecasting period. It is interesting to note that for buoy stations located close to the shore the model underestimated the measured wind gusts. This can be attributed to the representation of the coastline and topographical variation of the area, the grid structure of the NWP model and the air-sea-land interaction processes. On the contrary, over open sea areas the system overestimates the buoy observation. This may be due to the drag coefficient estimation through the parameterizations implemented in the modeling system and to problems associated with buoy measurements especially in high wave conditions. Similar values can be found in all the tested cases.

Table Ap-1: Statistical scores between measured wind gusts and the corresponding model results for 1, 2 and 3 days forecasts.

Station	Forecast	R^2	RMSE	Bias	Normalized	Nash-
St46002	1st	0,598	2,553	-0,511	0,102	-0,214
	2nd	0,580	2,671	-0,400	0,126	-0,293
	3rd	0,573	2,811	-0,442	0,116	-0,290
St46005	1st	0,699	3,281	-1,084	-0,112	0,273
	2nd	0,580	3,705	-1,045	-0,089	0,073
	3rd	0,605	3,612	-0,788	-0,067	0,119
St46025	1st	0,470	2,677	-1,159	-0,174	-0,266
	2nd	0,454	2,825	-1,200	-0,181	-0,209
	3rd	0,419	2,848	-1,236	-0,183	-0,232
St46028	1st	0.718	2.121	-0.512	-0.007	0.628
	2nd	0.637	2.317	-0.577	-0.014	0.579
	3rd	0.516	2.912	-0.588	-0.021	0.493
St46047	1st	0,431	3,120	-1,94631	-0,2872	-0,166
	2nd	0,383	3,112	-1,97285	-0,26805	-0,227
	3rd	0,319	3,160	-1,95709	-0,24519	-0,330
St46086	1st	0,496	2,652	-1,652	-0,241	-0,134
	2nd	0,456	2,684	-1,608	-0,221	-0,136
	3rd	0,392	2,821	-1,577	-0,207	-0,151

95th and 99th percentiles of wind speed and significant wave height

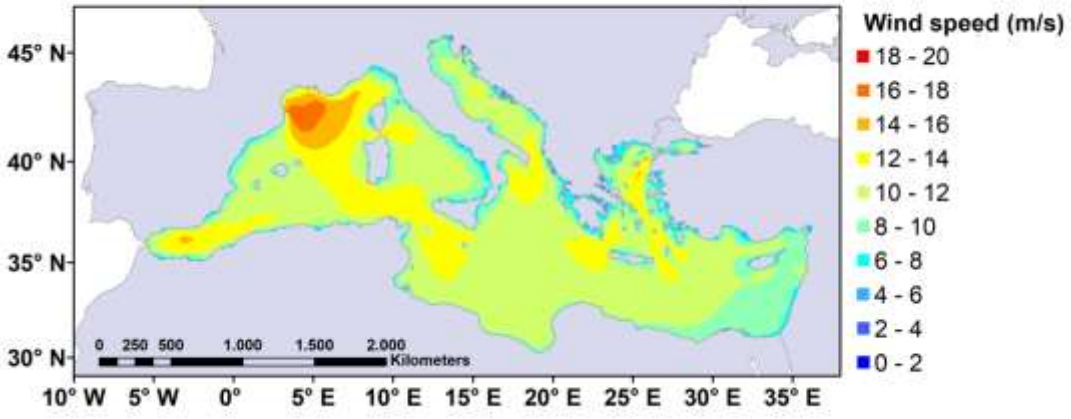

Figure Ap-4: 95th percentile of wind speed in the Mediterranean basin.

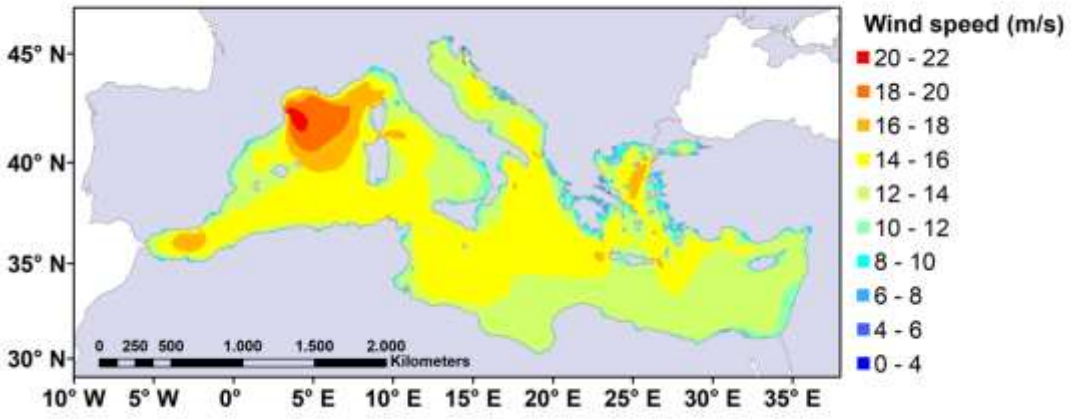

Figure Ap-5: 99th percentile of wind speed in the Mediterranean basin.

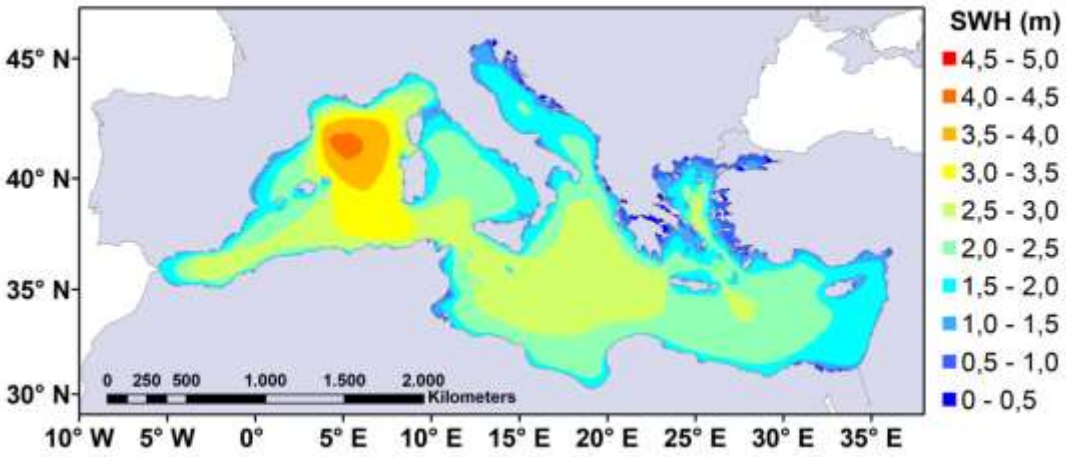

Figure Ap-6: 95th percentile of significant wave height in the Mediterranean basin.

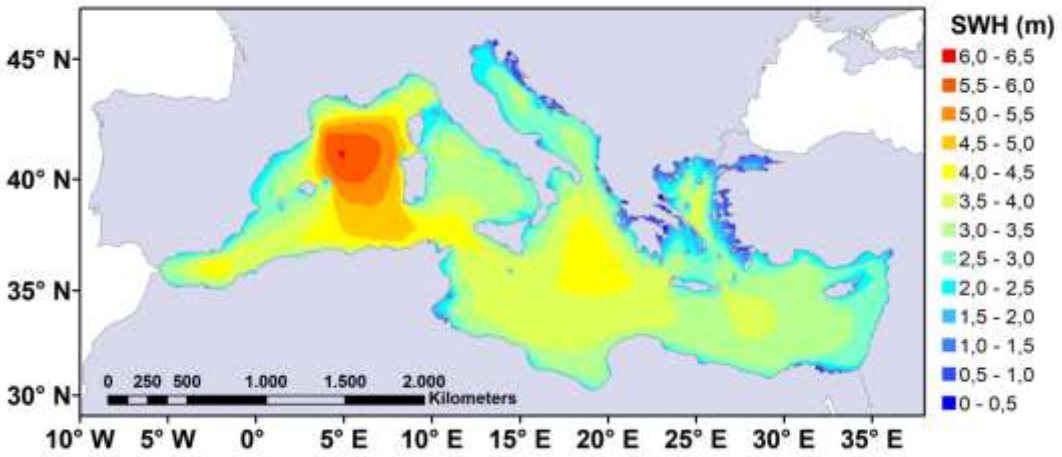

Figure Ap-7: 95th percentile of significant wave height in the Mediterranean basin.

Threshold selection

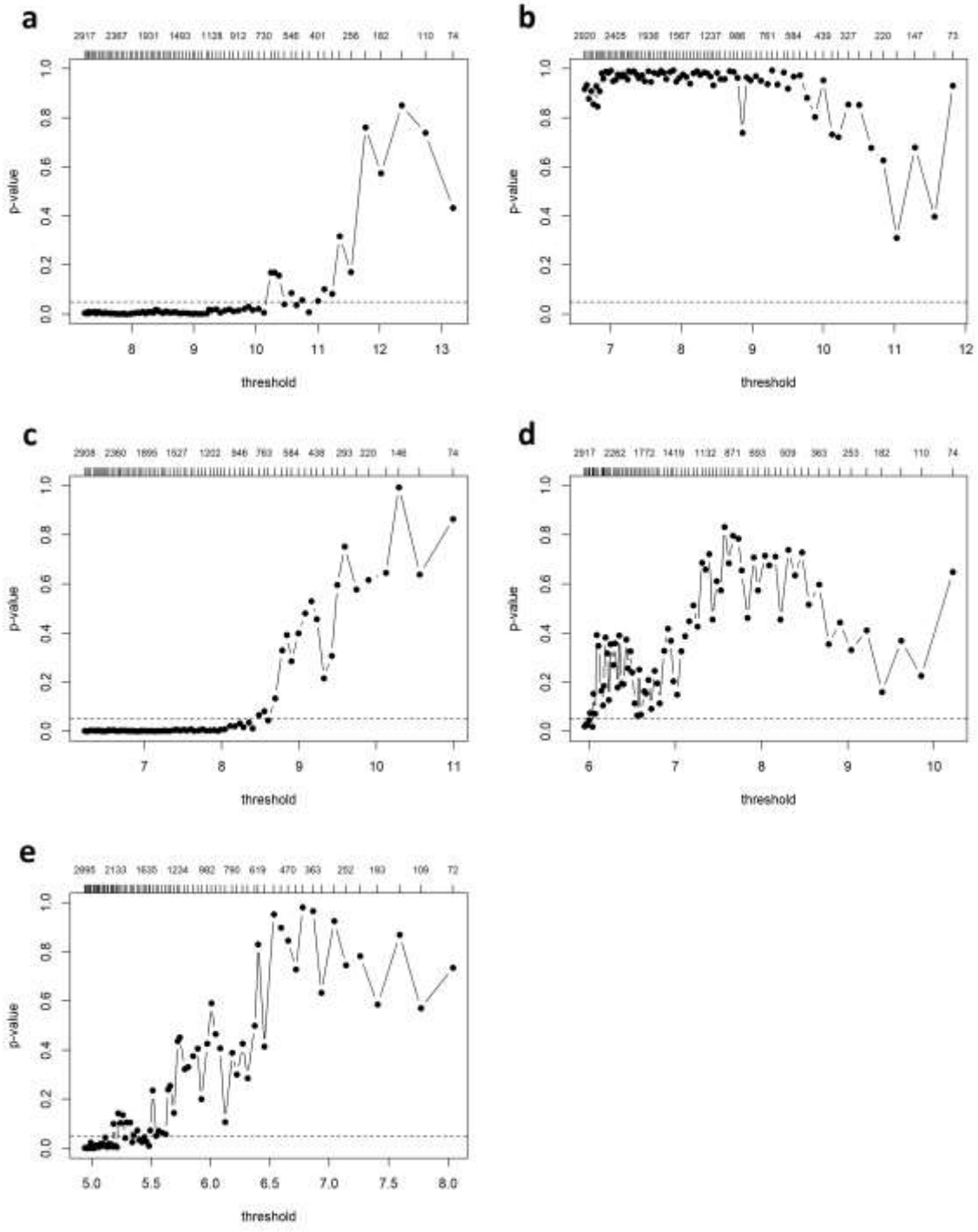

Figure Ap-8: NC diagram for the selection of the threshold for the wind speed extreme value analysis (POT), extreme index 1 and all sub-regions (a to e).

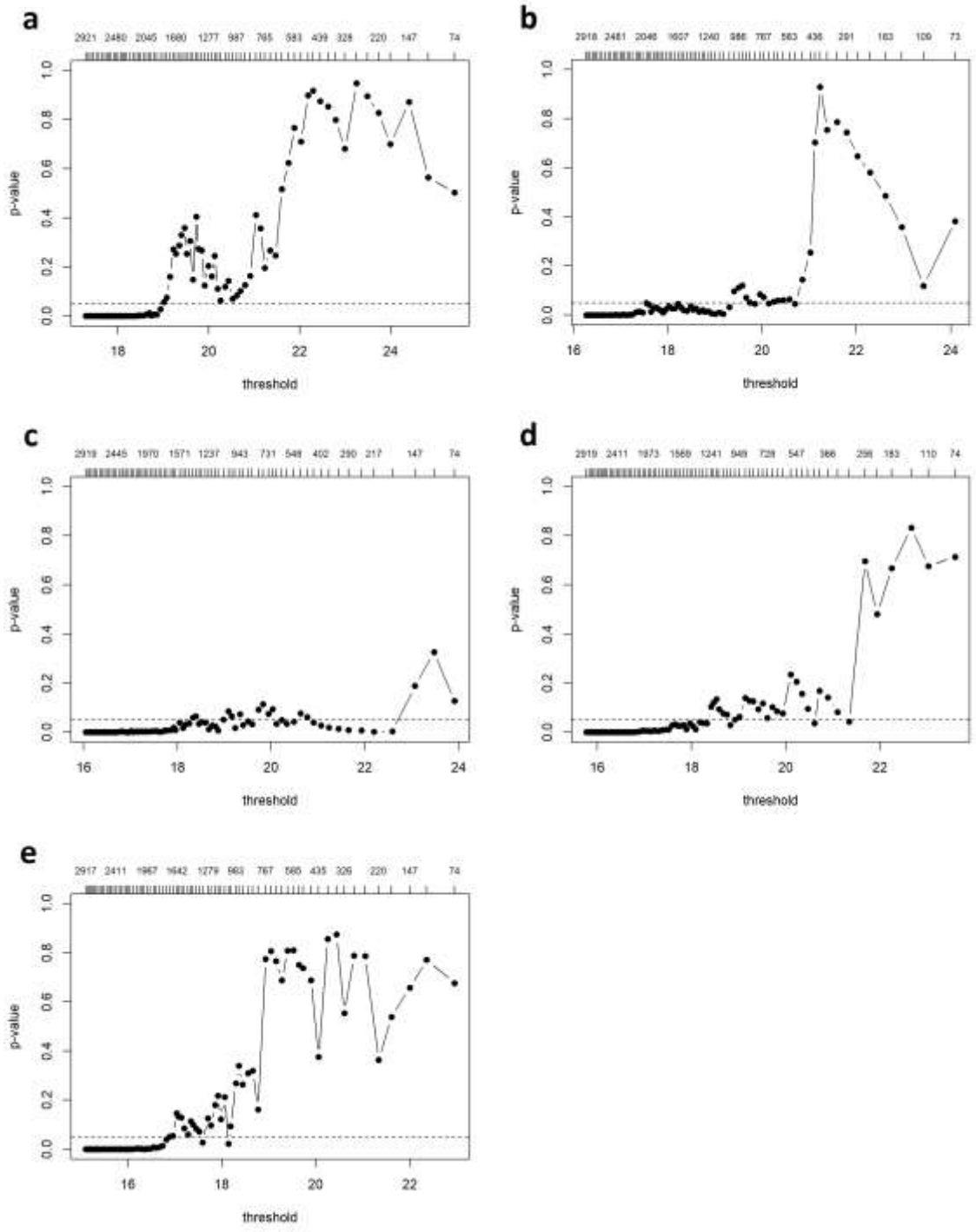

Figure Ap-9: NC diagram for the selection of the threshold for the wind speed extreme value analysis (POT), extreme index 2 and all sub-regions (a to e).

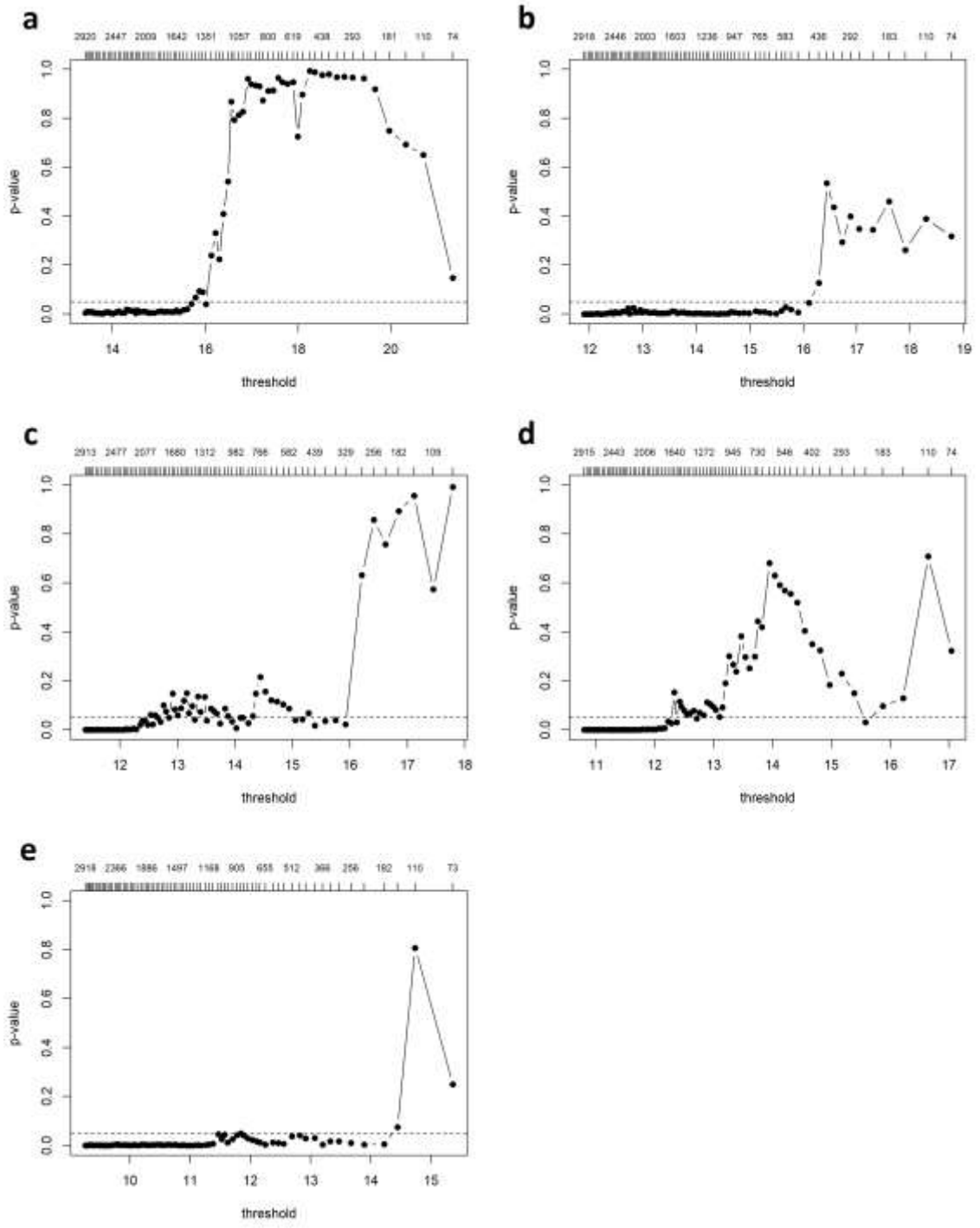

Figure Ap-10: NC diagram for the selection of the threshold for the wind speed extreme value analysis (POT), extreme index 3 and all sub-regions (a to e).

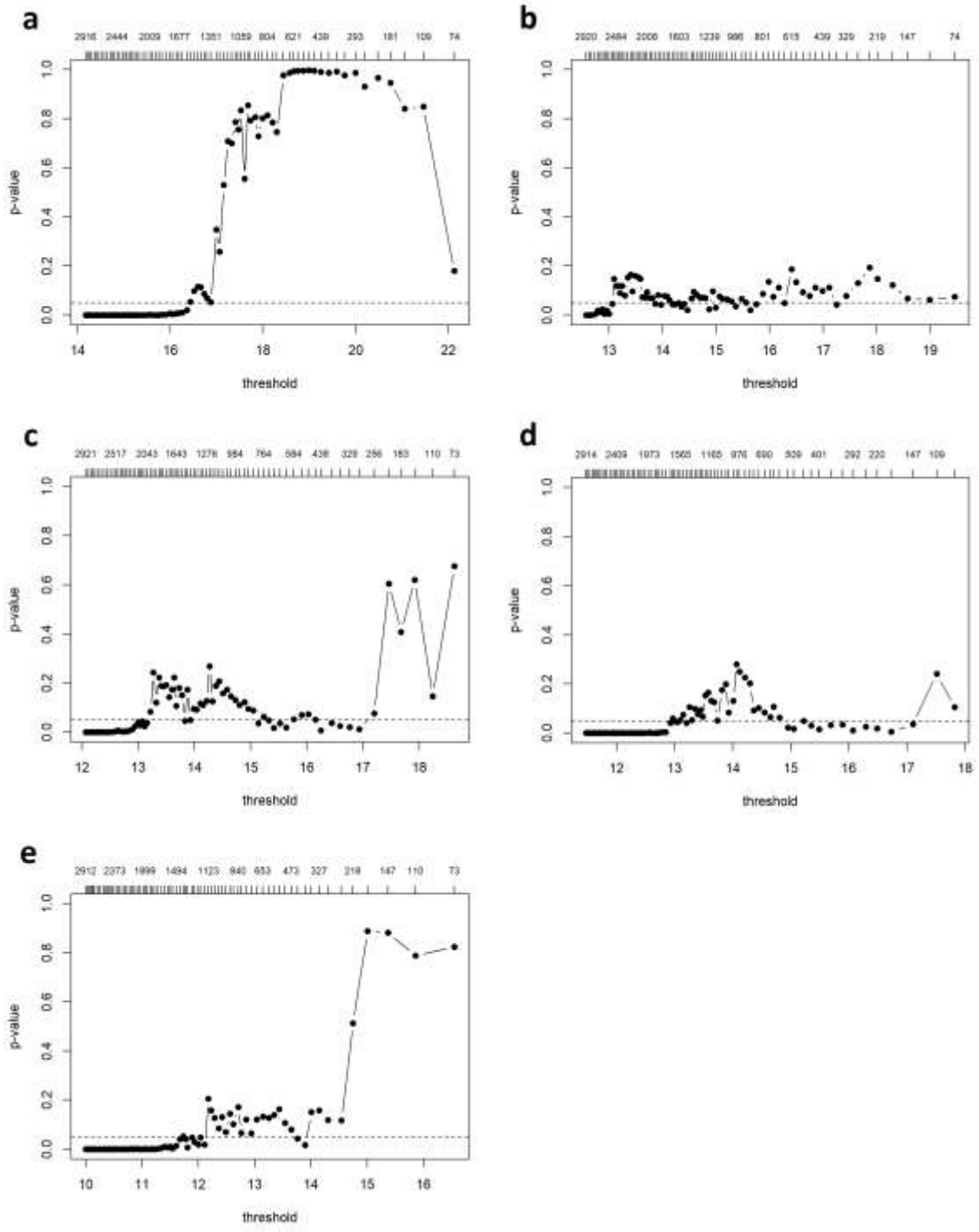

Figure Ap-11: NC diagram for the selection of the threshold for the wind speed extreme value analysis (POT), extreme index 4 and all sub-regions (a to e).

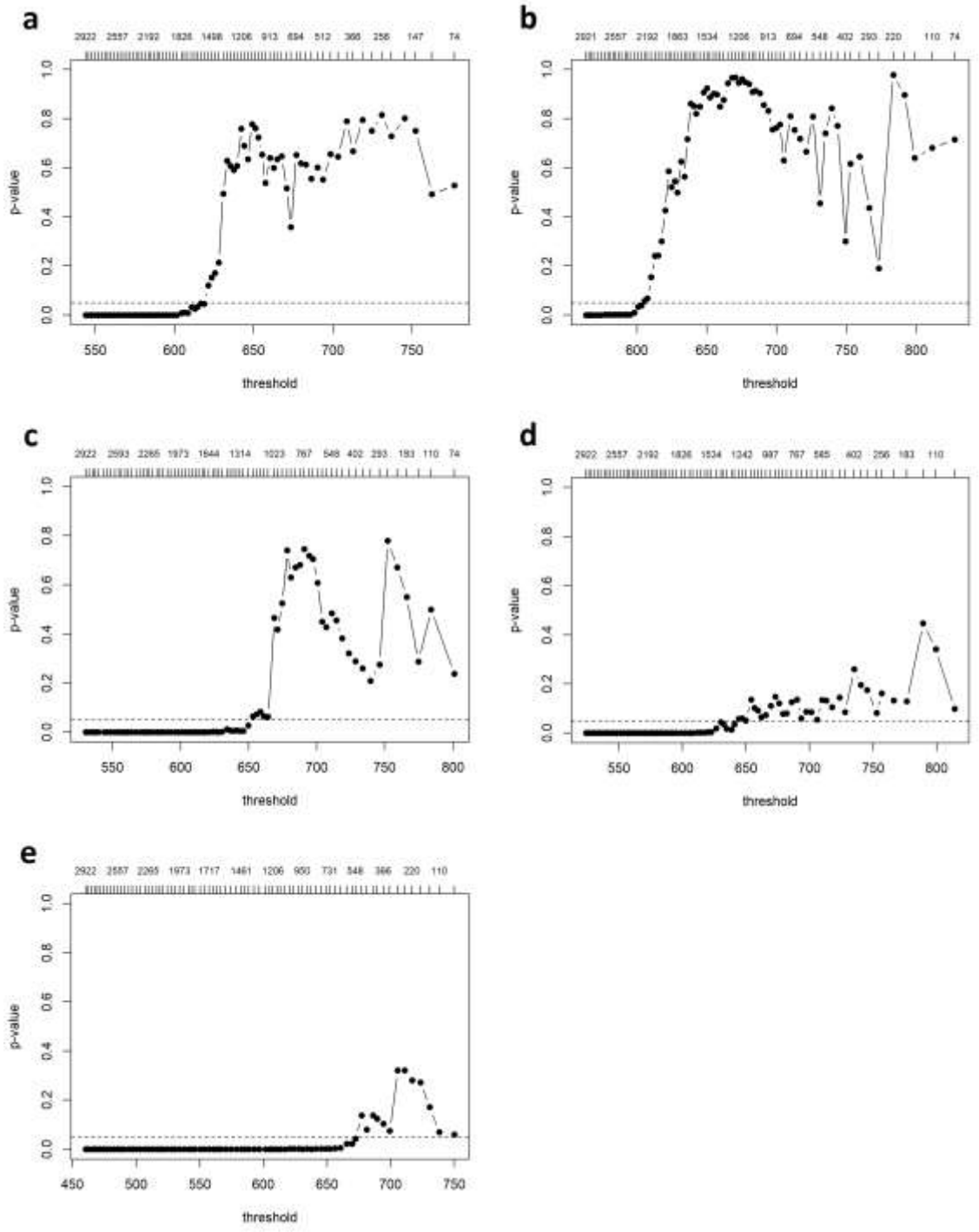

Figure Ap-12: NC diagram for the selection of the threshold for the wind speed extreme value analysis (POT), extreme index 5 and all sub-regions (a to e).

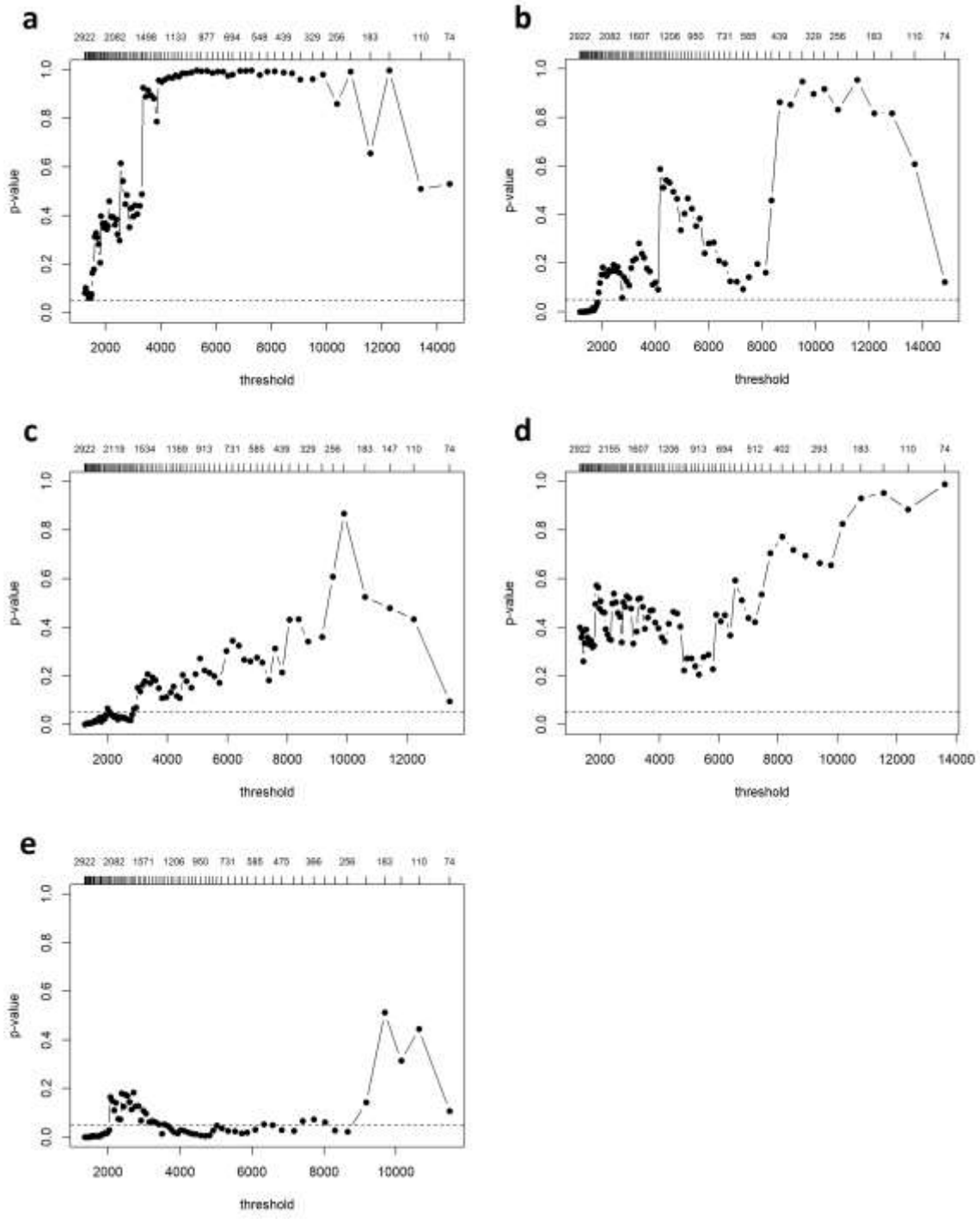

Figure Ap-13: NC diagram for the selection of the threshold for the wind speed extreme value analysis (POT), extreme index 6 and all sub-regions (a to e).

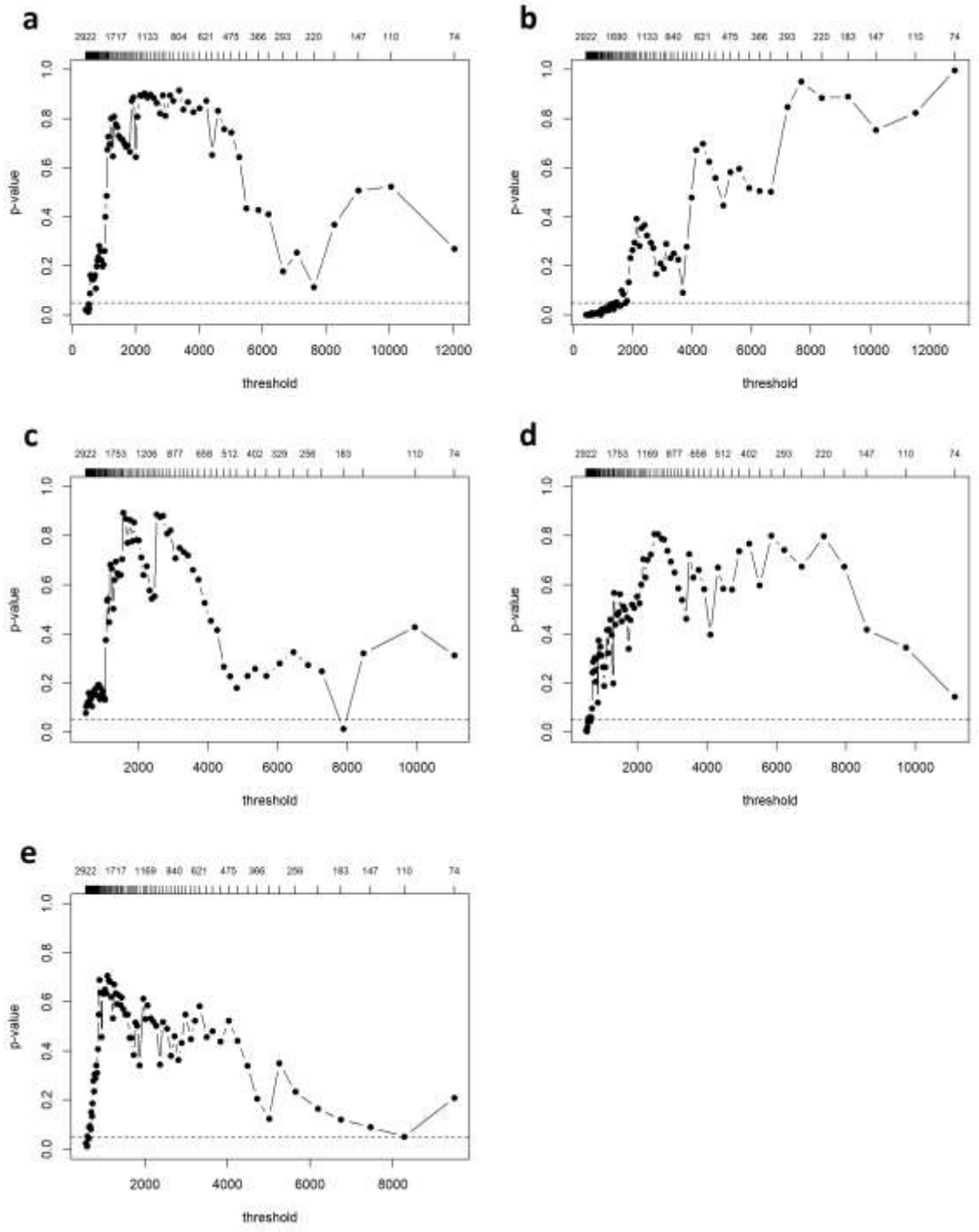

Figure Ap-14: NC diagram for the selection of the threshold for the wind speed extreme value analysis (POT), extreme index 7 and all sub-regions (a to e).

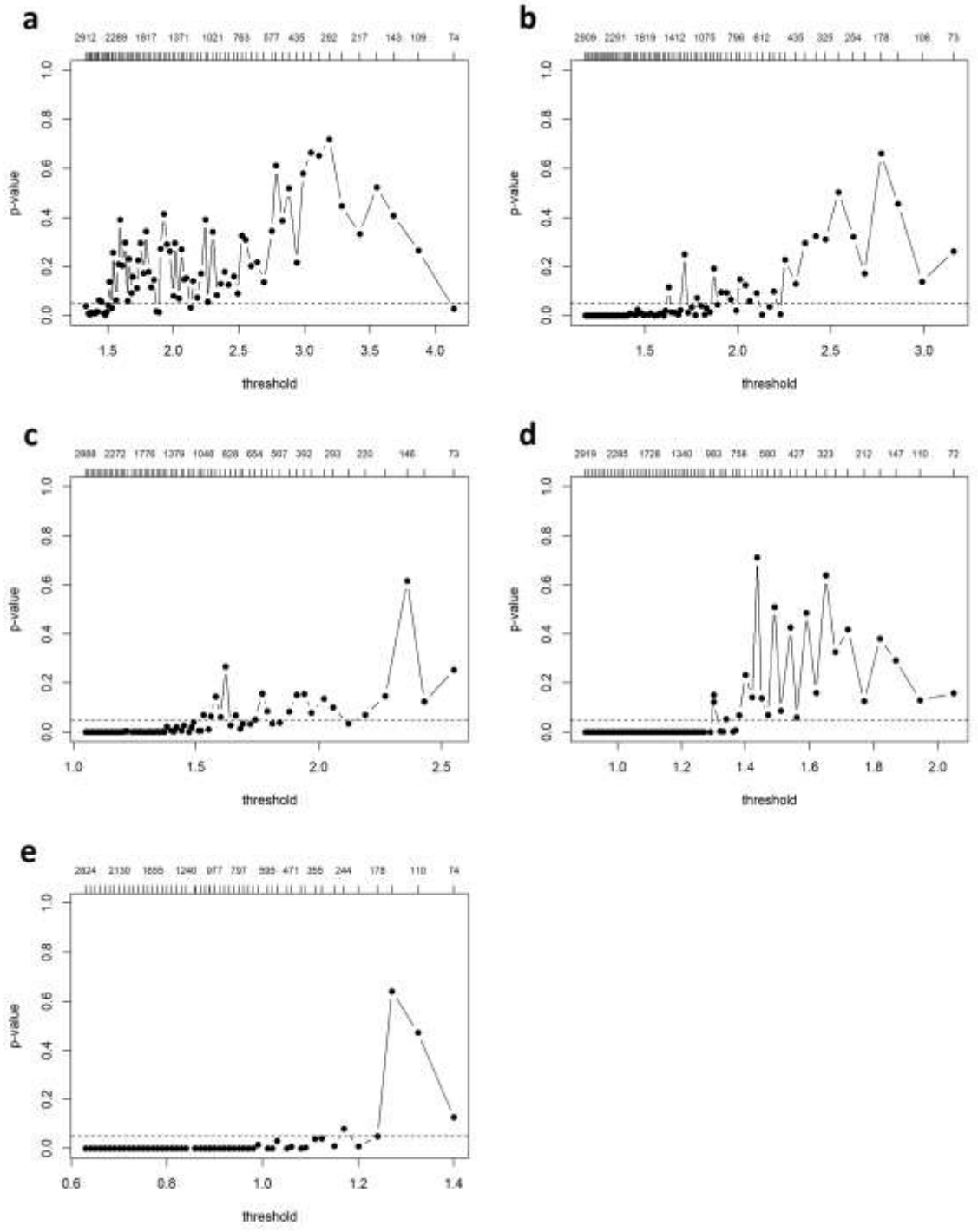

Figure Ap-15: NC diagram for the selection of the threshold for the significant wave height extreme value analysis (POT), extreme index 1 and all sub-regions (a to e).

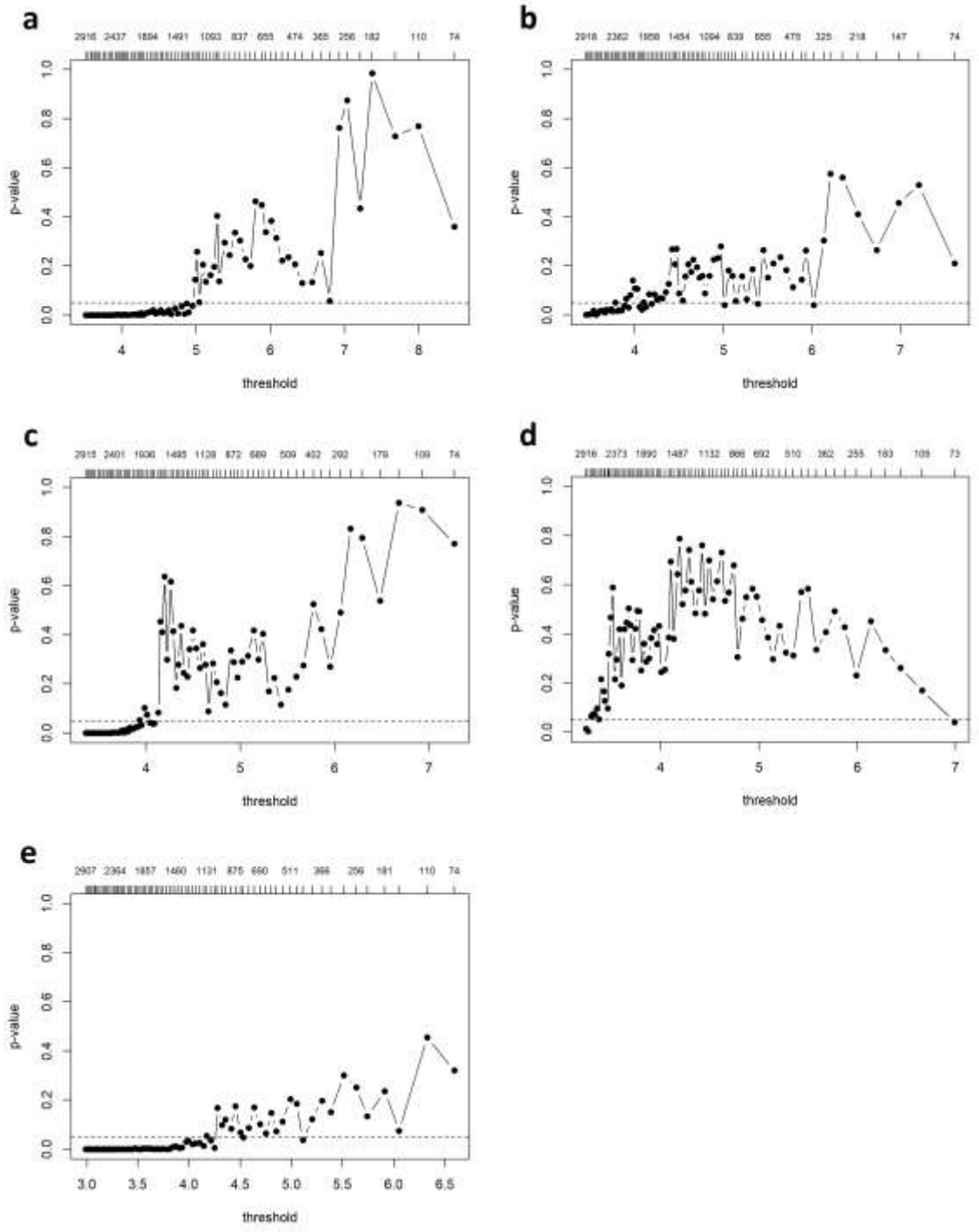

Figure Ap-16: NC diagram for the selection of the threshold for the significant wave height extreme value analysis (POT), extreme index 2 and all sub-regions (a to e).

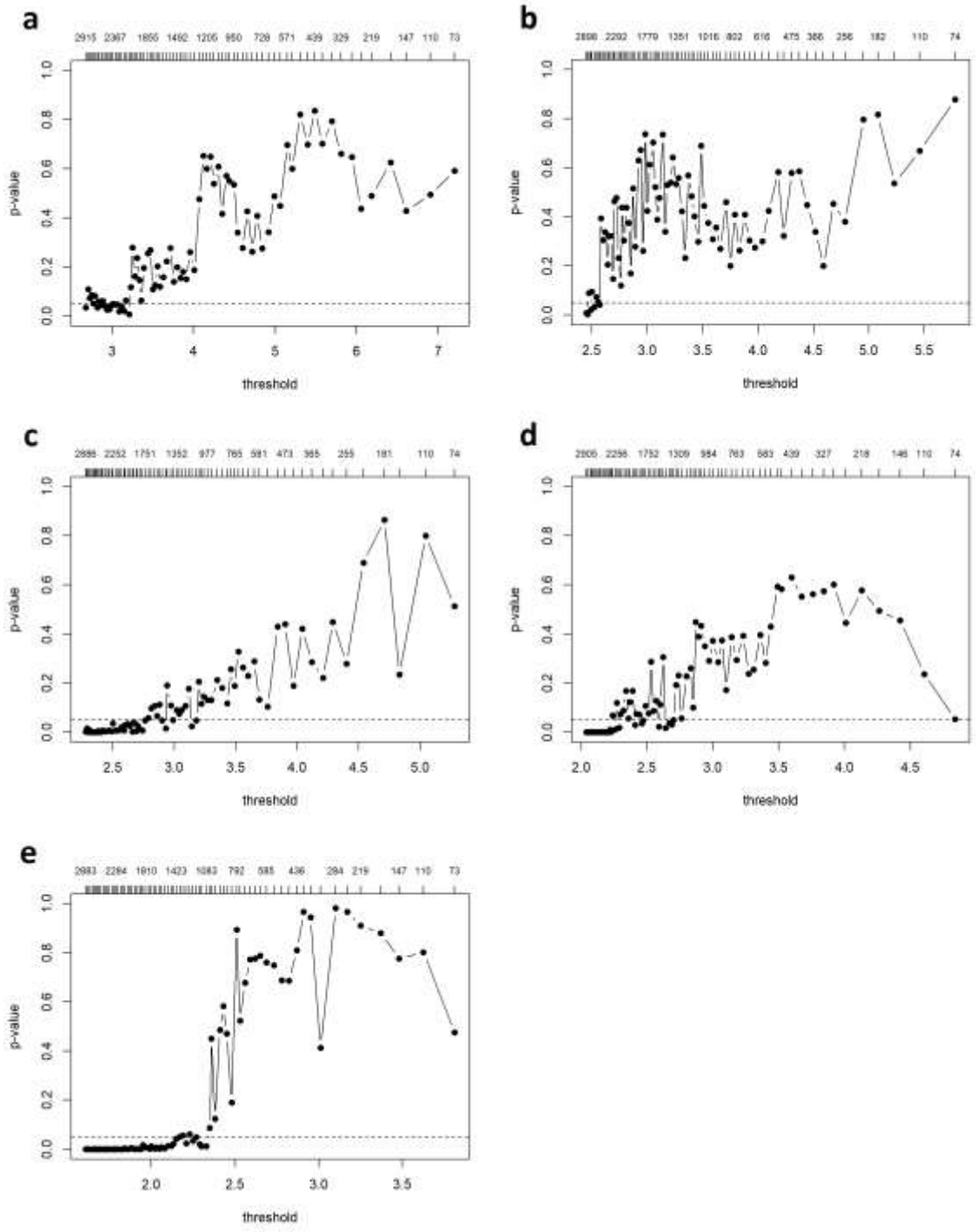

Figure Ap-17: NC diagram for the selection of the threshold for the significant wave height extreme value analysis (POT), extreme index 3 and all sub-regions (a to e).

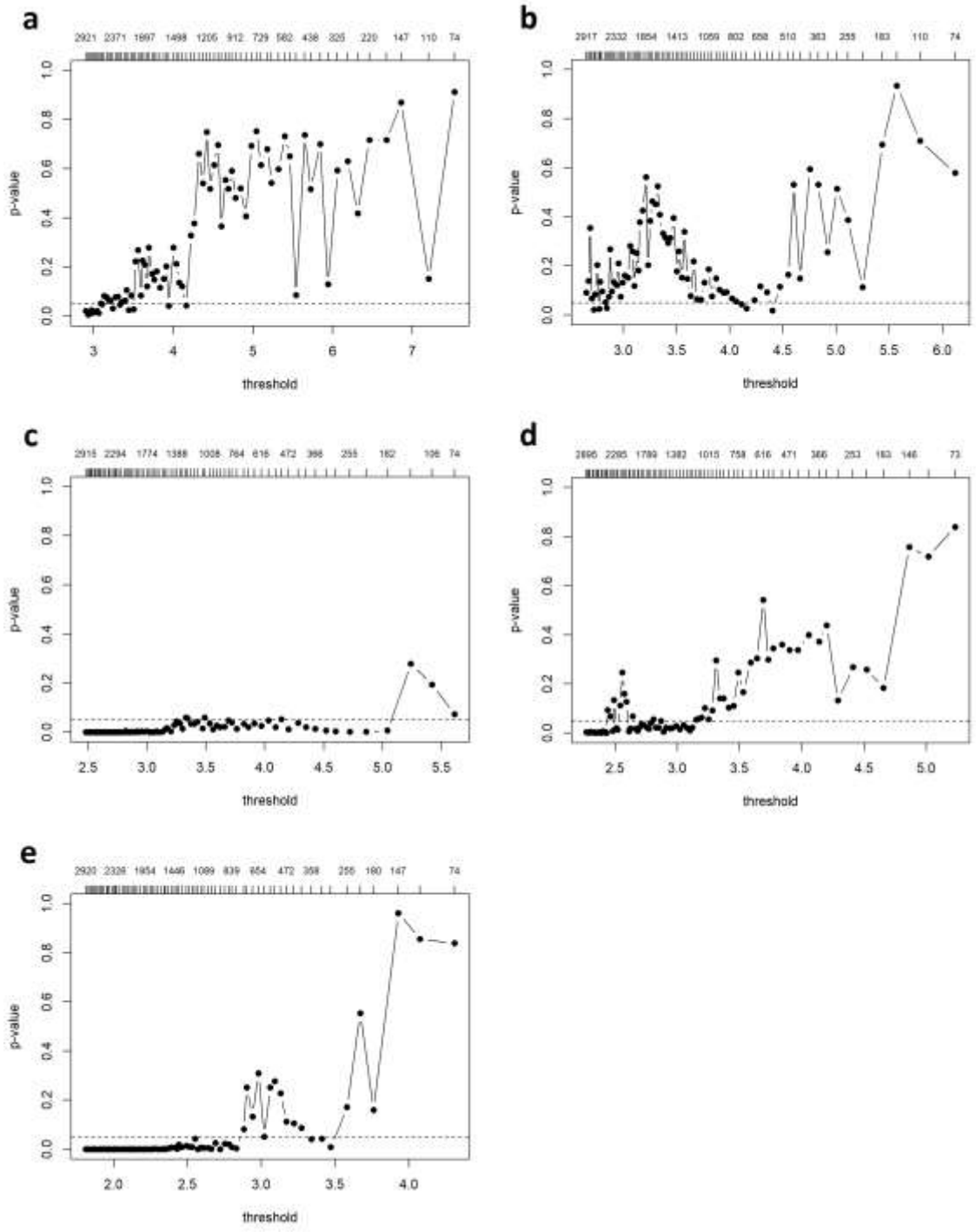

Figure Ap-18: NC diagram for the selection of the threshold for the significant wave height extreme value analysis (POT), extreme index 4 and all sub-regions (a to e).

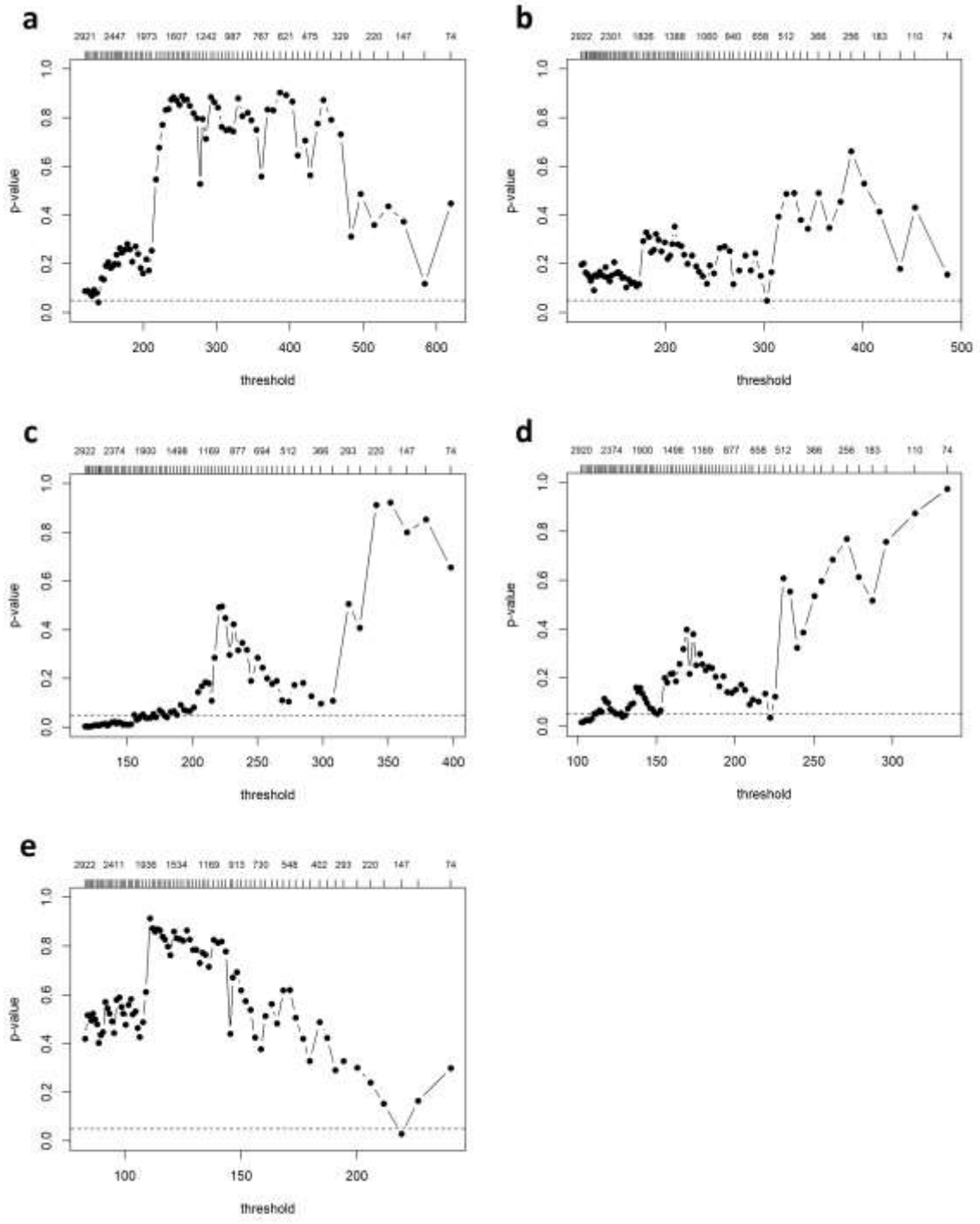

Figure Ap-19: NC diagram for the selection of the threshold for the significant wave height extreme value analysis (POT), extreme index 5 and all sub-regions (a to e).

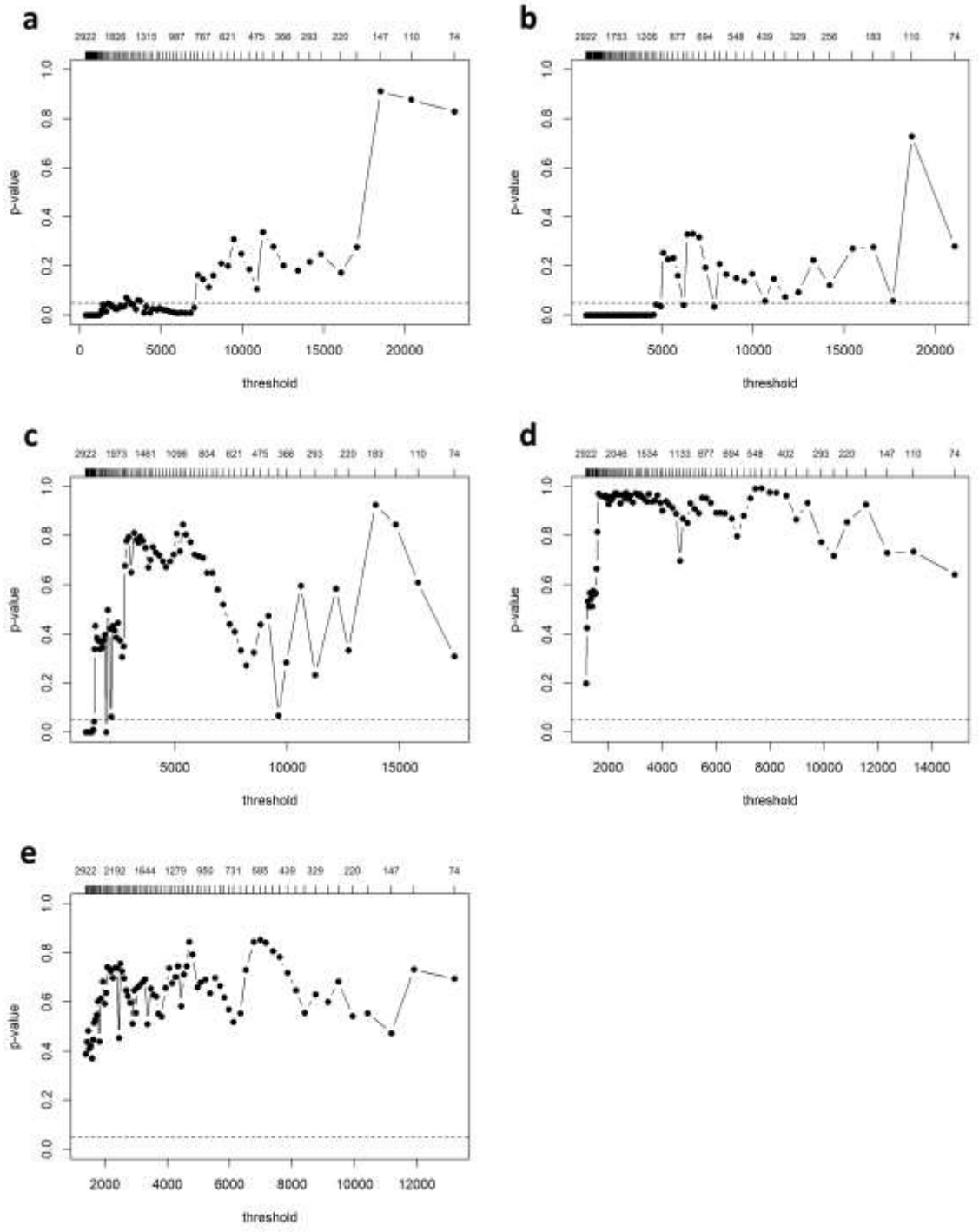

Figure Ap-20: NC diagram for the selection of the threshold for the significant wave height extreme value analysis (POT), extreme index 6 and all sub-regions (a to e).

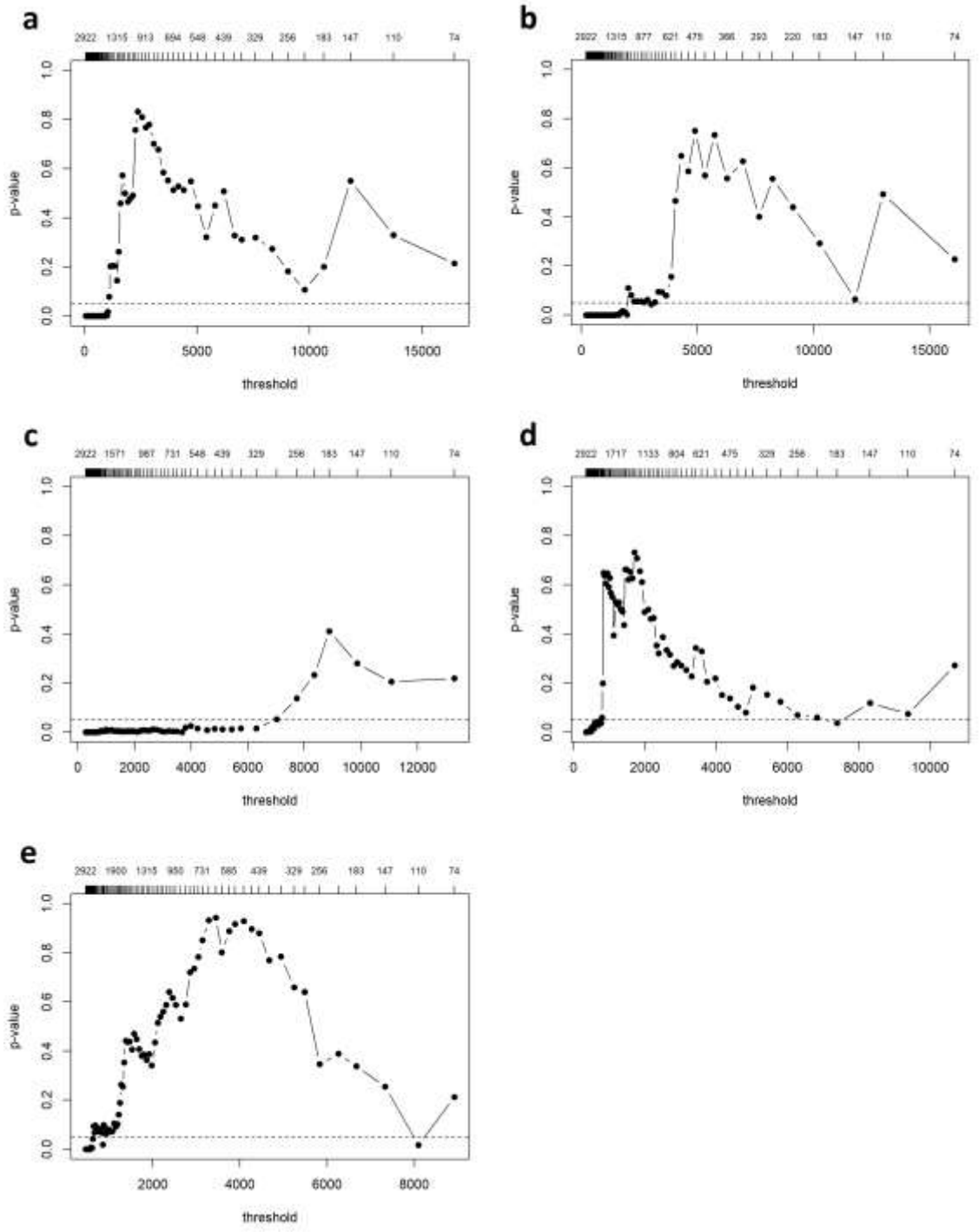

Figure Ap-21: NC diagram for the selection of the threshold for the significant wave height extreme value analysis (POT), extreme index 7 and all sub-regions (a to e).

Return periods of extreme indices - wind

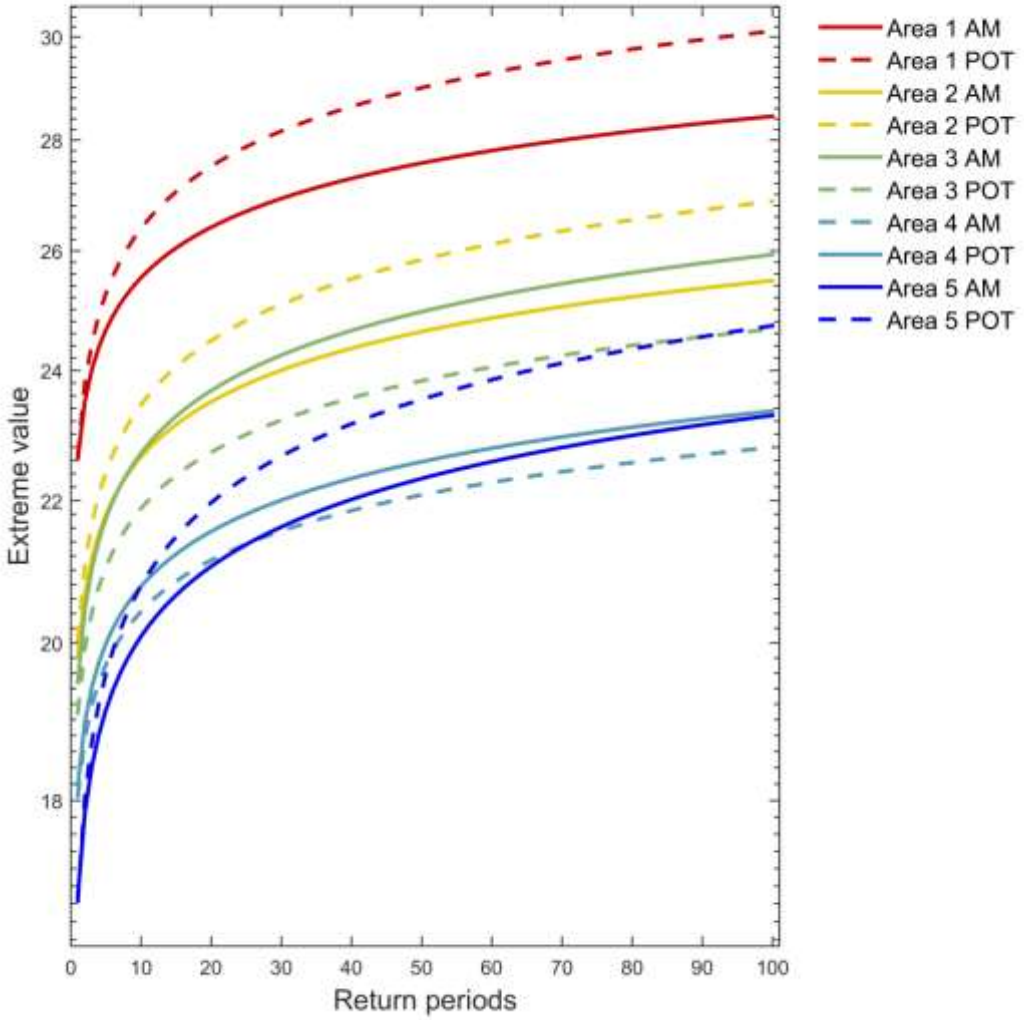

Figure Ap-22: Extreme values for the wind speed spatial 95th quantile and return periods ranging between 1 and 100 years.

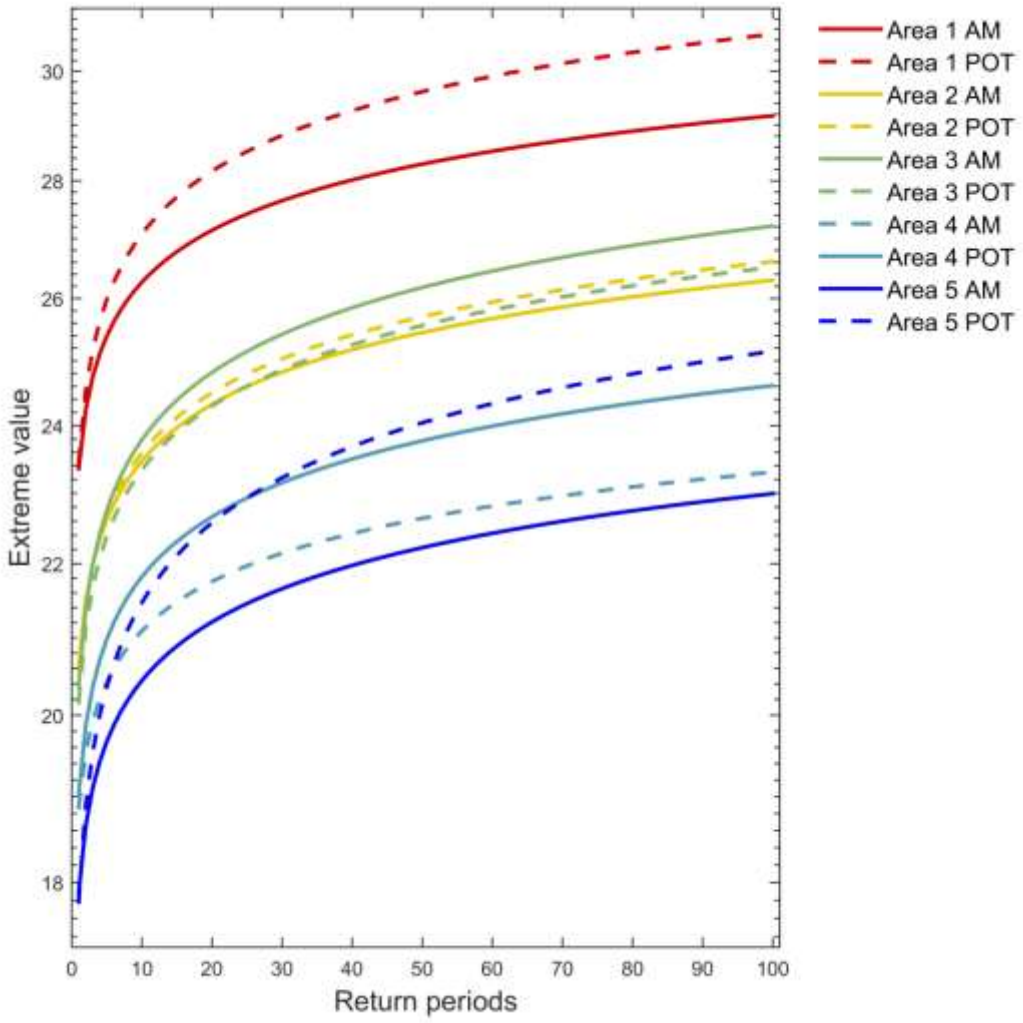

Figure Ap-23: Extreme values for the wind speed spatial 99th quantile and return periods ranging between 1 and 100 years.

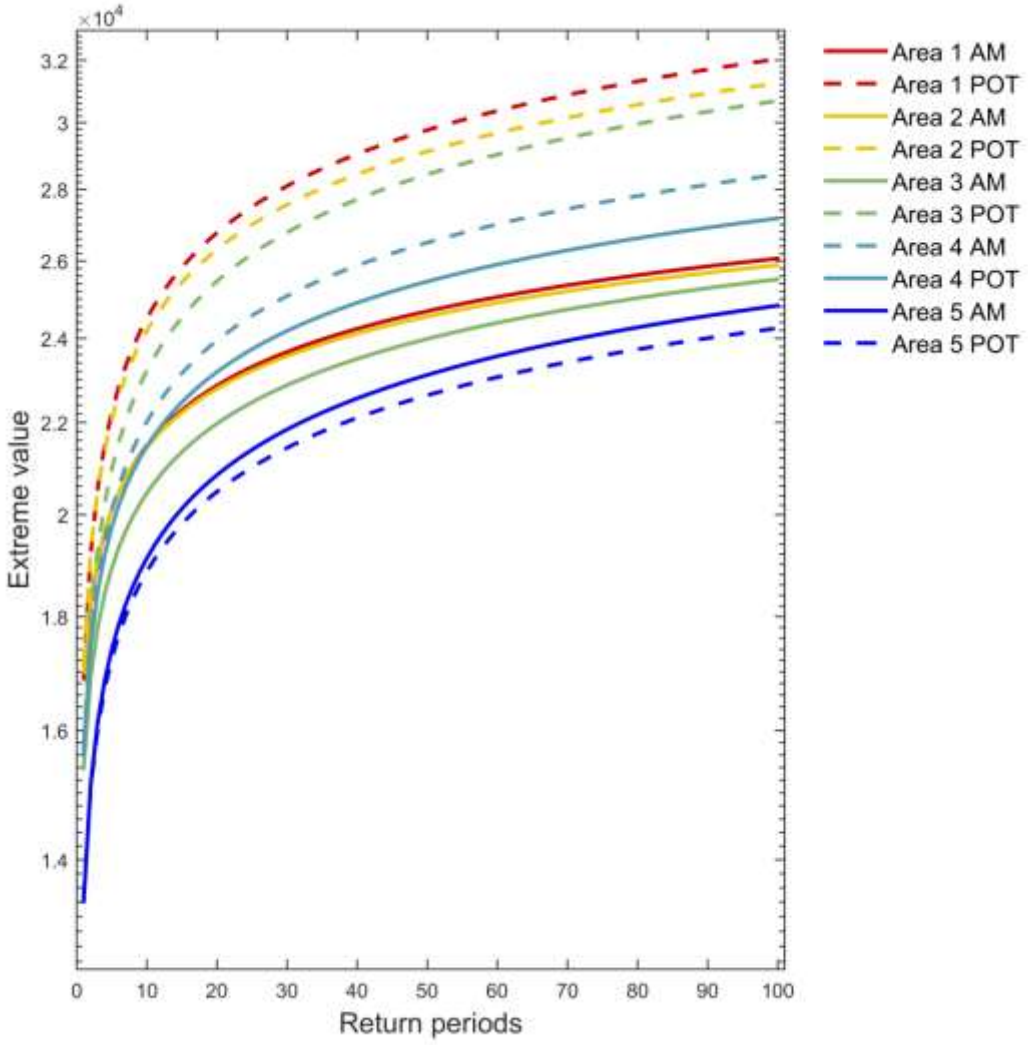

Figure Ap-24: Extreme values for the summary of the fraction of wind speed values divided by the grid-point climatological 95% quantile (Sfq95) and return periods ranging between 1 and 100 years.

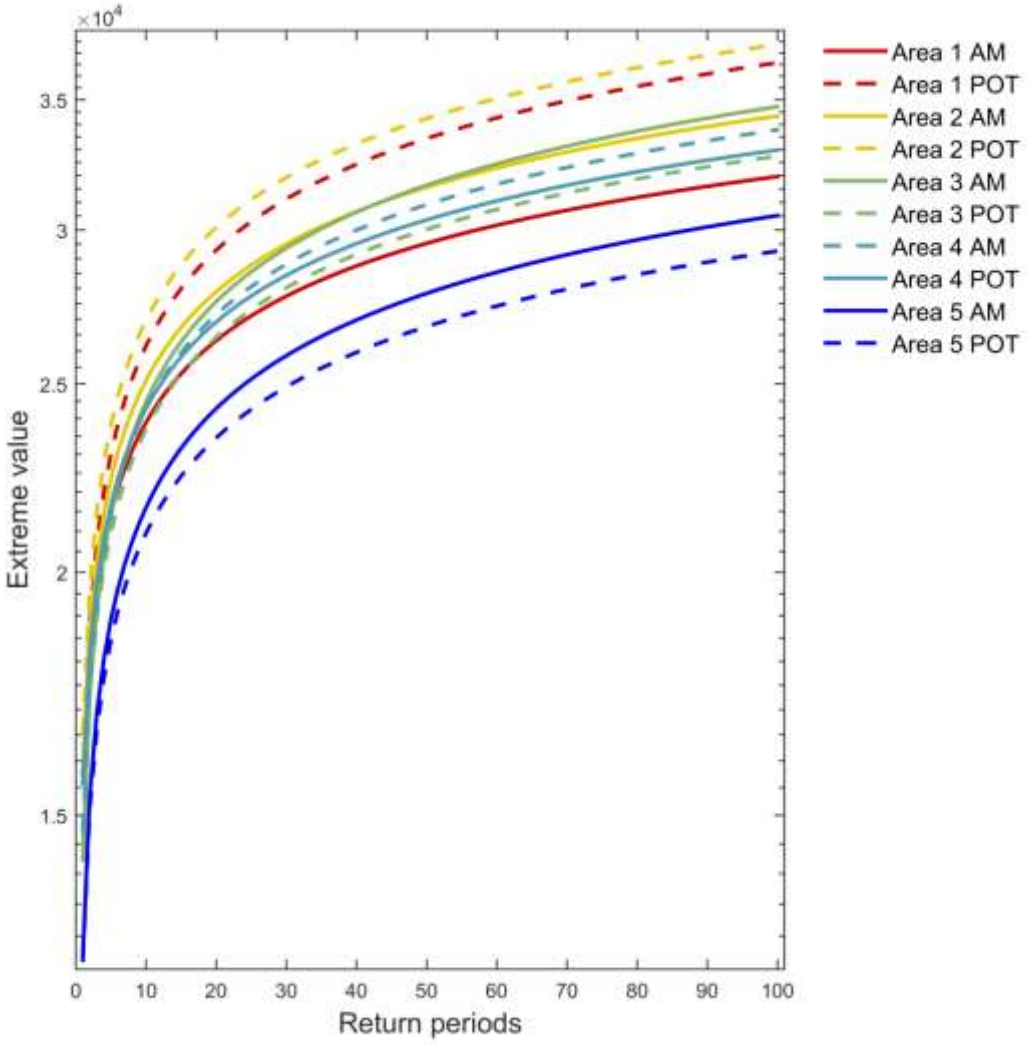

Figure Ap-25: Extreme values for the summary of the fraction of the highest wind speed values divided by the length of the distribution tail (Sfq95q99) and return periods ranging between 1 and 100 years.

Return periods of extreme indices - significant wave height

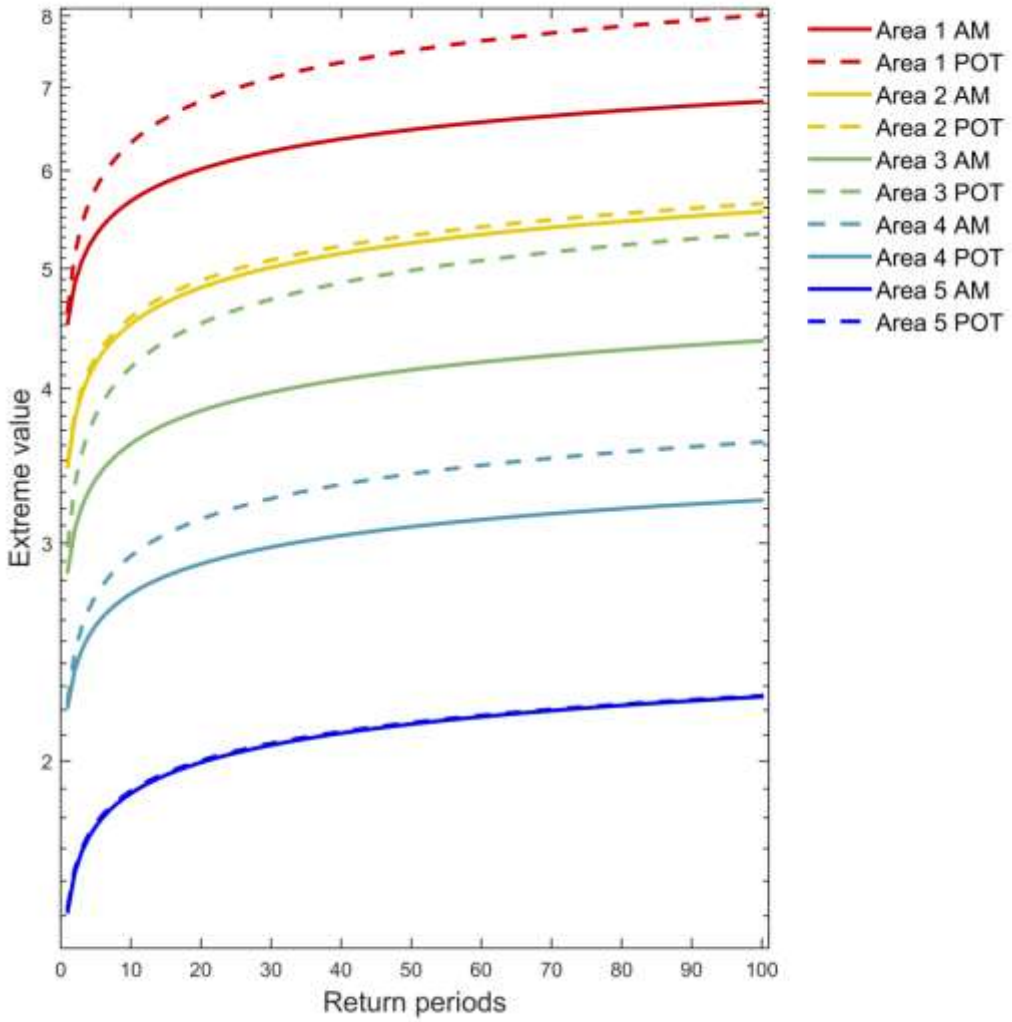

Figure Ap-26: Extreme values for the significant wave height spatial mean and return periods ranging between 1 and 100 years.

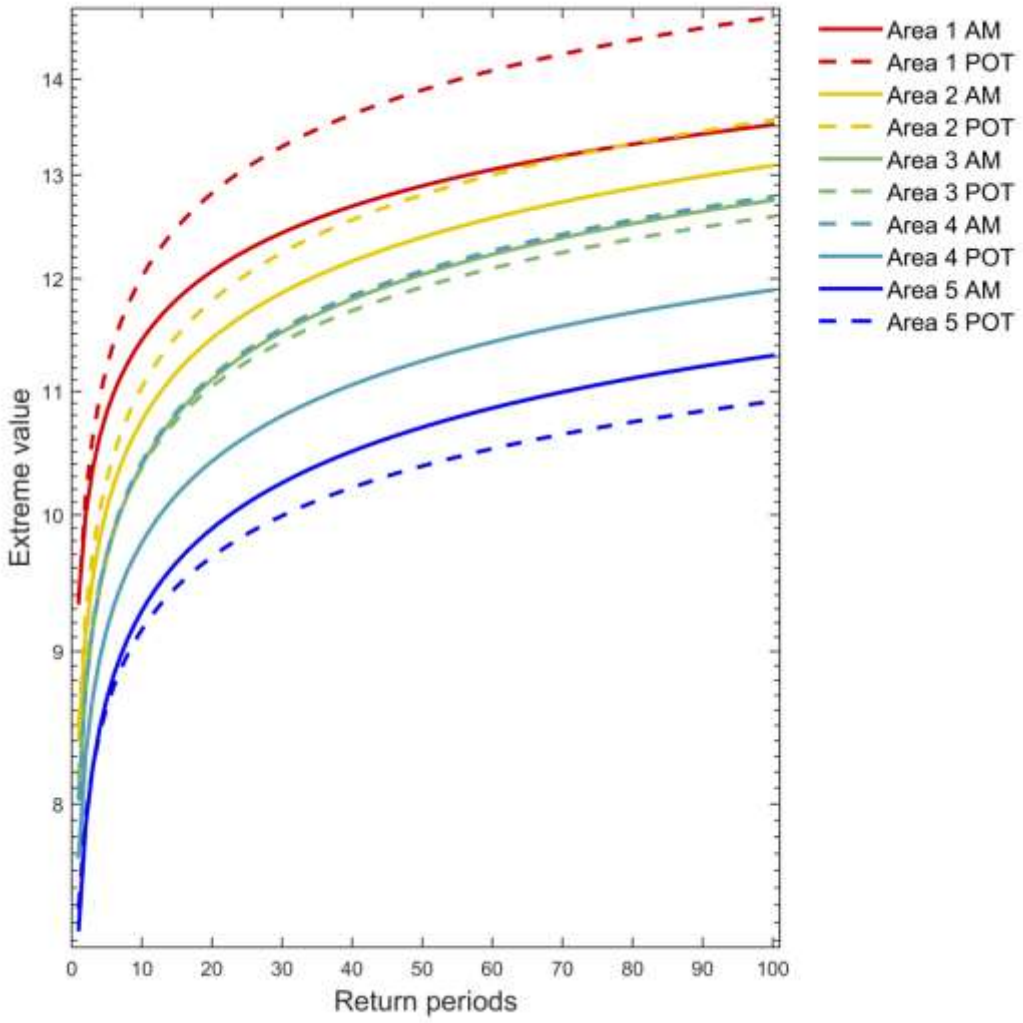

Figure Ap-270-1: Extreme values for the significant wave height maximum value and return periods ranging between 1 and 100 years.

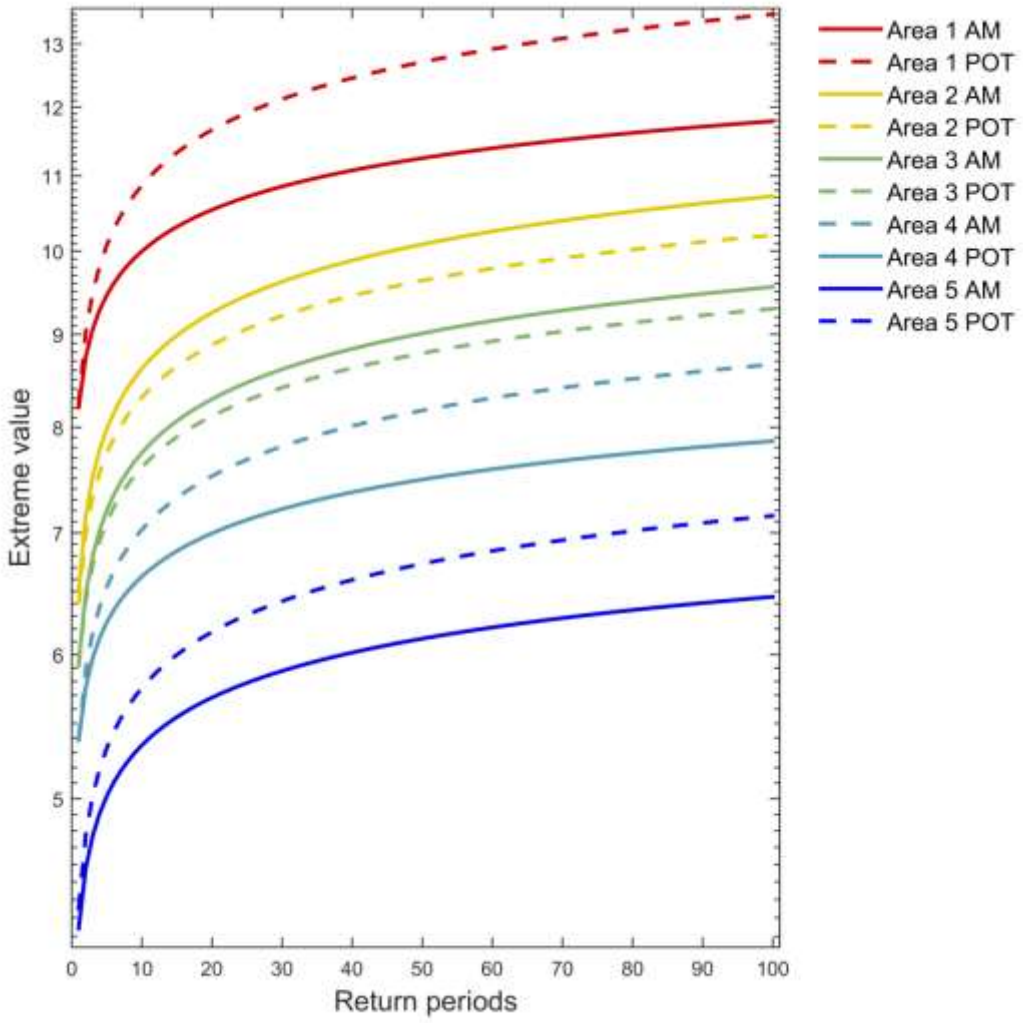

Figure Ap-28: Extreme values for the significant wave height spatial 95th quantile and return periods ranging between 1 and 100 years.

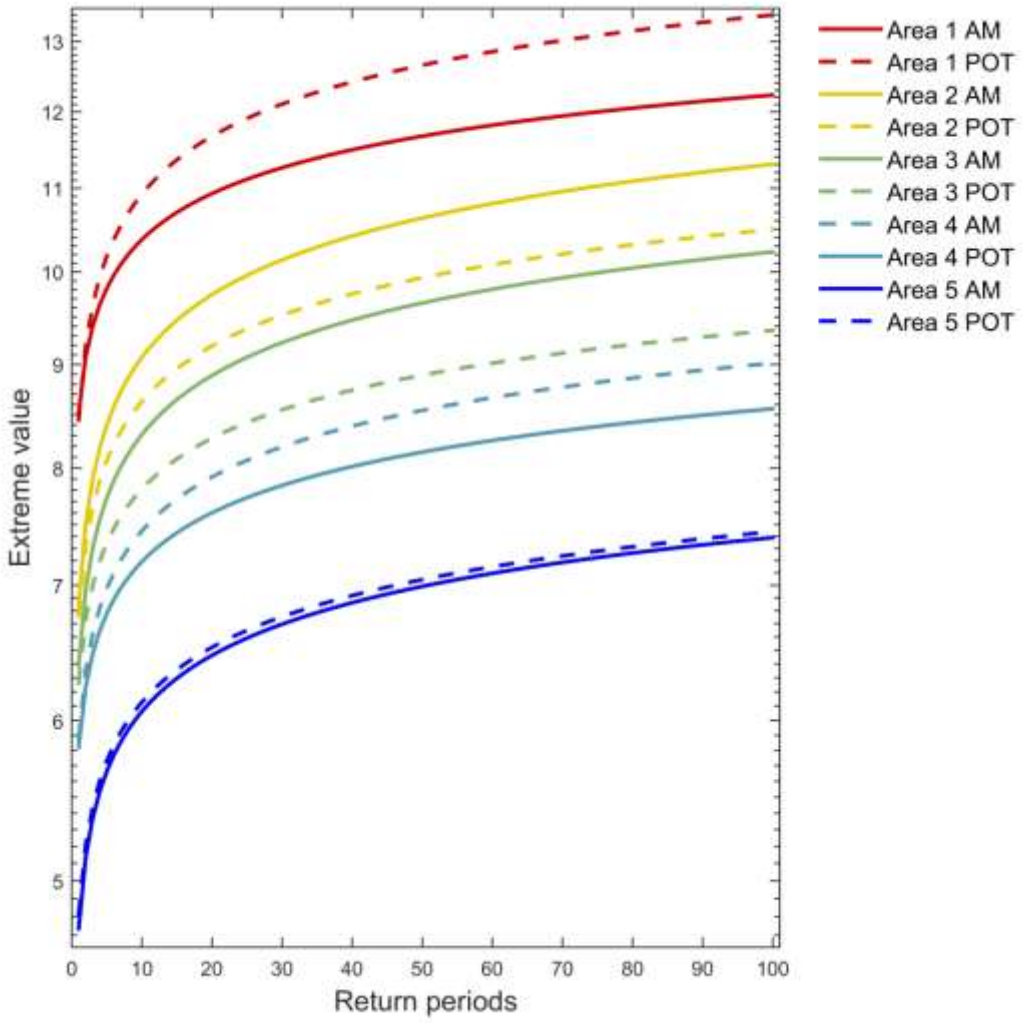

Figure Ap-29: Extreme values for the significant wave height spatial 99th quantile and return periods ranging between 1 and 100 years.

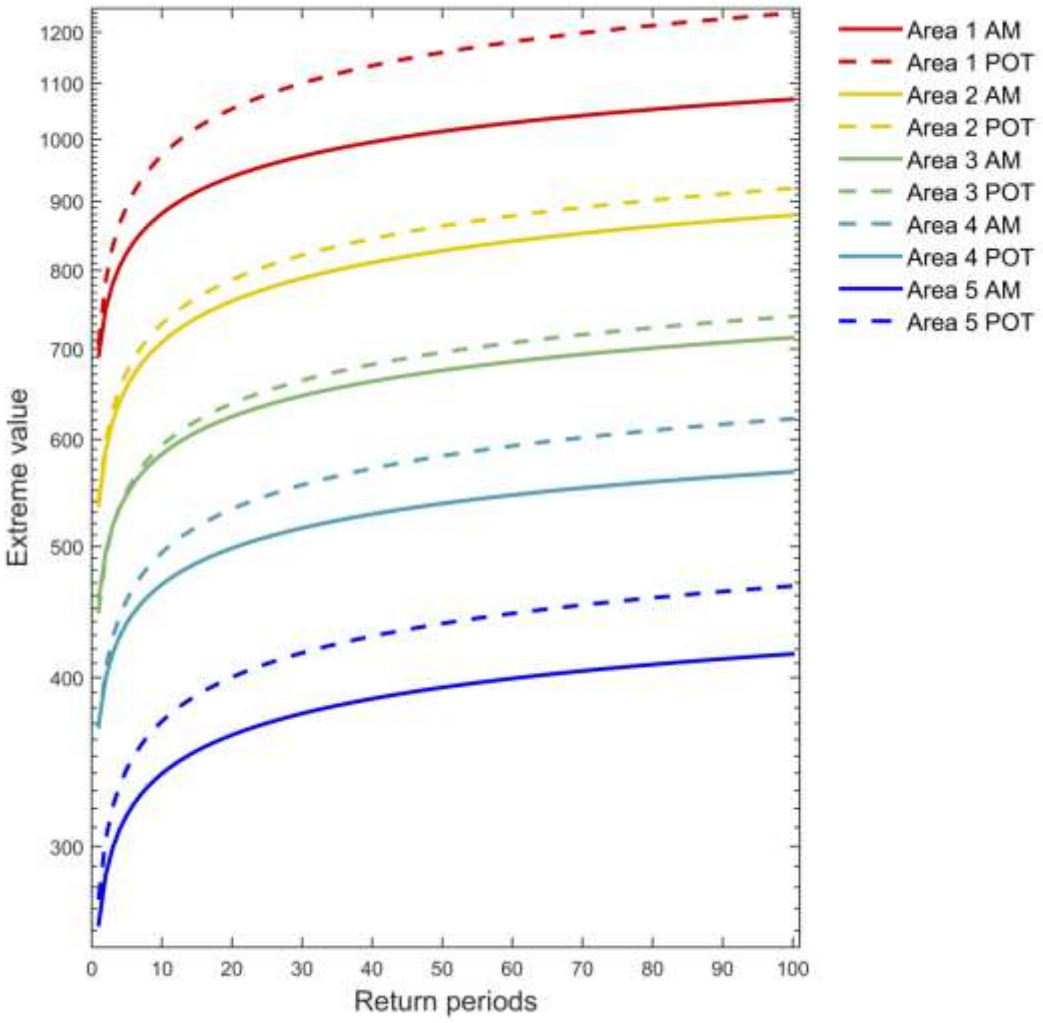

Figure Ap-30: Extreme values for the cube root of the sum of significant waae height cubed above the domain climatological 90% quantile (Sw3q90) and return periods ranging between 1 and 100 years.

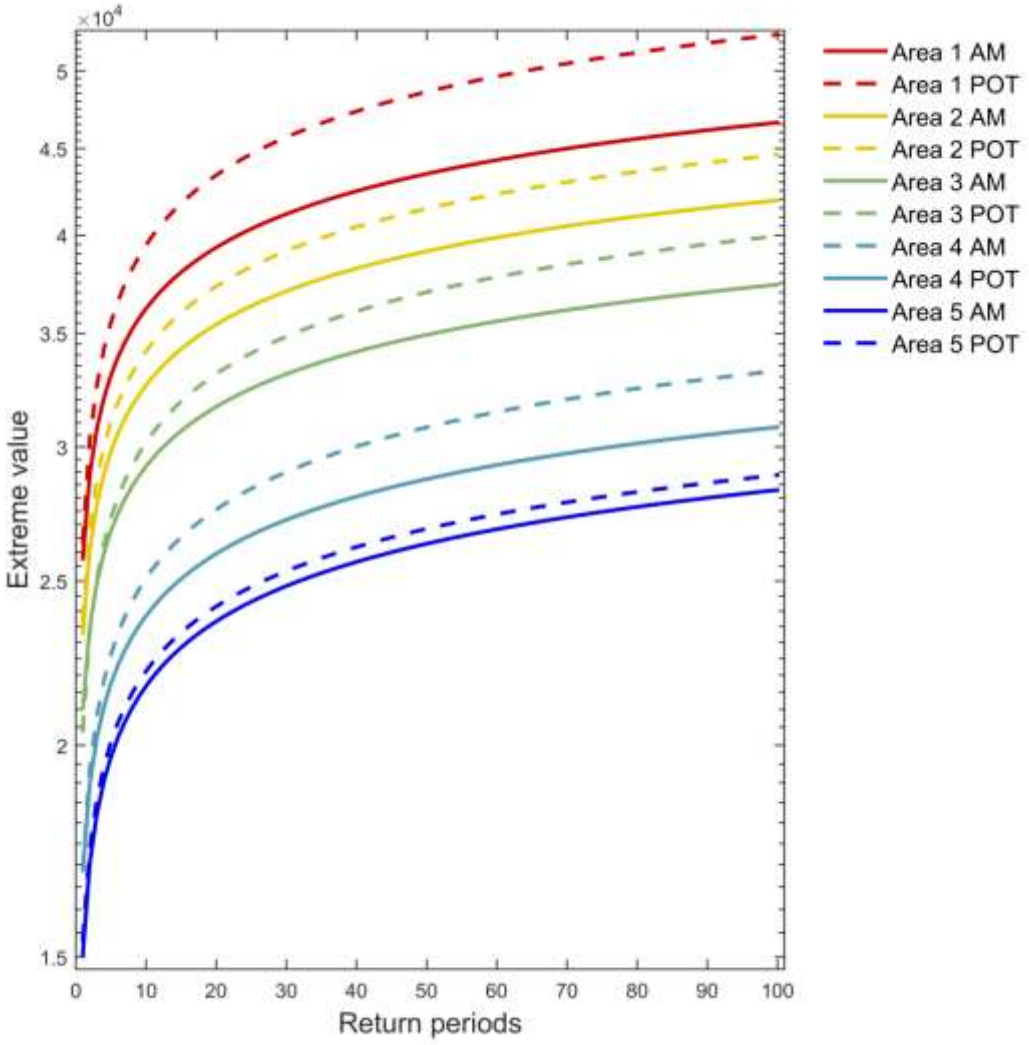

Figure Ap-31: Extreme values for the summary of the fraction of the significant wave height values divided by the grid-point climatological 95% quantile (Sfq95) and return periods ranging between 1 and 100 years.

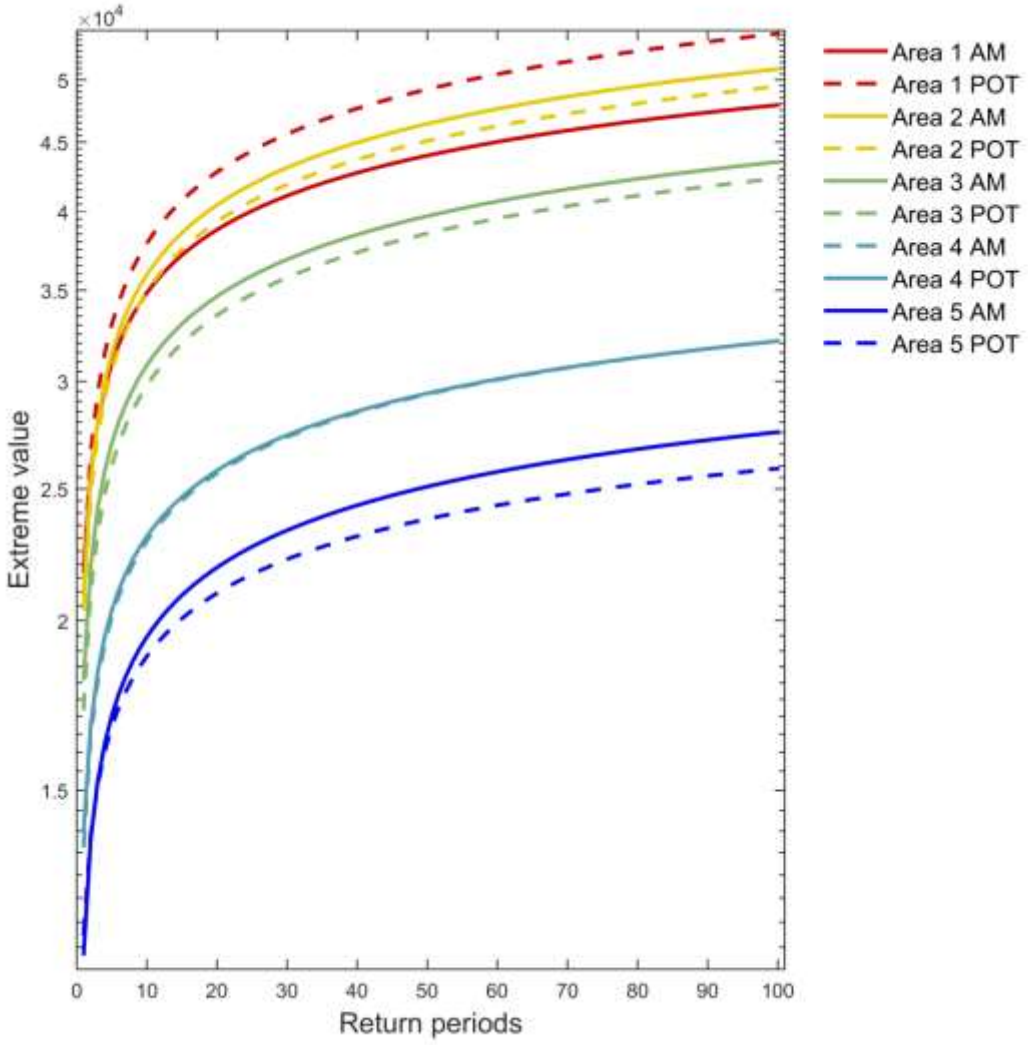

Figure Ap-32: Extreme values for the summary of the fraction of the highest significant wave height values divided by the length of the distribution tail (Sfq95q99) and return periods ranging between 1 and 100 years.

List of Publications (peer-review and conference presentations)

In peer review journals:

1. Tsalis, C., **Patlakas, P.**, Stathopoulos, C., Kallos, G. "Optimizing a new De-clustering approach for relatively small samples of wind speed with an application to offshore design conditions", *under review* on Ocean Engineering.
2. **Patlakas, P.**, Stathopoulos, C., Tsalis, C., Kallos, G. "Wind and wave extremes associated with tropical-like cyclones in the Mediterranean basin", *revisions submitted* on International Journal of Climatology.
3. Stathopoulos, C., **Patlakas, P.**, Tsalis, C., Kallos, G. "The Role of Sea Surface Temperature Forcing in the Life-Cycle of Mediterranean Cyclones", Remote Sens. 2020, 12, 825.
4. Otero-Casal, C., **Patlakas, P.**, Prósper, MA., Galanis, G.,Miguez-Macho, G. "Development of a High-Resolution Wind Forecast System Based on the WRF Model and a Hybrid Kalman-Bayesian Filter", Energies 2019, 12(16), 3050; https://doi.org/10.3390/en12163050
5. **Patlakas, P.**, Stathopoulos, C., Flocas, H., Kalogeri, C., Kallos, G. "Regional Climatic Features of the Arabian Peninsula". Atmosphere 2019, 10, 220. Doi: 10.3390/ATMOS10040220
6. **Patlakas, P.**, Drakaki, E., Galanis, G., Spyrou, C., Kallos, G. "Wind gust estimation by combining a numerical weather prediction model and statistical post-processing". Journal of Energy Procedia, Volume 125, September 2017, Pages 190-198. Doi:10.1016/j.egypro.2017.08.179
7. **Patlakas, P.**, Galanis, G., Diamantis, D., Kallos, G. "Low wind speed events: persistence and frequency". Journal of Wind Energy, Volume 20, Issue 6, June 2017, Pages 1033-1047. Doi:10.1002/we.2078
8. Solomos, S., Ansmann, A., Mamouri, R.E., Binietoglou, I., **Patlakas, P.**, Marinou, E., Amiridis, V. "Remote sensing and modeling analysis of the extreme dust storm hitting the Middle East and eastern Mediterranean in September 2015". Atmospheric Chemistry and Physics, Volume 17, Issue 6, 27 March 2017, Pages 4063-4079. DOI: 10.5194/acp-17-4063-2017
9. **Patlakas, P.**, Galanis, G., Barranger, N., Kallos, G. "Extreme wind events in a complex maritime environment: ways of quantification". Journal of Wind Engineering & Industrial Aerodynamics, Volume 149, February 2016, Pages 89–101. Doi:10.1016/j.jweia.2015.11.006

Conference presentations:

1. **Patlakas, P.**, Stathopoulos, C., Gavriil, A., Galanis, G., Kallos, G. "Wind energy potential assessment in western Mediterranean". EGU General Assembly 2020, Online | 4–8 May 2020.
2. Chaniotis, I., **Patlakas, P.**, Kallos, G. "A numerical study of dust particle effects on cloud microphysical processes and hail/precipitation impacts". EGU General Assembly 2020, Online | 4–8 May 2020.
3. **Patlakas, P.**, Stathopoulos, C., Tsalis, C., Kallos, G. "Tropical-Like Cyclones: Extreme Value Analysis and Risk Exposed Areas". AGU Fall Meeting 2019, 9 - 13 December, San Francisco, U.S.A.
4. Stathopoulos, C., **Patlakas, P.**, Tsalis, C., Kallos, G. "On the importance of the atmospheric-ocean feedback mechanisms in the Mediterranean storms". 10th European Conference on Severe Storms, Kraków, Poland, 4 – 8 November 2019.
5. **Patlakas, P.**, Stathopoulos, C., Tsalis, C., Kallos, G. "Estimating the risk exposed areas and the return periods of Medicanes". 10th European Conference on Severe Storms, Kraków, Poland, 4 – 8 November 2019.
6. Kallos, G., **Patlakas, P.**, Stathopoulos, C., Tsalis, C. "Optimizing a new declustering approach for extreme limited time series of high resolution with an application to wind speed design values". Extreme Value Analysis (EVA 2019) conference, July 1-5 2019, Zagreb, Croatia.
7. **Patlakas, P.**, Stathopoulos, C., Tsalis, C., Kallos, G. "Return periods of Medicanes: a wind-wave approach combining numerical weather prediction models and stochastic processes". AGU Fall Meeting 2018, 10-14 December, Washington, D.C., U.S.A.
8. Stathopoulos, C., **Patlakas, P.**, Tsalis, C., Kallos, G. "On the impact of air-sea feedback mechanisms under storm events". AGU Fall Meeting 2018, 10-14 December, Washington, D.C., U.S.A.
9. **Patlakas, P.**, Stathopoulos, C., Kalogeri, C., Flocas, H., Al Qahtani, J., Alexiou, I., Kallos, G. "Regional Climatology of the Arabian Peninsula based on a state of the art atmospheric model". 14th International Conference on Meteorology, Climatology and Atmospheric Physics October 15-17, 2018 Alexandroupolis, Greece.
10. **Patlakas, P.**, Stathopoulos, C., Kalogeri, C., Flocas, H., Al Qahtani, J., Alexiou, I., Kallos, G. "Regional climatology and climate trends in the Arabian Peninsula based on observational and modeling analysis". EMS Annual Meeting: European Conference for Applied Meteorology and Climatology 2018, 3–7 September 2018, Budapest, Hungary.
11. Stathopoulos, C., **Patlakas, P.**, Galanis, G., Al Qahtani, J., Alexiou, I. and Kallos, G. "Sea Spray Effects on Marine and Coastal Boundary Layer". 36th International Technical Meeting on Air Pollution Modelling and its Application May 14 - 18, 2018 – Ottawa, Canada.
12. **Patlakas, P.**, Stathopoulos, C., Kalogeri, C., Flocas, E., Bartsotas, N., Al Qahtani, J., Alexiou, I. "Dust Climatology for the Arabian Peninsula". EGU General Assembly 2018, Vienna, Austria, 8–13 April 2018.
13. Otero-Casal, C., **Patlakas, P.**, Prósper, M. A., Galanis, G., Miguez-Macho, G. "Development of a high resolution wind forecast system based on the WRF model and a hybrid Bayesian-Kalman Filter postprocess". EGU General Assembly 2018, Vienna, Austria, 8–13 April 2018.
14. Pinardi, N., Manzella, G., Simoncelli, S., Clementi, E., Moussat, E., Quimbert, E., Blanc, F., Valladeau, G., Galanis, G., Kallos, G., **Patlakas, P.**, Reizopoulou, S., Kyriakidou, C., Katara, I., Kouvarda, D., Skoulikidis, N., Gomez-Pujol, L., Vallespir, J., March, D., Tintoré, J., Fabi, G., Scarcella, G., Tassetti, A.N., Raicich, F., Cruzado, A., Bahamon, N., Falcini, F., Filipot, J.-F., Duarte, R., Lecci, R., Bonaduce, A., Lyubartsev, V., Cesarini, C., Zodiatis, G., Stylianou, S.,

Calewart, J.-B., Martín Míguez, B. “Stress testing the EU monitoring capacity for the Blue economy”. 8th EuroGOOS Conference, Bergen, 3-5 October 2017.

15. Kallos, G. with contribution from **Patlakas, P.**, Spyrou, C., Koukoula, M., Bartsotas, N. “Physical and Chemical Properties of Aerosols in the Mediterranean: Patterns and Impacts”. 15th International Conference on Environmental Science and Technology Rhodes, Greece, 31 August to 2 September 2017**.**
16. **Patlakas, P.**, Galanis, G., Kallos, G. “Studying the upper and lower tail of wind speed probability distribution: extreme value analysis”. Data Science & Environment workshop, Brest, France, 3-7 July 2017.
17. **Patlakas, P.**, Drakaki, E., Galanis, G., Spyrou, C., Kallos, G. “Wind gust estimation by combining a numerical weather prediction model and statistical post-processing”. EGU General Assembly 2017, Vienna, Austria, 23–28 April, 2017.
18. Stathopoulos, C., Galanis, G., **Patlakas, P.**, Kallos, G. “Assessing sea wave and spray effects on Marine Boundary Layer structure”. EGU General Assembly 2017, Vienna, Austria, 23–28 April, 2017.
19. Kallos, G., **Patlakas, P.**, Bartsotas, N., Spyrou, C., Al Qahtani, J., Alexiou, I., M Bar, A. “Modeling the dust cycle from sand dunes to haboobs”. EGU General Assembly 2017, Vienna, Austria, 23–28 April, 2017.
20. Kallos, G., **Patlakas, P.**, Koukoula, M., Stathopoulos, C., Rosenfeld, D. “Sea salt production and its role in warm clouds formation”. EGU General Assembly 2017, Vienna, Austria, 23–28 April, 2017.
21. Kallos, G., Stathopoulos, C., Galanis, G., **Patlakas, P.** “Modeling of Atmospheric-Wave Processes With a Fully Coupled System”. Ocean waves and wave-Coupled Processes workshop. Australia-China Centre for Maritime Engineering. Melbourne, Australia, December 2016.
22. Kallos, G., Nenes, A., **Patlakas, P.**, Drakaki, E., Koukoula. M., Rosenfeld, D., Mihalopoulos, N. “Aerosols in the Mediterranean Region and their role in cloud formation”. 35th International Technical Meeting on Air Pollution Modelling and its Application, 3-7 October, 2016, Chania, Crete, Greece.
23. **Patlakas, P.**, Kushta, J., Drakaki, E., Al Qahtani, J., Alexiou, I., Bartsotas, N., Spyrou, C. and Kallos, G. “The dust cycle in the Arabian Peninsula and its role in the urban air quality”.35th International Technical Meeting on Air Pollution Modelling and its Application, 3-7 October, 2016, Chania, Crete, Greece.
24. **Patlakas, P.**, Diamantis, D., Galanis, G., Kallos, G. “Towards a study of different types of extreme wind speed conditions”. 13th International Conference on Meteorology, Climatology and Atmospheric Physics, COMECAP 2016, 19-21 September 2016, Thessaloniki, Greece.
25. Kushta, J., Spyrou, C., **Patlakas, P.**, Kallos, G. “Sandblasting Mass Efficiency as a Function of Soil Clay Contents: A comparative modelling study”. 8th Internatıonal Workshop on Sand/Duststorms and Associated Dustfall, 1-4 May 2016 Lisbon, Portugal.
26. **Patlakas, P.**, Galanis, G., Péray, M., Filipot, J.F., Kalogeri, C., Spyrou, C., Diamantis, D. and Kallos, G. “An Integrated Methodology on the Suitability of Offshore Sites for Wind Farm Development”. EGU General Assembly 2016, Vienna, Austria, 17-22 April, 2016.
27. Kallos, G. with contribution from Galanis, G., Kalogeri, C., **Patlakas, P.**, Stathopoulos, C. and Liakatas, A. “The European offshore wind and wave energy resource analysis – Combined exploitation - Analysis of extremes”. Brazilian Symposium on Water Waves, Federal University of Rio de Janeiro, Brazil, 14-16 March, 2016.

28. Kallos, G., Kushta, J., **Patlakas, P.**, Bartsotas, N., Spyrou, C., Drakaki, E., Al Qahtani, J., Alexiou, I. "The dust cycle in the Arabian Peninsula: from sand dunes to haboobs". PetroEnvironment, 2016. 8th Symposium and Exhibition on Environmental Progress in the Petroleum & petrochemical, Dammam, Saudi Arabia 22-24 February, 2016.
29. **Patlakas, P.**, Galanis, G., Kallos, G. "Quantifying Extreme wind and uncertainties for energy applications". 8th GRACM – Intern. Congress on Computational Mechanics, Volos, Greece, 12-15 July, 2015.
30. Kallos, G., Kushta, J., Bartsotas, N., **Patlakas, P.**, Astitha, M., Al Qahtani, J. "The role of aerosols in low and upper atmospheric layers condensation". 34th International Technical Meeting on Air Pollution Modelling and its Application, Montpellier, France, 4-8 May, 2015.
31. **Patlakas, P.**, Galanis, G., Kallos, G. "Quantifying uncertainties in wind energy assessment". EGU General Assembly 2015, Vienna, Austria, 12-17 April, 2015.
32. Kallos, G., Galanis, G., Kalogeri, C., Barranger, N., **Patlakas, P.** "Advanced atmospheric modeling for engineering applications". 6th International Symposium on Computational Wind Engineering - CWE2014, Hamburg, Germany 2014.